**KTH Industrial Engineering
and Management**

Load Shifting and Storage of Cooling Energy through Ice Bank or Ice Slurry Systems

- modelling and experimental analysis

Doctoral Thesis

By

Marino Grozdek

Division of Applied Thermodynamics and Refrigeration
Department of Energy Technology
Royal Institute of Technology
Stockholm, Sweden 2009

Abstract

Ice based Cool Thermal Energy Storage (CTES) systems have attracted much attention during last few decades. The reasons are mainly of economical and environmental nature. Compared to conventional refrigeration and air-conditioning systems without cool thermal energy storage, implementation of CTES will increase environmental standards and overall efficiency of the energy systems as it contributes to the phase-out of synthetic refrigerants and reduces peak loads in electricity grids.

For the application of a cool thermal energy storages in refrigeration installations and HVAC systems in industry and building sector, it is necessary to have appropriate design tools in order to sufficiently accurate predict their performance. In this thesis theoretical and experimental investigations of two ice based cool thermal energy storage systems, namely static, indirect, external melt, ice-on-coil, i.e. ice bank system and dynamic, ice slurry cool thermal energy storage system are carried out.

An ice bank storage technology for cooling purposes is known for a long time. The main drawbacks which are hindering its wider use are the system complexity, high first costs, system efficiency which is highly dependant on design, control and monitoring of the system, etc. On the other hand, ice slurry technology was not well studied until recently, while in the current scientific literature there are still differences between results and conclusions reported by different investigators.

The aim of the present thesis is to extend the knowledge in the field of ice based CTES systems, thereby contributing in the development and wider utilization of those systems.

In the first part of the thesis a computer application, named "BankaLeda" is presented. It enables simulation of an ice bank system performance. In order to verify developed simulation model an experimental evaluation has been performed. Field measurements have been conducted on a two module silo which was installed as a part of the refrigeration system in dairy and cheese factory "Antun Bohnec" in the city of Ludbreg in Croatia. Experimental findings were compared to the simulation model. The software „BankaLeda" presents a strong optimization tool for designers and engineers in the field by providing a high degree of freedom in defining particular system design and operating parameters. It offers a basis for assessment and testing of a new energy efficient system arrangements and measures. Besides it will give decision-

makers the ability to test potential solutions in the process of CTES system design.

In the second part of the thesis ice slurry pressure drop and heat transfer in horizontal straight tubes have been experimentally investigated. In particular a mixture of 10.3 % of ethanol and water with an initial freezing point of -4.4 °C was considered. It was found that the behaviour of ice slurry flow is changing with time and that ice slurry pressure drop is generally higher than for single phase flow. However for ice concentrations of 15 % and higher, for certain velocities ice slurry pressure drop is found to be of a similar value as for single phase fluid. Moreover, if ice slurry is to be used as a energy transport media it is recommended to keep the ice mass fraction at a level of 20 %.

With tube geometry and thermophysical properties of a carrier fluid the heat transfer of ice slurry is generally a function of ice mass fraction and velocity. The imposed heat flux has no or has just minor influence on the heat transfer coefficient. Up to ice mass fraction between 10-15 % the mean heat transfer coefficient shows only slight (laminar flow) or no increase (turbulent flow) in comparison to single phase flow. Beyond that ice mass fraction the heat transfer coefficient is increasing significantly.

The test data for pressure drop and heat transfer in laminar and turbulent regime was compared to several correlations from the literature. A new correlations for ice slurry pressure drop and heat transfer in the laminar flow regime, for 10.3 % ethanol and water mixture, were derived based on the present experimental data. The correlation for pressure drop predicts 82 % of the experimental data with ±15 % accuracy, while the correlation for heat transfer predicts 75 % of the data with the same accuracy.

In order to investigate advantages and disadvantages of a dynamic, ice slurry system over a static, indirect, external melt, ice-on-coil CTES system and to assess their differences from economical aspects, a theoretical simulation model of an ice slurry CTES have been developed. It was found that the ice slurry based CTES systems posses higher economic and energy saving potential than static type systems. In the best case scenario the total energy consumption of dynamic CTES system was found to be approximately 25 % lower than for a static CTES system.

Keywords: refrigeration systems, cool thermal energy storage system, ice, modelling, simulation, field measurement, experiment, indirect system, ice-on-coil system, external melt, ice slurry, homogeneous storage, heterogeneous storage.

Acknowledgements

First of all I would like to express my sincere gratitude to my supervisors Professor Tonko Ćurko, of the University of Zagreb, Faculty of Mechanical Engineering and Naval Architecture (FSB) and Professor Per Lundqvist, of the Royal Institute of Technology (KTH) for the opportunity to become a part of your research teams and possibility to complete this thesis. Thank you for all the support, encouragement, guidance and belief in me. Above all I thank you for endless discussions on sailing and sailing itself.

My special gratitude goes to Professor Björn Palm who has always found time and energy to advise me. Thank you for stimulating discussions and valuable comments on published articles and this dissertation. Thank you for free time for sailing. I really like sailing your 470.

I would like to thank my co-supervisors Professor Boris Halasz (FSB) and Assistant Professor Rahmatollah Khodabandeh (KTH) for helping me with writing and publishing the articles, for your advices and patience with all my questions. I extend this gratitude to Professor Åke Melinder who has been an invaluable help in the early days of my ice slurry experience.

I am grateful to Zlatko Vojvoda, the owner and Dario Sekušak, the head engineer from the company Frigoterm d.o.o. for close cooperation on software development and technical backup during measurements.

Further, I wish to thank Đuro Bohnec, the owner, Miroslav Siladić, the head of production and all other employees of the dairy "Antun Bohnec", City of Ludbreg, Republic of Croatia for providing me with full support in conducting experiments in their company.

I would also like to thank to my roommate Samer Sawalha, and my friends at the Division of Applied Thermodynamics and Refrigeration, Oxana Samotewa, Claudi Martin, Primal Fernando, Yang Chen, Getachew Bekele, Ali Rashid, Jose Acuna, Hatef Madani, Hamayun Maqbool, Alaa Kullab, Stina Gustafsson, Richard Furberg, Wahib Owhaib, Raul Anton and Jaime Arias. Thank you for your friendship, lunches and table football championships. Many thanks to the all staff members at Department, to Inga Du Rietz, Benny Sjöberg, Benny Andersson, Peter Hill, Professor Eric Granryd, Hans Jonsson and Joachim Cleasson for the technical support.

Publications

The present thesis is based on six articles which have been written during the course of the projects. Of these, four have been published in scientific journals or presented at international conferences. The remaining two are submitted or are in process of submission to scientific journals for publication.

List of publications included in this thesis are:

Conference papers

Grozdek, M., Halasz, B., Ćurko, T., Soldo, V. Experimental Investigation of an Ice Bank System Performance. 3rd IIR Conference on Thermophysical Properties and Transport Processes of Refrigeration, Boulder, Colorado, USA, 2009.

Journal papers

Halasz, B., Grozdek, M., Soldo., V. Development of computer program for simulation of an ice bank system operation, Part I: Mathematical modelling. International Journal of Refrigeration, Volume 32, Issue 6, September 2009, Pages 1323-1335.

Grozdek, M., Khodabandeh, R., Lundqvist, P. Experimental investigation of ice slurry flow pressure drop in horizontal tubes. Experimental Thermal and Fluid Science, Volume 33, Issue 2, January 2009, Pages 357-370.

Grozdek, M., Khodabandeh, R., Lundqvist, P., Palm, B., Melinder, Å. Experimental investigation of ice slurry heat transfer in horizontal tube International Journal of Refrigeration, Volume 32, Issue 6, September 2009, Pages 1310-1322.

Articles submitted or to be submitted to scientific journals for publication:

Grozdek, M., Soldo., V., Ćurko, T. The economic justification of ice storage application in cooling systems within the process industry and building sector. To be submitted.

Grozdek, M., Soldo., V., Khodabandeh, R., Ćurko, T., Lundqvist, P. Performance Comparison of a Static Ice-Bank and Dynamic Ice Slurry Cool Thermal Energy Storage Systems. Submitted for publication.

Other papers

These articles have not been included in this thesis. They were published within the project in conference proceedings and were presented during the conferences or have been recently accepted to scientific journals for publication.

Halasz, B., Ćurko, T., Grozdek, M. Ice bank as a means for fast chilling of water. The 22nd International Congress of Refrigeration, Beijing, P.R. China, August 2007.

Nikolić, V., Grozdek, M., Halasz, B., Ćurko, T. Analiza isplativosti banke leda u rashladnim postrojenjima (Economic analysis of ice storage application in cooling systems within the industry). Strojarstvo, Journal for Theory and Application in Mechanical Engineering. Accepted for publication.

Table of contents

1 Introduction

Refrigeration, air conditioning and heat pump applications present one of the most important energy usage sectors in present day society. It is estimated that an average share in electricity use for the developed countries is between 10-20 % (UNEP, 2003). In the US one sixth of the electricity consumed goes to cool buildings (Lucas, 1998).

For different reasons, there is a steadily growing demand for air-conditioning or comfort cooling, mainly in commercial and institutional buildings. In the United States and Japan, more than 80 % of buildings in these categories have comfort cooling. Europe is responsible for only 6 % of the installed air conditioning equipment worldwide. However, the air conditioning market in Europe is expanding quickly in recent years. Although the intention of the EU is to decrease the need for cooling of buildings by using passive technologies, improved insulation and energy efficiency technologies, the air-conditioner world market is still expanding. The sales have been estimated at about 39.7 millions of units in 2000, among which 29.9 millions are room air conditioners and 9.8 millions are central air conditioners (CENERG, 2005). Market research shows that only 27 % of the European tertiary sector (schools, hospitals, offices, hotels, restaurants, shops) and 5 % of the residential sector are equipped with room air conditioners (CENERG, 2005). It is evident that the EU market is far from saturated. With a saturation rate of 60 % for the service sector and 40 % for the residential sector - "the European saturation rate" will be reached by 2018, i.e. the cooling market will show a four fold increase between 2000 and 2018, corresponding to cooling demand of 500 TWhc with electricity demand of 200 TWh for the countries of EU (EcoHeatCool, 2006).

For Croatia the total potential cooling demand is estimated to 5 TWhc, with an electricity demand of 1.8 TWh. The increase in electricity demand is closely followed by a peak load demand. Between 1990 and 2002, the average peak load in EU has increased by 20 % while in some Mediterranean countries the corresponding increase was more then 50 % (e.g. 54 % in Greece). The average peak-load increase is expected to continue at least at the same rate. In Mediterranean countries the forecasted increase is even higher.

According to Zanki (2006) the tourism market and with it related accommodation quality on the Croatian Adriatic coast is increasing rapidly. Currently, the majority of facilities have three stars while the four and five star hotels are scarce (approximately 10 %). Before the new rules of hotel classification, cooling systems were required only for four and five star hotels. Now, cooling of rooms and common facilitates is mandatory for three, four and five star hotels. This regulation forced the majority of hotels to enter renovation and implementation of a new cooling and air-conditioning systems. This has led to several electricity blackouts in recent years in August on the Adriatic coast (Dubrovnik, Vodice, island Murter).

To prevent exceeding the power system capacity limits and to avoid risks of future outages, Croatia is forced to import the required electric energy under adverse conditions. To cope with the problem a couple of key measures (remedies) were suggested and adopted under the Croatian Energy Strategy for the time period to 2030, namely building of new electricity generating capacity (2000 MW) and energy efficiency increase in production, transformation and use of energy including energy storage and transport (Croatian Parliament, 2002).

Instead of building new electricity generating installations to cover peak demand it is more economically and environmentally reasonable to bring the power system load curve into balance. Namely, Croatian power system daily maximum peaks between 2700-2900 MW (20 p.m.) while the minimum is at 1100-1500 MW (6 a.m.) depending on the period of the year (HEP, 2008).

In order to hinder the negative impact of the electricity power demand in the present day and with the forecasted increase in the future, that refrigeration and air conditioning equipment exerts on Croatian power system, the implementation of a cool thermal energy storage systems (CTES) as a part of refrigeration installations in industry and HVAC systems in commercial and residential buildings is proposed.

1.1 Motivation

Refrigeration systems in industry and air conditioning in commercial and residential buildings is the largest single contributor to electrical peak demand especially during summer daytime. This requires the electric suppliers to bring additional, more costly generating equipment on line or to import the required energy to handle this increased demand. Commercial users, whose large cooling loads greatly contribute to the need for these seldom used generating stations, are charged more for this

2

on-peak energy, in the form of demand charge which is based on their highest on-peak demand for electricity.

Implementation of a Cool Thermal Energy Storage (CTES) System enables to shift electric load to off-peak hours which significantly lower energy charges and reduces peak loads in power system during the cooling period. Besides, it can also lower total energy usage as well (Bahnfleth and Joyce, 1994; Fiorino, 1994). Generally, the electric supplier's generating capacity is under-utilized at night and, consequently, its rates are lowest then. In Croatia, difference between on- and off-peak rates is twofold, i.e. during day time (7 a.m. – 9 p.m.) consumer is charged with 0.085 €/kWh while during night shift (9 p.m. – 7 a.m.) with 0.042 €/kWh (valid for commercial low voltage customer, tariff model: white). Prices are dependant on customer profile and tariff model (HEP, 2008).

Basically, only few applications are <u>not</u> suited for cool thermal storage. Whenever the maximum cooling load is higher than the average load or the electric billing schedule includes high demand charges with difference between on- and off-peak rates, application of the thermal storage may be economically justified. The higher the load factor the more attractive is CTES to the customer. Particularly well suited to thermal storage are sports and entertainment facilities, convention centres, churches, airports, schools and universities, military bases and office buildings as well as various industrial applications (ASHRAE, 2007).

Office building cooling loads often peak at a level of two or more times higher than the daily average load (Dorgan and Elleson, 1994). Likewise, process cooling in various industrial applications such as food processing in food industry (milk cooling, carcass spray cooling, fish processing, beer and vine production) and drugs treatment in pharmaceutical industry have load peaks that rise much higher than the average load. Dairies are a good example where large short loads often are required. Typically once a day, in the morning, for a limited duration, a large quantity of incoming fresh milk must be quickly cooled. Such a high cooling demand requires either a large capacity refrigeration unit, which would be idle for the most of the day, and would consume high (electrical) power when busy, or a smaller refrigeration unit that would operate rather uniformly during low-load periods and accumulate the cooling energy to meet the peak load when needed.

Moreover, CTES not only can significantly cut operating costs but they can also substantially reduce capital outlays by downsizing the cooling equipment when systems are suitably designed for new commercial and industrial application (Andrepont, 2005).

If implemented, CTES's can increase environmental standards of the refrigeration system as it contributes to the phase-out of synthetic refrigerants. Today the ozone depletion potential (ODP) and global warming potential (GWP) of the synthetic refrigerants used in the majority of air-conditioning and refrigeration installations are the major environmental concerns. On an annual basis 20-35 % of refrigerant charge was emitted to the atmosphere in 1980 in developed countries (AEA, 2003). The worldwide main regulation addressing ozone depleting substances (ODS) is the Montreal Protocol adopted in 1987. On EU level that is European Regulation on Ozone-Depleting Substances No. 2037/2000 of June 29th, 2000. (Billiard, 2005).

With respect to the process for Croatia to enter the European Union, harmonization with the Montreal Protocol and the European community regulations and standards within strongly defined fields of application regarding safety and environmental criteria is summarized under Croatian bylaw on ozone depleting substances. According to the Bylaw, import of CFCs is banned from January 1st, 2006 and HCFC's were banned for new installation from 20 October 2005 (MZOPU, 2005). Complete phase out of HCFC's refrigerants and transfer to chlorine free HFC's in Croatia is planed by 2016.

Even though the HFC refrigerants were expected to be an acceptable replacement for the phased out CFC's and HCFC's, they turned out to be only a temporary solution due to their high global warming potential. Therefore, one of the key objectives set by International Institute of Refrigeration for the next period of 20 years is to reduce the refrigerant charge in refrigeration systems by 30 % to 50 % and to halve the refrigerant leakage (IIR, 2002). By implementation of the indirect cooling to CTES, the refrigerant charge and related emissions could be reduced by a factor of ten compared to a complete direct expansion installation (IIR, 2004). Besides, indirect systems are more suitable for use of environmentally friendly, natural refrigerants such as ammonia (R717), carbon dioxide (R744) or propane (R290).

In the energy sector the largest share of emissions is that of the carbon dioxide (CO_2). The largest contributors are energy production and transformation facilities. At present, more than 40 % of the total installed generating facilities in the Croatian electrical power system consists of thermal power plants, mainly oil-fired with the possibility of burning natural gas as an alternative fuel (HEP, 2008). As reported by MINGORP (2007) the CO_2 emissions in Croatia is steadily increasing. In 2005-2006 period the CO_2 emissions increased by 1.7 %. According to the Kyoto Protocol, which was signed and ratified by the Croatian Government in 2007, Croatia is obligated to cut greenhouse emissions by 5

% over the 2008-2012 period. It is reasonable to believe that the certain benefits could be achieved by implementation of CTES systems and load shifting, when it comes to reduction of carbon dioxide (CO_2) emissions in power plants, since the daily electric peaks are covered mainly by the thermal power plants. Baseline electricity needs are met by hydro power plants with total electricity production of approximately 58 %.

For the time being CTES's are being exclusively imported on Croatian domestic market. At the moment as a part of HVAC systems CTES's are implemented only in five hotels on the Adriatic coast (Zanki, 2006) and in not more than a few commercial buildings in Zagreb (concert hall Vatroslav Lisinski, business tower "Hrvatske vode", Zagreb "City Hall", sport facility "Handball hall Arena" Zagreb). Situation is slightly better in industry sector. As a part of refrigeration installations few dozens of CTES's are installed in a food industry (dairy "Antun Bohnec", "Dukat", "Vindija", food factory "PIK Rijeka", "Zvijezda", "PIK Vrbovec").

1.2 Background

In 2004 the Department of Thermodynamics, Thermal and Process Engineering of the Faculty of Mechanical Engineering and Naval Architecture under University of Zagreb started a technology project in cooperation with one major CTES producer in Croatia, Frigoterm d.o.o., a company involved in refrigeration technology and the Ministry of science, education and sport of the Republic of Croatia as a funder.

The overall aim of the technology project TP-03/0120-35, "Development and Production of an Indirect Cool Thermal Energy Storage Prototype – Ice Bank – with an Accumulation Capacity of 400-7000 kWh" was to develop and produce a prototype of a static, indirect, external melt, ice-on-coil cool thermal energy storage system, i.e. an ice bank system.

The project was divided in four stages. In the first stage development of a simulation model of a static, indirect, external melt, ice-on-coil CTES, i.e. ice bank, and building of a computer application which would allow simulation of an ice bank system operation was carried out. The simulation model was designed to account for numerous parameters that influence ice bank operation and to offer basis for an ice bank prototype design. On basis of the simulation results the design of a CTES components were carried out in the second stage.

The third phase comprised of the ice bank prototype production and commissioning. A two module silo was produced and installed in a dairy and cheese factory "Antun Bohnec" in city of Ludbreg, Croatia. In the

final fourth phase on-site measurements of ice bank performance were conducted in order to verify a validity of the simulation model.

In December 2006 I have joined the research project "A New machine for producing ice-slurry at -35 °C for a completely environmentally friendly refrigeration process, ICE-COOL" as a postgraduate PhD student at Department of Energy Technology of the Royal Institute of Technology, Sweden in order to broaden initiated investigation to more advanced ice based CTES technologies, i.e. to conduct investigation on ice slurries.

1.3 Aim of the study

This thesis are dedicated to ice based cool thermal energy storage systems, namely static, indirect, external melt, ice-on-coil system, i.e. ice bank and dynamic, ice slurry cool thermal energy storage system.

The purpose of this thesis is to investigate and put into relation the afore mentioned technologies and to provide a basis for decision makers who are involved in the design and preinstallation planning of such systems.

The main tasks of this thesis are:

- o The development of a simulation model of an indirect, external melt, ice-on-coil cool thermal energy storage system,

- o Verification of a developed simulation model by means of the field measurements,

- o Identification of a strengths and weakness points of an ice bank storage and pointing out potential improvements,

- o Investigation of the economic potential and benefits gained by implementation of an ice bank systems in industry and air conditioning systems in commercial and residential buildings, in Croatia,

- o A comparison with more advanced ice based cool thermal energy storage systems, i.e. ice slurry systems,

- o Experimental investigation of ice slurry flow behaviour, i.e. pressure drop and heat transfer in horizontal tubes,

o   Investigation of advantages and disadvantages of static, indirect, external melt, ice-on-coil cool thermal energy storage system over dynamic, ice slurry system,

o   Recommendations for future research work.

1.4 Methodology

In this thesis two ice based cool thermal energy storage technologies are investigated. The investigation methods are of numerical (theoretical) and experimental nature.

In order to evaluate the performance of a static, indirect, external melt, ice-on-coil cool thermal energy storage system for different design arrangements and under various operating conditions a computer simulation model have been developed. In the first phase development of a mathematical model that includes components of an ice bank system and their interconnections have been carried out. Due to the high complexity of the system and numerous design and operating parameters that influence its performance a computer application "BankaLeda" was designed. Mathematical models of system components are integrated in a stand alone computer program. Input of design and operating parameters is enabled through drop down menus while the results are presented via figures, diagrams and pictures. Programming was done in Fortran 95 language standard. (*Chapter 3. Published in International Journal of Refrigeration, Volume 32, Issue 6, September 2009, Pages 1323-1335).*

In order to verify the developed simulation model an extensive experimental evaluation has been performed. Field measurements have been conducted on a two module silo which was installed as a part of the refrigeration system in dairy and cheese factory "Antun Bohnec" in the city of Ludbreg, Croatia. Experimental findings were compared to the simulation model. (*Chapter 4. Presented and published in conference proceedings of the 3rd IIR Conference on Thermophysical Properties and Transport Processes of Refrigeration, Boulder, Colorado, USA, 2009).*

Two actual cases of ice bank application in process industry and building sector are studied in order to investigate their economic potential on the Croatian market. For both cases static, indirect, external melt, ice-on-coil cool ice bank system was considered. In the first case ice bank application within the dairy industry "PIK, Rijeka" is considered. In the second case implementation of the ice bank system as a part of chilled water system for the purpose of building cooling (Elderly Persons Home in Sisak) is discussed. (*Chapter 5. To be submitted for publication.*).

Based on findings and observations of the experimental tests it was possible to identify the advantages and limitations of the ice bank system. Suggestions for improvements and recommendations for future research and further development of the simulation model and ice bank design have been pointed out. *(Chapter 6).*

A transition to more advanced ice based CTES systems, i.e. dynamic ice slurry systems have been undertaken. As a part of research on ice slurries, experimental investigation of ice slurry pressure drop and heat transfer in horizontally laid tubes have been conducted whereby existing experimental rig, originally designed for freezing temperatures have been modified for cooling applications. The research activities conducted on ice slurries greatly contributed to better understanding of an ice slurry technology which finally served as a base for subsequent investigations. *(Chapter 8. Published in Experimental Thermal and Fluid Science, Volume 33, Issue 2, January 2009, Pages 357-370; Chapter 9. Published in International Journal of Refrigeration, Volume 32, Issue 6, September 2009, Pages 1310-1322).*

In order to perform theoretical evaluation of the performance of a dynamic ice slurry storage system and to assess its possible economic and energy saving potential over conventional ice-on-coil static type a theoretical simulation model of an ice slurry CTES have been developed. In particular, heterogeneous storage with chilled secondary fluid extraction and warm spray return was considered. *(Chapter 10. Submitted for publication).*

8

2 Ice based cool thermal energy storage systems

2.1 Introduction

A thermal energy storage system remove heat from or add heat to a storage medium to meet a system load at another time. Basically it separates generation of heating or cooling from the use in time. This allows the generation of heating or cooling to be moved to periods when conditions are more favourable.

Thermal energy storage systems are primarily classified according to a temperature level at which the stored energy is being used. If stored energy is used for heating purposes thermal storage is referred to as heat thermal energy storage and if it is used for cooling, thermal storage is referred to as cool thermal energy storage.

Implementation of thermal energy storage in HVAC&R systems can offer certain benefits (ASHRAE, 2007):

- o cost savings in energy by reduction of total operating costs in case when the electricity is primary energy source,

- o reduced equipment size,

- o capital cost savings from downsizing the heating or cooling generation equipment,

- o energy savings in case when the generation of cooling is performed during the night resulting in higher efficiency of refrigeration equipment due to lower ambient and therefore condensing temperatures,

- o increased operating flexibility,

- o extending existing systems capacity and

- o back-up capacity.

Cool thermal energy storages involve a variety of applications and by it related temperature levels. Basically they are grouped in three main application fields. For air-conditioning purposes energy storage at temperatures above 0 °C is desired. Energy storage for cooling applications is associated with temperature levels between 0 °C and -18 °C and for freezing applications between -18 °C and -35 °C. Certain temperature level depends on particular process requirements.

Moreover, cool thermal energy storages can be divided according to the type of the storage medium and storage technology. If classified according to the storage medium they can be of sensible or latent type.

Sensible type cool storage media include aqueous or nonaqueous fluids, in most cases plain water, while latent type storage media include phase-change materials, mostly water-ice.

In comparison to the sensible type, latent type storage offers higher energy storage density and temperature stability of the fluid being discharged from the storage. Higher energy density allows compact system design resulting in capital cost savings while temperature stability means preserving the quality of the product.

Phase-change materials can be either pure substances or mixtures. In comparison to single component pure substances, mixtures exhibit a temperature glide, i.e. continuous transition, as in case with mixture of water and freezing point depressant (alcohol, salts, etc.), micro-emulsions or microencapsulated slurries.

2.2 Applications of cool thermal energy storages

For comfort cooling of buildings chilled water CTES systems have been commonly accepted and widely applied. Bahnflet and Joice (1994), Fiorino (1994) and Henze et al. (2008), report on sensible cold water type storage systems as a measure to raise efficiency of air-conditioning systems for cooling of university complex, electronic manufacturing facilities and pharmaceutical buildings. Although requires large storage tanks and space for installation, chilled water storage technology offer use of standard water chillers operating at high rates of efficiency. It is a simple, low maintenance and reliable technology. Moreover, it becomes most economical for applications with cooling loads requiring storage of more than 7000 kWh (Dorgan and Elleson, 1994).

If phase-change material is considered as a storage media for comfort cooling of buildings, appropriate material with phase change temperature around +5 °C is desired (for standard temperature regime of chilled wa-

ter +7/+12 °C used for air cooling). As a potential solution aqueous micro-emulsion or micro-encapsulated slurries based on paraffin are proposed (He et al., 2004; Gschwander et al, 2005); in particular tetradecane or hexadecane paraffin with melting temperature of +6 °C and +18 °C. Since these types of advanced secondary fluids have many problems yet to overcome (coagulation, coalescence, Ostwald ripening, resistance to shear stresses) they are still in a phase of development.

Nevertheless, today in most of the CTES installations water or water-ice is used as a storage medium. The reasons are its good thermodynamical and general properties, such as high density, specific heat, heat of fusion and good heat transfer characteristics. Moreover it is available and of low cost, environmentally benign, nontoxic, nonflammable, nonexplosive, noncorrosive and inert.

If water-ice is considered as a CTES media for air-conditioning purposes, temperature level of energy stored will be lower than usually required, namely fixed to 0 °C. However it will enable use of a cooler air distribution temperature of +12 °C compared to +15 °C which is a normal design practice. Reduction in air flow will at the end compensate for reduced refrigeration unit efficiency due to lower operating temperatures (Bellas and Tassou, 2005).

Today two ice based technologies for storage of cold are known, namely static, where ice is built and stored on surfaces of a heat exchanger and dynamic where ice is removed from a heat exchanger surface. In the latter case a mixture of liquid and ice particles is formed and it is referred to as ice slurry.

Another interesting ice based technology suitable for colder climate is to collect or make snow in the winter season and then use it for cooling of buildings in spring or summer period (Skogsberg and Nordell, 2001). This is known as a Seesonal Snow Storage technology and it will not be further treated in this thesis. The systems studied in this thesis are mainly short therm (Diurnal) ice storage systems for day to night load shifting.

Saito (2002) summarized examples where ice based or ice slurry CTES systems have been applied as a part of air-conditioning installations with success. Most of them are located in USA and Japan. In Chicago, USA, two-third of the peak-load air-conditioning demands of the downtown area is supplied by ice based CTES. In Osaka, Japan, for cooling of CAPCOM and Herbis buildings an ice slurry system is used (Kuriyama and Sawahata, 2001). A similar solution is applied for cooling of Kyoto Station Building complex (Ise et al, 2001). Many other countries encourage implementation of CTES's by electricity rates or by regulations. In

Croatia the peak electricity rate is twice that of off-peak rate for commercial users while in Korea for new or renewed buildings of more than 3000 m² it is an obligation to provide air-conditioning with CTES system or by an absorption chiller.

Beside air-conditioning, there are many industrial process where the temperature of the products should be kept at a temperature slightly above freezing point of water. Naturally for such applications, water-ice as a phase change media is logical by itself. In food processing plants, namely dairy and cheese factories, the temperature of products that is to be reached in a relatively short period of time is approximately +3 °C. In order to provide it, low temperature water from +0.5 to +1.5 °C is supplied from the CTES system to the load. There are many examples of successful operation of static, ice bank CTES systems for cooling of milk in the world as well as in Croatia (dairy "Antun Bohnec", "Dukat", "Vindija", food factory "PIK Rijeka", "Zvijezda", "PIK Vrbovec"). Dynamic CTES systems are however scarce. As reported by Gladis (1997) a dynamic type CTES sytem using ice slurry as a storage material and chilled water as a distribution media was successfully installed in a cheese plant in Hanford, California. As reported by Ralph and Breisch (1997) dynamic ice harvesting CTES systems was successfully installed in a factory producing powdered eggs.

Water-ice as a phase change media is also applicable for rapid cooling of fish, meat and vegetables. Fish lose quality because of bacterial or enzymatic activity or both. Reduction of storage temperature retards these activities significantly, thus delaying spoilage and autolytic deterioration. The shelf life of species such as haddock and cod is doubled for each 4 to 5.5 K decrease in storage temperature within the range of 16 to -1°C. Therefore fresh fish should be cooled as quickly as possible to a temperature of approximately +2 °C (ASHRAE, 2007). Usually flake ice or ice slurry is sprayed over the fresh fish. The ice crystals melt by the direct contact with the fish providing necessary cooling. As reported by (Bellas and Tassou, 2005) ice slurry was showed to perform better ensuring higher product quality.

For carcass chilling rapid temperature reduction is important in reducing the growth rate of microorganisms that may exist on carcass surfaces. Spraying cold water intermittently on beef carcasses for 3 to 8 h during chilling is currently the normal procedure in commercial beef slaughter plants. A final product temperature of +5 °C should be reached and it should be maintained during storage, shipping and display. (Gigiel and Badran, 1988) found that chilling of pig carcasses with low water temperature from ice bank gave a savings in weight loss over 48 hours of chilling and storing in comparison to conventional methods. Anyway,

most of the CTES installations in the world are designed especially for the purpose of milk cooling or fish processing.

For cooling applications, at temperatures lower than 0 °C, such as for retail food applications in supermarkets where temperature at which the food is preserved in display cabinets is around -4 °C, aqueous-brine/ice solutions, i.e. ice slurries or eutectic salts as a CTES media are of interest. Ice slurries can be generally applied for a temperature range of 0 °C down to approximately -35 °C. They are however most promising for cooling applications, i.e. for temperatures above -10 °C (IIR, 2005a). Typical applications of ice slurry for food preservation in supermarkets are reported in (IIR 2005b).

Eutectic salts, as phase change materials are engineered to store energy at certain temperature levels. Basically, the material is composed of inorganic salts, water and a nucleating agent in a proportion which ensures phase change at temperatures from +27 °C to -33 °C (Cristopia, 2008). The material is confined within plastic spherical containers around which secondary coolant circulates, allowing freezing and melting of eutectic mixture in containers. This technology is widely applied, primarily for air-conditioning of buildings ("Hrvatske vode" and "City Hall" in Zagreb) and cultural and sport facilities (concert hall "Vatroslav Lisinski" and "Handball hall Arena" Zagreb).

2.3 Solutions of ice based CTES's

Design and performance of cool thermal energy storage depends on the temperature level at which the cooling energy is being stored and the technology used. The temperature level of storage depends on the application. According to storage technology, ice based cool storage systems can be divided to internal melt ice-on-coil, external melt ice-on-coil, encapsulated ice, ice harvesters and ice slurry systems (Dorgan and Elleson, 1994).

Internal melt ice-on-coil circulates a secondary coolant or refrigerant through a tubular heat exchanger that is submersed in a tank of water. The charging (ice making) and discharging (ice melting) are accomplished by circulating the secondary heat transfer fluid. Ice forms on the heat exchanger tubes during charging, and melts from the inside out during discharging. The tubular heat exchanger is typically constructed of polyethylene or polypropylene plastic or steel or copper. Tube spacing is closer than in external melt heat exchangers since there is no need to maintain a liquid channel between individual tubes. An important characteristic of the internal-melt design is the relationship between the charging and discharging process. During discharge, ice in contact with the

heat exchanger is melted first. Initial discharge rates can be very high, and initial available temperatures approach the phase change temperature. As ice melts an annulus of water develops between the heat exchanger and ice surfaces which results in variable performance. The available discharge temperatures for internal melt and encapsulated ice systems depend mainly on discharge rate. Due to the insulating effect of water around tubes, internal melt ice storage tanks show a steadily falling discharge rate if a constant discharge temperature is maintained or a steadily rising temperature if a constant discharge rate is maintained. The close tube spacing needed for good discharge performance provides excellent ice making performance, because the thermal conductivity of ice is about 3.5 times greater that that of liquid water. The charge cycle begins with coolant temperatures of -3 °C entering storage and 0 °C leaving. As the ice making cycle advances an average supply temperature diminishes to approximately -4 °C. At the end of the ice making cycle the average supply temperature decreases at a much faster rate with a minimum at approximately -5 °C.

Encapsulated storage systems use a phase-change material, water or eutectic salts, contained in relatively small polymeric vessels. In case of eutectic salts, the temperature level at which phase change occurs is not limited to 0 °C as in case of pure water, it can be in the range of +27 °C down to -33 °C in dependence on the chosen PCM type (Cristopia, 2008). A large number of these plastic containers are immersed in a bath of secondary coolant. As for the case with internal melt ice-on-coil system charging (ice making) and discharging (ice melting) are accomplished by circulating the secondary heat transfer fluid. To charge the storage coolant at -3 to -6 °C is circulated through the tank causing the water to freeze inside the container. In discharge mode, if a constant discharge rate is maintained it has a steadily rising temperature, or if a constant temperature is desired it has a steadily falling discharge rate. These characteristics result from the decreasing area of ice in contact with the container walls as the ice melts. Limiting factor is a heat transfer characteristics of encapsulated ice container.

External melt ice-on-coil storage system builds ice on exterior surfaces of a heat exchanger coil submerged in a water tank. The system is charged by refrigerant of secondary coolant circulating through the coils, while the discharging is accomplished by circulating the water surrounding the heat exchanger where ice melts from outside in. The heat transfer fluid and phase-change material is water. Charging and discharging circuits are separated. Since the secondary coolant pipes are more distant than in the case of internal ice-on-coil system, charging temperatures of secondary coolant are lower in range of -4 to -9 °C. They depend on charging rate and the amount of ice on the pipes at a given time. Discharge tempera-

tures are in range of 1 to 2 °C up to 80 % of the ice in the tank melted. These temperatures are relatively stable during discharge mode with no or just minor influence of the discharge rate.

An ice harvesting system separates the formation of ice from its storage. Ice is built directly on the evaporator surfaces installed above the storage tank and is removed mechanically or by hot-gas defrost cycles. Sheets or flakes of ice are stored in a water tank below. The charging performance remains the same throughout the charge cycle independent of the amount of ice stored. Due to a high ratio of stored ice surface area to ice volume ice harvesting system can release stored cooling very quickly with discharging temperatures almost constant (in range of 1 to 2 °C) and with minor or no effect of the discharge rate on the discharge temperature.

In comparison to large ice flakes produced by harvesting type generators ice slurry is a mixture of liquid and small ice particles with sizes in the range of 0.1 to 1 mm. Beside the ability to store the energy ice slurry is very interesting as a secondary refrigerant from an energy transport point of view. In relation to static ice based systems ice slurry offer higher temperature stability, better heat transport capability, enhanced heat transfer, higher ice packing factor and therefore smaller storage size. Moreover, the temperature level of ice slurries is not limited to 0 °C if the basic fluid is a mixture of water and a freezing point depressant additive. Different methods are used to produce ice slurry. Each method has its particular advantages and weaknesses. The key problems which are hindering wider use of the ice slurry technology are basically related to production of ice slurry.

In Table 2.1 a summary of ice based storage technologies is given (Dorgan and Elleson, 1994).

Table 2.1 Summary of ice based storage technologies

Technology / Characteristics	Energy storage density [kWh/m³]	Charging temperature [°C]	Chiller charging efficiency, COP [-]	Discharging temperature [°C]	Discharge fluid	Strengths	Weakness
Internal melt ice-on-coil	40-50	-3 to -6	4.1 to 2.9	1 to 3	Secondary fluid	- ice inventory control - control of fully charge state - modular tanks, good for small or large installations	- discharge temperatures highly dependant on discharge rate and remaining ice - low heat transfer coefficient in charging and discharging
External melt ice-on-coil	40-50	-4 to -10	4.1 to 2.5	1 to 2	Water	- high instantaneous discharge rates - steady near zero discharge temperatures	- ice inventory control - control of fully charge state - efficiency penalty if all ice is not melted during discharge cycle
Encapsulated ice	40-50	-3 to -6 (for water)	4.1 to 2.9	1 to 3	Secondary fluid	- tank shape flexible - control of fully charge state - can be applied with both large and small loads - temperature level not limited to 0 °C	- low energy storage density - discharge temperatures highly dependant on discharge rate and state of the storage charge - low heat transfer coefficient in charging and discharging - subjected to supercooling
Ice harvester	30-50	-4 to -9	> 4 to 2.7	1 to 2	Water	- instantaneous response to short term cooling needs - high continuous discharge rates - steady near zero discharge temperatures - high refrigeration unit COP (not in case of defrost type ice harvester) - efficiency and charging performance of ice harvester not affected by state of the storage charge	- require overhead clearance above the storage tank - tank geometry affects the storage capacity and performance - high cost of ice harvesting equipment
Ice slurry	30-50	Dependant on fluid type	> 4 to < 2	Dependant on fluid type	Water or Secondary fluid	- high continuous discharge rates - steady discharge temperatures - temperature level not limited to 0 °C - energy transport ability - enhanced heat transfer	- expensive ice slurry production equipment - problems in operation (subjected to clogging) - system control

3 Static CTES systems – ice banks

Since the use of simple calculation methods in the process of ice bank performance evaluation offers neither adequate flexibility nor accuracy, the aim of this research was to provide a powerful tool for an industrial design of an ice storage system allowing to account for the various design parameters and system arrangements over a wide range of time varying operating conditions. In this chapter development of a computer application for the prediction of an ice bank system operation is presented. Static, indirect, cool thermal storage systems with external ice-on-coil building/melting were considered. The mathematical model was developed by means of energy and mass balance relations for each component of the system and is basically divided into two parts, the model of an ice storage system and the model of a refrigeration unit. Heat transfer processes in the ice silo were modelled by use of semi-empirical correlations while the performance of a refrigeration unit components were based on manufacturers data. Programming and application design were made in Fortran 95 language standard. Input of data is enabled through drop down menus and dialog boxes, while the results are presented via figures, diagrams and data (ASCII) files. In addition, to further demonstrate the necessity for development of a simulation program a case study was performed. Simulation results clearly indicate that no simple engineering methods or rule of thumb principles could be utilised in order to validate performance of an ice bank system properly.

3.1 Introduction

Dynamic, time-dependant operating conditions are rather common in process industry. Many plants adjust their operation to the time-varying input parameters. Dairies are very good examples of such time-varying conditions: typically once a day, in the morning, for a limited duration, a large quantity of incoming fresh milk must be quickly cooled. To cope with such a task, a large capacity refrigeration unit might be installed, but it would be idle for the most of the day, and would consume much (electrical) power when busy. Switching such a large unit on or off would

cause a great impact on the electrical distribution system, not to mention that electric companies usually charge high costs for such awkward loads. A much better solution is to build a smaller refrigeration unit that operates rather uniformly during the whole day (or when the electric energy is cheaper, i.e. during night) and accumulate its cooling effect in a convenient way that will make possible short bursts of greater cooling effect. Such an accumulator is usually called an "ice bank" (Dorgan and Elleson, 1994). During operation of the refrigeration unit, its cooling effect is used to freeze water so that ice is accumulated and melted when cooling is needed.

Ice banks can be designed as various shapes – rectangular basins, cylindrical reservoirs (silos) etc. filled with water. Submerged pipe coils containing a flow of refrigerating fluid are used to build ice on their outer surface. As a refrigerating fluid either a primary refrigerant (ammonia, HFC's etc.) or a secondary cooling fluid (brine cooled by a primary refrigerant elsewhere) can be used. The periods of ice building and melting can be either separated (first the refrigerating unit is switched on without warm water inlet, so that ice is built-up, later ice is melted by warm incoming water, while refrigerating unit is switched off), or these periods can be more or less overlapped.

In any case, due to the high process complexity and a large number of influencing parameters no standard engineering procedures or rules of thumb are adequate for design or rating the ice bank system performance. To be able to provide results with sufficient accuracy, a more complex computer tool is needed.

In the past, several attempts were made to build dynamic mathematical model of an ice bank systems. The most referenced static thermal storage systems which can be found in an open literature are those classified as direct, external ice-on-coil (Finer et al., 1993; Lopez and Lacarra, 1999) or indirect, internal ice-on-coil ice bank system (Chaichana et al., 2001). Finer et al. (1993) and Lopez and Lacarra (1999) developed simple mathematical models of a direct, ice-on-coil ice bank systems. Finer et al. (1993) came to the conclusion that for cases when heat release by the refrigeration user changes relatively slowly with time, heat transfer can be considered as the process limiting factor. This assumption allowed them to neglect hydrodynamic aspects of a refrigeration unit performance and to build the ice bank model solely by energy balance relations. This was proven experimentally as a good approach except for periods immediately after startup. For all of these publications one feature is common, all of the models are built for a specific case with limiting flexibility in definition of design and operating conditions.

18

In this project the objective was to develop a computer program for simulation of an ice bank system operation with the intention to offer a basis for industrial design of such systems over wide a range of time varying operating conditions. Static, indirect, cool thermal storage system with external ice-on-coil building/melting was considered.

The program was made as flexible as possible, allowing the user to define and change numerous parameters in design and operating conditions. This feature makes the application a strong optimization tool for particular system requirements.

The results presented in Part I of the current study focuses on the development of a mathematical model and computer application for the prediction of an ice bank system operation. In addition, identification of the problems encountered while designing such systems is presented through an actual case study.

In Part II validation of the mathematical model is discussed. The tested system was designed and constructed on the basis of the developed computer program after which it was installed as a part of a production line in the dairy factory "Antun Bohnec" in the city of Ludbreg, Croatia.

3.2 Ice bank model description

The considered ice bank system falls under the category of static, indirect cool thermal storages with external ice-on-coil building/melting where ice is built by circulating the brine solution cooled by refrigeration unit.

For the description of the ice bank operation, several limitations and assumptions were made. A vertical cylindrical shape (vertical silo) was assumed, consisting of one or more (stack up to ten) equal modules, Figure 3.1. The outer part of the silo (of annular cross-section) is used for the ice build-up or melting during upwards flow of water, the central part is used for the downward recirculation of water by means of the propeller (agitator).
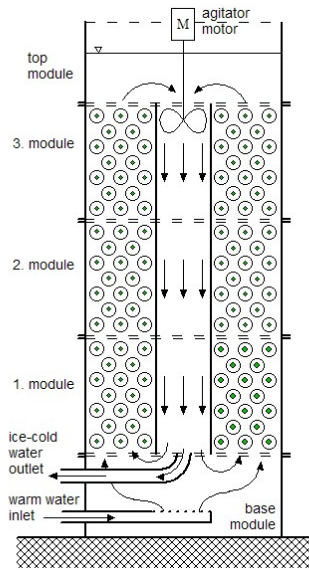
Figure 3.1 Vertical section of the ice bank silo

Within each module, in an outer annular part, pipes for the flow of refrigerant are spirally wound in a horizontal plane; each pipe has its own plane, the two vertically adjacent spirals form a staggered or in line arrangement for the upwards flow of water, Figure 3.2.
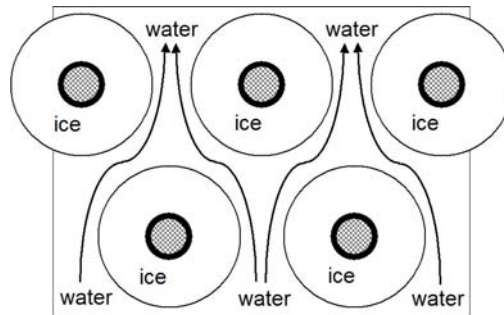
Figure 3.2 Staggered arrangement of the tubes in the silo

Only secondary cooling fluids (brines) are envisaged for the flow through pipes of the modules. The heated brine is then cooled in an ordinary refrigeration unit. On the secondary coolant (brine) side, modules are connected in parallel, so that a total flow of cold brine, coming from a refrigerating unit, is distributed amongst modules and later collected to be returned to the refrigerating unit, Figure 3.3.
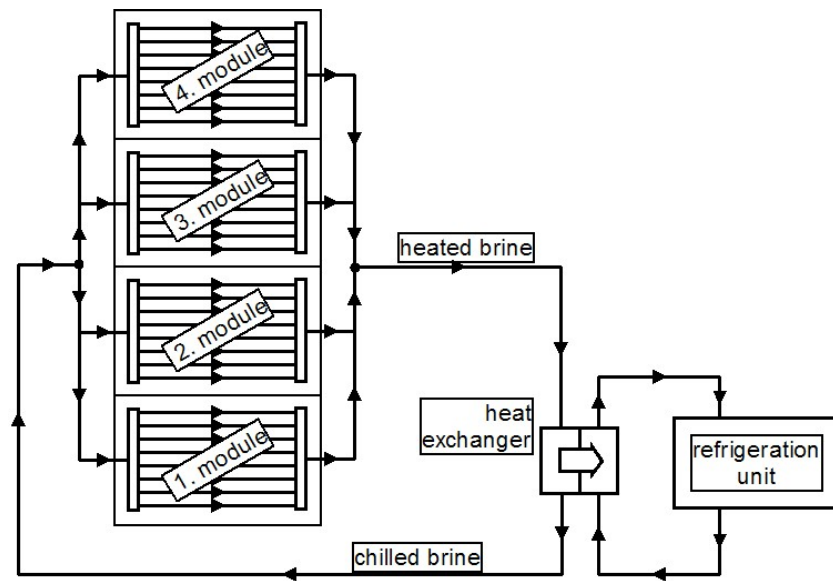
Figure 3.3 System layout of a four module silo ice bank

Within the above restrictions, the program was meant to be as flexible as can be, making it possible:

o to define any reasonable value of all the dimensions of the pipe, module, or a silo as a whole. The arbitrary choice of the number of pipes in a module, number of modules in a silo and, finally, a number of silos (up to five in parallel) is allowed;

o allow for various building materials for the hardware and various brines to be taken into account;

o allow for any mode of operation and arbitrary heat load on the water side of the process to be taken into account by taking water flow rate and its inlet temperature as input parameters. Any timing (automatic or manual) of switching on and off of the refrigeration unit is possible;

o to use a flexible description of the refrigeration unit, to allow various types of compressors, evaporators, condensers and the regulation of the unit to be taken into account;

o to assume that each module can be switched off separately when the ice thickness within it reaches some prescribed limit. The limit takes into account the average ice thickness along

the tubes as well as the maximum one (at the brine entrance region of the tubes).

3.3 Application description

The computer application is divided in two parts, the preprocessing part where all necessary input variables are defined and the calculation procedure where actual computation is taking place.

Mathematical models are integrated in form of a stand-alone program with a standard visual interface. Input of data is enabled through drop-down menus, while the results are presented via figures, diagrams and data files (ASCII). All programming was done in Fortran 95 language standard.

The preprocessing part includes definition of the ice bank system design (module/silo geometry, secondary coolant loop and refrigeration unit), system management and time schedule of a heat load. To be able to input access and change parameters with ease windows based application with graphical interface was built. The main application window is composed of five menu groups, named "Design and Dimensions", "Silo Management", "Refrigeration Unit", "Results" and "Calculation". Each of these menus contains several sublevels. The layout and brief description of drop down menus is as follows:

1. Design and Dimensions

   o *Pipeline Network*; dimensions of supply and return pipelines as well as number of fittings and bends between refrigeration unit and silos.

   o *Silo Design*; number of connected silos in parallel, number of modules per silo, water agitator characteristics, dimensions of brine distribution connections within silo.

   o *Module Geometry*; module design parameters; tube arrangement, tube bundle characteristics (tube dimensions, tubes length, transverse and longitudinal distance between adjacent tubes, number of tubes in bundle etc), main module dimensions, brine distribution method.

   o *Materials*; predefined tube materials and their related thermo-physical properties (conductivity) and surface condition (roughness),

22

2. Silo Management

- *Initial State*; state of the system variables at the beginning of the calculation process, such as initial brine and water temperatures at different locations in the system, initial ice thickness, water level in a silo, refrigeration unit intermittence,

- *Heat Load Histogram*; time schedule of warm water heat load,

- *Refrigeration Unit Intermittence*; operational time schedule of the refrigeration unit,

- *Silo System Control*; maximum ice thickness, manual or automatic module regulation; it displays time passed since the beginning of the calculation process; it enables any module to be shut off or turned on manually or automatically,

- *Brine Pump Characteristics*; pump characteristics and regulation (pressure head-mass flow rate, i.e. pump curve),

3. Refrigeration Unit

- *Refrigeration Unit Design*; components of refrigeration unit and related features, compressor, evaporator, condenser, expansion control device, working fluid,

- *Secondary Fluid*; choice of predefined secondary fluid (brine),

- *Refrigeration Unit Regulation*; refrigeration unit performance regulation; by defining either lowest temperature of brine at evaporator outlet or/and brine temperature drop on evaporator, or by setting temperatures at inlet and outlet of silos as constant, which in turn determines brine mass flow rate, i.e. brine pump must be selected in such a way to be able to deliver the required flow rate.

- *Evaluation/Estimation of Input Parameters*

4. Results and Print Out Options

- *Project Name*, enter or change the name of the project,

- *Print Out Management*, choice between various types of output formats, options to print out calculated results for each component, to set printout time interval, e.g. print out of water

23

and ice results, refrigeration unit performance and brine circuit variables in short or long format.

- o *Write All Input Parameters*, saves all parameters defined on input in a file for later use,

- o *Load All Input Parameters*, loads all parameters necessary to start calculation procedure from a previously saved file,

- o *Print Out Input Parameters,* prints out ice bank design parameters in formatted output with descriptions for engineers use,

5. Calculation

- o *Run*, starts the calculation procedure,

- o *Pause*, pause the calculation procedure,

- o *Stop*, terminates the calculation procedure,

- o *Continue*, continues the previously paused calculation procedure.

3.4 Modelling approach

The mathematical model of the ice bank system was developed by means of energy and mass balance relations for each component of the system and it is basically divided into two parts, the model of an ice storage system and the model of the refrigeration unit.

3.4.1 Ice storage mathematical formulation

During the operation of an ice bank, a very non-uniform distribution of temperatures of both water to be cooled and the cooling brine within the ice storage part of device takes place. Also the thickness of the ice varies from one tube to another and along each tube from the brine entrance to its exit. Such a process must be described by a set of differential equations.

Therefore, the whole volume is divided into smaller control volumes containing a section of the tube (of the area ΔA^{cv}) and the accompanying brine flow inside the tube ($\dot{m}_b^{cv}$) and water flow around the segment of the tube ($\dot{m}_w^{cv}$). The original differential equations are written below in the form of finite difference equations.

The governing equations that describe the operation of the ice bank system are written separately for the two cases:

- o if there is no ice around the tube section, it acts as an ordinary recuperative heat exchanger with known (predictable) convective heat transfer coefficients on the brine and water side and the known thermal conductivity of the tube wall; the heat flow exchanged between water and brine rises the brine temperature and lowers the water temperature;

- o if there is a layer of ice around the tube, the temperature of the ice layer outer surface (in contact with water) is known and fixed at 0 °C. This interface surface receives the heat flow by convection from warm water around it and gives away the heat flow through the ice layer and tube wall to the cold brine inside the tube; If more heat flow is received from water than given away, ice on the outer surface is melted, otherwise the water particles in contact with outer surface are frozen and ice is accumulated. In any case, water is cooled by the released heat flow and brine is heated by the received heat flow;

3.4.1.1 First case – no ice around the tubes

A mass balance of water (for each control volume, water outlet mass flow rate equals water inlet mass flow rate):

$$\dot{m}_{w,out}^{cv} = \dot{m}_{w,in}^{cv} \tag{3.1.}$$

An energy balance of water; for each calculation time step and for every segment in a silo, the change in water temperature is calculated by the relation:

$$c_{pw}\, \dot{m}_w^{cv}\, \Delta \vartheta_w = -k_2\, \Delta A_2^{cv} \left(\vartheta_w - \vartheta_b \right) \tag{3.2}$$

where ϑ_w and ϑ_b are the (average) values of water and brine temperature within the particular control volume, and

$$\frac{1}{k_2} = \frac{r_2}{r_1 \alpha_1} + \frac{r_2}{\lambda_t} \ln\left(\frac{r_2}{r_1} \right) + \frac{1}{\alpha_2} \tag{3.3}$$

and

$$\Delta A_2^{cv} = 2\, r_2\, \pi\, \Delta L^{cv} \tag{3.4}$$

are the overall heat transfer resistance (reduced to the tube outer surface) and an area of the segment of the tube outer surface contained within the control volume, respectively.

In the same manner, the temperature change of the secondary fluid (brine) is given by

$$c_{pb}\,\dot{m}_b^{cv}\,\Delta\vartheta_b = k_2\,\Delta A_2^{cv}\left(\vartheta_w - \vartheta_b\right) \qquad\qquad 3.5.$$

These are the finite difference equations governing the operation of an ordinary recuperative heat exchanger of somewhat peculiar flow arrangement (here similar to a cross flow type), but they do not represent the typical operation mode of an ice bank system, because there is no ice layer around the tubes!

3.4.1.2 Second case – a layer of ice around the tubes (Emblik, 1951)

A mass balance of water (for each control volume, water outlet mass flow rate equals water inlet mass flow rate minus the time-increase of the mass of ice around the tube in the particular control volume):

$$\frac{\Delta m_i^{cv}}{\Delta t} \cong \dot{m}_{w,in}^{cv} - \dot{m}_{w,out}^{cv} \qquad\qquad 3.6.$$

When water just in the vicinity of outer tube surface reaches the solidification point, it starts to deposit ice on tube bundles. Now, the heat is transferred from bulk water to water/ice interface at temperature of 0 °C, Figure 3.4.

Again the energy relations for water and brine are set, this time at the water-ice interface

$$c_{pw}\,\dot{m}_w^{cv}\,\Delta\vartheta_w = \alpha_i\,\Delta A_i^{cv}\left(\vartheta_w - 0\right) \qquad\qquad 3.7$$

$$c_{pb}\,\dot{m}_b^{cv}\,\Delta\vartheta_b = k_i\,A_i^{cv}\left(0 - \vartheta_b\right) \qquad\qquad 3.8$$

where heat transfer resistance $1/k_i$ consists of one convection term on the fluid side, and two heat conduction terms, of the tube wall and the ice layer:

$$\frac{1}{k_i} = \frac{r_i}{r_1\alpha_1} + \frac{r_i}{\lambda_t}\ln\left(\frac{r_2}{r_1}\right) + \frac{r_i}{\lambda_i}\ln\left(\frac{r_i}{r_2}\right) \qquad\qquad 3.9.$$

26
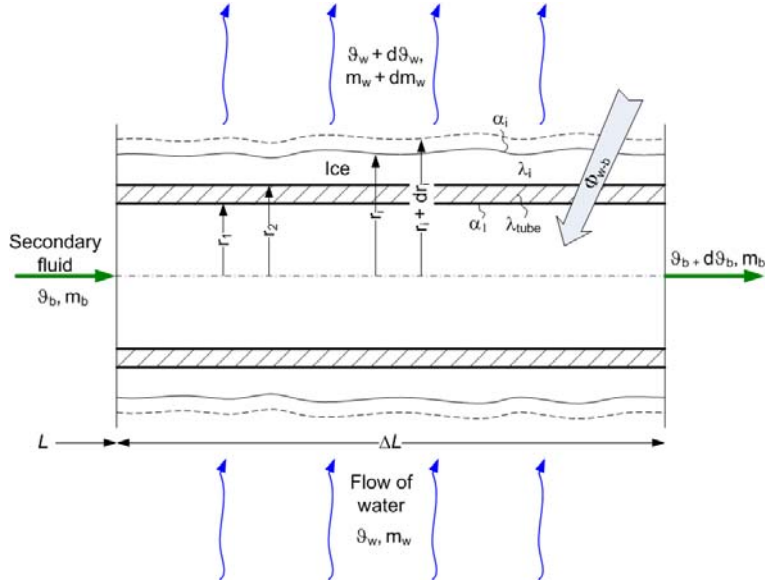
Figure 3.4 The control volume associated with the tube segment

The surface area of ice is calculated by

$$A_i^{cv} = 2\, r_i^{cv} \pi\, \Delta L^{cv} \qquad\qquad 3.10.$$

The mass rate of ice formation/melting around a tube segment is given by the relation

$$\frac{\Delta m_i^{cv}}{\Delta t} = \frac{k_i\, A_i^{cv}\left(0 - \vartheta_b\right) - \alpha_i\, A_i^{cv}\left(\vartheta_w - 0\right)}{c_{pw}\, \vartheta_w + \Delta h_{sl} - 0.5\, c_{pi}\, \vartheta_b} \qquad\qquad 3.11.$$

Equation 3.11 is derived from an energy balance at ice-water interface. The first term in the numerator at the right hand side of the equation presents heat transferred from an ice-water interface to bulk brine while the second term presents heat transferred from bulk water to ice-water interface.

The denominator on the right-hand side of Equation 3.11 represents the release of heat at the ice surface during water solidification. It consists of the sensible part of water cooling from bulk to ice interface temperature ($c_{pw}\, \vartheta_w$), the latent heat of freezing (Δh_{sl}) and the sensible term which accounts for cooling of ice below freezing temperature. The last term ($-0.5\, c_{pi}\, \vartheta_b$) assumes that ice layer will cool to temperature halfway between 0 °C and of the brine temperature. As it can be seen it is just an

approximation of the energy needed to subcool the ice layer. It is based on the assumption that the mean ice temperature is approximately the arithmetic mean between 0 °C and the brine temperature, and that approximately half the ice mass is below the mean temperature and the other half is above it. It is adopted primarily in order to avoid calculation of the non-steady-state temperature field in the ice layer of a particular element and finally to save computational time. The error induced by adopting such an approximation where cooling of all the ice mass to the same mean temperature, or cooling every ice particle to its real temperature is considered small at least in comparison to the latent heat of freezing.

By assuming cylindrical shape of ice, the radius of the ice formed around tube is given by

$$r_i = \left(\frac{m_i^{cv}}{\pi \, \rho_i \, \Delta L^{cv}} + r_2^{\,2} \right)^{0.5} \qquad\qquad 3.12.$$

The radial growth rate of ice formation is expressed by

$$\frac{\Delta r_i}{\Delta t} \cong \frac{k_i \, A_i^{cv} \left(0 - \vartheta_b \right) - \alpha_i \, A_i^{cv} \left(\vartheta_w - 0 \right)}{2 \, r_i \, \pi \, \rho_i \, \Delta L^{cv} \left(c_{pw} \, \vartheta_w + \Delta h_{sl} - 0.5 \, c_{pi} \, \vartheta_b \right)} \qquad\qquad 3.13.$$

The transition criterion between modes of calculation for pure water cooling and solidification is for the relation on the right hand side of eq. 3.13 in the numerator to be positive

$$k_i \, A_i \left(0 - \vartheta_b \right) - \alpha_i \, A_i \left(\vartheta_w - 0 \right) > 0 \qquad\qquad 3.14$$

and ice thickness in previous calculation step to be equal to 0

$$\delta_i = 0 \qquad\qquad 3.15$$

with k_i and A_i set equal to k_2 and A_2.

The convective water side heat transfer coefficients are calculated according to the proposed correlation for tube bundles by Zhukauskas (Incropera et al., 2006) while brine heat transfer coefficient inside tubes are calculated in dependence on flow regime for helically wound tubes (Inženjerski priručnik, 1996).

28

The brine mass flow rate inside the tube ($\dot{m}_b^{cv}$) passing through a particular control volume is obtained by the distribution of the total brine mass flow rate over all the tubes according to the pressure drop within each tube. Brine total mass flow rate $\dot{m}_b$ depends on the circulation pump characteristics with associated control and flow resistance of the brine circuit. It is determined by using iterative loop procedure in which the pressure drop of components in the coolant circuit is calculated and then brought to balance with the available head pressure. To find the temperature of the brine at the inlet of ice bank silo, a coupling with the refrigeration unit is necessary. Interaction between the brine circuit and the refrigeration loop is closed on evaporator/heat exchanger.

In the base module, recirculation cold water is mixed with incoming warm water from the consumer. The resulting water temperature, just before entering the first tube stack, is determined according to the first law of thermodynamics for the two streams (mixing rule). On the other hand, a heat load imposed on the ice silo by warm water inflow depends on the consumer's particular need. It is usually provided in form of chart data diagram, which displays time dependence of either heat flow rate or volume flow rate and water inlet temperatures.

Water mass flow rate around a tube segment $\dot{m}_w^{cv}$ is obtained by distributing the total water flow rate $\dot{m}_w$ (it depends on the agitator performance) over all the control volumes along one whole spirally wound tube. Temperature of the cold water at the exit from the last module is calculated as the average value over all control volumes along the last tube.

Within the program, equations from 3.1 to 3.15 (written for every control volume) along with procedures for determination of pressure drop balance in coolant circuit, refrigeration unit performance, consumers heat load and water temperatures in a base and top module are solved for each calculation time step.

3.4.2 Refrigeration unit mathematical formulation
Modelling the refrigeration unit included building models of compressor, condenser, and evaporator with flow control device.

All components were modelled according to the manufacturers' data. Various compressors, evaporators, condensers and refrigerants are considered as well as several types of control, i.e. compressor speed control, on/off and temperature control.

29

The compressor behaviour was modelled through a set of algebraic functions, obtained by curve fitting method from manufacturers data, describing compressor mass flow rate, effective power and cooling oil heat load in dependence on evaporation and condensation temperature, compressor speed, refrigerant type and way of compressor cooling/lubricating with oil (thermosiphon, injection or water cooling type).

$$\dot{m}_{RT} = \dot{m}_{RT}\left(\vartheta_{e}, \vartheta_{c}, n, RT, OCT\right) \qquad\qquad 3.16$$

$$P_{comp} = P_{comp}\left(\vartheta_{e}, \vartheta_{c}, n, RT, OCT\right) \qquad\qquad 3.17$$

$$\Phi_{ol} = \Phi_{ol}\left(\vartheta_{e}, \vartheta_{c}, n, RT, OCT\right) \qquad\qquad 3.18$$

The refrigerant thermophysical properties were obtained from standard reference database REFPROP v6.0 (1998) which subroutines were compiled and linked with the main program.

The condenser and evaporator were modelled by energy and mass balances around them. The overall heat transfer coefficient and heat exchanger area were obtained from manufacturers data for plate type heat exchangers.

In addition, correlations for single phase pressure drop on the secondary loop side were obtained by curve fitting method again from manufacturers' data. With respect to the heat exchanger model, type of plates and flow regime, dependence between Fanning friction factor and Reynolds number is found for each evaporator and expressed as

$$c_f = aRe^b \qquad\qquad 3.19$$

3.4.3 Computational procedure layout

A simplified program flow diagram of calculation procedure (without preprocessing) is shown in Figure 3.5.

The program begins with initialization, under which all system variables are set to their predefined initial values. The calculation is continued by increasing computational time for a given interval and by calculating the time dependant input variables; for a given time it checks if the refrigeration unit is operational and calculates the mass flow rate and temperature of warm water at silos inlet. It proceeds with evaluation of silos performance. In the first part of the procedure, the brine circuit is hydraulically balanced. Calculation is carried out in an iterative loop until coolant circuit pressure drop is in balance with available pump head pressure. Un-

der this loop the program performs calculations of all relevant variables in the silo, but does not change the ice thickness from the previous step. Once the brine flow is hydraulically balanced, the whole step is repeated, now taking into account the change of the ice layer thickness.
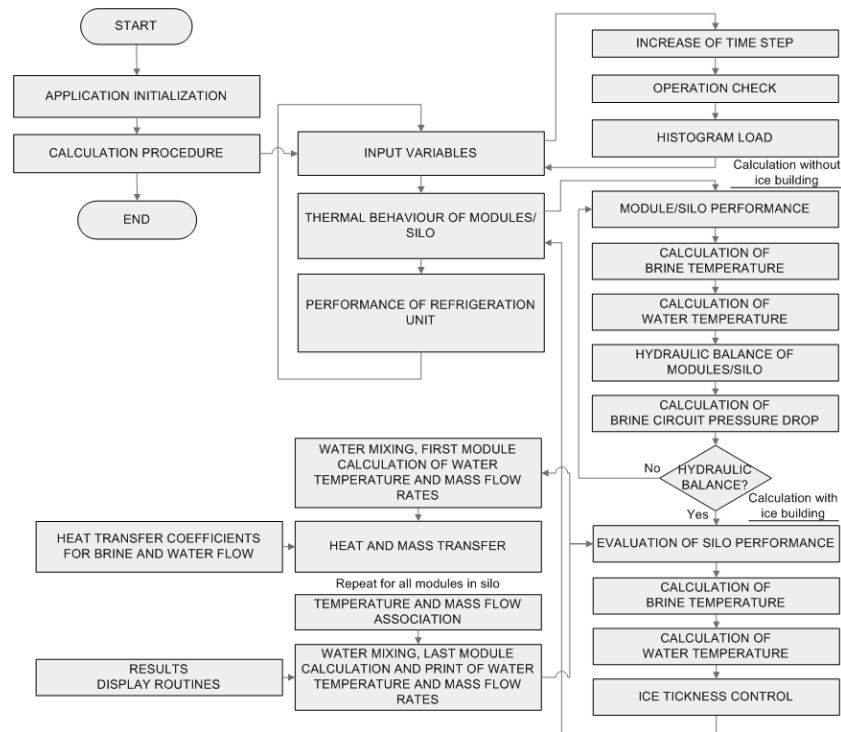
Figure 3.5 Flow diagram of calculation procedure

After new ice thickness is calculated for each tube segment, program control is directed to evaluation of refrigeration unit necessary performance. Upon calculation of the evaporation and condensation temperature, compressor refrigeration capacity and power, as well as the brine temperature drop in evaporator, program control is returned to the beginning of the main program loop where calculation procedure is repeated for the next time step.

3.5 Results

To demonstrate the importance and necessity for development of a simulation program for prediction of an ice bank system operation a case study was performed. On the basis of a specific user supplied data for a design day, acquired as an actual case, the task was to offer an ice bank system which would meet (satisfy) requirements set by a user. The emphasis was on the determination of adequate ice silo size (number of

modules), arrangement and operating conditions. As an input parameter the existing module design and its related geometry was used. The ice bank design procedure started by implementation of standard engineering methods while the verification of the first step solution and the subsequent optimization was done with the developed software.

User supplied data are specified through the storage system load, supply water temperature to the load and return water temperature from load according to ARI Guideline T (2002). In addition to the high peak cooling load during on-peak period to be covered, the user demands that water temperature leaving the ice bank is always lower than 0.5 °C. Temperature of return water to ice bank is set to constant value of 8.0 °C.

First step in design process of a cool storage system is to make decision on operating and control strategies. This choice highly depends on the shape of the system load curve. Out of the load schedule curve displayed in Figure 3.6, one can observe a cooling peak load of 1933 kW at 10 a.m. which is several times higher than the average load of roughly 500 kW.
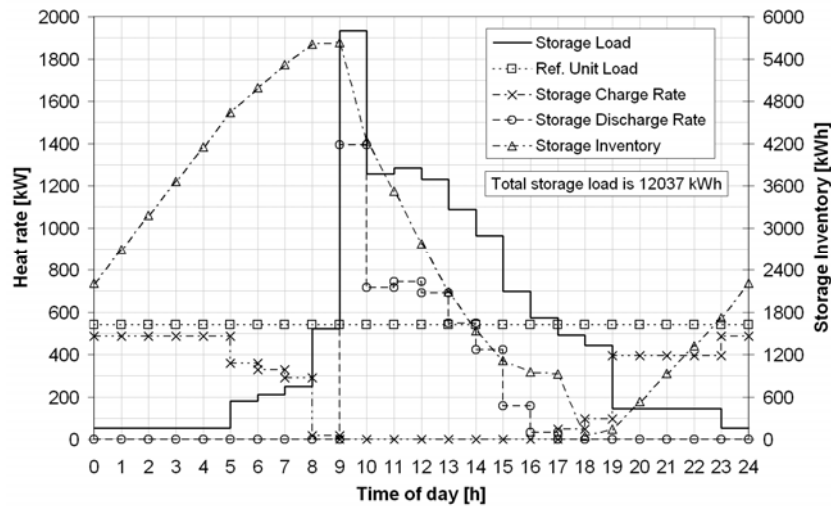
Figure 3.6 User specified data for a design day and initial storage system sizing results

Due to the high ratio of peak to average load the choice for operating and control strategy falls on partial storage (load levelling system) and daily charging cycles. Such arrangement of a cool thermal storage system should yield minimal required refrigeration and storage capacity (Dorgan and Elleson, 1994).

The total cooling load required by a user is 12037 kWh with water temperature available from the storage less or equal to 0.5 °C. Estimates of a

chiller size and storage capacity are calculated based on the total system load, number of hours in charging and discharging mode and chiller performance. Results are presented in Figure 3.6.

It is assumed that the refrigeration unit is running at full capacity of 540 kW for the entire day. When the load is less than the chiller output, from 0 a.m. to 9 a.m. and from 5 p.m. to 12 p.m. of a design day, excess cooling is stored. When the load exceeds the chiller capacity (period from 9 a.m. to 5 p.m.) the additional cooling load is discharged from storage.

As it can be seen from the net storage curve (Figure 3.6), 5631 kWh is stored into the ice bank silo and 4708 kWh is discharged from it during the day, while 923 kWh remains in storage at 5 p.m. According to the manufacturers data the total nominal capacity of one module with ice thickness of 30 mm is 940 kWh. Hence, to cover the daily system load one silo with six modules stacked one on top of the other seems to be sufficient.

To calculate and display charging and discharging characteristics of the ice storage, the computer program developed for this purpose was used. In total, fourteen cases were considered. The parameters that were held constant during the calculation are summarized in Table 3.1. The operating conditions of the ice bank system being examined is given in Table 3.2.

In the first five cases only the number of modules for one-silo storage system was varied. The lowest brine temperature at evaporator outlet was set to -6 °C and held constant during the calculation, as well as the brine temperature drop of 3 °C. For the cases six to nine, the brine temperature drop through the evaporator was lowered to 2 °C.

Table 3.1 Design parameters

Menu group	Submenu	Parameter	Value
Design and Dimensions	Pipeline network		
	Silo design	water agitator characteristics	1500 m3/h
	Module geometry		
	Materials	thermo-physical properties	PPE
Silo Management	Initial state	brine temperature	-6 °C
		water temperature	0 °C
		ice thickness	30 mm
	Heat load schedule		as indicated in Figure 3.6
	Refrigeration unit operation	time schedule	0 to 24 h
	Silo system control	maximum ice thickness	30 mm
		ice thickness hysteresis	0.5 mm
		module regulation	automatic
	Brine pump characteristics	regulation	frequency controlled
Refrigeration Unit	Refrigeration unit regulation	target refrigeration capacity	540 kW

Table 3.2 Operating conditions for case 1-14

	Variable				
	No. of silos in parallel	Number of modules	Available system pressure drop [bar]	Minimal brine temperature at evaporator outlet [°C]	Brine temperature drop on evaporator [°C]
Case no.	Value				
1	1	6	2.25	-6	3
2	1	7	2.25	-6	3
3	1	8	2.25	-6	3
4	1	9	2.25	-6	3
5	1	10	2.25	-6	3
6	1	6	5.0	-6	2
7	1	7	5.0	-6	2
8	1	8	5.0	-6	2
9	1	9	5.0	-6	2
10	2	4	2.15	-6	3
11	1	7	2.25	-9	3
12	1	8	2.25	-9	3
13	1	7	9.0	-6	1.5
14	1	8	9.0	-6	1.5

While in case ten, two parallel four-module silo system was examined, in cases eleven and twelve again the number of modules for one-silo system was varied but with minimum brine temperature on evaporator outlet as -9 °C. In the last two cases, a one-silo arrangement with seven and eight modules and the brine temperature drop of only 1.5 °C was considered. In all cases the maximum refrigeration unit capacity was targeted to be 540 kW.

Calculation was conducted with a time increment of 1 minute up to five days depending on case. Summary of results is presented in Table 3.3.

Table 3.3 Simulation results

Case no.	Day of Simulation	Ref. Equipment Load [kWh]	Storage Charging [kWh]	Storage Discharging [kWh]	Min. Net Storage Inventory [kWh]	Max. Net Storage Inventory [kWh]	Max. Water Supply Temp. to Load [°C]	Max. Fluid Temp. Entering Storage [°C]	Max. Fluid Temp. Leaving Storage [°C]	Max. Brine Pumping Load [kW]	Brine Pumping Power [kWh]
1	3	10820,7	4281,5	4249,5	0,0	4200,0	4,0	-0,3	2,7	10,6	239,2
2	3	11432,7	4790,9	4773,4	0,0	4710,0	3,1	-1,0	2,0	10,7	244,8
3	4	11541,0	4824,2	4928,6	4,0	4883,0	1,3	-2,4	0,6	10,7	245,8
4	3	10866,7	4249,6	4926,8	2,0	4882,0	1,6	-2,0	1,0	10,6	237,0
5	3	10447,1	3899,5	5170,4	266,0	5396,0	0,8	-2,7	0,3	10,4	230,2
6	3	11048,8	4458,0	4438,3	0,0	4379,0	3,6	-0,1	1,9	35,4	798,9
7	3	11717,0	4935,0	4924,4	0,0	4887,0	1,5	-1,8	0,2	35,6	823,2
8	3	11850,6	4989,3	5002,5	147,0	5120,0	0,6	-2,5	-0,5	35,8	830,7
9	3	11068,2	4371,2	5122,4	163,0	5257,0	0,7	-2,1	-0,1	36,0	805,7
10	4	11784,8	4938,6	5022,8	128,0	5126,0	0,5	-3,5	-0,5	10,4	241,1
11	3	11469,4	4728,6	4737,3	0,0	4650,0	2,6	-1,4	1,6	10,7	237,2
12	4	11559,9	4784,0	4904,1	10,0	4832,0	1,2	-2,5	0,5	10,7	237,5
13	4	11728,5	4894,7	5002,1	28,0	4996,0	0,7	-2,3	-0,8	86,5	1992,3
14	5	11727,7	4879,6	5049,4	181,0	5198,0	0,5	-2,3	-0,8	87,0	1995,8

3.6 Discussion

In the first case, the dynamic behaviour of a one six module silo was examined, since this came as a result of an initial calculation procedure. Results are showed in Figure 3.7 for the third day of simulation.
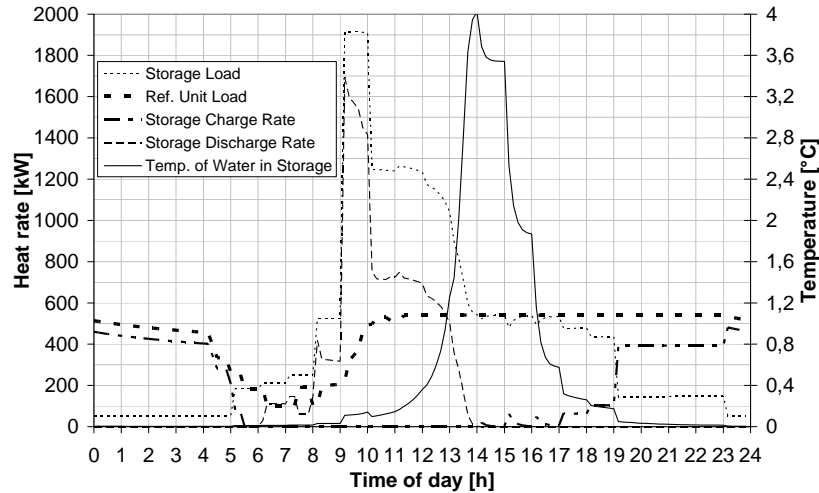
Figure 3.7 Dynamic behaviour of one silo with six modules, case 1, day 3

Figure 3.7 shows that the available cooling capacity of one silo with six modules is not sufficient, i.e. the system is not capable to store enough energy to compensate for the system load during one day. 12037 kWh in total is required and only 10820.7 kWh is provided by the refrigeration unit. During the day 4281.5 kWh of energy is stored and 4249.5 kWh is discharged from the silo. Lack of capacity reflects on temperature of water leaving the silo, which exceeds the imposed limit of 0.5 °C and rises up to 4 °C at 2 p.m. At 1.30 p.m. one can notice that there is no ice present in the silo, see Figure 3.8. At that time silo is used purely as a recuperative heat exchanger.

In the next case, case 2, one module is added to the silo and studied as in the previous example. Even though the total nominal capacity of the silo (with 30 mm of ice thickness) is now increased to 6580 kWh, with this new arrangement the situation is not proportionally changed for better. Still the silo capacity is insufficient and temperature of water leaving silo is too high (3.1 °C on "day 3").

With eight modules in the silo, case 3, the system behaviour is slightly improved. Figure 3.9 shows "day 3" scenario where total silo capacity is high enough and on a critical hour some ice still exists on tube coils. Yet

the supply water to the load reaches the highest temperature of almost 0.8 °C for day three what is higher than required.
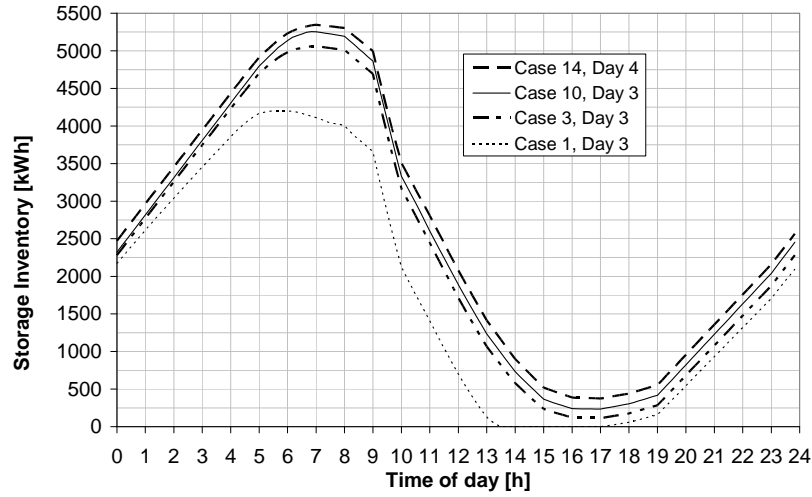
Figure 3.8 Accumulated ice capacity in the ice bank system

Having continued calculation on "day 4" an interesting feature might be observed. The maximum stored capacity that day is less (4883 kWh) than for the day before (5061 kWh) and water temperature has increased considerably (from ~0.8 °C on "day 3" to 1.3 °C on "day 4"). The reason for this occurrence is that the ice remaining at the end of the discharging cycle is not evenly distributed on coils through the silo. The remaining ice is primarily located in the last (top) module, most of it at the brine entrance end of the tube. Due to the fact that the brine temperature is lowest at the tube entry, ice is thicker at that location than at the brine exit tube end. Therefore, when charging cycle begins again (at 5.00 p.m. chiller cooling capacity exceeds the load), the maximum ice thickness in the last, uppermost module is now easily reached. Consequently, automatic regulation due to safety reasons switches off this module leaving it without full capacity.

In the following cases, 4 and 5, extra modules were added. While the capacity and temperature fluctuations for the case 4 between simulation days were more emphasized (maximum temperature reached on a "day 5" in hour 3 p.m. was 1.8 °C and 0.5 °C on "day 4" in hour 3 p.m.) than in the previous example, case 5 with ten modules showed more stable operation with respect to temperature and capacity, yet with highly non-symmetric behaviour between first and last module. The highest temperature of 0.8 °C for case 5 occurred on day three.

36
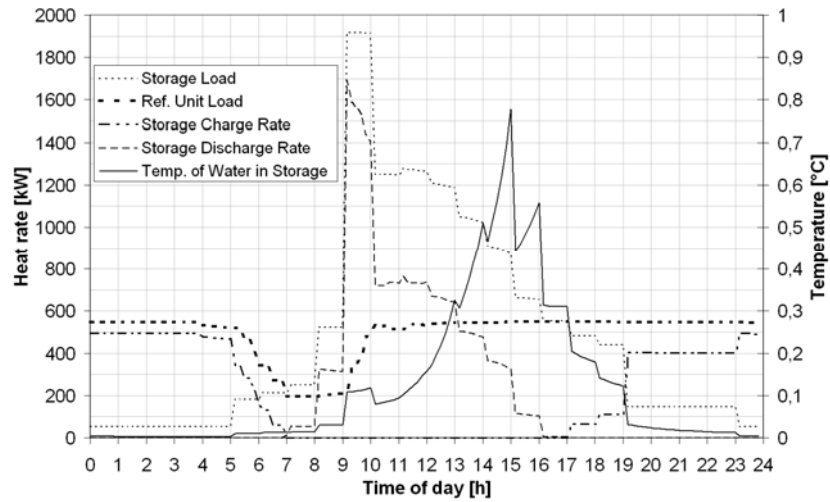
Figure 3.9 Dynamic behaviour of one eight module silo, case 3, day 3

Since all examined cases up to now provided unsatisfying results, a different approach had to be taken. The reason why adding extra modules in the first five cases provided no result is twofold: too high brine temperature rise through the silo in conjunction with the lack of symmetry when observing the behaviour of first to last module. A brine temperature rise of 3 °C results in the conical ice shape along the tube and the loss in capacity in relation to nominal. Thus, the next four cases, from 6 to 9, were performed with brine temperature rise of 2 °C again with a target refrigeration capacity of 540 kW.

In case 6 and case 7, again the silo capacity was insufficient and the water temperature was too high. The situation was improved for case 8, where the highest outlet water temperature reached 0.6 °C. In this case the system showed stable operation for simulation days three to five with minimum deviation in operating variables.

Case 9, as in previous cases 4 and 5, showed high instability and asymmetry without gaining in desired result.

To solve the silo operation instability, a case with two parallel four module silos was considered as case 10. Brine temperature rise across the silo was set to 3 °C with the lowest possible temperature of -6 °C. The maximum chiller capacity target was 540 kW. As showed in Figure 3.10 the desired results were reached, the capacity was sufficient and the water temperature was below prescribed limit of 0.5 °C for all five simulation days.
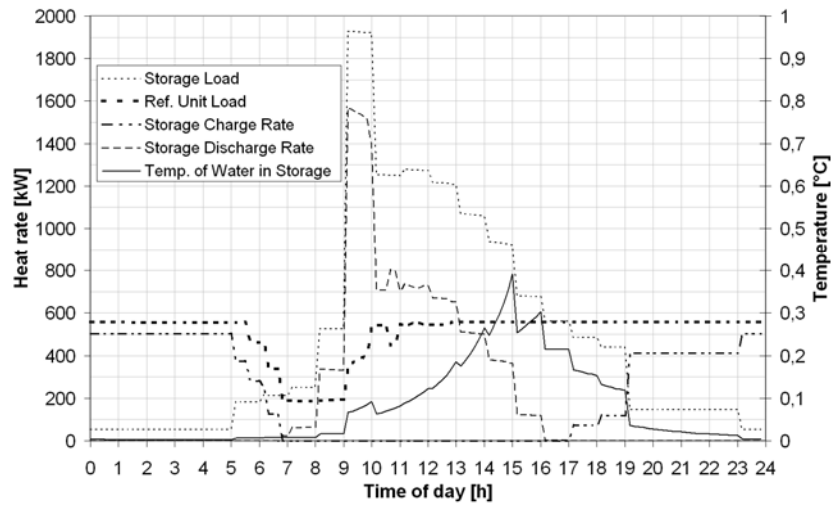
Figure 3.10 Dynamic behaviour of two parallel four module silos, case 10, day 3

For cases 11 and 12, a single silo with seven and eight modules and lowest possible brine temperature of -9 °C was envisaged. In both cases target result was not reached.

In the last two examples, case 13 and 14, to override the problem of nonuniform ice thickness, temperature rise across silo was reduced to 1.5 °C. Both cases showed adequate silo capacity and stability in operation. Yet for case 13 on the fourth day of simulation maximum water temperature was found to be 0.7 °C. In case 14, the capacity, the system stability as well as the water temperature at storage outlet were found to be satisfactory. Figure 3.11 shows system performance for case 14 on day four.

While a lower brine temperature rise across the silo improved the storage charge and discharge characteristics, higher operating capacity and better overall system behaviour, it heavily reflected on the required pumping power. In case 10, for two parallel four-module silo system, maximum brine pumping power was only 10.4 kW with 241 kWh of energy consumed during day, while in the latest case 14, for one eight-module silo, maximum pumping load was increased to 87 kW with nearly ten times more energy consumed, 1996 kWh.
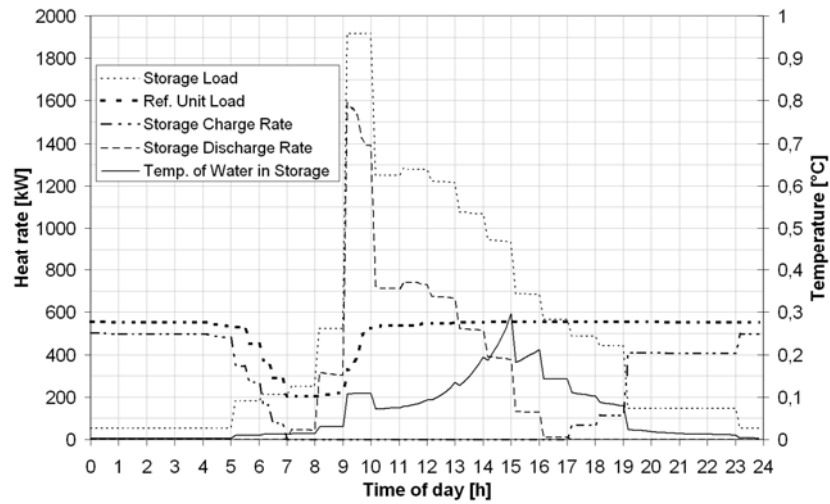
Figure 3.11 Dynamic behaviour of one eight module silos, case 14, day 4

3.7 Conclusion

Due to the high process complexity and nonuniformity throughout the ice bank system (situation can drastically differ between pipe segments, pipes and modules in a same silo) it is impossible to find rather simple, fast, yet sufficiently accurate method to describe the performance of such systems over time. A complex computer model is thus needed.

Simulation results clearly show that in order to propose adequate ice bank system design, no simple engineering methods or rule-of-thumb principles could be utilised. As indicated, results of an initial sizing procedure are far from the "real" behaviour of an ice bank system. While a quick storage size estimate suggested use of one six-module silo as sufficient, simulation results showed that only two ice bank system arrangements offer satisfactory operation behaviour, i.e. the case 10, two parallel four module silos and the case 14, single eight module silo with temperature rise across silo of 1.5 °C.

4 Static CTES system – ice bank – verification

In order to verify the mathematical model of an ice bank system developed for the purpose of predicting the system performance, experimental measurements on the ice bank thermal storage system were performed. Static, indirect, cool thermal storage system, with an external ice-on-coil building/melting was considered. The tested system was installed as a part of a production line in the dairy "Antun Bohnec" in the city of Ludbreg, Croatia. Cooling energy stored in a form of ice during night is used for rapid cooling of milk after the process of pasteurization during day time.

The ice bank system was tested under real operating conditions to determine parameters such as time varying heat load imposed by a consumer, refrigeration unit load, storage capacity, supply water temperature to the load and to find storage charging and discharging characteristics, i.e. ice building and melting rate. Experimentally obtained results were then compared to the computed ones. It was found that calculated and experimentally obtained results are in a good agreement as long as there is ice present in the silo.

4.1 Introduction

In the past several attempts were made to build and test dynamic mathematical models of an ice bank system. The most referenced static thermal storage systems which can be found in an open literature are those classified as direct, external ice-on-coil (Finer et al., 1993; Lopez and Lacarra, 1999; Lee and Jones, 1996) or internal ice-on-coil ice bank system (Chaichana et al., 2001). Finer et al. (1993) and Lopez and Lacarra (1999) developed simple mathematical models of a direct, ice-on-coil ice bank systems. Finer et al. (1993) came to the conclusion that for cases when heat release by the user changes relatively slowly with time, heat transfer can be considered as the process limiting factor. This assumption allowed them to neglect hydrodynamic aspects of a refrigeration unit performance and to build the ice bank model solely by energy balance re-

lations. This was proven experimentally as correct except for period immediately after start-up. Likewise, Lee and Jones (1996a) developed analytical models for an indirect, ice-on-coil thermal energy storage system for both charging and discharging modes. As such, the models were simplified to a large extent. Nevertheless, error analysis indicated that the model predictions were within 5 and 12 % of the experimental values. Moreover, they (Lee and Jones, 1996b) conducted laboratory testing's of a direct, ice-on-coil thermal energy storage system for air-conditioning applications and offered a basis for performance rating procedures for the residential and light commercial CTES systems.

For all of these publications one feature is common, all of the models were built for specific case with limited flexibility in definition of design parameters and operating conditions. In order to allow the definition of numerous design parameters and operating conditions and still provide results with sufficient accuracy, a more complex computer model of a static, indirect, cool thermal storage system with external ice-on-coil building/melting was developed (Halasz et al. 2009).

In the first part of this study the performance testing of an indirect ice-on-coil ice bank system is outlined, while in the second part a validation of the developed mathematical model is discussed.

4.2 Experimental details

4.2.1 Experimental apparatus and instrumentation

Ice bank system under consideration, designed and manufactured by company Frigoterm, was installed in a dairy "Antun Bohnec" in the city of Ludbreg, Republic of Croatia, as a part of a production line. It is a static, indirect cool thermal storage with external ice-on-coil building/melting, where ice is built around the tubes by the brine solution which is cooled by the refrigeration unit circulating through the tubes. Ice bank system consists of the refrigeration unit cycle, storage unit, i.e. ice silo and consumer cycle, Figure 4.1.

Storage unit is a vertical cylindrical silo built as a stack of two equal modules. The outer part of the silo (of annular cross-section) is used for the ice build-up or melting during upwards flow of water, the central part is used for the downward recirculation of water by means of the propeller (agitator). The agitator (nominal capacity 300 m³/h) was in operation only in a discharge mode while during the charging time it was idle.

Within each module, in an outer annular part, pipes for the flow of brine are spirally wound in a horizontal plane. Each pipe has its own plane.

The two vertically adjacent spirals form a staggered arrangement for the upwards flow of water. Submerged pipe coils containing a flow of secondary fluid are used to build ice on their outer surface. Pipes are made of polypropylene.
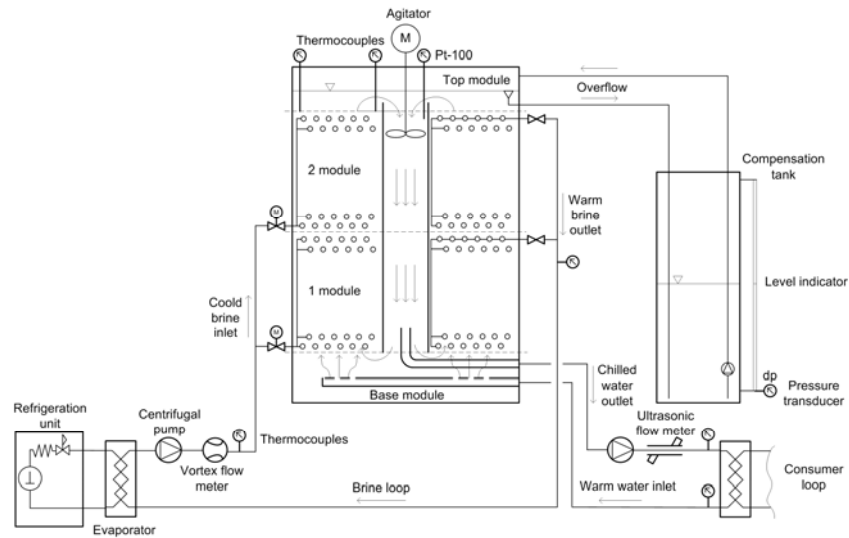
Figure 4.1 Ice bank system

On the secondary coolant side, modules are connected in parallel, so that a total flow of cold brine coming from the refrigerating unit is distributed amongst modules and later collected to be returned to the refrigerating unit. Secondary fluid (brine), 30 % mixture of ethylene glycol and water was used.

In the consumers loop, chilled water is circulated from the ice silo to a plate heat exchanger in production line to provide milk cooling. Heated return water from the consumer is returned to the base module of the silo to be mixed with chilled silo recirculation water.

Process variables, i.e. temperatures, flow rates and pressures are measured at several locations in the system, as indicated in Figure 4.1. In the secondary fluid loop, two temperatures and one flow rate have been measured, i.e. brine temperatures at the silo inlet and outlet and the total brine flow rate through the silo. Four thermocouples were used for this purpose. Two of them were bonded on an outer pipe wall (steel pipe with dimensions O.D. 89.7 x 2.9 mm) just after the mass flow meter and before brine distribution joint to all modules. The other two thermocouples were placed in the same manner as previous ones at distance of 20 outer pipe diameters after brine collector joint of the modules. The pipe section with attached thermocouples was heavily insulated outside to

prevent the influence of the environment and to make sure that the measured temperature was close enough to the temperature of the fluid flowing through the pipe. Measurement of the brine flow rate was carried out with the vortex type flow meter. It was installed in the brine distribution line at the safe distance from the brine pump and bends.

In the chilled water cycle (consumer loop), two temperatures and one flow rate have been measured, chilled water temperature at the silo outlet and warm return water temperature at silo inlet as well as total chilled water flow rate. Again four thermocouples were used, two for measurement of chilled water temperature at silo outlet and two for the warm return water from the consumer. Thermocouples were placed on the tube wall (stainless steel pipe O.D. 51 mm with wall thickness of 1.5 mm) and have been heavily insulated. Chilled water flow rate was measured by a clamp-on ultrasonic type flow meter.

Since the ice silo was physically closed, detailed ice thickness measurements inside the silo could not be conducted even though some visual inspection was possible through the hatch on the top of the silo and through the two inspection glasses mounted on the side of each module.

Inside the ice silo, three water temperatures were recorded during testing as indicated in Figure 4.1.

Ice level inside silo was measured by monitoring the change of a water level. In order to make level monitoring more sensitive, beside the ice silo a compensation tank with a pump and flexible pipes was added. Any increase of water level inside ice silo would cause overflowing of surplus water to the compensation tank. In this way, water level inside ice silo was kept artificially constant at all times, on maximum, and any difference in water level change caused by the ice building or melting inside the silo would return as a water level difference in the compensation tank. Water level inside the compensation tank was measured by sensitive differential pressure transducer with range from 0 to 350 mbar.

To minimize the influence of the ambient, outer surface of the ice silo was covered with 100 mm thick polystyrene insulation. The heat gain through the ice silo walls was estimated to be around 250 W (heat flux of 40 W/m²) at the ambient temperature of 20 °C. The compensation tank was insulated as well, but the tubes connecting the ice silo and compensation tank were not. The heat gained through the compensation tank loop was found to be approximately 1.5 kW during day time (discharging mode), while during night (charging mode) it was less than 1 kW.

The data acquisition system used consisted of personal computer and a Data acquisition/Switch unit Agilent 34970 A. All the data were scanned and recorded at 5 second intervals.

Table 4.1 List of measuring instrumentation

Instrument	Type	Calibrated Range	Accuracy
Differential pressure transducer	Omega, PX750	0 – 350 mbar	± 0.1 %
Temperature sensors	Pt100, Hart engineering	-5 °C – + 5 °C	± 0.015 °C
	K-type thermocouples	-15 °C – + 5 °C	± 0.1 °C
Vortex flow meter	Yokogava, DY80	0 – 100 m³/h	± 0.75 %
Ultrasonic flow meter	Sitrans FUE clamp on	0 – 50 m³/h	± 1 %
Data acquisition unit	Agilent 34970 A	-	-

Calibration of measuring instruments and uncertainty analysis is outlined in Appendix A and Appendix B of this thesis.

4.2.2 Experimental procedure

To determine ice bank charging and discharging characteristics series of 16 tests has been conducted. The system was tested under real operating conditions in both charging and discharging modes.

Operation of the considered system can be characterized as a full storage (load shifting operation mode (Dorgan and Elleson, 1994)). Charging of the ice silo was carried during the night time (from 9 p.m. to 7 a.m.), limited by a period of cheap electricity and was finished either manually or automatically at any time by the ice thickness sensors. Cool energy stored in the silo is then used during day time. Chilled water consumption usually starts at 7.30 a.m. and ends at 3 p.m.

Ice bank system performance was continuously measured for the period of one week. Discharging and charging test were taken consecutively. First experiment was carried out in a discharge mode. In this case the test was started with unknown quantity of ice stored in the silo and was continued until all ice was melted and the temperature of water in the storage has reached approximately 4 °C. Second testing was continued in a charging mode. Except of the first test all other discharge experiments have been finished with some ice still remaining in the silo. Since the ice bank system was operated in real conditions, and the real production process depended on the supply of the chilled water from the storage, no special discharging and charging scenarios were allowed.

4.3 Results and Discussion

4.3.1 Charging process

First charging process (experiment no. 2) started at fully depleted tank condition at 9.53 p.m. and lasted to 7.43 a.m. the next day. Figure 4.2 shows water temperature and ice mass build up inside the silo.
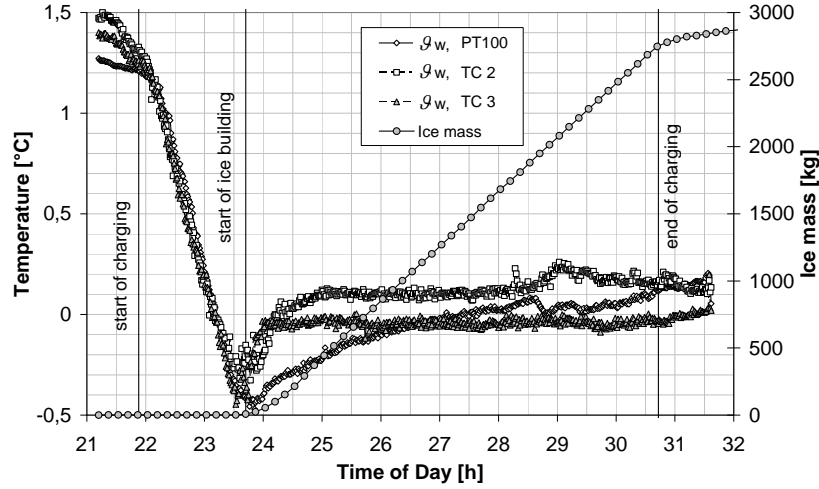
Figure 4.2 Water temperature and ice mass in the silo

At the beginning of the process the temperature of the uppermost water layer was between 1.3 and 1.5 °C. As the cold brine entered the tube bundles the temperature of the water started to decrease. In the period from the start to 11.30 p.m. water temperature followed a linear trend indicating that only water was present inside the silo. At 11.10 p.m. water reached freezing point but its temperature continued to decrease until the 11.30 p.m. when it reached the lowest value of approximately -0.4 °C. At that moment freezing of water inside the tank commenced. With instantaneous release of supercooling large size ice particles were formed (around 5 mm). This was observed through the hatch at the top of the silo. Creation of the ice crystals in the bulk water away from the tube bundles is accompanied with a sudden water temperature rise after which it was stabilized for the rest of the process at ±0.1 °C. Occurrence of the water supercooling and the forming of ice crystals is attributed to the fact that there is no water agitation during the charging process. As seen in Figure 4.2 in the moment when the water temperature reached minimum and crystallisation was observed the building of ice is recorded as well. The trend of the ice growth appears to be linear even though it should be decreasing with time due to the decrease in cooling charge

46

rate. The same trend can be observed for the rest of the charging tests as shown in Figure 4.3.
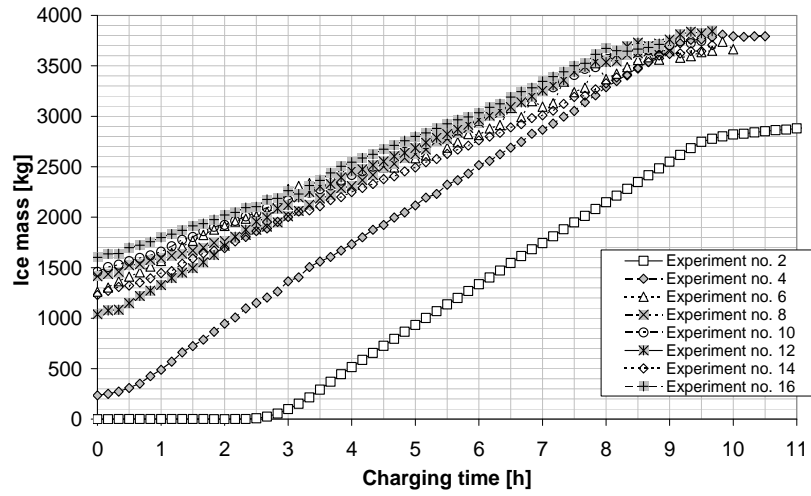
Figure 4.3 Ice mass in the silo for all charging processes

As it may be seen the charging rate depends on the ice inventory in the silo, i.e. the ice thickness around the tubes. Second and fourth experiments show highest charging rates while for all the other cases charging rates are lower. This is logical since for the second experiment the tubes were bare without ice while for the fourth experiment ice was observed only in the second module on the uppermost tubes. For all other cases a charging mode started with a significant amount of ice already present in the silo.

A plot of charging rate versus ice content is shown in Figure 4.4. Content of ice present in the silo is calculated as a ratio of the measured ice mass over ice mass calculated for uniform ice thickness of 25 mm. As already anticipated the highest charging rates, around 37 kW, are observed for the first two charging experiments, no. 2 and 4, while the rest of the experiments show much lower charging rates of approximately 25 kW. Only for few experiments with initially high mass of ice inside the silo, no. 6, 12 and 14, charging rates are high but only up to some point in the charging process.
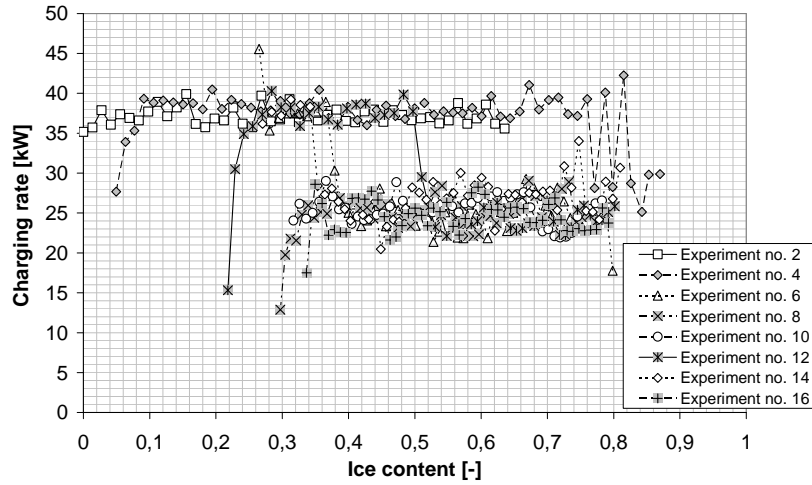
Figure 4.4 Charging rate versus ice content for all charging experiments

The reason for high charging rate at the first part of the cycle 12 is the high performance of the refrigeration unit. In this case, due to unknown reasons refrigeration unit was performing more efficiently than in rest of the cases. Nevertheless, different phenomenon was observed in case of cycles 6 and 14. It is believed that the reason for such behaviour lays in the uneven distribution of ice inside the silo which is a result of the pre-ceding discharging process. During discharging process the first, lower module is the most affected one where depending on a discharging rate and warm water temperature, the ice is melted rapidly. Another factor which influences the variation of ice thickness regarding the position in-side the silo is uneven distribution of the recirculation water across the annular cross-section of the silo. Uneven distribution of the recirculation water in the silo is the result of an ice thickness variation along the tubes.

Both charging rate levels are fairly constant over the period of ice build-ing, i.e. they are not decreasing as it might have been expected. The rea-son is only a slight decrease of the brine inlet temperature over the charging process (around 0.5 °C) due to which the cooling capacity of the refrigeration unit is not decreasing notably as well.

In the Figure 4.5, the product of overall heat transfer coefficient and heat transfer area, calculated as a ratio of the charging rate and logarith-mic mean temperature between brine and a water temperature inside silo, is plotted versus ice content for all charging experiments. Generally the more ice stored inside the silo the lower the *kA* product. The significant drop in *kA* product can be observed with the ice content higher than 0.2. The deviations between results of the individual experiments are

small. Only experiments 6 and 14 are showing approximately 20 % higher kA product in comparison to the other experiments.
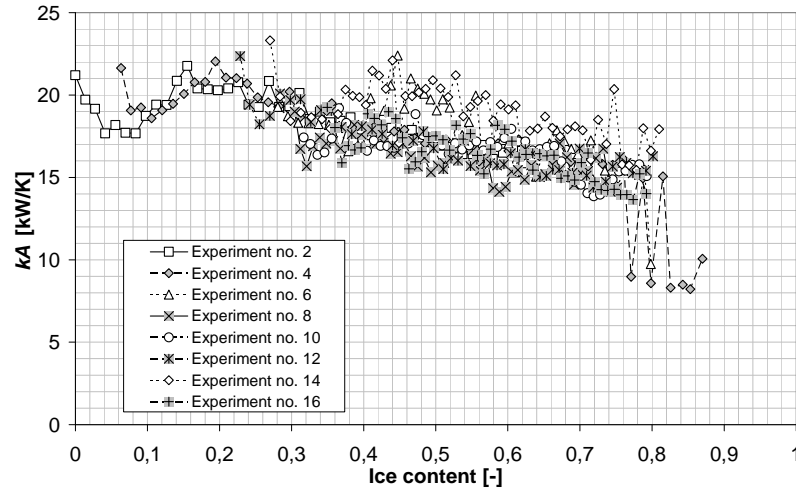
Figure 4.5 Product of overall heat transfer coefficient and heat transfer area versus ice content

4.3.2 Modelling results, charging mode

Figure 4.6 and Figure 4.7 are showing the comparison of the experimental and calculated results for cycle 2.
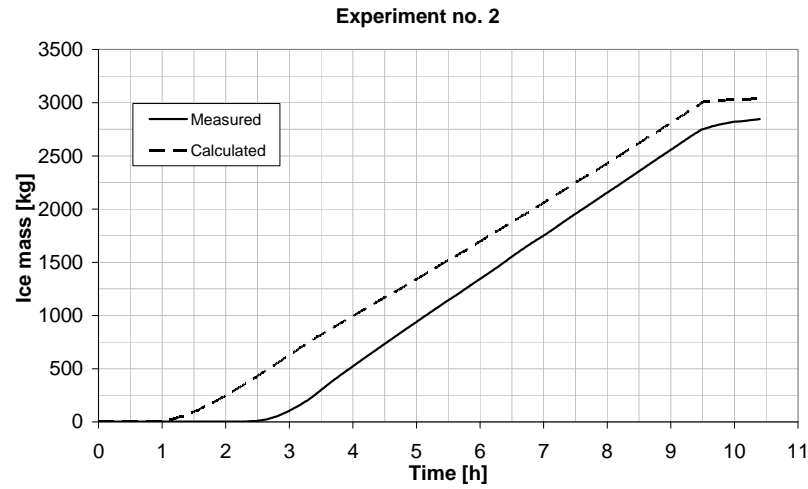
Figure 4.6 Experimental and calculated ice mass building versus charging time, experiment no. 2

It can be seen that calculated results deviate from the experimental ones. According to the calculated results ice started to build just after the water temperature reached the freezing point. According to the measurements the ice building commenced approximately one and half hour later after the water reached the freezing point.

If Figure 4.7 is observed it can be seen that calculated outlet brine temperature is always lower than the measured one. The reasons are at least twofold. First, in the mathematical model thermal capacity of the tubes, construction material and water inside the silo was not taken into account. Secondly, mathematical model does not support low, near zero flow rates of the recirculation water.
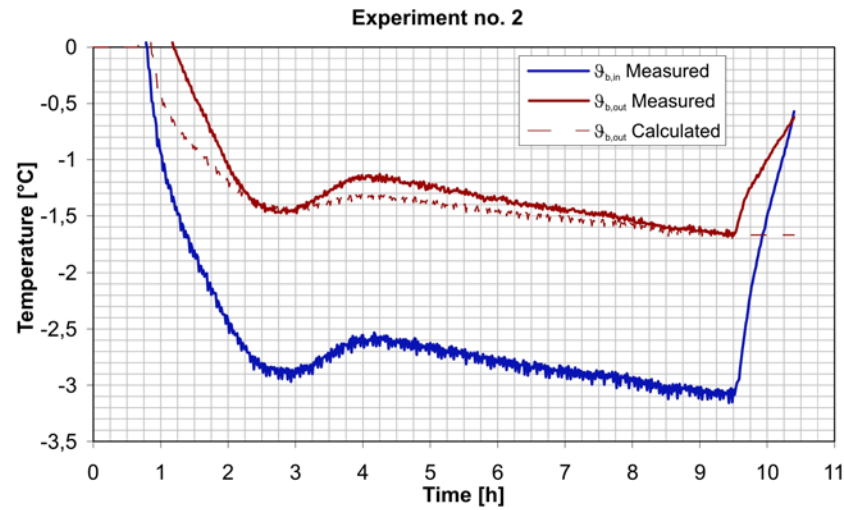
Figure 4.7 Experimental and calculated brine inlet/outlet temperatures versus charging time, experiment no. 2

Much better results are obtained for cycle 4. As it is shown on Figure 4.8 the difference between calculated and experimental results of ice building is negligible. Slight deviation is notable at the beginning of the ice building period and at the end of the process. Again, before the new ice layer has started to build, a certain supercooling of the water is observed, even though some ice was already present in the silo. Consequently a slower ice growth rate is measured than calculated in the initial stage. The occurrence of the water supercooling might have been expected since most of the tube coils were without ice.
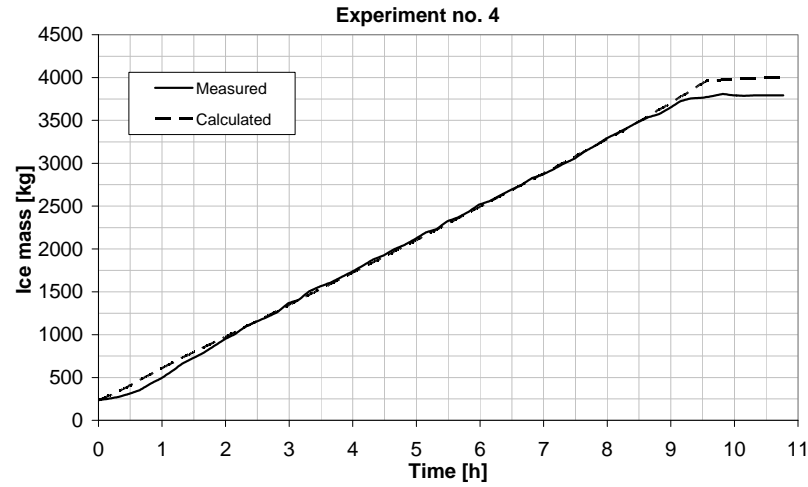
Figure 4.8 Experimental and calculated ice mass building versus charging time, experiment no. 4

In Figure 4.9 plot of brine inlet and outlet temperatures versus charging time is shown. The deviation between measured and calculated results is notable only at the beginning and the end of the process. The fluctuation of the brine temperatures in the last stage of the process is caused by the periodical closing and opening of the brine solenoid valve at the second module.
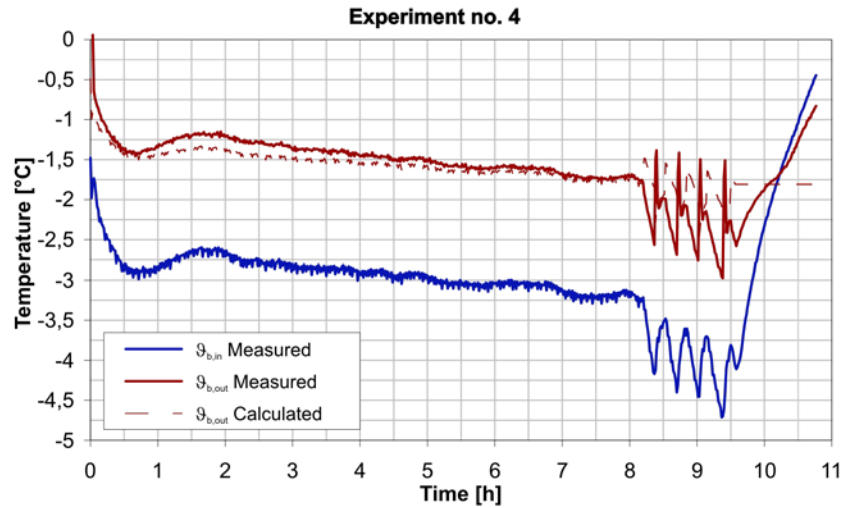
Figure 4.9 Experimental and calculated brine inlet/outlet temperatures versus charging time, experiment no. 4

51

Solenoid valve is regulated by the ice thickness sensor which acts when the measured ice thickness is greater than preset as maximum allowed value. Since it wasn't possible to close the imaginary solenoid valve of the second module during the simulation procedure now lower brine flow rate to the silo was equally distributed to the both modules resulting in a lower average brine velocity and thereby higher brine temperature rise through the silo which finally led to the higher ice growth rate than actually measured. Since the temperature of the water inside the silo was already at the freezing point the experimental results in this case were predicted with a high accuracy. Even better conformity between calculated and experimental results is found for the rest of the charging experiments, i.e. for cases 6, 8, 12, 14 and 16.

4.3.3 Discharging process
In following figures experimental results for cycle 3 are shown.
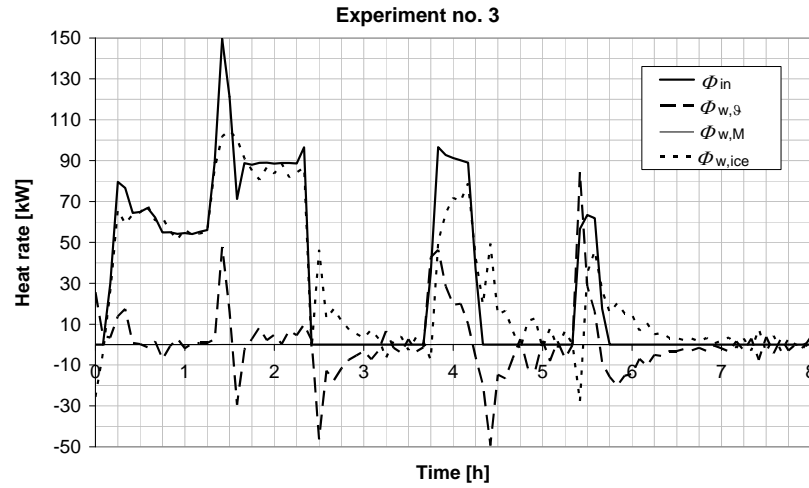
Figure 4.10 Heat rates versus discharging time, experiment no. 3
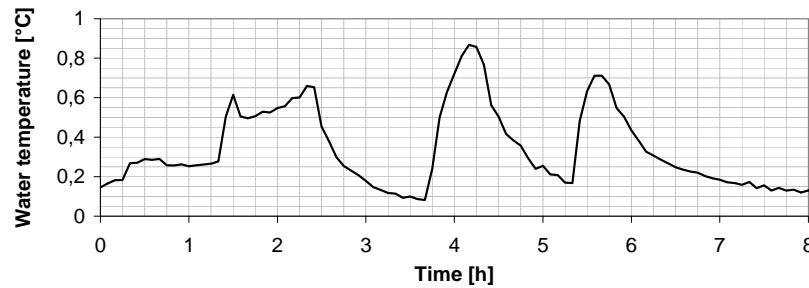
Figure 4.11 Water temperature at silo outlet, experiment no. 3

52

As it may be observed, the discharge rate imposed on the ice silo is highly dynamic with the maximum cooling load (150 kW) of more than two times higher than the average load (65 kW). Discharging period of the ice bank is separated in three stages. The discharging sequence is dependant on the fresh milk departure and pasteurisation process. Temperature of the water coming from the consumer varies from 4 to 13.5 °C depending on the cooling load requirements. In the period when the cooling load is not needed chilled water pump is idle. Figure 4.10 shows different heat rates and energy terms versus discharging time.

Φ_{in} presents the heat rate input to the silo by the consumer:

$$\Phi_{in} = \dot{m}_w c_{pw} \left(\vartheta_{w,in} - \vartheta_{w,out} \right) \qquad 4.1.$$

$\Phi_{w,\vartheta}$ is the sensible heat rate due to change in bulk water temperature:

$$\Phi_{w,\vartheta} = M_w c_{pw} \frac{d\vartheta_w}{dt} \qquad 4.2.$$

$\Phi_{w,M}$ is the sensible heat rate due to change in mass of water in the tank:

$$\Phi_{w,M} = c_{pw} \left(\vartheta_w - \vartheta_{ice} \right) \frac{dM_w}{dt} \qquad 4.3.$$

Heat transfer rate from the water in the tank to the ice, $\Phi_{w,ice}$ is described by the relation:

$$\Phi_{w,ice} = \alpha A_{ice} \left(\vartheta_w - \vartheta_{ice} \right) \qquad 4.4.$$

On the other hand $\Phi_{w,ice}$ can be calculated from the energy conservation equation as:

$$\Phi_{in} = \Phi_{w,\vartheta} + \Phi_{w,M} + \Phi_{w,ice} \qquad 4.5.$$

In the first discharging period basically all required cooling heat rate was provided by melting of ice without significant temperature rise. In order to cover the peak load neither the heat transfer coefficient water to ice nor the area of the ice surface were sufficient to transfer the necessary heat at the present water temperature level of approximately 0.3 °C. Therefore at the period of the highest cooling load water temperature has risen to 0.6 °C where it remained to the end of the first discharging stage, see Figure 4.11.

After the first discharging stage, and at the beginning of the standstill period the temperature of water is still high enough for ice to melt which in turn causes water temperature to decrease. This process would continue until thermal equilibrium of the water and ice inside the tank is reached or the other charging period commences. During the second discharging period input heat rate was approximately at the same level as at the end of the first stage, but now the water temperature increased to above 0.8 °C. The reason could be found in Figure 4.12 where the product of water to ice heat transfer coefficient and ice interface area as well as ice percentage are plotted versus discharging time.
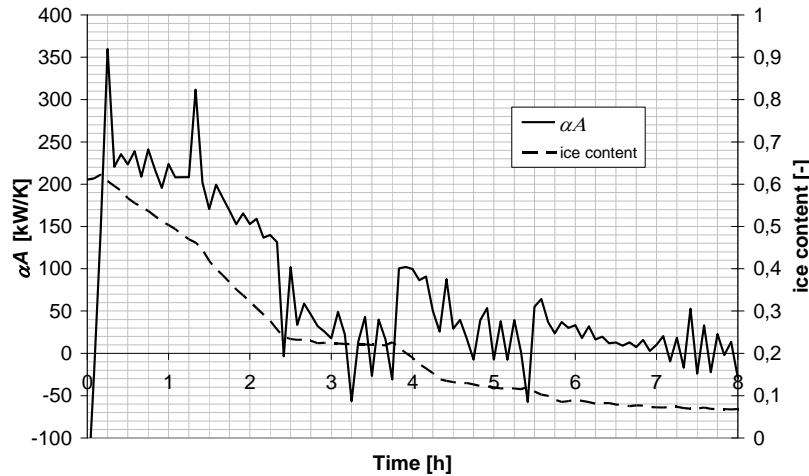
Figure 4.12 αA and ice content versus discharging time, experiment no 3

As seen in Figure 4.12 during the first period product of heat transfer coefficient and ice interface area was at high level (more than 200 kW/K), after which it gradually decreased with time and ice quantity inside the silo. At the beginning of the second stage only 22 % of ice still remained inside the silo. Due to the reduced ice-water interface area and the heat transfer coefficient between water and ice as well (due to lower flow velocity caused by increased water flow cross sectional area which is caused by increase of spanwise clearance between ice layers) water had to take over the part of a imposed heat rate which finally resulted with water temperature rise.

The third stage is characterized with lower heat rate load (60 kW) for which the product of ice-water interface area and the heat transfer coefficient is high enough to provide water temperature of only 0.7 °C. Having examined Figure 4.10 to Figure 4.12, the following conclusion could be made; the greater the ice-water interface area and heat transfer coeffi-

cient between water and ice, the higher the ice melting rate and lower the final water temperature.

4.3.4 Modelling results, discharging mode

In order to asses the ability of the mathematical model to simulate the processes inside the ice bank silo during discharging, computer program was put to the test.

In Figure 4.13 to Figure 4.15 comparisons of calculated and experimental results for the experiment 3 is shown. As it can be seen the calculated and measured results are in good agreement. Still there is a slight deviation between calculated and measured results.
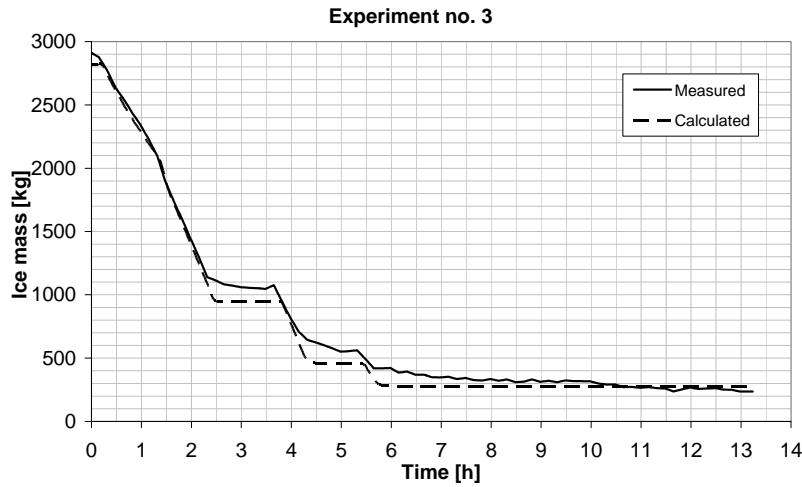
Figure 4.13 Experimental and calculated ice mass versus discharging time for experiment no. 3

As seen in Figure 4.13 during the first discharging period curves of the calculated and measured quantity of ice are falling together with one exception, at the end of the cycle according to the calculations more ice have been melted than measured. The similar but less emphasized can be observed for the second and the third discharging period. The background could be found if Figure 4.14 and Figure 4.15 are examined more closely.

It can be seen that almost during the entire cycle calculated heat transfer from water to ice is more intense than the measured one. This causes water temperature to be lower than measured (as indicated in Figure 4.15) and finally the calculated amount of ice melted to be higher than actually recorded.
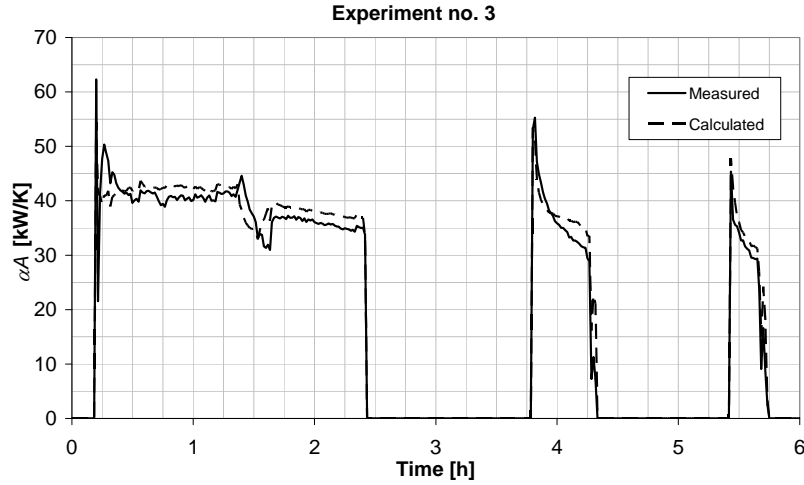
Figure 4.14 Experimental and calculated αA versus discharging time for experiment no. 3

The reasons for such behaviour could be at least twofold. First is the error in calculation of the water-ice surface area. Namely, in the calculation procedure circularity of the ice layer at any instant is assumed while in the reality conditions are much different. During the discharging experiments high noncircularity of ice layer was observed, i.e. the ice that is under direct influence of the incoming warm water will be melting faster while the ice in a shadow of the water flow (caused by the tube) will be melting with a slower rate. Respectively, it happens that there is no ice at the bottom of the tube while on top of the tube very thick ice layer is still present. In this case ice-water interface area is lower than anticipated by assuming circularity.

The second factor which influences the heat transfer behaviour at the water-ice interface relates to the uneven water flow distribution over the annular cross-section of the silo due to ice thickness variation along the tubes. In the mathematical model a uniform water flow distribution over the silo cross section was assumed. This assumption was adopted in order to make calculation procedure less time-consuming and is supported by the fact that the heat transfer can be considered as the process limiting factor (Finer et al., 1993). One more feature could be noticed in Figure 4.15. At the beginning of the standstill period when there is no heat load, calculated temperature of the water in the silo is decreasing rapidly while the measured temperature is decreasing more slowly. One of the reasons is the capacity of the agitator which could not be changed in the calculation procedure, i.e. it had the same value for both discharging and standstill period (300 m³/h) while in reality during the standstill

56

period the chilled water pump and silo agitator were idle. Consequently, the calculated heat transfer at water-ice interface was more intense and temperature drop was faster. Another reason is neglected thermal capacity of mass of the water present in the silo in the mathematical model. Nevertheless, the differences between calculated and experimental results in discharge mode are acceptably small.
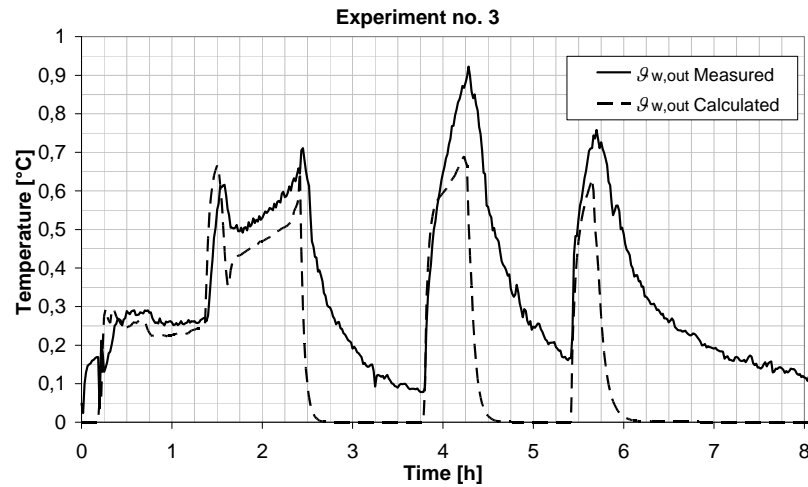
Figure 4.15 Experimental and calculated outlet water temperatures for experiment no. 3

4.4 Conclusion

Experimental investigation on the ice bank thermal storage system was performed. Static, indirect, cool thermal storage system, with an external ice-on-coil building/melting was considered. The tested system was installed as a part of the production line in the dairy "Antun Bohnec" in the city of Ludbreg, Croatia.

In charging mode, the ice building rate followed a linear trend although in theory it should be decreasing with time. Due to just slight change in brine temperature, charging rate was fairly constant during the charging process. Unlike in some other investigations formation of ice was observed when the bulk water temperature reached certain degree of the supercooling (-0.4 °C). With increasing quantity of ice inside the silo, thermal resistance of the ice layer increased, deteriorating the overall heat transfer characteristics of the ice bank which negatively reflected on the heat transfer curve. Namely, the product of the overall heat transfer coefficient and heat transfer area decreases with increasing ice quantity in silo.

Consumer cooling load curve is found to be extremely dynamic with a peak load of 150 kW and an average load of around 60 kW. The higher the cooling load required the more rapid the ice melting. For all discharging experiments outlet water temperature from the ice bank was below 0.8 °C indicating that even in very different heat load conditions, the output of the ice bank is spontaneously adjusted to deliver water at almost constant near zero temperature. The ability to provide low water outlet temperatures regardless of the heat load conditions could be quantified by the product of the water to ice heat transfer coefficient and ice surface area. The higher the water to ice heat transfer coefficient and higher the area of the water-ice interface the lower the water temperatures can be reached. At the 80 % of the silo capacity the αA is found to be 250 kW/K, at 40 % αA is 150 kW/K and at 20 % αA is 100 kW/K.

In the second part of the study experimental results are compared to the calculated result obtained by use of a computer model. In the charging mode calculated results are in very good agreement with experimental data as long as there is ice present inside the silo. In the initial period when the simple water cooling is considered, results do not match satisfactorily. In the discharging mode calculated results are closely following the experimental data, although, slight deviation could be observed. The possible reasons are simplifications introduced to the mathematical model. Namely, circularity of the ice layer and uniform water flow distribution over the annular cross-section of the silo is assumed, while the thermal capacity of the water present in the silo is neglected.

5 The economic justification of ice storage application in cooling systems within the process industry and the building sector

In general, implementation of the CTES systems may be of interest when one or more of the following conditions apply (Dorgan and Elleson, 1994; ASHRAE, 2007):

- o the peak cooling load is higher than the average load,

- o difference between on- and off-peak electric billing rates exists,

- o charges for peak power demand are high,

- o the cooling load profile is too dynamic to be handled with non-storage system,

- o loads are of short duration and/or they occur infrequently,

- o loads are not coincident with energy source availability,

- o energy supply is limited,

- o an existing facility expansion is planned, and the cooling equipment is insufficient to meet the new peak load but has spare nonpeak capacity,

- o backup capacity is desirable.

Whether the CTES system will be economically justifiable or not depends on the parameters that will influence the investment and operating costs of cooling system, which are:

- o shape of the cooling load curve (cooling load profile),

- o operating and control strategy (full or partial storage),

- o optimized operation, i.e. chiller or storage priority,

- o maximum refrigeration load, i.e. the size of the refrigeration unit, connection to the electrical grid,

- o size of the ice bank, the higher the quantity of ice stored the larger the storage is required.

In order to investigate economic potential of an ice storage application in cooling systems within the process industry and the building sector two actual cases are studied. For both cases the static, indirect, external melt, ice-on-coil cool ice bank system was considered. In the first case, ice bank application within the dairy industry "PIK, Rijeka" is considered. In the second case implementation of the ice bank system as a part of chilled water system for the purpose of building cooling (Elderly Persons Home in Sisak) is discussed.

The economic evaluation of a CTES system implementation is based on the design load profile and the electricity billing rates. According to the adopted operating and control strategies (full or partial storage) required refrigeration unit capacity and storage capacity can be calculated. These estimates are used to determine operating and first costs.

Investment costs to be considered:

- o purchase and commissioning of the equipment, i.e. refrigeration unit, CTES, heat exchangers, pumps, pipelines, regulation, instrumentation etc. In this study only the cost of refrigeration unit, storage silo, heat exchangers and pumps as a capital components are taken into account,

- o connection to the Croatian power grid.

Operating costs consist of:

- o electrical energy cost,

- o power demand charge.

The design load profile for the dairy "PIK, Rijeka" was determined from the current load data acquired for the period of one year (2008), while the design load profile of Elderly Persons Home in Sisak was calculated. It was based on cooling load calculations previously made for a design of a non-storage cooling system according to the German standard VDI 2078 (1996). The adopted load profile referees to the hottest day of the year (July 23).

In the first case the cooling load profile is highly dynamic with infrequent loads of short duration and with a maximum peak load which is 6.5 higher than the average load. In the second case the maximum cooling load is only 2.5 times higher than the daily average load.

The fact that in both cases the cooling load profile peaks at a level of more than twice the average load and the fact that in Republic of Croatia difference between on- and off-peak electricity rates exists makes these cases potentially interesting for application of CTES system.

5.1 System configurations

A non-storage cooling system configuration is shown in Figure 5.1. It consists of a refrigeration unit loop, a secondary fluid loop and a consumer loop. Capital components of the system are refrigeration unit, secondary fluid circulation pump and a heat exchanger. Any cooling demand required by the consumer must be covered directly by the refrigeration unit which has to have ability of capacity control.
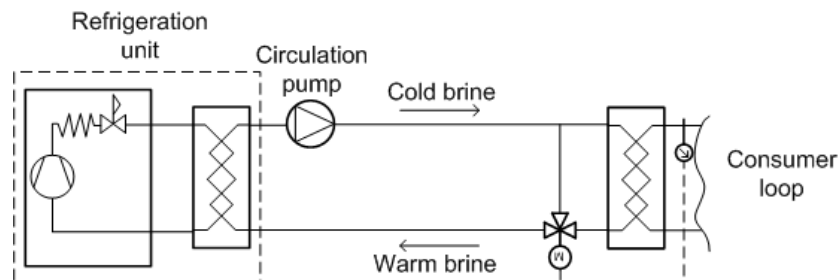
Figure 5.1 Non-storage cooling system

A configuration of a cooling system with an ice storage is shown in Figure 5.2. In contrast to non-storage system, cooling system with ice storage has one additional heat transfer level (water loop). Capital components of the cooling system with storage are: refrigeration unit, ice storage, intermediate heat exchanger, brine and water circulation pumps and a heat exchanger in a consumer loop.
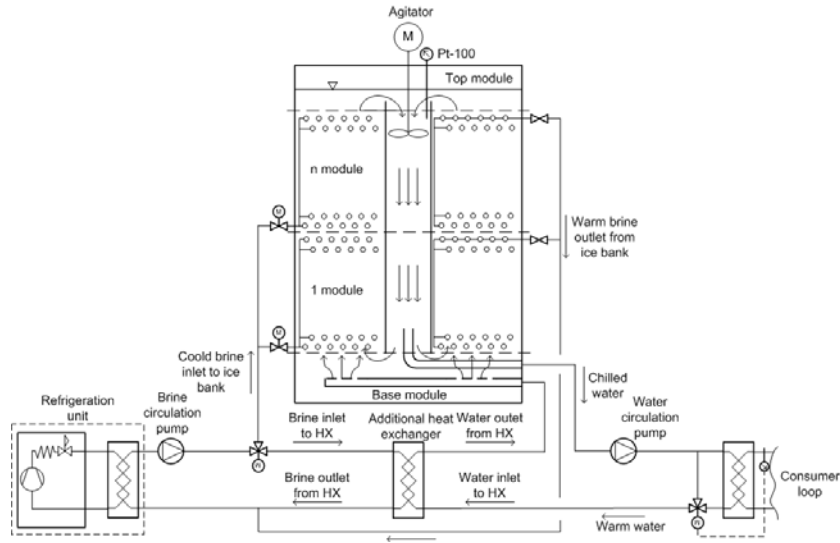
Figure 5.2 Storage cooling system

Due to additional temperature level between primary refrigerant and a consumer loop, a cooling system with storage will always have lower refrigeration unit COP than the non-storage system. This implies larger electricity power demands. However, in addition of storage it allows downsizing of the system components which at the end can lead to savings in both first cost and operating costs since inefficient part load operation may be avoided.

5.2 Investment costs

Investment costs of the components which the ice bank system consists of are partially acquired from the companies present at the local Croatian market and partially deduced from the literature.

Investment cost of the CTES generally depends on the storage technology, capacity and application. For external melt, ice-on-coil, ice bank storage for industrial application investment costs can be expressed by the following relation:

$$I_{\text{ice silo}} = 1020 \cdot Q_0^{0.64} \text{ [EUR] valid for } Q_0 > 250 \qquad 5.1$$

where Q_0 presents storage capacity in kWh. The price includes all the hardware (silo, agitator, insulation, control, instrumentation) and work necessary to implement the silo into the refrigeration system. It has to be noted that these prices are acquired from the one single producer on Croatian domestic market.

Investment costs of the chillers generally depend on the nominal refrigeration capacity and its application. Investment cost of water and glycol using chillers for high temperature application (-10 °C to 5 °C) can be approximated by the following expression:

$$I_{chiller} = 745.4 \cdot \Phi_0^{0.77} \text{ [EUR]} \qquad 5.2$$

where Φ_0 presents nominal chiller's refrigeration capacity in kW (source: Carrier, Daikin).

The price of plate type heat exchangers for the purpose of fluid cooling in food industry (acquired from company AlfaLaval) can be approximated by relation:

$$I_{pthx} = 58.78 \cdot \Phi_0^{0.94} \text{ [EUR] valid for } 100 < \Phi_0 < 600 \qquad 5.3.$$

According to Pronk (2006), the costs of 304 grade stainless steel shell-and-tube heat exchangers can be approximated by:

$$I_{s\&thx} = 1500 \cdot A_{he}^{0.65} \text{ [EUR]} \qquad 5.4$$

where A_{he} is heat transfer surface of the heat exchanger in m².

The last capital components of the system are circulation glycol and water pumps. According to Nikolić et al. (2009) initial cost of the pumps is in range of 4-7 % of the total investment cost of the ice bank system. Furthermore the electricity consumption for pumping is in range of 5-10 % of the total electricity consumption. Investment pump price is estimated as 5 % of the initial cost of the chiller, storage and heat exchangers. Furthermore energy consumed by the glycol and water pumps in ice bank systems is estimated as 5 % of energy consumed by chiller.

Significant part of one time investment costs is the initial connection to the Croatian power grid (power lease) which can be expressed with the relation:

$$I_{conn} = 240 \cdot P_{el} \text{ [EUR] with } P_{el} \text{ in kW} \qquad 5.5.$$

5.3 Operating costs

In the Republic of Croatia, electric energy charge is time dependant. Electricity prices are thus dependant on customer profile and chosen tar-

iff model (HEP, 2008). During day time, from 7 a.m. to 9 p.m. consumer is charged with 0.085 €/kWh. During night shift from 9 p.m. to 7 a.m. the electricity price is 0.042 €/kWh. Besides, power demand charge is 11.54 €/kW per month. VAT is included. These prices are valid for commercial low voltage customer (0.4 kV) and the tariff model "red", which is the most suitable for power demands up to approximately 750 kW.

For electricity power demands higher than 750 kW transfer to medium voltage system (10 or 20 kV) would be economically more reasonable. On-peak electricity price under this model is 0.073 €/kWh, off-peak is 0.037 €/kWh while the power demand charge is 9.5 €/kW per month (VAT is included). In this case investor is obligated to build the power system substation with approximate price of 165 €/kW. Nevertheless these expenses are compensated through lower price of the electrical energy in period of 3 to 5 years dependant on consumption.

Since in the above mentioned examples required chiller electric power doesn't exceeds 750 kW, investment and operating costs are calculated for low voltage customer and tariff model "red".

5.4 Ice based CTES application in dairy industry "PIK Rijeka"

In this chapter an economic comparison of ice based CTES storage system and non-storage system for the purpose of milk cooling in dairy factory is conducted. In order to investigate the influence of operating strategy on system economy ten scenarios are considered; in particular one non-storage system and nine storage system scenarios. In all storage scenarios daily charging cycles are assumed.

In Figure 5.3 and Figure 5.4, refrigeration unit load and storage inventory versus time and operating strategy is shown. Two groups of scenarios could be distinguished. In the first group (scenario: partial 4, 1, 3, 2, 7) upper chiller capacity is limited, i.e. cooling load profile is "shaved" at certain levels determined by the maximum chiller capacity. The rest of the required capacity to meet the current cooling load is recovered from the storage. Whenever the cooling demand is lower than the full capacity of the chiller a refrigeration unit is unloaded in order to reduce the operating costs during on-peak period. During off-peak period the chiller is operated at maximum capacity until the storage is completely charged.

The second group consists of four scenarios, partial 5, partial 6, full storage and load levelling. For partial 5, partial 6 and full storage strategies refrigeration unit is operated at a reduced capacity during the on-peak

period. The part of the cooling load which is not covered by the refrigeration equipment is met from the storage. Whenever the cooling load is lower than the actual chiller capacity the storage is charged.
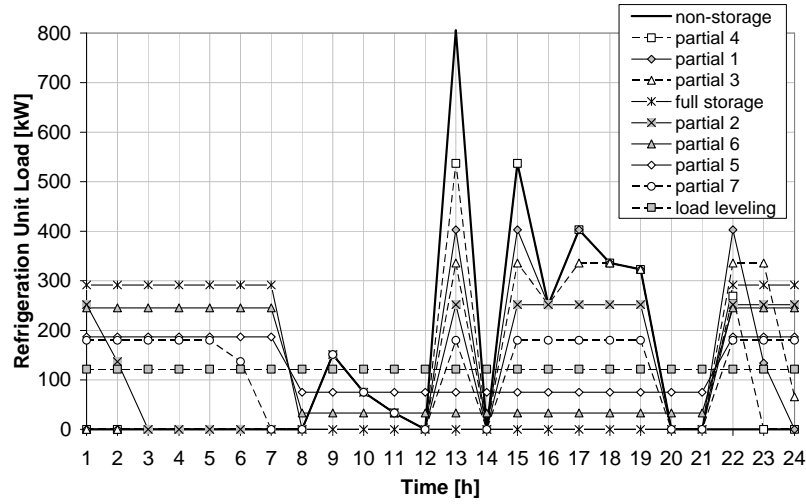
Figure 5.3 Refrigeration unit load versus time and operating strategy

As seen in Figure 5.3 the largest chiller size (besides non-storage system) is required for the partial 4 scenario and the smallest for the load levelling strategy. In the other hand the largest silo size is required for the full storage while the smallest is for the partial 4 scenario (Figure 5.4).
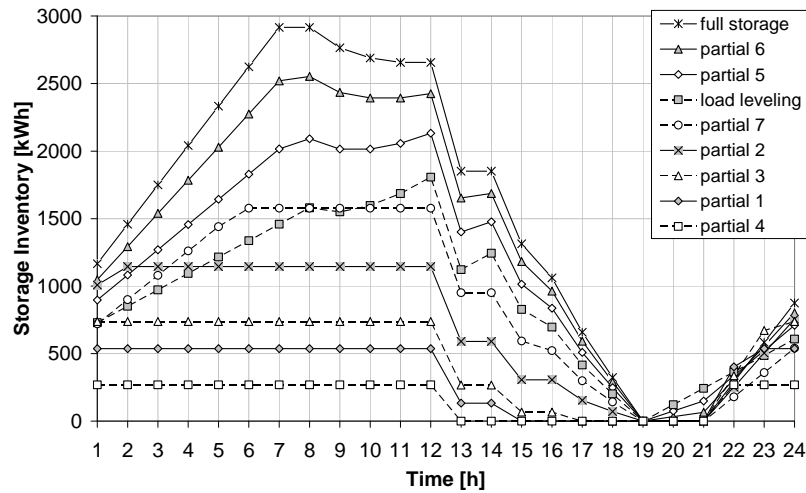
Figure 5.4 Storage inventory load versus time and operating strategy

On basis of refrigeration unit capacity, storage capacity and scheduling of the chiller operation the first cost and operating cost are calculated. For a non-storage system refrigeration unit a COP of 4.5 is assumed (Dorgan and Elleson, 1994). In case of storage system COP of 3.5 is assumed for all options. Calculation of the operating costs was based on system operation of 330 days per year. Results are shown in Figure 5.5.
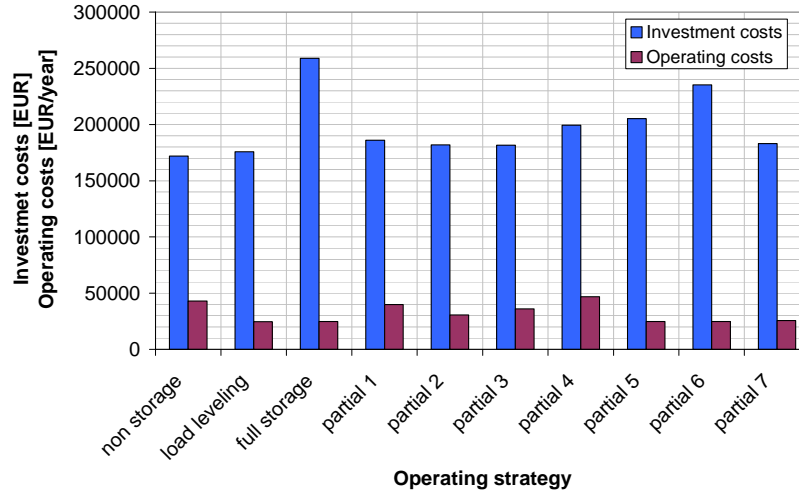
Figure 5.5 Investment and annual operating costs vs. operating strategy

As shown investment cost of storage systems for all options is greater than that of a non-storage system. In contrary, operating costs for storage systems are lower than those for a non-storage system. The highest first cost shows full storage (load shifting) strategy while the lowest operating cost is offered by a load levelling strategy. The second lowest operating costs shows partial system strategy 5, then 6 and then full storage.

On basis of first cost as well as operating costs the simple payback period in relation to the non-storage system is calculated. The results are shown in Figure 5.6. As it may be seen in the application of the ice storage system for process cooling in dairy industry is favoured in almost all cases with investment payback period below five years. Only system scenario partial 4 is not economically feasible due to operating costs which are higher than in the case of non-storage system. The most economically viable option is offered by the load levelling strategy. The closer the strategy to the load levelling the shorter the payback period.
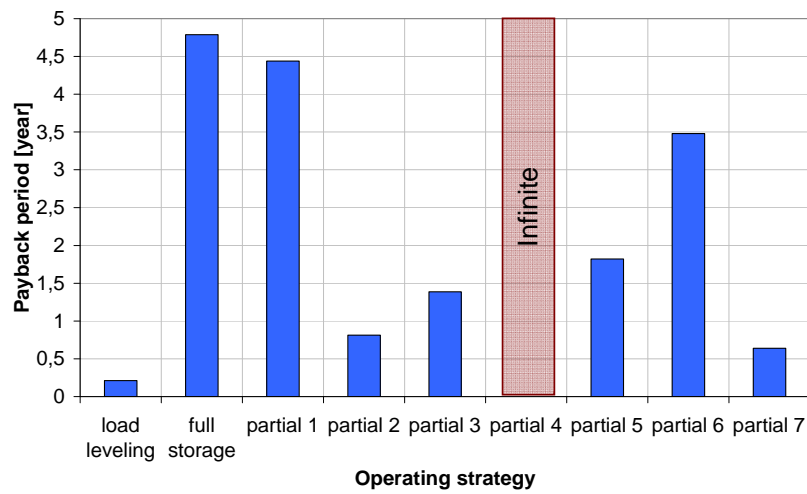
Figure 5.6 Simple payback period versus operating strategy

Due to large the size of the storage silo and the relatively large refrigeration unit (see Figure 5.3 and Figure 5.4) the full storage strategy seams unfavourable when compared to the other options. However if additional operating safety and back up capacity is desirable or a system expansion is planned in the near future its application can be justified as well.

In Figure 5.7 annual savings in operating costs for storage systems are extrapolated to the period of system life time expectancy. Expected life time of the CTES system is more than 20 years.
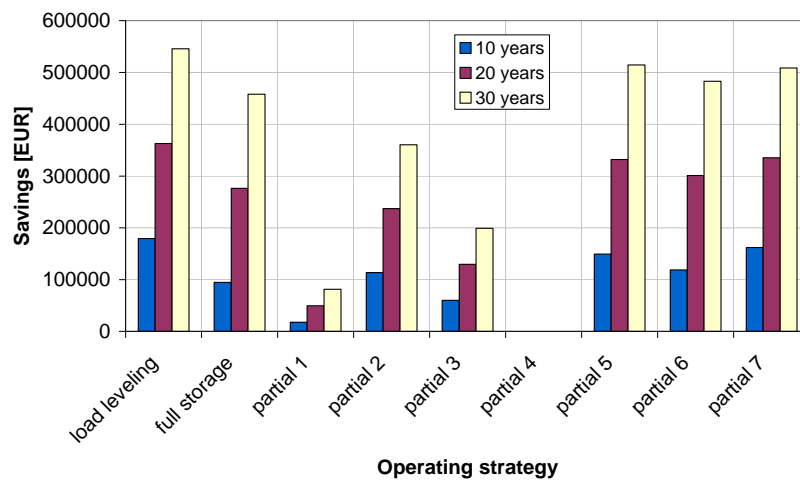
Figure 5.7 Operating cost savings versus operating strategy

Figure 5.7 shows that the most economically justified operating strategy is load levelling strategy. For longer system life time expectancies strategies with larger storage capacities are favoured, i.e. for a period over 20 years the second best option is partial storage, strategy 5 (demand-limiting).

5.5 Ice based CTES application for building cooling "Elderly Persons Home in Sisak"

In Figure 5.8 and Figure 5.9 refrigeration unit load and storage inventory is shown versus time and two operating strategies. In particular load levelling and full storage options are considered.
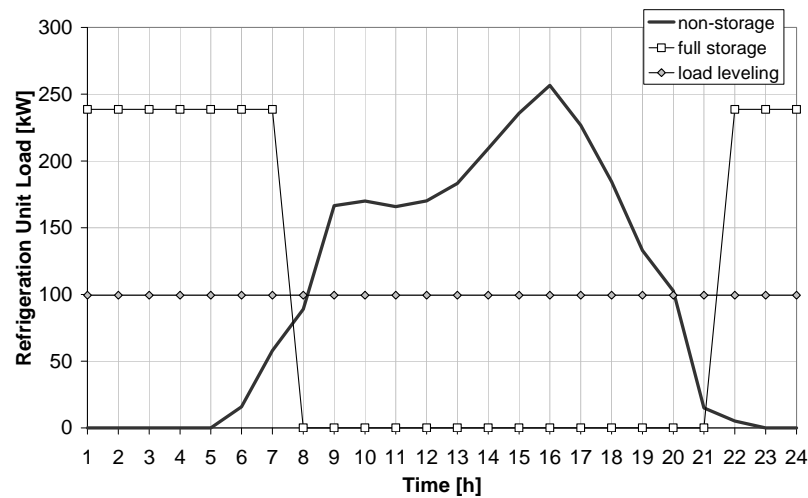
Figure 5.8 Refrigeration unit load versus time and operating strategy

The need for cooling starts at 6 a.m. and rises to a maximum of approximately 250 kW at 4 p.m. which is 2.5 higher than the average daily load. As it may be observed the required chiller refrigeration load for non-storage and full storage system is approximately the same. In this example the full storage strategy offers no benefits in first cost in terms of refrigeration equipment downsizing. On the contrary, with a refrigeration unit COP of 5 (Dorgan and Elleson, 1994) for non storage system and with COP of 3.5[1] for ice storage system the electrical power demand for storage system is approximately 25 % higher than for a non-storage

---

[1] The COP of 3.5 is based on the assumption that the evaporation temperature is around -10 °C. For the non-storage system an evaporation temperature at +2 °C may be kept!

system. Moreover, the required size of the storage is 2.3 times higher than for load levelling operation (Figure 5.9).
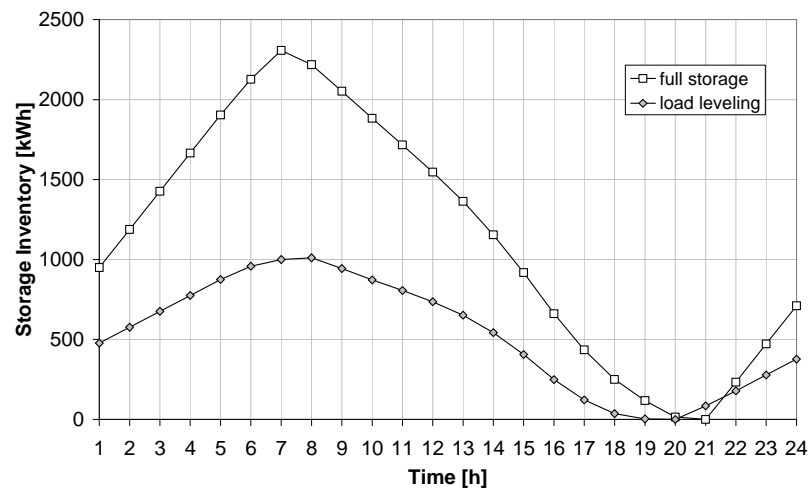
Figure 5.9 Storage inventory versus time and operating strategy

In Figure 5.10 first and operating costs versus operating strategy are shown. Calculations of the operating costs are based on a required annual energy for building cooling which was estimated to 200 MWh.
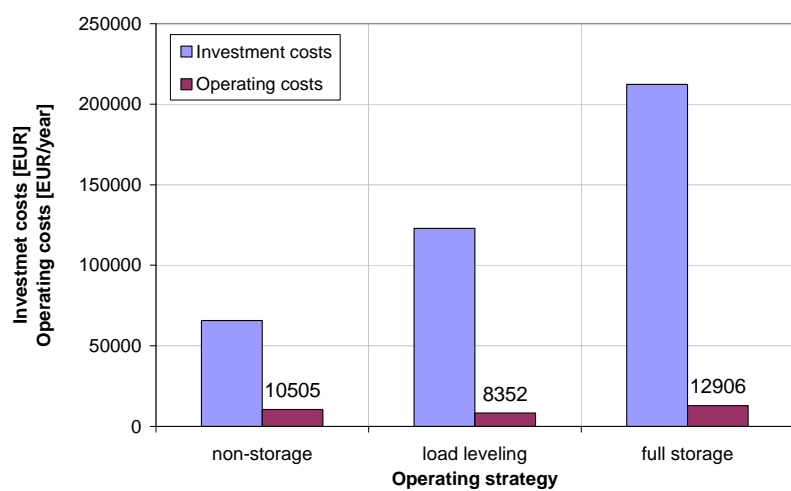
Figure 5.10 Investment and annual operating costs versus operating strategy

The investment cost of the load levelling storage system is two times higher than that of a non-storage system. It is even higher for a full stor-

age system (more than three times higher). In both cases the reason is high cost of ice storage which couldn't be compensated by the lower chiller price. The annual operating costs of a load levelling system are approximately 20 % lower than for a non-storage system. This reduction is a direct consequence of the monthly power charge cost which is in this case 40 % lower.

Opposite of what might have been expected is a 15 % higher annual electricity energy cost for the storage system in comparison to a non-storage system. The reason is large difference in refrigeration unit COP of storage to non-storage system and energy consumption of additional pumps. Due to large difference in first cost of load levelling to a non-storage system the simple period of investment payback is 26.5 years.

The annual operating cost of the full storage exceeds operating costs of a non-storage system (Figure 5.10). In spite of low expense for electrical energy in case of full storage system, due to low chiller COP, annual charge for electrical power demand brings total operational cost to the level higher than in case of a non-storage system. Therefore, this type of system is not profitable.

From the foregoing analysis it can be concluded that the implementation of an ice type CTES systems in industry is economically well justified with generally short payback period. On the other hand it is not viable for cooling applications in building sector in the continental region of Croatia under current equipment prices. The application of an ice type CTES system for the purpose of cooling of buildings could become economically interesting if:

     o   the ice based CTES equipment price decreases and/or

     o   ice storage system design allow higher COP for the refrigeration unit in the charging mode.

The price of the ice based CTES equipment depends on many factors on which is not possible to influence directly. However by careful development and optimization of the storage design one can not only to decrease the price of the storage but at the same time to increase the storage charging and discharging efficiency.

By increasing the chiller COP to a level of 4 - 4.4 the payback period would shorten to 17.5 - 14.5 years. By decreasing the storage price by 40 % the payback period would shorten to 10.5 years.

6 Conclusions and suggestions for future work

6.1 Conclusions

The application of static, external melt, ice-on-coil CTES system has been theoretically investigated and a thorough experimental study has been performed in a dairy industry. The following conclusions can be drawn with relevance to the both theoretical analysis and experimental work.

6.2 Theoretical analysis

A detailed mathematical model and a computer application have been developed to simulate the performance of a static, indirect cool thermal storage system with external ice-on-coil building/melting. The mathematical model has been compared to experimental results and these showed reasonable agreement.

The results from the computer simulations showed that the development of more complex mathematical model was justifiable. A very large number of parameters determine the operation of such a complex device as the ice bank. In the first place the design data, such as dimensions and the number of the pipes, modules, and a silo. Then the characteristics of the equipment used, such as refrigeration unit, the brine circulation pump and water agitator and their control equipment, determine the behaviour of the device as a whole. And finally the conditions which prevail when the plant is operated, such as the warm water incoming flow and temperature, the chosen mode of operation, the ambient data contribute to the complexity of the process. Due to the complexity it is impossible to find simple and sufficiently accurate method to describe the performance of such systems over time. The developed program allows for high flexibility in definition of design and operating parameters. The computer model presents strong optimization tool for particular system requirements and offers a basis for fast and simple system design.

The simulation results showed that an ice bank can be used as an effective means for fast chilling of large amount of water, for a relatively small installed power of a compressor. By properly choosing the operating parameters one can achieve water outlet temperatures that are practically constant and almost equal to 0 °C regardless of the water inlet temperature and its flow rate. Furthermore, using the ice melting and building as a buffer, the variation of required compressor power is smaller than the variation of the heat load usually imposed by the incoming water.

6.3 Experimental analysis

An experimental investigation of a static, indirect CTES system with external ice-on-coil building/melting was conducted on site. A two module ice bank system was installed in a dairy plant as a part of a production line. A series of testing's under real operating conditions have been conducted to determine ice bank charging and discharging characteristics.

The measurements confirmed theoretical predictions reasonably well. By using ice as a buffer with relatively small refrigeration capacity of the compressor it is possible to satisfy much higher cooling load requirements. The ratio of peak cooling load to installed capacity of the refrigeration unit was in the range of 4 to 6. Moreover, the shape of the cooling load curve has only small influence on the outlet water temperature. Regardless of imposed inlet water temperature (3 to 15 °C), flow rate (9 to 13 m³/h) and their fluctuation frequency, the water outlet temperature remained low within the range of 0.3 to 0.8 °C.

A comparison of the simulation results and measured data confirm that the developed computer program can be used for performance prediction of the ice bank systems with acceptable accuracy. As long as there is ice present inside the silo the results are in good agreement in both charging and discharging mode. Nevertheless, certain deviations are observed. They can be attributed mainly to the simplifications introduced to the mathematical model; the neglected water thermal capacity, the presumption of circular ice around the tubes and uniform water flow distribution across the tube bundles which is dependant on distribution of ice thickness in the silo. Moreover, the circulation capacity of the agitator in the model is considered constant while in realty it depends on the accumulated mass of ice in the silo.

During the experimental investigation the following operative characteristics of the ice bank are observed.

It is difficult to determine and to control the termination of the process of ice building. If the process is stopped earlier than foreseen the ice in-

ventory will be lower than expected. If it is stopped to late overcharging may occur. The overcharging of the ice silo and bonding of two adjacent tubes into an ice block should by all means be avoided. Extensive formation of bridging can prevent water flow and ice melting, resulting in increased outlet water temperatures or even in complete silo dysfunction. There are two known methods to determine when the process of ice building should end: by measurement of water level difference and by measurement of the ice thickness at certain locations within the tank. Both methods have weaknesses. In a first place the water level measurements within the tank are not sufficiently accurate due to large silo diameter resulting in low water level change. Secondly if there is a consumption or leakage of cold water somewhere in the process, which is usually the case, the information on water level is irrelevant. Moreover, the water level measurement gives an integral state of the silo inventory, with no information on local ice thickness and indication on possible ice bridging whatsoever.

The problem which may arise by measurement of local ice thickness is uneven ice growth. Thus placement of more than a few sensors on different locations within the tank recognized as critical is necessary to ensure proper silo operation. To promote even ice building it is recommended to leave the agitator in operation during charging process. Without active agitator, formation of long ice crystals (ice web between tubes) has been observed. It affected the thickness sensors which signalled the end of ice making too early.

Since circulation of the secondary working fluid is used for ice building, formation of a conical shape of ice along a tube axis is unavoidable. Ice is thicker at brine tube inlet and thinner at brine tube outlet. Difference in ice thickness causes non-symmetrical flow of water inside silo. Consequently some regions are melting faster resulting in water shortcuts and increased outlet water temperatures. In order to diminish an influence of conical ice shape high secondary working fluid flow rate is required which is energy demanding.

6.4 General

According to the studies reported in this thesis from a technical point of view, the static, indirect, external ice-on-coil CTES system present an efficient solution for load shifting and storage of cold in refrigeration installations and HVAC systems in industry and building sector.

From the economical aspects application of ice type CTES systems for milk cooling within the process industry is well justified with generally short payback period. However, this is not the case for cooling applica-

tions in the building sector in the continental region of Croatia. In order to ensure a wider utilization of such systems in the building sector they must become more economically attractable and more energy efficient. With the total price of the storage installed cost (including tank, heat transfer surface, insulation, agitator, foundation, instrumentation and commissioning) within 40 to 50 EUR/kWh for systems with required storage capacity of 500 to 1000 kWh they would yield the acceptable pay back period under 8 years. Therefore simpler and more efficient storage designs adapted for building sector application are needed.

6.5 Suggestions for future work

The computer simulation model used to evaluate the performance of the ice bank systems can be refined by expanding the mathematical model to account for thermal capacity of the water. Moreover it could be improved by taking into account a variable operation of the propeller (agitator) used for recirculation of water within the silo since ice thickness has significant influence on the water flow resistance and performance of the agitator respectively.

To develop a mathematical model of the water flow within the silo and to couple it with existing software. The flow of water affects the thermodynamic performance of the ice bank to a certain degree. Solidification of water around tubes and melting of ice causes water velocity and flow patterns to change resulting in varying heat transfer. In this way poor designs with high probability of ice bridging and improper water distribution across ice tank could be recognized and avoided.

Optimization of the module geometry and ice silo design in general in order to maximize charging and discharging efficiency of the ice bank system. Optimized solutions would cause investment costs as well as the operating costs of the ice bank systems to decrease.

Design of the particular ice bank systems designated for air cooling applications would stimulate the wider spread of such systems beyond the boundaries of an industrial sector.

Monitoring and control of the ice bank system performance seems to be an important issue in the application of this system solution. A satisfactory solution of this problem would make it possible to exploit the ice bank characteristics to a full extent.

7 Dynamic CTES system – ice slurry

Ice slurry as an advanced two-phase secondary working fluid presents a promising substitute for cold energy transport and storage compared to single phase fluids mainly due to the benefit from the latent heat of the ice phase change. If ice slurry is used for cold energy storage it is possible to shift electric load to off-peak hours which significantly lower energy and demand charges and leads to reduction in total energy usage. Beside lower operating costs it can substantially cut capital investment through reduced installed refrigeration (and electrical) power. Furthermore, with single phase secondary fluid in the traditional indirect system the refrigerant charge (HFC) and related emissions are greatly reduced compared to a complete direct expansion system.

Today, cold energy storages installed as a part of refrigeration and air conditioning systems in industry and commercial buildings are mainly designed as ice bank systems with ice formed around tube bundles. Only a small percentage of CTES systems in the world are built on ice slurry technology despite their numerous advantages over static types such as higher temperature stability, highly improved heat transport capability in comparison to single-phase fluids, enhanced heat transfer, higher ice packing factor and smaller storage size of simpler design (IIR, 2005a). Moreover, temperature level is not limited to 0 °C if the ice slurry fluids are mixtures of water and freezing point depressant additives. Nevertheless, the key problem which is prohibiting wider spread of the ice slurry technology is the high cost of ice slurry production.

For optimum design of cold energy storage systems with an ice slurry knowledge of flow and heat transfer behaviour of two phase slurry is of high importance.

Ice slurry is a mixture of liquid and fine ice crystals with size in range of 0.1 to 1 mm (IIR, 2005a). In most cases the liquid is plain water or a blend of water and freezing point depressants, the same that are used for single-phase secondary working fluids; glycols, alcohols and salts. For

instance, ethylene and propylene glycol, ethyl and methyl alcohol, potassium formate, acetate and carbonate, sodium chloride, ammonia etc.

Opposite to the single phase fluids the working temperature of ice slurries is below the freezing point of the mixture. The decision on the level of freezing point temperature depends on the system application. Generally, water based ice slurries can be applied for temperature range of 0 °C down to approximately -35 °C depending on type of additive and additive concentration (Hägg, 2005)[2]. Decision on operating point temperature is a system design issue. The greater the temperature difference between the freezing point and the operating temperature the greater the ice content. Dependant of application ice mass fractions may vary from 0 up to 60 %. If ice slurry is used for transport of energy ice mass fractions may vary from 0 up to 30 %. In this range ice slurry is still pumpable. If used for purpose of storage of energy, ice mass fractions may be as high as 60 %. Except for pure water ice slurry, higher design ice mass fractions require lower design operating temperatures. Ice slurries with higher ice mass fractions have higher energy density. They offer higher energy storage, heat transport, heat transfer capabilities. Therefore smaller piping system, storage tanks and heat exchangers can be used. On the contrary, a lower operating temperatures give lower COP of the refrigeration unit and a higher viscosity of the remaining liquid which in turn, with higher ice mass fractions, increases the pressure drop and required pumping power.

7.1 Ice slurry properties

The thermo-physical properties of working fluid depend on the choice of carrier fluid and a freezing point depressant. Since water has excellent thermo-physical properties it is mostly used as a carrier fluid. The additives used to lower the freezing point affects the thermo-physical properties of a mixture in an unfavourable way. The decision on appropriate type and concentration of the freezing point depressant depends on desired ice slurry application. The chosen fluid should have good heat transport and heat transfer properties. Moreover it should have low viscosity to facilitate small pumping power (Melinder, 2003; Guilpart et al., 2006).

The selection of most appropriate secondary refrigerant for the efficient ice slurry generation should take into account many properties such as

---

[2] Although the low temperatures are difficult to achieve. It is also hard to reach a high ice mass fraction at these low temperatures.

freezing point, ice concentration, density, enthalpy, apparent heat capacity, thermal conductivity and viscosity.

7.1.1 Freezing point and ice concentration

Figure 7.1 shows freezing point curves of some aqueous solutions. The initial freezing temperature depends on the type and concentration of additive used. The higher the additive concentration the lower the freezing point temperature of the mixture. When the temperature drops below the freezing temperature, ice crystals are starting to form. Since ice crystals during freezing contain only water, the concentration of the additive in the remaining liquid increases. Consequently, the freezing point temperature of remaining liquid decreases. Therefore by increasing the mass fraction of ice the equilibrium temperature of ice slurry decreases.

The ice mass fraction is calculated from

$$c_i = \frac{c_{cf}(\vartheta) - c_A(\vartheta_0)}{c_{cf}(\vartheta)} \qquad\qquad 7.1$$

where $c_A(\vartheta_0)$ is the initial additive concentration giving the solution freezing point and $c_{cf}(\vartheta)$ is the additive concentration of the carrier fluid.
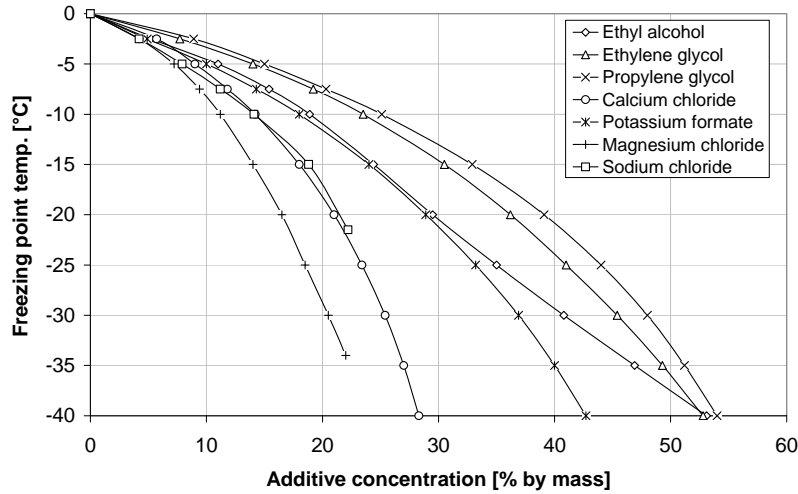
Figure 7.1 Freezing point temperature vs. additive concentration (Melinder, 1997)

Equation 7.1 shows that the ice concentration is closely linked to the slope of the freezing point curve between considered temperatures. Therefore a fluid with flatter freezing point curve will give higher ice mass fractions for a given temperature difference in comparison to the fluid with a steeper curve. Moreover ice slurries with lower additive concentration will be more "efficient" since the additives affect the thermophysical properties of the fluid unfavourably.

7.1.2 Density
The density of ice slurries can be estimated with following equation

$$\rho_{is} = \frac{1}{\dfrac{c_i}{\rho_i} + \dfrac{1-c_i}{\rho_{cf}}} \qquad\qquad 7.2$$

where ρ_i is ice density and ρ_{cf} is density of the remaining liquid.

Generally, density of ice slurry is lower than the density of the single phase fluid due to the low density of ice. The difference between ice and liquid densities result in buoyancy forces to the ice particles which causes stratification of the fluid in pipes and storage tank. The problem is more emphasized for salts and low temperature applications than for alcohols and medium temperature applications. In the other hand ice slurries with higher density have better transport and transfer properties.

7.1.3 Enthalpy, apparent heat capacity and volumetric enthalpy change
The enthalpy of ice slurry can be expressed as follows

$$h_{is} = h_i(\vartheta) \cdot c_i + h_{cf}(c_{cf}, \vartheta) \cdot (1 - c_i) \qquad\qquad 7.3$$

where h_i is enthalpy of ice. The enthalpy of the carrier fluid is given by

$$h_{cf}(c_{cf}, \vartheta) = h_{w,R} + \Delta h_M(c_{cf}, \vartheta) + \int_{\vartheta_R}^{\vartheta_{cf}} c_p \cdot d\vartheta \qquad\qquad 7.4$$

where c_{cf} is concentration of the carrier fluid, is $h_{w,R}$ the enthalpy of water at reference temperature (at 0 °C the enthalpy is 0 kJ/kg) and Δh_M is heat of mixing (IIR, 2005a).

The enthalpy of ice is expressed by equation

$$h_{\mathrm{i}} = -332.4 + \vartheta \cdot \left(2.12 + 0.008 \cdot \vartheta\right) \qquad\qquad 7.5.$$

Since heat capacity of ice slurry includes both sensible and latent heat it is referred to as an apparent heat capacity. It is calculated as

$$c_{p,\mathrm{is}} = \left(\frac{\partial h_{\mathrm{is}}}{\partial \vartheta}\right)_{p=\mathrm{const}} \qquad\qquad 7.6.$$

Since apparent heat capacity is directly proportional to the slope of the freezing curve a flatter freezing curve would yield higher apparent heat capacity. Available latent heat has its maximum at low additive concentrations and at temperatures just below the freezing point where a certain concentration of ice can be produced or melted with a small temperature change. Thereby ice slurries with low additive concentrations and initial freezing temperature close to 0 °C would show higher apparent heat capacities than ice slurries with higher solute concentrations.

Change of ice slurry density and apparent heat capacity with ice mass fraction for ethyl-alcohol and sodium chloride water mixture for initial freezing temperature of -4.4 °C is shown in Figure 7.2.

The volumetric heat transport capability of a fluid is equal to the volumetric enthalpy change for a certain temperature change between the fluid inlet and outlet of the cooling object and is calculated as

$$\frac{\Phi}{\dot{V}} = \rho_{\mathrm{is}} \cdot \Delta h_{\mathrm{is}} \qquad\qquad 7.7$$

where Φ is cooling capacity and $\dot{V}$ volume flow rate of ice slurry.

The higher the volumetric enthalpy change the more reduced size of the piping system. For cooling, i.e. medium temperature applications, the volumetric enthalpy change can be 7 to 10 times higher for ice slurries than for single phase fluid. For freezing applications this ratio is between 2 and 2.5. As reported by Melinder (2003) calcium chloride, potassium formate and ethyl alcohol show the highest values.
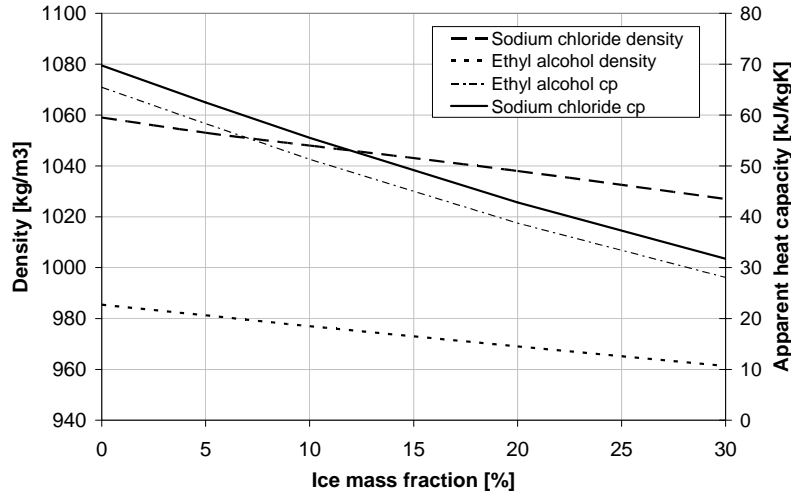
Figure 7.2 Density and apparent heat capacity versus ice mass fraction of ethyl-alcohol and sodium chloride water mixture for initial freezing temperature of -4.4 °C

7.1.4 Thermal conductivity

Thermal conductivity of the fluid affects the heat transfer in heat exchangers. There are several models to calculate thermal conductivity of the ice slurry. In the thesis the Maxwell-Eucken model was used,

$$
\lambda_{is} = \lambda_{cf} \cdot \frac{1 + 2 \cdot c_{i,vol} \cdot y}{1 - c_{i,vol} \cdot y}; \quad y = \frac{1 - \dfrac{\lambda_{cf}}{\lambda_i}}{2 \cdot \dfrac{\lambda_{cf}}{\lambda_i} + 1} \qquad 7.8
$$

where λ_{cf} and λ_i are thermal conductivities of the carrier fluid and ice, and $c_{i,vol}$ is the volume fraction of ice calculated as

$$
c_{i,vol} = \frac{c_i}{c_i + (1 - c_i) \cdot \dfrac{\rho_i}{\rho_{cf}}} \qquad 7.9.
$$

Due to the high thermal conductivity of ice the thermal conductivity of ice slurry increases with increase of ice content (Figure 7.3). For cooling applications and for temperature change of 3 to 5 °C the thermal conductivity of ice slurry is 1.5 to 2 times higher than for single phase fluid.

According to Melinder (2003) salts (sodium chloride and potassium formate) show highest values for both cooling and freezing applications.

7.1.5 Dynamic viscosity

Dynamic viscosity of the fluid affects the pressure drop of the system and its required pumping power. There are many models to estimate the viscosity of ice slurries. In the thesis the Thomas model was used,

$$\eta_{is} = \eta_{cf} \cdot \left(1 + 2.5 \cdot c_{i,vol} + 10.05 \cdot c_{i,vol}^2 + 0.00273 \cdot e^{16.6 \cdot c_{i,vol}}\right) \qquad 7.10.$$

It is an empirical model for calculating the dynamic viscosity of a Newtonian suspension which takes both concentration of the solid phase and the interaction between the particles (spherical) into consideration. The model is valid for particle concentration up to 62.5 %.

The dynamic viscosity of ice slurry increases rapidly with increase of ice concentration. For cooling applications and for ice concentration of 30-34 %, dynamic viscosity of ice slurry become 1.5 to 3 times higher than for single phase fluid. According to Melinder (2003) the fluid with the highest viscosity is ethyl-alcohol followed by propylene and ethylene glycol. Viscosity of salts is typically half the viscosity of ethyl alcohol.
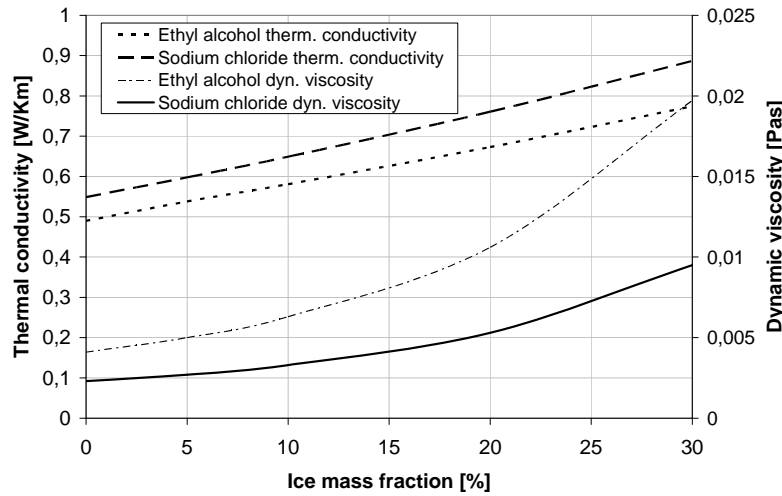
Figure 7.3 Thermal conductivity and dynamic viscosity versus ice mass fraction of ethyl-alcohol and sodium chloride water mixture for initial freezing temperature of -4.4 °C

For freezer applications the ice slurry viscosity of salts are the lowest. The viscosity of propylene glycol is by far the highest and generally not

acceptable. The viscosity of ethyl alcohol is also rather high but maybe acceptable.

The relative property change of ethyl-alcohol water mixture, with initial freezing temperature of -4.4 °C, versus ice mass fraction is shown in Figure 7.4. As may be seen the dynamic viscosity shows highest relative increase, more than 4.5 times higher than for single phase fluid for an ice mass fraction of 30 %. In the same range of ice mass fraction thermal conductivity increased approximately 50 % while apparent heat capacity decreased 50 %. Density showed only slight relative change.
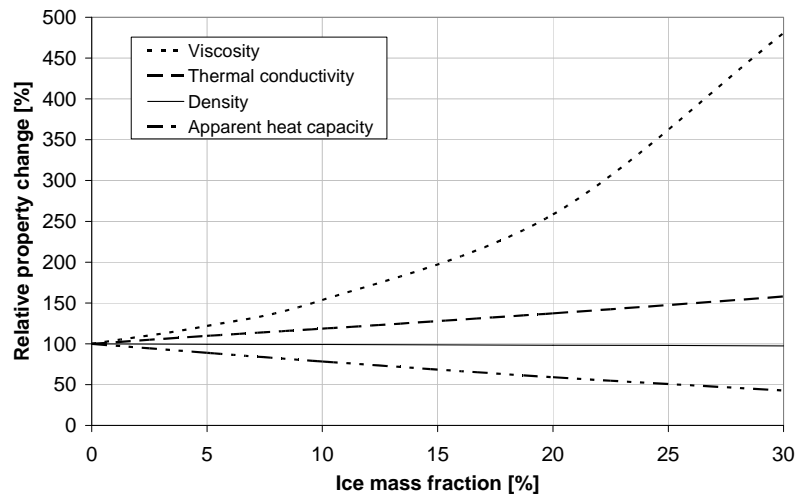
Figure 7.4 Relative property change versus ice mass fraction for ethyl-alcohol water mixture with initial freezing temperature of -4.4 °C

8 Experimental investigation of ice slurry flow pressure drop in horizontal tubes

Pressure drop behaviour of ice slurry based on ethanol-water mixture in circular horizontal tubes has been experimentally investigated. The secondary fluid was prepared by mixing ethyl alcohol and water to obtain initial alcohol concentration of 10.3 % (initial freezing temperature -4.4 °C). The pressure drop tests were conducted to cover laminar and slightly turbulent flow with ice mass fraction varying from 0 % to 30 % depending on test conditions. Results from flow tests reveal much higher pressure drop for higher ice concentrations and higher velocities in comparison to the single phase flow. However for ice concentrations of 15 % and higher, certain velocity exists at which ice slurry pressure drop is same or even lower than for single phase flow. It seems that higher ice concentration delay flow pattern transition moment (from laminar to turbulent) toward higher velocities. In addition experimental results for pressure drop were compared to the analytical results, based on Poiseulle and Buckingham-Reiner models for laminar flow, Blasius, Darby and Melson, Dodge and Metzner, Steffe and Tomita for turbulent region and general correlation of Kitanovski which is valid for both flow regimes. For laminar flow and low buoyancy numbers Buckingham-Reiner method gives good agreement with experimental results while for turbulent flow best fit is provided with Dodge-Metzner and Tomita methods.

Furthermore, for transport purposes it has been shown that ice mass fraction of 20 % offers best ratio of ice slurry transport capability and required pumping power.

8.1 Introduction

During the last ten years a lot of research has been done in field of ice slurry technology but with varying outputs and different conclusions. Many researchers reported investigation on ice slurry pressure drop and rheology (Hansen and Kauffeld, 2000; Zelasko and Zalewski, 2006; Jen-

83

sen et al., 2000; Frei and Egolf, 2000; Guilpart et al., 1999; Kauffeld et al., 1999; Knodel et al., 2000; Kitanovski and Poredos, 2002; Doetsch, 2001; Stutz and Reghem, 2001). Regarding ice slurry rheology they basically agree that ice slurry shows non-Newtonian behaviour for ice content higher than 10 %, where the viscosity is a function of shear rate. Several models of viscosity have been proposed among which the Thomas relation is the most stressed out. According to Hansen and Kauffeld (2000) and Zelasko and Zalewski (2006) Thomas equation overpredicts the viscosity at ice content higher than 15 %.

Reports on ice slurry pressure drop by Jensen et al. (2000), Frei and Egolf (2000), Kauffeld et al. (1999) indicate increase in pressure drop with increasing ice mass fraction what is generally supported by other researchers (IIR, 2005a; Doetsch, 2001). In contrary, Knodel et al. (2000) reported decrease in pressure drop up to the ice mass fraction of 15 %. They have experimented with large size of ice particles; 5 mm in average. Liu et al. (1997) came to similar conclusions, i.e. pressure drop increases with increasing velocity but decreases with increasing ice mass fraction. Recently Zelasko and Zalewski (2006) conducted extensive research on ice slurry flows. For the same ice slurry velocity and at the certain ice concentration threshold they observed rapid decrease in pressure drop as an ice mass fraction increased. This phenomenon was attributed to changes in flow behaviour, i.e. shift from turbulent to laminar. Once the flow became laminar an increase in ice concentration resulted in pressure drop to start rise again.

In order to investigate pressure drop behaviour of ice slurry in horizontal tubes and to contribute to clarification of these contradicting results published to this date series of experimental pressure drop experiments have been conducted.

8.2 Experimental setup

8.2.1 Experimental apparatus
The experimental set-up designed and built at the Division of Applied Thermodynamics and Refrigeration, Royal Institute of Technology consists of an ice generator, a measurement loop and a data acquisition system, Figure 8.1. An ice slurry storage tank of 60 litres separates the ice generator and measurements cycles. The main components of the measurement loop are: the volumetric pump of lobe type, the Coriolis mass flow meter, and four measurement loops. Three of the measurement loops serves for pressure drop investigation under isothermal conditions. They are stainless steel circular horizontal tubes with inner dimensions of 9, 15 and 25 mm in diameter. Each tube is equipped with two pressure

taps with a distance of 1.2 m connected to three parallel Druck pressure transducers (range of 0.35, 1 and 3.5 bar). For the purpose of this investigation the pressure transducer with the smallest range, 0.35 bar, was used. The fourth pipe is 21 mm in diameter and is intended to serve for heat transfer measurements. The pipe consists of two measuring sections of stainless steel as inlet and outlet of the pipe and the pipe section in between the measuring sections are made of transparent plastic. Both measuring sections are equipped with 20 thermocouples to measure the wall temperature. The thermocouples are soldered to the wall in grooves that are 1 mm deep, i.e. approximately 3 mm from inner tube surface. The wall temperature is measured at five positions along each measuring section and at each position the temperature is measured on top, below and on each side of the pipe. On top of each measuring section with their 20 thermocouples a resistance thread is twisted. By means of a variable voltage transformer one can control the supplied voltage to the resistance thread.

All four loops are equipped with two PT-100 temperature sensors at inlet and outlet which has been calibrated with an accuracy of 0.015 °C (Table 8.1). The velocity in the loops is regulated by means of the frequency controlled pump. A Coriolis mass flow meter is used to measure mass flow rate and density of the ice slurry prior inlet to the test section. The ice mass fraction was measured continuously, i.e. simultaneously determined based on two parameters, temperature and density.

Table 8.1 List of measuring instrumentation

Instrument	Type	Range	Accuracy
Differential pressure transducers	Druck PCDR 2100	0 – 0.35 bar	± 0.1 %
Temperature sensors	Pt100 Omega engineering	-100°C – 400°C	± 0.015 °C
	T-type thermocouples	-100°C – 350°C	± 0.1 °C
Mass (density) flow meter	Micro Motion	density	± 0.5 kg/m3
		mass flow	± 0.1 %
Power meter	Hameg HM8115	0 – 8 kW	± 0.5 %
Data acquisition unit	Agilent 34970A	-	-

The ice generator is of brush type where the ice is formed on the bottom disc in the storage tank. The ice is then removed by means of the brush that rotates in the middle of the tank. On the shaft in the middle of the tank two agitators are placed, one "boat propeller" and one Visco-jet. Both the brush and the agitators are frequency controlled. The agitators are rotating in the opposite direction to the brush. The brush, the agitators and the pump guarantee a homogenous suspension in the tank. The refrigerant in the vapour compression cooling machine is R404A. The evaporator of the cooling machine is placed in the bottom of the tank and forms the bottom disc of the tank on which the ice is formed.
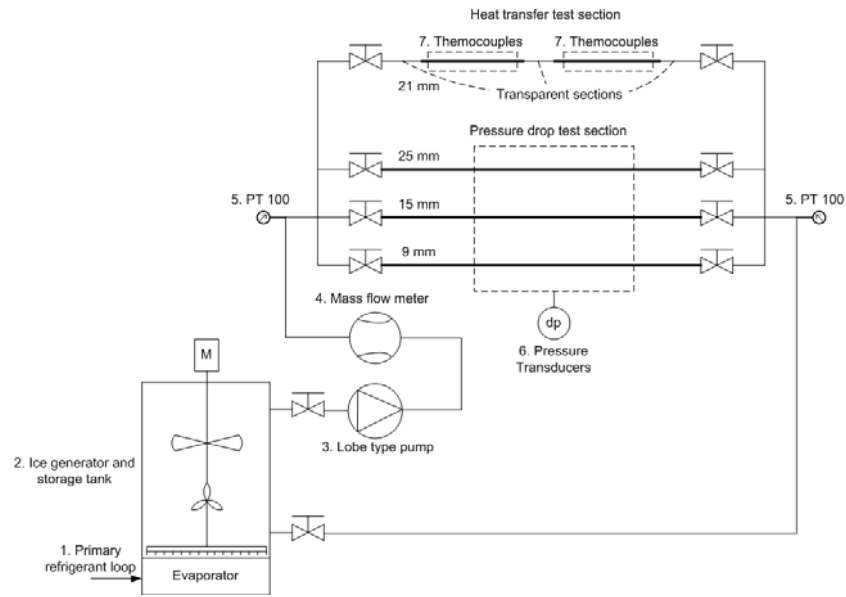
Figure 8.1 Layout of the simplified flow chart of the experimental setup

8.2.2 Experimental procedure

The experimental investigation of the ice slurry flow behaviour was conducted on the aqueous solution of ethyl alcohol with initial concentration of 10.3 % by weight (freezing point -4.4 °C).

For pressure drop measurements the ice slurry was produced continuously until desired ice concentration level was reached. During ice production the ice generator as well as pump was running continuously to ensure a homogeneous fluid in the tank. Since the quality of ice slurry mixtures are time dependant, pressure drop tests were carried out approximately seven hours after the liquid reached the freezing point. Tests were designed to cover laminar and slightly turbulent flow.

Each series contained pressure drop measurements at thermodynamic equilibrium at one temperature level and for a range of different velocities. Bulk temperatures of ice slurry were measured at inlet and outlet of the measuring section by Pt100 temperature sensors. During tests no heat flux was applied. One batch of ice slurry was used for measurements in all three tubes. Each point in a series was measured during 8 minutes and included approximately 70 readings. To minimize the influence of the ambient all test sections were heavily insulated.

Ice mass fraction of flowing slurry was calculated as an arithmetic average of ice concentrations determined by density measurements

86

$$c_i = \frac{\rho_i(\vartheta) \cdot \left[\rho_{cf}(\vartheta) - \rho_{is}\right]}{\rho_{is} \cdot \left[\rho_{cf}(\vartheta) - \rho_i(\vartheta)\right]}$$

8.1

and temperature measurements

$$c_i = \frac{c_{cf}(\vartheta) - c_A(\vartheta_0)}{c_{cf}(\vartheta)}$$

8.2

where $c_A(\vartheta_0)$ is the initial additive concentration giving the solution freezing point and $c_{cf}(\vartheta)$ is the additive concentration of the carrier fluid, i.e. remaining liquid obtained according to Melinder (1997). According to Hansen et al. (2002) estimation of ice concentration by combining both methods leads to more accurate results than by using solely temperature or density measurements.

The maximal uncertainty of the determination of the ice concentration based on combination of temperature and ice slurry density measurements was calculated as $u_{ci}=\pm0.26$ % where the individual methods were weighted with u^{-2} (Hansen et al., 2002).

8.3 Results and Discussion

An overview of the operating conditions for performed experiments are presented in Table 8.2.

Table 8.2 Operating conditions

Exp. series	Experiment	Pipe diameter (inner) [mm]	Ice mass fraction	Heat flux [kW/m²]	Mean velocity range [m/s]
1	Pressure drop	9	5-30 %	0	0.2 – 2
2		15	5-30 %	0	0.2 – 2
3		25	5-30 %	0	0.2 – 1.2

8.3.1 The behaviour of ice slurries over time

Since ice slurries are time dependant, i.e. ice crystal size and shape are changing with time due to processes of attrition, agglomeration and Ostwald ripening (IIR, 2005a) a temporal pressure drop variation during stable operating condition is expected. In order to investigate the effect of this phenomenon pressure drop was monitored during period of 8 hours for which the solution was subjected to cooling. Figure 8.2 shows pressure drop and ice mass fraction versus time for 15 mm tube. Varia-

tion in temperature and density during test is displayed on Figure 8.3 From the point where the temperature reached its target value of -5.25 °C which corresponds to ice concentration of approximately 15 %, mass flow rate, i.e. velocity of ice slurry was held constant as shown on Figure 8.4.
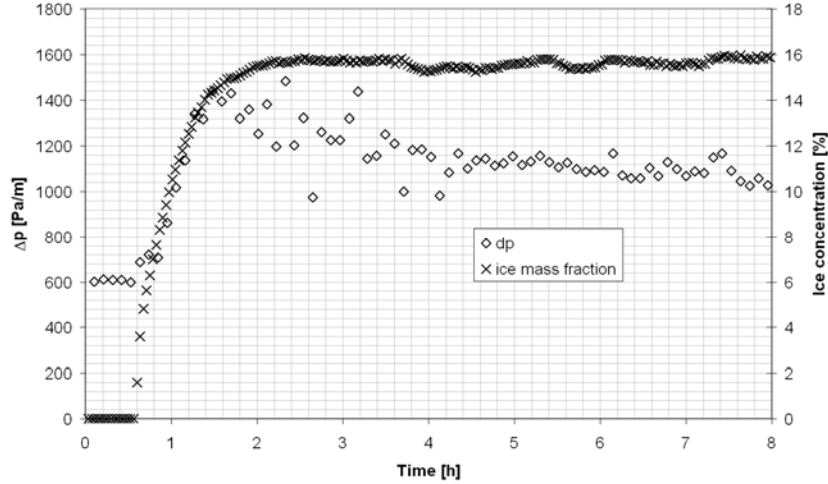
Figure 8.2 Ice slurry pressure drop and ice mass fraction versus time for d_i=15 mm

In this process four different zones could be clearly distinguished as presented from Figure 8.2 to Figure 8.4. The first zone corresponds to a period from the experiment start up to 40th minute where the point of freezing is reached. During this period the mixture is in liquid phase and shows constant pressure drop of 600 Pa/m while the temperature is linearly decreasing from -3.7 °C to -4.3 °C. Due to the small temperature change density of solution decreases slightly from 981.8 kg/m³ to 981.6 kg/m³. During this first period of experiment the temperature of the solution was above freezing point indicating that only liquid was present inside the test section. Velocity was constant, Figure 8.4, and only the temperature of the solution was decreasing due to cooling, causing only a small change in density and viscosity and consequently Reynolds number. Due to the small change in Reynolds number, and the fact that the solution is in liquid state (common Blasius correlation for friction factor applies) it is obvious to expect pressure drop to be fairly constant during the observed period.

The second period lasts from 40th minute where the first ice particle is formed up to one hour and 40 minutes where the desired ice slurry concentration is reached. In that period temperature is decreasing as well as ice slurry density indicating that more ice particles have been produced,

88

see Figure 8.4. Due to the rise of ice concentration during that period viscosity of ice slurry increases respectively. At the same time velocity has increased slightly, 0.1 m/s on the average, which is directly connected to the characteristics of the lobe pump used to transport the ice slurry from ice generator to the test section. During the course of experiment the rotational speed of the pump was held constant. The viscosity increase and density decrease during this period is more emphasized than the influence of velocity, yielding the Reynolds number to decrease from 2500 to 1500. As it can be seen from Figure 8.2 in that period the pressure drop increases from 600 Pa/m up to 1400 Pa/m. At the second hour ice concentration of approximately 15 % is reached and the corresponding pressure drop is the maximal 1400 Pa/m. For that time ice slurry is fresh and ice crystals have just been created in the ice generator.
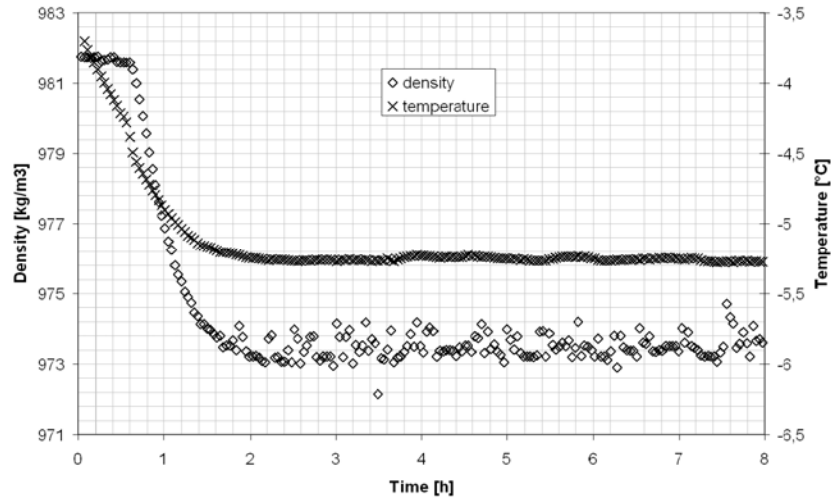
Figure 8.3 Ice slurry temperature and density versus time for d_i=15 mm

The third section (starts at one hour and 40th minutes and lasts to four hours and 30th minutes) is characterized with a decrease in pressure drop from 1400 Pa/m to 1050 Pa/m and by larger scattering of data than for other periods. During that time operating conditions are held constant yielding a constant Reynolds number and ice concentration. It is believed that the change in size and shape of ice particle due to high shear stresses to which ice slurry is subjected in pump and during mixing inside ice generator tank can explain pressure drop behaviour. Also it is believed that higher fluctuations in pressure drop in this region is connected with pump behaviour since it is transporting the fluid in pulses.

The fourth region lasts from 4:30 to 8:00 and shows almost constant pressure drop over time. During that period velocity, temperature, ice slurry density and corresponding ice fraction are constant.

In the third and fourth period one can notice certain variations in density. It is believed that these variations are not connected to the accuracy of the mass flow meter. They are probably the result of small air bubbles which are incorporated in slurry flow during vigorous mixing in ice generator tank. This was observed by taking ice slurry samples from generator tank during the course of experiment. Due to influence of air bubbles on overall density of ice slurry, the ice mass content was determined as an average of density or temperature method.
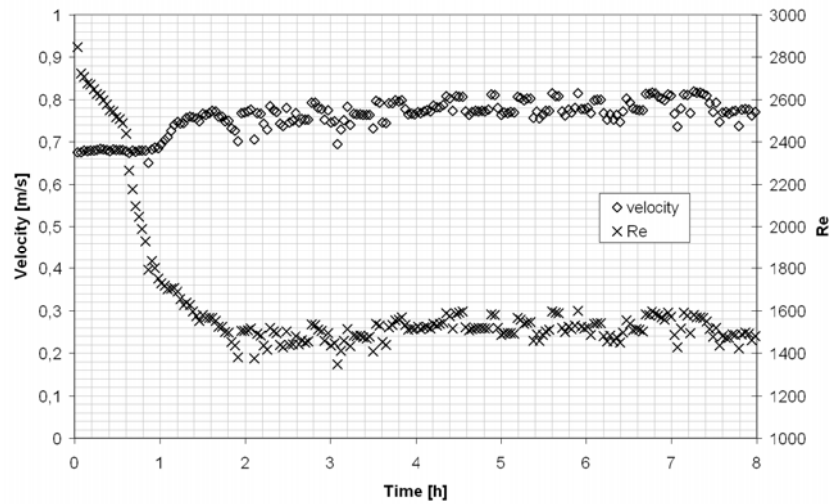
Figure 8.4 Ice slurry velocity and Reynolds number versus time for d_i=15 mm

This test revealed the time dependency of an ice slurry mixture and that it is necessary to run each pressure drop test after certain period of time allowing for mixture to reach the point where the time variation of pressure drop is reasonable small. Although the process of ice ripening doesn't stop at that time, it is a rather slow process; the pressure drop decrease after seventh hour is small enough to allow for the testing process to commence.

8.3.2 Pressure drop

Generally the pressure drop for single phase incompressible, adiabatic flows inside circular tubes is dependant on solution velocity, density, viscosity, tube length, and diameter and wall roughness

$$\Delta p = \Delta p(w_m, \rho, \eta, L, d, \varepsilon) \qquad 8.3.$$

If dimension analysis is performed pressure drop can be expressed with relation

$$\frac{\Delta p \cdot d}{\frac{1}{2} \cdot \rho \cdot w_m^2 \cdot L} = F\left(\frac{\rho \cdot w_m \cdot d}{\eta}, \frac{\varepsilon}{d} \right) \qquad 8.4$$

where pressure drop term is function of two dimensionless numbers, first representing Reynolds number and second the surface roughness term. For ice slurry flow three variables which influence pressure drop could be added, ice mass fraction, diameter and density of ice particles.

$$\frac{\Delta p \cdot d}{\frac{1}{2} \cdot \rho \cdot w_m^2 \cdot L} = F\left(\frac{\rho \cdot w_m \cdot d}{\eta}, \frac{\varepsilon}{d}, c_i, \frac{d_{ip}}{d}, \frac{g \cdot \Delta \rho \cdot d}{\rho \cdot w_m^2} \right) \qquad 8.5$$

where c_i stands for ice mass fraction, $\dfrac{d_{ip}}{d}$ ice particle diameter term and the last term $\dfrac{g \cdot \Delta \rho \cdot d}{\rho \cdot w_m^2}$ is a ratio of buoyancy and inertial forces responsible for stratification processes during flow. Influence of the buoyancy term becomes important for low flow velocity, large tube diameters and high density differences between ice particles and carrier fluid. These three variables, ice mass fraction, diameter and density of ice particles are directly related to the thermophysical properties of ice slurry, i.e. they determine its density and viscosity. Therefore it is physically correct to make correlation with non-dimensional numbers dependant on ice slurry properties. In this way ice concentration is not any more a parameter that is directly connected to friction factor, it is rather incorporated through ice slurry thermophysical properties. In the case of ice slurry flow eq. 8.5 is still valid, but thermophysical properties are now related to the ice slurry instead of carrier fluid

$$\frac{\Delta p \cdot d}{\frac{1}{2} \cdot \rho_{is} \cdot w_m^2 \cdot L} = F\left(\frac{\rho_{is} \cdot w_m \cdot d}{\eta_{is}}, \frac{\varepsilon}{d}, \frac{d_{ip}}{d}, \frac{g \cdot \Delta \rho \cdot d}{\rho_{cf} \cdot w_m^2} \right) \qquad 8.6.$$

According to the eq. 8.6 the pressure drop is function of ice slurry mean velocity, tube diameter, length and wall roughness, diameter and density

of ice particles, density of the carrier fluid and density and viscosity of ice slurry. The latest two properties are function of ice mass fraction, density and diameter of ice particles and the thermophysical properties of the carrier fluid, i.e. density and viscosity which are dependant on solution temperature and initial additive concentration.

Size of ice particles were not experimentally determined, instead it is believed that the average size of ice particles is 0.3 mm (IIR, 2005a). Moreover surface roughness was not considered in this analysis; it is assumed that the pipes are hydraulically smooth.

In order to explain pressure drop of ice slurry flow inside horizontal tubes and to find proper correlations to describe it, series of experimental tests were carried out as indicated in Table 8.2. Three main variables were varied during the test, ice mass fraction, and tube diameter and ice slurry velocity. In Figure 8.5 to Figure 8.7 measured pressure drop as a function of a mean velocity for 9 mm, 15 mm and 25 mm tube is shown.
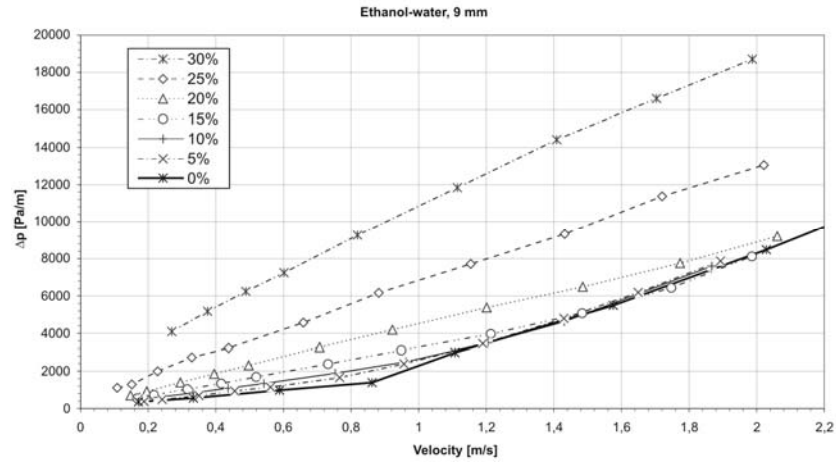
Figure 8.5 Pressure drop versus ice slurry velocity for d_i=9mm

Basically one can notice increase in pressure drop with increasing velocity, higher ice fraction (i.e. lower operating temperature) and reduced pipe dimension. In addition to the measured pressure drop of ice slurry, pressure drop for single phase flow (0 %) is plotted on figures as well. As it can be seen from Figure 8.8 and Figure 8.11 the measured pressure drop of a single phase flow is in a good agreement with the Poiseuille correlation for laminar flow and the Blasisus correlation for turbulent flow regime for 9 mm and 15 mm tube. Somewhat higher pressure drop and corresponding friction factor is observed for 25 mm tube in both flow regimes.

92
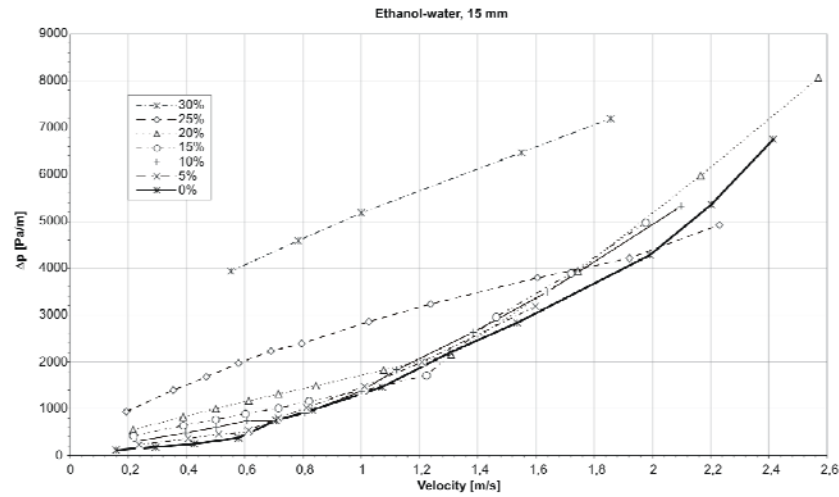
Figure 8.6 Pressure drop versus ice slurry velocity for d_i=15 mm

For 9 mm tube one can see that in laminar region pressure drop of ice slurry is always higher than for single phase flow. In turbulent region for velocities greater than 1.5 m/s pressure drop of ice slurry up to 15 % of ice mass fraction is the same as for single phase fluid.
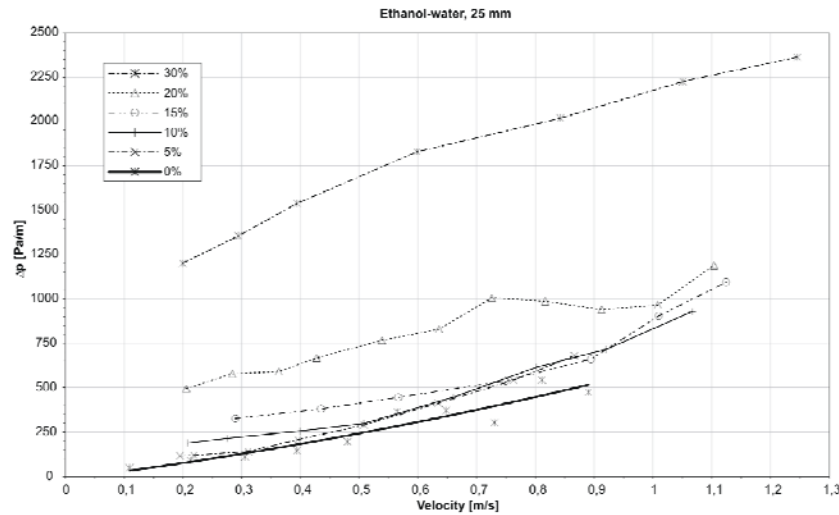
Figure 8.7 Pressure drop versus ice slurry velocity for d_i=25 mm

As can be seen in Figure 8.6 for the 15 mm tube pressure drop increases with increasing ice mass fraction and velocity. Yet for flow with ice concentrations of 15 % and more one can notice several experimental points with lower pressure drop of ice slurry flow than for single phase fluid. Higher ice concentrations seem to delay flow pattern transition moment

93

(from laminar to turbulent) toward higher velocities. After turbulent flow is established pressure drop starts to rise again and shows larger pressure drops than single phase flow.

The 25 mm tube shows that even for low ice concentrations the pressure drop of ice slurry is higher than for liquid only flow. Still, the same phenomenon as for 9 mm and 15 mm tubes can be observed; with increasing ice concentration the flow pattern transition moment is shifting to higher velocities.

To investigate the influence of non dimensional parameters to pressure drop, friction factor:

$$f = \frac{\Delta p \cdot d}{\frac{1}{2} \cdot \rho_{is} \cdot w_{m}^{2} \cdot L}$$
8.7

is plotted against ice slurry Reynolds number for fixed ice concentration and tube diameter on Figure 8.8 Reynolds number was calculated according to mean velocity, tube diameter, density and viscosity of ice slurry

$$Re = \frac{d \cdot w_{m} \cdot \rho_{is}}{\eta_{is}}$$
8.8

whereas density and flow velocity were measured while viscosity of ice slurry was determined according to Thomas relation

$$\eta_{is} = \eta_{cf} \cdot \left(1 + 2.5 \cdot c_{i,vol} + 10.05 \cdot c_{i,vol}^{2} + 0.00273 \cdot \exp^{16.6 \cdot c_{i,vol}}\right)$$
8.9

where $c_{i,vol}$ stands for volume fraction of ice in the ice slurry mixture

$$c_{i,vol} = \frac{c_{i}}{c_{i} + (1 - c_{i}) \cdot \dfrac{\rho_{i}}{\rho_{cf}}}$$
8.10.

In addition to the measured results, the Poiseulle correlation for laminar and the Blasius correlation for turbulent single phase flow are drawn in Figure 8.8 as well.

It is possible to observe three groups of experimental data formed, each corresponding to a different tube diameter. As the tube diameter in-

94

creases friction factor increases as well. The highest deviation from theoretical friction factor based on Poiseulle correlation is observed for the largest tube. Difference in friction factor between each tube is increasing as Reynolds number decreases, i.e. inclination angle of experimental data group to Reynolds axis is getting higher with increasing ice concentration and with increasing tube diameter. Furthermore, it is shown that in laminar flow regime the friction factors based on experimental measurements are always higher than analytically determined according to Poiseulle correlation. For certain tube diameter, with increasing ice concentration, for the most cases the friction factor rises as well. This effect is hardly notable for ice concentrations of 5, 10 and 15 %, but even for this ice fractions the deflection from theoretical friction factor is observed and it is more emphasised with decreasing Reynolds number. For ice concentrations ranging from 20 % to 30 % significant increase in friction factor is observed compared to lower ice concentrations.
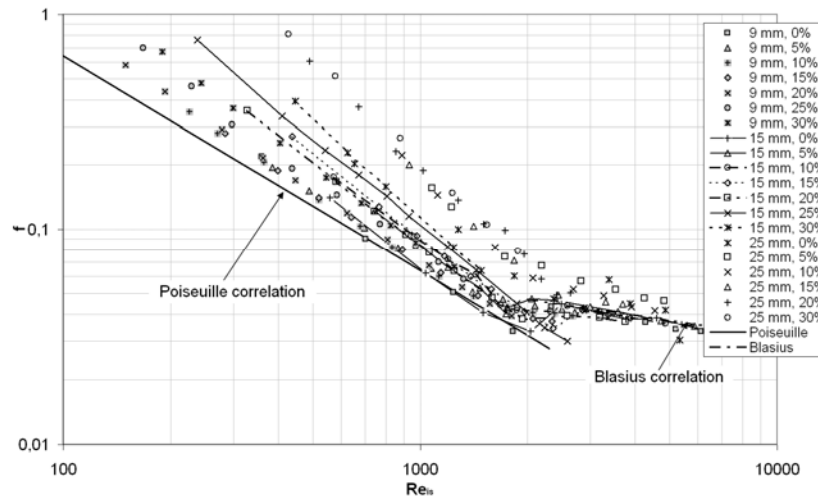
Figure 8.8 Friction factor versus ice slurry Reynolds number

Flow pattern transition, from laminar to turbulent is observed within range of Reynolds number from 1700 to 2500, depending on tube diameter and ice concentration. As the ice concentration increases critical Reynolds number where transition occurs increases as well and can reach higher values than for single phase flow, Re_c=2300. This phenomenon allows for pressure drop of concentrated ice slurry flow to be lower than pressure drop for single phase fluid, see Figure 8.5, Figure 8.6 and Figure 8.8. This is in consent with findings of other researchers (IIR, 2005a; Zelasko and Zalewski, 2006), since higher ice concentrations tend to homogenize the flow making it more resilient to higher kinetic turbulence energies.

95

As it is shown in Figure 8.8 classical model for prediction of laminar friction factor for single phase flow based on Poiseulle flow in tubes,

$$f = \frac{64}{Re_{is}}$$

8.11

for Reynolds numbers up to 2300, poorly predicts experimental results. As it can be seen discrepancies between measured and calculated friction factor is increasing with decreasing Reynolds number.

Only for the smallest tube (9 mm), for very limited span of Reynolds numbers (from 700 to 1700) and ice concentrations below 20 % the discrepancy between calculated and measured pressure drop is below 10 %. This is not the case for tubes of 15 and 25 mm which basically show much higher pressure drop even for low ice mass fractions than calculated with eq. 8.11.

The reason for such behaviour is that larger mean velocities (but still laminar flow regime) in smaller tubes tend to make the flow more homogeneous, with more uniform distribution of ice particles across the tube cross section, while for low mean velocities and large tube diameters, a heterogeneous flow occurs with higher ice concentration at the pipe top and lower at the bottom. In turn this affects local ice slurry viscosity (which is higher at pipe top and lower at pipe bottom) and as a result distorted velocity profile, with lower velocities at pipe top and higher at pipe bottom which consequently lead to higher mean friction factor.

The most referred correlation for friction factor prediction of a non Newtonian fluids in laminar flow regime which is found in literature is given by Buckingham-Reiner (IIR, 2005a):

$$f = \frac{64}{Re_{is}} \cdot \left[1 + \frac{He}{6 \cdot Re_{is}} - \frac{He^4}{3 \cdot f^3 \cdot Re_{is}^7} \right]$$

8.12

where Hedstrom number is defined as:

$$He = \frac{d^2 \cdot \tau_0 \cdot \rho_{is}}{\eta_{is}^2}$$

8.13

The correlation was derived for fluids which can be classified as Bingham type.

Comparison between experimental and calculated pressure drop results based on Buckingham-Reiner method is shown on Figure 8.9. As it can be seen from Figure 8.9 experimental and calculated pressure drop are fitted with an accuracy of ±15 % for only 60 % of all experimental results in laminar region. Measurements that didn't fit the proposed correlation are mostly those for 25 mm tube. For 15 mm and 9 mm tubes the measurements that didn't fit have high ice mass concentration and low average velocities, more precisely those with high values of buoyancy term. For these conditions correlation is underestimating measured pressure drop. The lower the buoyancy term is the more accurate prediction is. The reason for such poor accuracy lays in fact that the correlation was not derived for suspensions with density difference between solid particles and liquid which is the case for ice slurry flow. The correlation was developed for fluids which exhibit symmetrical plug type velocity profile during flow. On contrary, velocity profile during laminar flow of ice slurry in horizontal tubes is never symmetric (Kitanovski and Poredos; 2002) due to buoyancy forces that act on ice particles causing uneven concentration distribution across tube cross section. Only for higher average velocities and lower ice mass concentrations, concentration profile and therefore velocity profile tends to get more symmetrical shape.
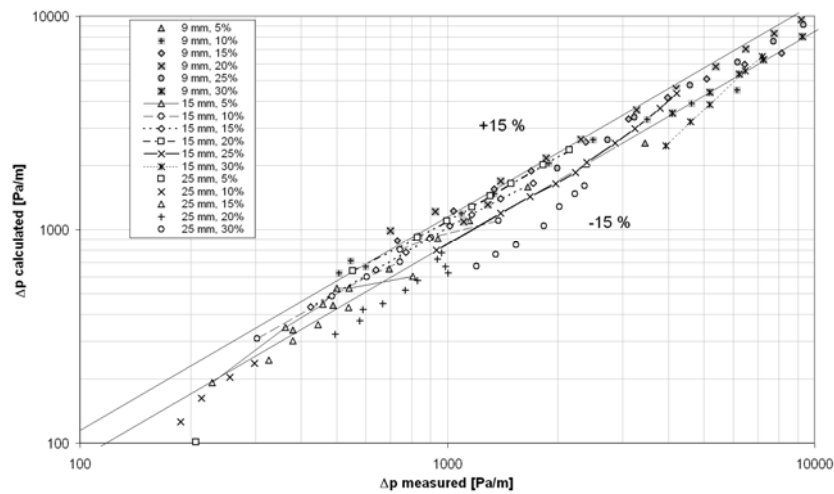
Figure 8.9 Comparison between measured and calculated pressure drop according to Buckingham-Reiner method for laminar flow

Thus, on basis of experimental results Buckingham-Reiner correlation can be used for prediction of laminar friction factor for ice slurry flow in horizontal tubes for buoyancy term less than 0.065 which is in consent to Kitanovski and Poredos (2002).

To account for stratification effect in laminar flow regime next correlation for friction factor is derived

$$f = \frac{64}{Re_{is}} \cdot \left[1 + C_1 \cdot Re_{is}^{C_2} \cdot \left(\frac{d_{ip}}{d} \right)^{C_3} \cdot \left(\frac{g \cdot \Delta \rho \cdot d}{\rho_{cf} \cdot w_m^2} \right)^{C_4} \right] \qquad 8.14$$

with coefficients C_1= 0.022, C_2= -1.480, C_3=-3.110, C_4= -0.315. It predicts 82 % of all experimental data in laminar region, up to Reynolds number of 2300 with accuracy of ±15 %. Comparison between experimentally obtained and calculated pressure drop is presented on Figure 8.10.
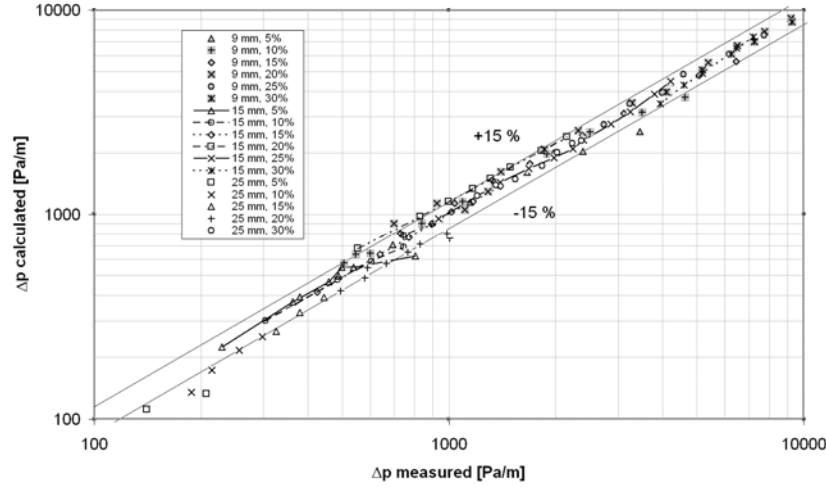
Figure 8.10 Comparison between measured and calculated pressure drop for laminar flow according to eq. 8.14

Laminar to turbulent flow transition is observed within the range of 1700 < Re_{is} < 2500. With increasing ice concentration transition moment is shifted towards higher Reynolds numbers. For turbulent flow regime, friction factor is in a good accord with Blasius correlation,

$$f = 0.316 \cdot Re_{is}^{-1/4} \qquad 8.15$$

for 9 mm and 15 mm tube and up to 15 % ice mass concentration, for which the accuracy is better than 10 %, while relatively large discrepancy was found for 25 mm tube and higher ice concentrations. 81 % of experimental data from Re_{is} > 2300 are found to satisfy Blasius equation within ±15 % margin. Points that didn't fit the correlation are those with

high ice concentration and tubes with larger diameter. Since the maximum test velocity for 25 mm tube was only 1.25 m/s due to lack in pump capacity, turbulent region was not reached for tests with ice mass concentration above 20 %.
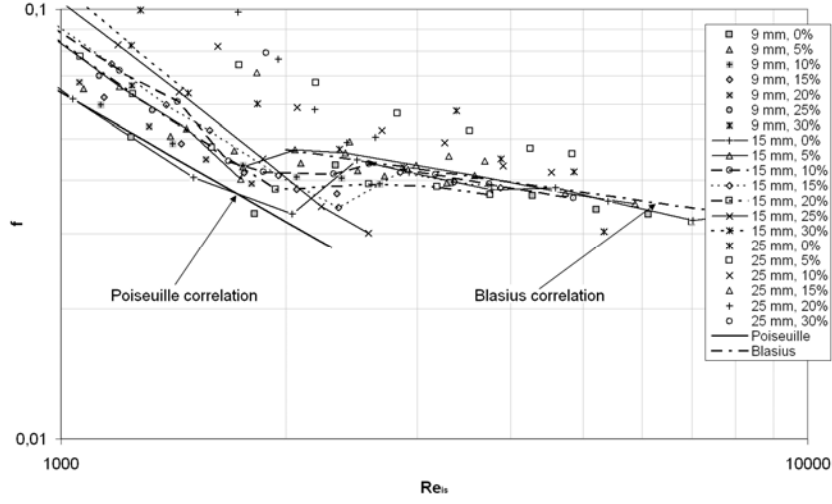
Figure 8.11 Friction factor versus ice slurry Reynolds number; turbulent region

To account for the influence of large diameter tubes and higher ice concentrations a modified Blasius correlation is proposed by Darby and Melson based on Hanks and Dadias theory for Bingham type fluids (IIR, 2005a):

$$f = \left(f_1^m + f_t^m\right)^{1/m}$$

8.16

where

$$f_t = 4 \cdot 10^a \cdot Re_{is}^{-0.193}$$

8.17

$$a = -1.378 \cdot \left[1 + 0.14 \cdot \exp^{-2.9 \cdot 10^{-5} \, Re_{is}}\right]$$

8.18

$$m = 1.7 + \frac{40000}{He}$$

8.19

and laminar friction factor f_1 which is calculated by eq. 8.12.

As it is shown on next figure proposed correlation under-predicts measured pressure drop for approximately 29 % for entire range. If adapted it would give almost 100 % fit.
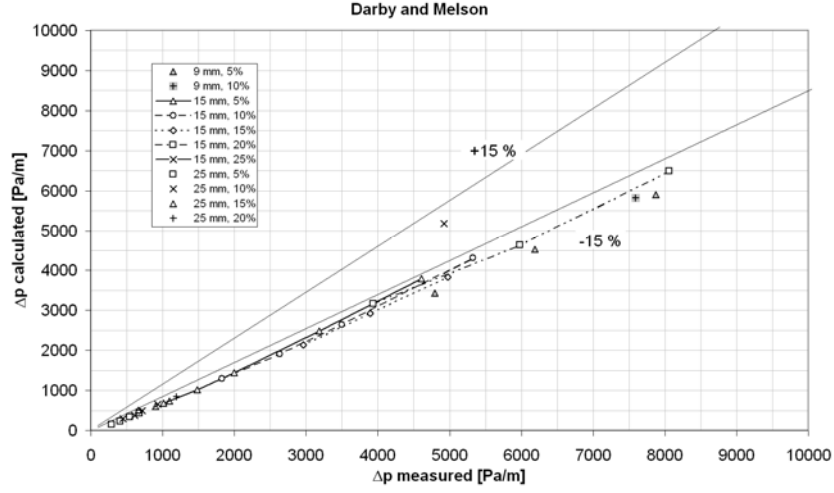
Figure 8.12 Comparison between measured and calculated pressure drop according to Darby and Melson correlation

Dodge and Metzner (IIR, 2005a) proposed correlation for turbulent friction factor of power law fluids:

$$\frac{1}{\sqrt{f}} = \frac{2}{n^{0.75}} \cdot \log_{10}\left(Re_{is} \cdot \left(\frac{f}{4}\right)^{\frac{2-n}{2}} \right) - \frac{0.2}{n^{1.2}} \qquad 8.20$$

where n is fluid behaviour index. If it is assumed that ice slurry is behaving according to Bingham fluid (n = 1) then correlation predicts measured pressure drop very good, with accuracy of ±15 % for 78 % of all experimental data above Reynolds number of 2300. Points that didn't fit the correlation are those of low Hedstrom number and are still in laminar region (see Figure 8.13, points: 9 mm tube and 10 % ice fraction; 15 mm 20 % ice fraction, one point; 15 mm 25 % ice fraction; 25 mm and 5 % ice fraction) even though the Reynolds number is quite high.

As reported by Steffe (Ayel et al., 2003) turbulent friction factor for Bingham fluid can be determined according to:

$$\frac{1}{\sqrt{f}} = 2.265 \cdot \log_{10}\left(1 - \frac{\tau_0}{\tau_{wall}}\right) + 2.265 \cdot \log_{10}\left(Re_{is} \cdot \sqrt{f}\right) - 1.832 \qquad 8.21$$

100

Only 47 % of experimental data are fitted with accuracy of ±15 % with this correlation as it tends to over predict the measured pressure drop.
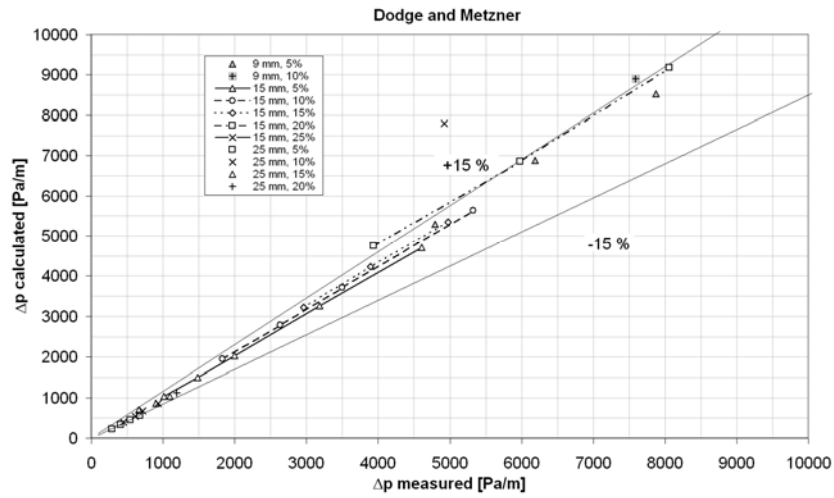
Figure 8.13 Comparison between measured and calculated pressure drop according to Dodge-Metzner correlation
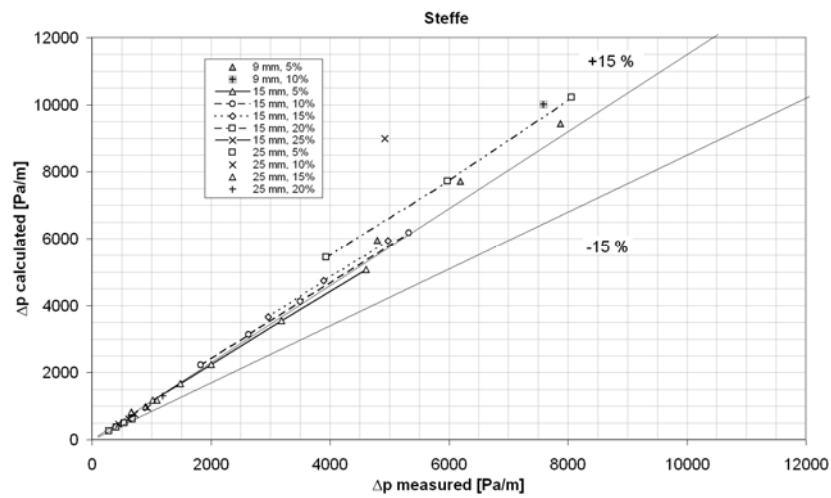
Figure 8.14 Comparison between measured and calculated pressure drop according to Steffe

Tomita (Zelasko and Zalewski, 2006) proposed a more accurate method for pressure drop calculation of ice slurry flow in turbulent region

$$\frac{1}{\sqrt{f}} = 2 \cdot \log_{10}\left(Re_{t,is} \cdot \frac{f}{2}^{0.5}\right) - 0.2 \qquad\qquad 8.22$$

$$Re_{t,is} = Re_{is} \cdot \frac{(1-\varepsilon) \cdot (\varepsilon^4 - 4 \cdot \varepsilon + 3)}{3} \qquad\qquad 8.23$$

$$\varepsilon = \frac{\tau_0}{\tau_{wall}} = \frac{4 \cdot L \cdot \tau_0}{d \cdot \Delta p} \qquad\qquad 8.24.$$

More than 68 % of experimental results are predicted in the range of ±15 %, Figure 8.15. However, it seems that correlation slightly tends to over predict the experimental results for the most values.
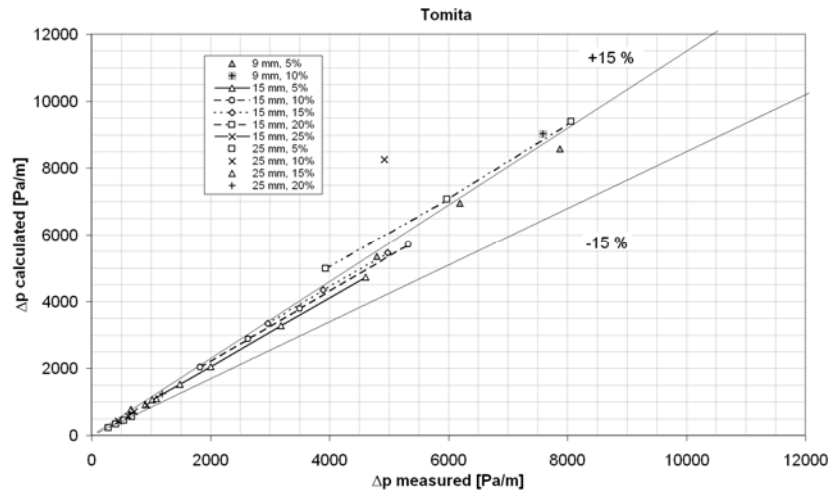
Figure 8.15 Comparison between measured pressure drop and calculated according to Tomita

Furthermore, experimental results were compared to correlation proposed by Kitanovski (IIR, 2005a) for both laminar and turbulent ice slurry flow with friction factor of a single phase flow f_f determined according to eq. 8.15

$$f_{is} = f_f + b_1 \cdot c_i^{b_2} \cdot f_f^{b_3} \cdot c_A^{b_4} \cdot \left(\frac{w_m^2}{d_i \cdot g \cdot \left| \frac{\rho_i}{\rho_{cf}} - 1 \right|} \right)^{b_5} \qquad 8.25.$$

Coefficients $b_{1...5}$ are taken for 10 % initial concentration of the additive ethanol as, b_1=650.1835; b_2=1.147015; b_3=3.8707498; b_4=1.089962; b_5=-0.649095. As it can be seen from Figure 8.16 only 40 % of all experimental data is predicted within ±15 %. With this correlation experimental results are under predicted for the most of the values. Only experimental points with high velocity are predicted within the range.
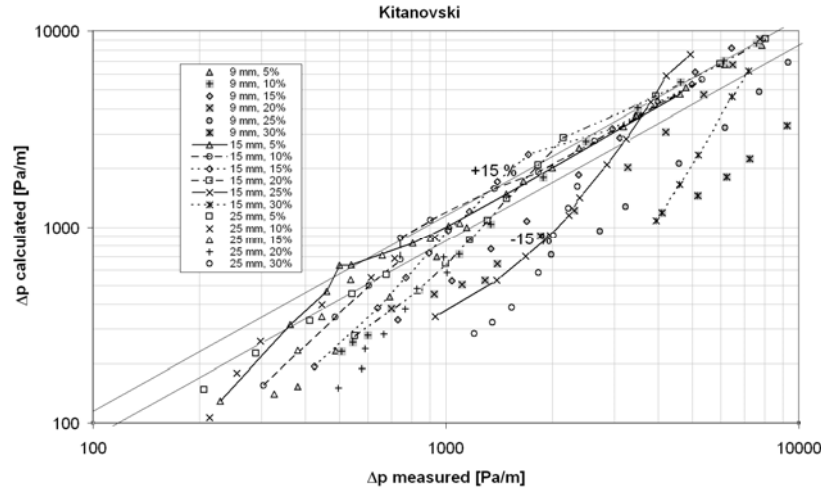
Figure 8.16 Comparison between measured pressure drop and calculated according to Kitanovski for laminar and turbulent flow

8.3.3 Transport characteristics of ice slurry

In order to evaluate transport characteristics of ice slurry flow in horizontal tubes transport capacity and required pumping power was determined on basis of experimental results. In Figure 8.17 transport capability and required pumping power of ice slurry is shown for different velocities and ice concentrations for 15 mm tube. Transport capability is calculated as cooling energy that could be provided at "full melt off" to the initial freezing temperature given by the initial ethyl alcohol concentration, i.e. -4.4 °C, while the required pumping power is determined according to pressure drop and volume flow and is expressed per meter of tube length. One can observe linear dependence of transport capacity with ice concentration, i.e. with ice fraction increase the capacity in-

103

creases as well. On the other hand one can clearly observe that required pumping power is fairly constant up to ice concentrations of 20 to 25 % when it starts to increase rapidly.
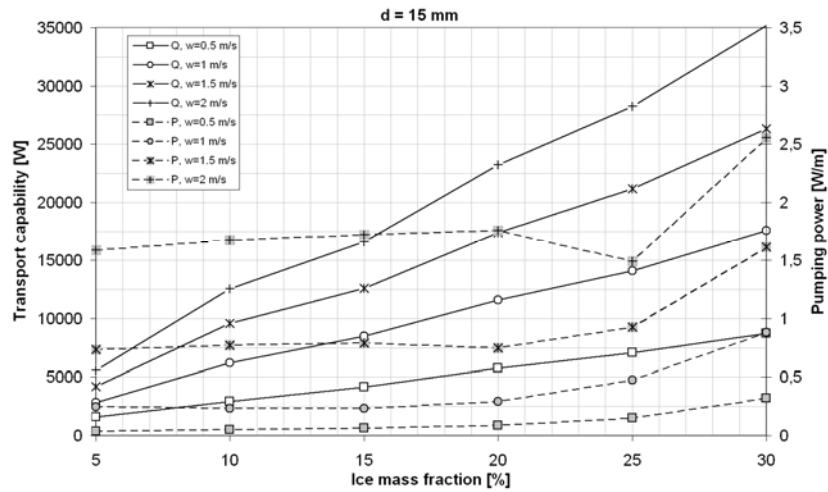
Figure 8.17 Ice slurry transport capability and required pumping power for 15 mm tube

This was to expect and is in concord with previous analysis. This suggests existence of local maximum for transport capacity and pumping power ratio at certain velocity and tube diameter as shown in Figure 8.18.
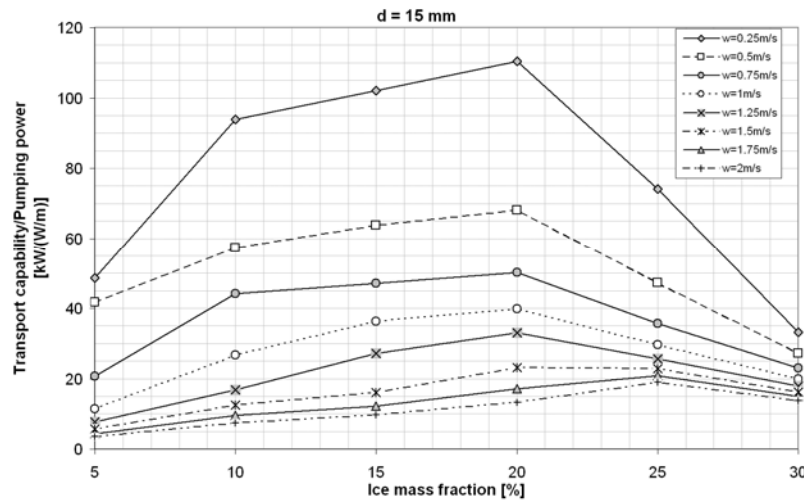
Figure 8.18 Ratio of ice slurry transport capability and required pumping power versus ice fraction for 15 mm tube

If transport capacity and required pumping power ratio is plotted versus ice concentration for constant velocity and tube diameter, one can clearly observe that maximum values of this ratio are found for ice mass fraction of 20 %. The same trend is found for other tubes and velocities. Although low flow velocities offer high ratio of transport capacity to pumping power, too low velocities are not desired from operational point of view, as flow is no longer homogeneous and can lead to system blockage.

In Figure 8.19 transport capacity to pumping power ratio is displayed versus velocity for constant ice concentration. Up to velocity of 1.5 m/s, 20 % ice mass fraction yields the best result. For higher velocities higher ice fractions, 25 % and 30 % offer better or at least the same result as 20 %. Lowest ratio in almost entire velocity range is given for ice concentration of 5 %. With velocity being increased higher ice concentrations are in favour.
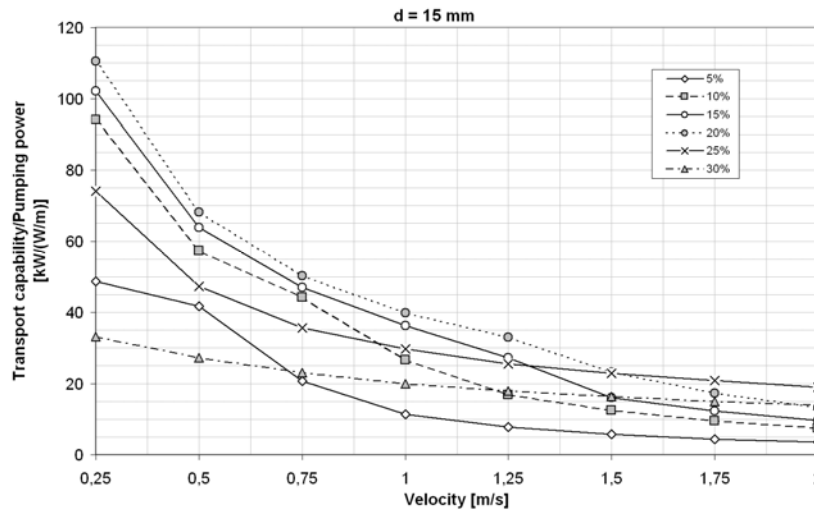
Figure 8.19 Ratio of ice slurry transport capability and required pumping power versus average velocity for 15 mm tube

Therefore, in order to exploit advantages of ice slurries over conventional fluids to full extent it is recommended to keep the concentration of ice particles at 20 % while the flow velocity should be generally in the range of laminar flow regime. Basically, when designing the piping system the choice of ice slurry velocity is a matter of operating strategy. If the benefit of small tube diameters, in terms of lower initial costs for piping system, are favoured over operating costs, the velocity should be kept as high as possible but still in laminar flow regime to avoid excessive pump work. For an ice concentration of 20 % and tube diameter of

9 mm this means velocity up to 2 m/s, for 15 mm around 1.4 m/s and for 25 mm tube approximately 1 m/s.

On the other hand if minimum consumption of pumping is put as a priority over initial costs, the flow velocity should be kept as low as possible but still high enough to meet cooling requirements and more than minimum velocity to prevent phase separation and system blockages. During the course of experiments no problem or blockages occurred as long as velocity was higher than 0.2 m/s for all tested tubes. According to Guilpart et al. (1999) minimum recommended velocity can be calculated from

$$w_{\min} = 2.8 \cdot \sqrt{g \cdot d \cdot \left(1 - \frac{\rho_i}{\rho_{cf}}\right)} \qquad 8.26$$

which means 0.2 m/s for 9 mm tube, 0.25 m/s for 15 mm and 0.35 m/s for 25 mm tube.

8.4 Conclusion

Experimental investigation of flow behaviour in straight tubes of an ice slurry based on 10.3 % of ethanol water-mixture for cooling applications was conducted with aim to provide and/or confirm existing analytical methods for prediction of ice slurry pressure drop.

According to the foregoing investigation it was found that the behaviour of the ice slurry flow is time dependant, i.e. ice slurry pressure drop for certain temperature and ice concentration changes with time. Decrease in pressure drop is observed immediately after ice production, i.e. from the point where the desired ice concentration was reached and for the next three hours. This was attributed to change in size and shape of ice crystals. After approximately seven hours of having ice slurry stirred and circulated through the test section no further significant pressure drop change was observed.

Results from the pressure drop tests reveals higher pressure drops for higher ice concentrations and velocities in comparison to the single phase flow, which is in agreement with most of other reported work. However for ice concentrations of 15 % and higher certain velocity exists at which ice slurry pressure drop is same or even lower than for single phase flow. It seems that higher ice concentrations delay flow pattern transition moment (from laminar to turbulent) toward higher velocities, i.e. for the same velocity ice slurry flow is still in laminar regime while the flow of single phase fluid would be in turbulent regime.

106

For the ice mass fractions up to 10 % to 15 % the ice slurry can be treated as a purely Newtonian fluid. Above ice mass concentration of 15 %, ice slurry can no longer be regarded as Newtonian fluid.

In addition experimental results for pressure drop were compared to the analytical results, based on Poiseulle and Buckingham-Reiner models for laminar flow and Blasius, Darby-Melson, Dodge-Metzner, Steffe and Tomita for turbulent flow and also general correlation of Kitanovski which is valid for both flow regimes. The evaluated model based on Poiseulle shows good agreement with the experimental results only for smallest tube and for low ice concentrations up to 15 %. The Buckingham-Reiner method gives good prediction only for data with low value of buoyancy term. In addition, based on experimental data empirical correlation is presented which takes buoyancy effect into account. The proposed correlation predicts 82 % of all experimental data in laminar region with an average accuracy of ±15 %. In turbulent region the methods of Dodge-Metzner and Tomita give good agreement with the experimental data. Calculated and experimental results are fitted with accuracy better than ±15 % for both methods. Correlation of Darby and Melson under-predicts measured pressure drop for approximately 35% for entire range.

From transport point of view in order to exploit advantages of ice slurries over conventional fluids it is recommended to keep the concentration of ice particles at 20 % while for velocity it is concluded that:

- o if the benefit of small tube diameters are desired the velocity should be kept as high as possible but still in laminar regime; which means velocity up to 2 m/s for 9 mm tube, around 1.4 m/s for 15 mm and approximately 1 m/s for 25 mm tube.

- o If minimum pumping power is desired, the flow velocity should be kept as low as possible but still high enough to meet cooling requirements and more than minimum velocity to prevent system blockages. For velocity higher than 0.2 m/s no problem or blockages occurred during the course of experiment.

9 Experimental investigation of ice slurry heat transfer in horizontal tube

Heat transfer of ice slurry flow based on ethanol-water mixture in a circular horizontal tube has been experimentally investigated. The secondary fluid was prepared by mixing ethanol and water to obtain initial alcohol concentration of 10.3 % (initial freezing temperature -4.4 °C). The heat transfer tests were conducted to cover laminar and slightly turbulent flow with ice mass fraction varying from 0 % to 22 % depending on test performed.

Measured heat transfer coefficients of ice slurry are found to be higher than those for single phase fluid, especially for laminar flow conditions and high ice mass fractions where the heat transfer is increased with a factor 2 in comparison to the single phase flow.

In addition, experimentally determined heat transfer coefficients of ice slurry flow were compared to the analytical results, based on the correlation by Sieder and Tate for laminar single phase regime, by Dittus-Boelter for turbulent single phase regime and empirical correlation by Christensen and Kauffeld derived for laminar/turbulent ice slurry flow in circular horizontal tubes. It was found that the classical correlation proposed by Sieder and Tate for laminar forced convection in smooth straight circular ducts cannot be used for heat transfer prediction of ice slurry flow since it strongly underestimates measured values, while, for the turbulent flow regime the simple Dittus-Boelter relation predicts the heat transfer coefficient of ice slurry flow with high accuracy but only up to an ice mass fraction of 10 % and $Re_{cf} > 2300$ regardless of imposed heat flux. For higher ice mass fractions and regardless of the flow regime, the correlation proposed by Christensen and Kauffeld gives good agreement with experimental results.

9.1 Introduction

This paper reports on an experimental investigation of heat transfer behavior of ice slurry based on ethanol water-mixture in straight tubes for cooling applications. In the last ten years much research has been made in the field of ice slurry technology but with varying outputs and conclusions. Heat transfer measurements performed on ice slurries inside horizontal circular pipes were reported by many (Ayel et al., 2003; Egolf et al., 2005; IIR, 2005a).

Christiansen and Kauffeld (1997), Guilpart et al. (1999), Kauffeld et al. (1999), Jensen et. al (2000), Sari et al. (2000), Hägg (2005) and Zelasko (2006) reported increase of the heat transfer coefficient with increasing ice fraction and velocity but rather small or no influence on the heat transfer coefficient with increasing heat flux. Knodel et al. (2000), reported decreased heat transfer coefficients with increased ice fraction up to a fraction of about 4 %. At higher ice fractions, the Nusselt number was more or less constant. The experiments were done with ice water slurry in 24 mm horizontal pipe and velocity between 2.8 to 5 m/s.

Only Snoek and Bellamy (1997) observed decrease in Nusselt number with increasing ice fraction. In their experiments they used ethylene glycol with initial concentration of 8-10 %, with ice concentration, i.e. ice mass fraction up to 33 %.

A number of experiments have thus been performed to investigate local and average heat transfer coefficients but the results differ from one report to another. The most possible reason for differences in the reported heat transfer behaviour is the size and shape of the ice slurry particles. In the early age of ice slurry research the ice particles were large. The influence of the ice generation method and the time influence on the geometrical characteristics of the ice crystals were not known. Consequently, large ice particles lead to superheating phenomena which may significantly influence the heat transfer results. Hansen et al. (2002) reported on an investigation on ice agglomeration during storage, i.e. on ice crystal growth mechanisms during ice generation and its dependency on time during storage, while Pronk et al. (2004) reported on the influence of the ice crystal size on ice slurry heat transfer and superheating phenomenon. With present day ice generation methods, the ice particles have much finer crystalline form which, it seems, has an impact on the thermal boundary and in turn on heat transfer.

In this study, a series of heat transfer experiments have been conducted in order to investigate heat transfer of ice slurry in horizontal tubes with the intention to contribute to the clarification of the contradicting results published to this date.

9.2 Experimental details

9.2.1 Experimental apparatus

The experimental set-up designed and manufactured at the Division of Applied Thermodynamics and Refrigeration of the Royal Institute of Technology consists of an ice generator/storage tank, the test loop and the data acquisition system, see Figure 9.1, Hägg (2005).
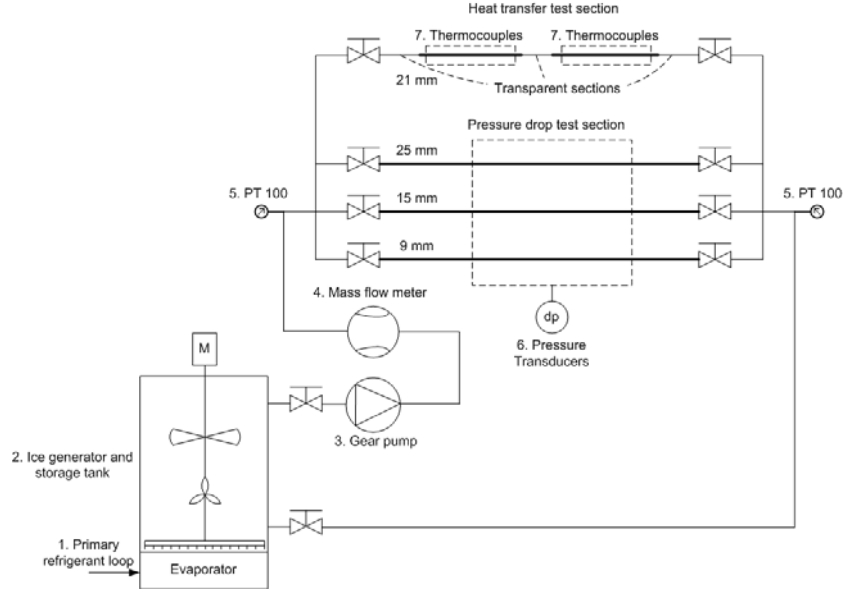
Figure 9.1 Simplified flow chart of the experimental setup

An ice slurry storage tank of 60 liters is built together with the ice generator and is connected to the test circuit. The main components of the test circuit are: the volumetric pump of lobe type, the Coriolis mass flow meter, and four measurement sections. Three of the measurement sections serve for pressure drop investigation under isothermal conditions. They consist of stainless steel circular horizontal tubes with inner diameters of 9, 15 and 25 mm. Each tube is equipped with two pressure taps with a distance of 1.2 m connected to three parallel Druck pressure transducers (range of 0.35, 1 and 3.5 bar). The fourth tube has an inner diameter of 21 mm and is intended to serve for heat transfer measurements. The tube consists of two measuring sections of stainless steel while the inlet and outlet of the tube, as well as the tube section in between the measuring sections are made of transparent plastic. The length of one heated test section is 940 mm with a total internal heat transfer surface of 0.062 m². Each measuring section is equipped with 20 ther-

mocouples to measure the wall temperature. The thermocouples are soldered to the wall in grooves that are 1 mm deep, i.e. approximately 1 mm from inner tube surface. The wall temperature is measured at five positions along each measuring section and at each position the temperature is measured on top, below and on each side of the tube. Around each measuring section with their 20 thermocouples a resistance wire is wound, Figure 9.2. By means of a variable voltage transformer it is possible to control the supplied voltage to the resistance wire.
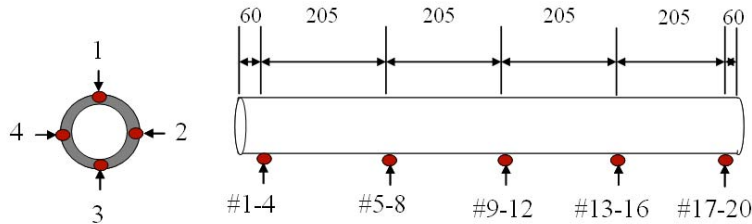
Figure 9.2 Heat transfer measuring section

All four loops are equipped with Pt-100 temperature sensors at inlet and outlet to measure the bulk temperatures of the ice slurry. All Pt-100 sensors have been calibrated to an accuracy of $\pm$ 0.015 °C, while the thermocouples have been calibrated to an accuracy of $\pm$ 0.1 °C at 0 °C (Table 9.1). The velocity in the test sections is regulated by means of the frequency controlled pump. A Coriolis mass flow meter is used to measure mass flow rate and density of the ice slurry prior to the inlet of the test section. The ice mass fraction was measured continuously, i.e. simultaneously determined based on two parameters, temperature and density.

Table 9.1 List of measuring instrumentation

Instrument	Type	Range	Accuracy
Differential pressure transducers	Druck PCDR 2100	0 – 0.35 bar	$\pm$ 0.1 %
Temperature sensors	Pt100 Omega engineering	-100°C – 400°C	$\pm$ 0.015 °C
	T-type thermocouples	-100°C – 350°C	$\pm$ 0.1 °C
Mass (density) flow meter	Micro Motion	density	$\pm$ 0.5 kg/m3
		mass flow	$\pm$ 0.1 %
Power meter	Hameg HM8115	0 – 8 kW	$\pm$ 0.5 %
Data acquisition unit	Agilent 34970A	-	-

The evaporator of the cooling machine is placed in the bottom of the tank and forms the bottom disc of the tank on which the ice is formed. The refrigerant in the cooling machine of the ice generator is R404A. The ice is removed by means of the brush connected to a shaft that rotates in the center of the tank. On the shaft, in the middle of the tank, two agitators are placed, one boat propeller and one visco jet. Both the

112

brush and the agitators are frequency controlled. The agitators are rotating in the opposite direction to the brush. The brush, the agitators and the pump contribute to a homogenous suspension in the tank.

9.2.2 Experimental procedure

Experimental investigations of ice slurry heat transfer behaviour were conducted on the aqueous solution of ethyl alcohol with initial concentration of 10.3 % by weight (freezing point -4.4 °C).

Ice slurry was produced until desired ice concentration or ice mass fraction level in the tank was reached. The ice generator and the pump were running continuously during ice production to ensure uniform dispersion of the ice particles in the tank. Since the particle size and shape of ice slurry mixtures are time dependant, heat transfer tests were carried out approximately seven hours after the liquid reached the freezing point.

When a desired ice mass fraction of 22 % was reached in the tank (which was the upper limit that could be reached considering the pump capacity and test conditions), and retention conditions were satisfied, ice generation was stopped and heat was applied to the test section by an AC power supply.

The power supply consisted of a 2 kW manually controlled power transformer and power meter. The heating rate to the test section was controlled by the power transformer and measured by the power meter and was set to 4, 8, 12 and 16 kW/m². During the experiments, the velocity of the ice slurry was maintained constant by means of the frequency controlled pump. A certain portion of the ice was melted in each pass through the test section. The highest ice mass concentration reduction recorded per pass was 3.3 % for the lowest ice slurry velocity of 0.5 m/s and the highest heat flux of 16 kW/m2. The melting process was continued until all ice was melted and the tank contained only liquid.

To minimize the influence of the ambient the test section was heavily insulated resulting in heat balance errors within ± 5 %, and for the majority of the data the error is less than ± 3 %.

Based on the measured temperature and density of the flowing ice slurry, the ice mass fraction at the test section inlet was determined as an arithmetic average of the ice concentrations determined by density measurements and temperature measurements,

$$c_i = \frac{\rho_i(\vartheta) \cdot \left[\rho_{cf}(\vartheta) - \rho_{is}\right]}{\rho_{is} \cdot \left[\rho_{cf}(\vartheta) - \rho_i(\vartheta)\right]}$$

9.1

$$c_i = \frac{c_{cf}(\vartheta) - c_A(\vartheta_0)}{c_{cf}(\vartheta)}$$

<div align="right">9.2</div>

where $c_A(\vartheta_0)$ is the initial additive concentration giving the solution freezing point and $c_{cf}(\vartheta)$ is the additive concentration of the carrier fluid, i.e. remaining liquid, obtained from Melinder (1997). According to Hansen et al. (2002) estimation of ice concentration by combining both methods leads to more accurate results than using solely temperature or density measurements.

However, the ice concentration at the outlet of the test section was determined solely on temperature according to eq. 9.2 since the density of the ice slurry was not measured after the test section.

For high ice mass fractions, i.e. c_i=15-20 %, the difference in ice concentration obtained by using both methods separately was not large, less than 1 %, while for the ice content of 10 % and lower combining the methods was beneficial since that difference was around 2 %.

9.3 Results and Discussion

The objective of the heat transfer tests was to determine heat transfer coefficients as function of ice concentration and mean velocity for ice slurry flows in horizontal circular tubes. An overview of the experimental conditions is presented in Table 9.2.

Table 9.2 Operating conditions

Exp. Series	Experiment	Tube diameter (inner) [mm]	Mass concentration of ethanol [%]	Ice mass fraction [%]	Heat flux [kW/m^2]	Mean velocity [m/s]
1		21	5	0	4	0.06;0.1;0.15;0.35; 0.5;0.75
2		21	5	0	16	0.06;0.1;0.2;0.35; 0.5;0.75;1;1.25
3		21	10	0	4	0.5;0.75;1.25
4	Heat transfer	21	10	0	8	0.5;1;1.25
5		21	10	0	12	1;1.25
6		21	10	0	16	0.5; 0.75; 1
7		21	10	0-22	4	0.5; 1; 1.25
8		21	10	0-22	8	0.5; 1; 1.25
9		21	10	0-22	12	1; 1.25
10		21	10	0-22	16	0.5; 0.75; 1

Local wall temperatures were measured by means of thermocouples at twenty locations placed at five positions as described in previous section. The ice slurry bulk temperature was measured at the inlet and outlet of

the test section. Local heat transfer coefficients between the inner tube wall surface and the ice slurry flow is defined as

$$\alpha_{is,x} = \frac{\dot{q}}{\vartheta_{wall,x} - \vartheta_{is,x}}$$

9.3.

The local ice slurry bulk temperature $\vartheta_{is,x}$, was calculated assuming a linear temperature dependency along the test section and on the ice slurry inlet and outlet temperatures.

The mean heat transfer coefficient for a certain tube cross section was calculated as

$$\alpha_{is,cs} = \frac{1}{n} \cdot \sum_{i=1}^{n} (\alpha_{is,x})_i$$

9.4

where n is the number of measurement points around the tube perimeter, i.e. $n=4$.

The average heat transfer coefficient for the entire test section was determined as

$$\alpha_{is,m} = \frac{1}{n} \cdot \sum_{i=1}^{n} (\alpha_{is,x})_i$$

9.5

where n represents the total number of locations where measurements were taken, i.e. $n=20$.

The local Nusselt number was calculated according to

$$Nu_{is,x} = \frac{\alpha_{is,x} \cdot d}{\lambda_{is}}$$

9.6

and the average Nusselt number for the entire heat exchanger (test tube) was calculated as

$$Nu_{is,m} = \frac{\alpha_{is,m} \cdot d}{\lambda_{is}}$$

9.7.

Reynolds and Prandtl numbers are determined on the basis of average ice slurry properties between inlet and outlet conditions.

The thermal conductivity of ice slurry was determined according to Maxwell-Eucken model (Hansen et al., 2002) and the dynamic viscosity according to Thomas relation (IIR, 2005a).

Each heat transfer test was performed under constant heat flux and velocity. Experimental uncertainties of the measured data are determined with respect to the accuracy of the measuring equipment. The maximum relative error of the heat transfer coefficients is between ± 1.5 % and ± 6.4 %. The lower margin corresponds to high heat fluxes and low velocities while the higher limit to low heat fluxes and high velocities.

Heat applied to the flowing ice slurry results in heating up of the liquid and in melting of ice crystals. According to Hansen et al. (2002) and Pronk et. al (2004) superheating of the carrier liquid is likely to occur while melting ice in an ice slurry mixture, especially when the ice crystals are relatively large or a large percentage of the ice is being melted. This superheating phenomenon may negatively affect the heat transfer and can lead to a decrease in the heat exchanger capacity. Therefore, the superheating of the ice slurry at the test section end was calculated from the heat balance. The maximum superheating of the ice slurry was found to be around 2 °C (at ice mass fraction of 2 %) for the case with the highest heat flux (16 kW/m²) and lowest velocity (0.5 m/s). For the same case the maximum ice mass fraction reduction recorded during the tests was found and was found to be 3.3 %. For all other cases, i.e. for higher velocities and lower heat fluxes, the superheating and reduction of the ice mass fraction per one pass were much lower. Since the degree of liquid superheating was relatively small in almost the entire range of ice mass fractions its influence on heat transfer was neglected.

Experimentally obtained results in terms of mean Nusselt versus ice slurry Reynolds number are shown in Figure 9.3 for the entire range of operating conditions, i.e. single phase and ice slurry flow. The diagram is divided in three parts, laminar, transitional and turbulent region. The region of transition occurs in the range 1700 < Re_{is} < 2500. In addition theoretical values for single phase laminar and turbulent heat transfer are plotted in the diagram. The latter values are obtained by use of Dittus-Boelter correlation assuming a Prandtl number of 36 derived for the fluid in liquid state at the initial freezing temperature.

As seen in Figure 9.3 heat transfer of ice slurry is generally increasing with increasing ice mass fraction and flow velocity but is not changing considerably with imposed heat flux.

The figure legend contains:

- □ 20% ice, 16kW/m2
- ◇ 20% ice, 12kW/m2
- △ 20% ice, 8kW/m2
- × 20% ice, 4kW/m2
- ▣ 15% ice, 16kW/m2
- ◈ 15% ice, 12kW/m2
- ▲ 15% ice, 8kW/m2
- ✕ 15% ice, 4kW/m2
- —□— 10% ice, 16kW/m2
- --◇-- 10% ice, 12kW/m2
- ···△··· 10% ice, 8kW/m2
- --×-- 10% ice, 4kW/m2
- ■ 5% ice, 16kW/m2
- ◆ 5% ice, 12kW/m2
- ▲ 5% ice, 8kW/m2
- ▨ 5% ice, 4kW/m2
- —□— 0% ice, 16kW/m2
- --◇-- 0% ice, 12kW/m2
- --△-- 0% ice, 8kW/m2
- ···✕··· 0% ice, 4kW/m2
- --○-- 0% ice, 5%eth-h2o, 4kW/m2
- --✳-- 0% ice, 5%eth-h2o, 16kW/m2
- —— Dittus-Boelter
- — — Single phase, laminar

Chart axes: Nu is (vertical), Re is (horizontal). Annotations: "Single phase laminar flow", "Dittus-Boelter correlation for Pr=36".

Figure 9.3 Experimental results in terms of average Nusselt versus Reynolds number

9.3.1 Single phase heat transfer

To be able to compare ice slurry heat transfer coefficients with single phase, separate tests with 0 % ice concentration were performed for similar operating conditions as for ice slurry flow. The experimental conditions for the single phase heat transfer measurements are summarized in the first six rows in Table 9.2 and the results are also shown in Figure 9.3.

9.3.2 Laminar single phase flow

According to the theoretical analysis in Kakac and Yener (1995) Nusselt number for fully developed laminar flow and constant heat flux in circular tubes is 4.36. As can be observed from Figure 9.3 single phase flow of 5 % ethanol-water mixture and heat flux of 4 and 16 kW/m² yields much higher average Nusselt numbers than theoretically derived.

The reason for the higher heat transfer coefficients is the influence of the entry region, i.e. the flow is still not fully developed thermally and hydraulically on locations where the measurements were taken.

The thermal entrance length after which the temperature distribution becomes fully developed can be estimated by

$$L_{th} / d \cong 0.05 \cdot Re_{in} \cdot Pr_{in}$$ 9.8

while the hydrodynamic entrance length required for the velocity distribution to develop varies with the Reynolds number as

$$L_h / d \cong 0.056 \cdot Re_{in} \qquad\qquad 9.9.$$

For the experimental conditions, the minimum thermal entrance length is calculated as 10 m while the hydrodynamic is 30 m. Therefore, for single phase heat transfer measurements in the laminar region neither the temperature nor the velocity profile could be considered as fully developed.

Furthermore, due to test section design, thermal and hydraulic boundary layers are not developing simultaneously. Development of velocity profile starts much earlier. Figure 9.4 shows experimentally obtained results for single phase laminar flow heat transfer in the entrance region.
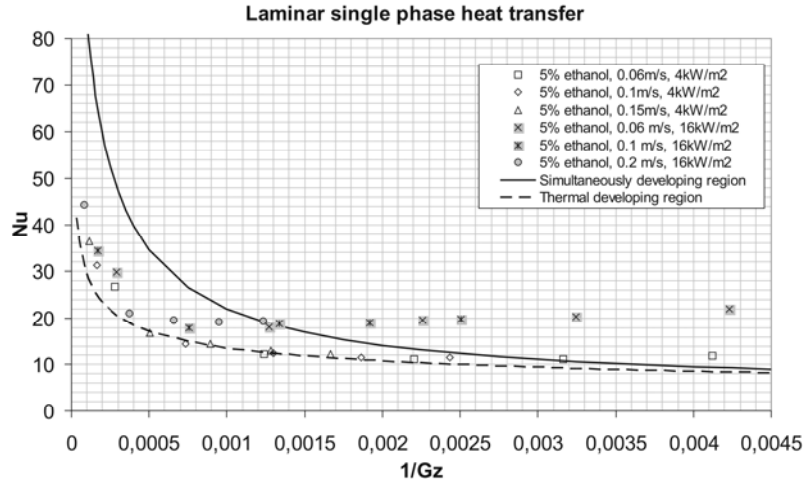
Figure 9.4 Experimental results of laminar single phase heat transfer in terms of Nusselt versus inverse Graetz number

Experimental results are plotted for initial ethanol concentration, velocity and heat flux against inverse Graetz number which is defined as

$$Gz(z) = \frac{d}{z} \cdot Re \cdot Pr \qquad\qquad 9.10$$

where z stands for axial downstream location from the entrance, i.e. where heating starts. All thermophysical properties are evaluated at the average value of the inlet and outlet temperatures.

Beside experimentally obtained results, proposed correlations according to Shah and London (1978) for thermal entry region and by Hausen (Kakac and Yener, 1995) for simultaneously developing region (thermal and hydraulic) are plotted in Figure 9.4 as well.

The empirical correlation for local Nusselt number and combined entry region under constant wall heat flux, proposed by Hausen (Kakac and Yener, 1995) is as follows:

$$Nu = 4.36 + \frac{0.023 \cdot (Gz)}{1 + 0.0012 \cdot (Gz)^{0.8}}$$

9.11.

For uniform heat flux thermal entry region, the correlation suggested by Shah and London (1978) is

$$Nu = \left[1.302 \cdot \left(\frac{1}{Gz} \right)^{-\frac{1}{3}} - 0.5 \right] \cdot \left(\frac{\eta_b}{\eta_{wall}} \right)^{0.14} \text{ for}$$

$$0.00005 \leq Gz^{-1} \leq 0.0015$$

9.12

and

$$Nu = \left[4.36 + 8.68 \cdot \left(10^3 \cdot \frac{1}{Gz} \right)^{-0.506} \cdot e^{-41 \cdot \frac{1}{Gz}} \right] \cdot \left(\frac{\eta_b}{\eta_{wall}} \right)^{0.14} \text{ for}$$

$$Gz^{-1} > 0.0015$$

9.13.

As seen in Figure 9.4 the experimental results are falling between the theoretically obtained results for simultaneously and thermal developing region, i.e. experimental results show slightly higher values than for uniform heat flux thermal entry region. For 5 % ethanol water mixture, 4 kW/m², calculated and experimental results are in good agreement. Results for 16 kW/m² and $Gz^{-1} > 0.0005$ show much higher heat transfer than expected from the correlations. It is believed that in this case heat transfer augmentation is a result of combined free and forced convection. In this case the fluid velocity and temperature profile are not symmetrical as buoyancy effects will induce a rotationally asymmetric flow which can lead to increase in heat transfer. To support the suggested mechanism, Figure 9.5 shows the tube wall temperature distribution versus normalized tube length L/L_0 (ratio of length where the temperature measurement is taken over total test section length), for 5 % ethanol water mixture, velocity of 0.06 m/s and heat flux of 16 kW/m². The wall temperature on the pipe top for these conditions is much higher than on

the bottom which indicates presence of free convection superimposed on stream-wise main flow.

5% ethanol-water, 0.06 m/s, 16 kW/m2
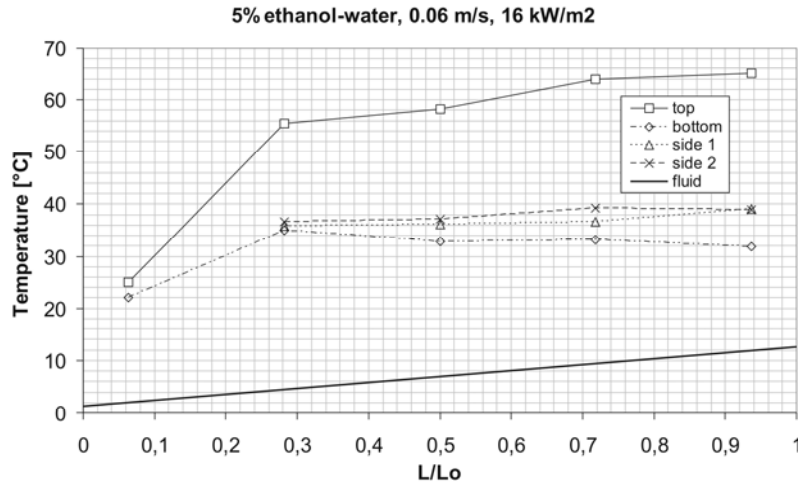
Figure 9.5 Pipe wall temperature distribution for laminar single phase flow against normalized tube length, 5% ethanol water, 0.06 m/s, 16 kW/m²

Similar results can be observed for 5 % ethanol water mixture, velocity of 0.06 m/s and heat flux of 4 kW/m². In this case the temperature differences between top and bottom are by far lower with consequently less emphasized free convection.

A more practical correlation for estimation of the mean heat transfer coefficient for laminar forced convection in smooth straight circular ducts, for thermal entrance region is proposed by Sieder and Tate (Kakac and Yener, 1995):

$$Nu = 1.86 \cdot \left(Re \cdot Pr \cdot \frac{d}{L} \right)^{0.33} \cdot \left(\frac{\eta_b}{\eta_{wall}} \right)^{0.14} \text{ valid for } 0.48 < Pr < 16700,$$

$$0.0044 < \eta_b / \eta_{wall} < 9.75 \text{ and} \left(Re \cdot Pr \cdot \frac{d}{L} \right)^{0.33} \cdot \left(\frac{\eta_b}{\eta_{wall}} \right)^{0.14} > 2 \qquad 9.14$$

where fluid properties are evaluated at bulk mean fluid temperature.

For heat flux of 4 kW/m², this correlation predicts the measured values with relative error less than ± 5 % while for a heat flux of 16 kW/m²

only one point, i.e. for 0.2 m/s, falls inside an error margin of $\pm$ 15 % (Figure 9.6).
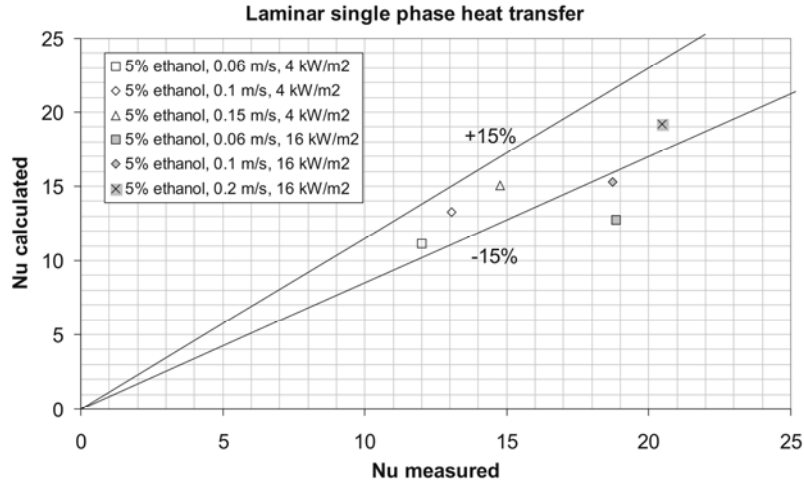
Figure 9.6 Comparison between measured and calculated laminar heat transfer according to Sieder-Tate correlation for single phase developing flow

9.3.3 Turbulent single phase flow

For turbulent flow in circular ducts, the hydrodynamic entrance length may be estimated according to Kakac and Yener (1995) as

$$L_\mathrm{h} / d \cong 1.359 \cdot Re^{1/4}$$ 9.15

while the thermal entrance length over which the temperature distribution becomes fully developed in general is given by

$$L_\mathrm{th} / d < 30$$ 9.16.

The calculated hydrodynamic entrance length for the given experimental conditions is approximately 0.25 m while the thermal entrance length is around 0.6 m. Therefore, the velocity profile for single phase heat transfer measurements in turbulent region is fully developed but the temperature profile can be considered fully developed only in the last section (after two thirds of the total tube length).

In case of turbulent flow, i.e. $Re > 2300$, one of the most widely used correlations for prediction of single phase heat transfer coefficient is the one recommended by Dittus-Boelter (Kakac and Yener, 1995):

121

$$Nu_{cf} = 0.023 \cdot Re_{cf}^{0.8} \cdot Pr_{cf}^{0.33} \qquad\qquad 9.17.$$

The comparison between the experimental and calculated values is presented in Figure 9.7.

Turbulent single phase heat transfer
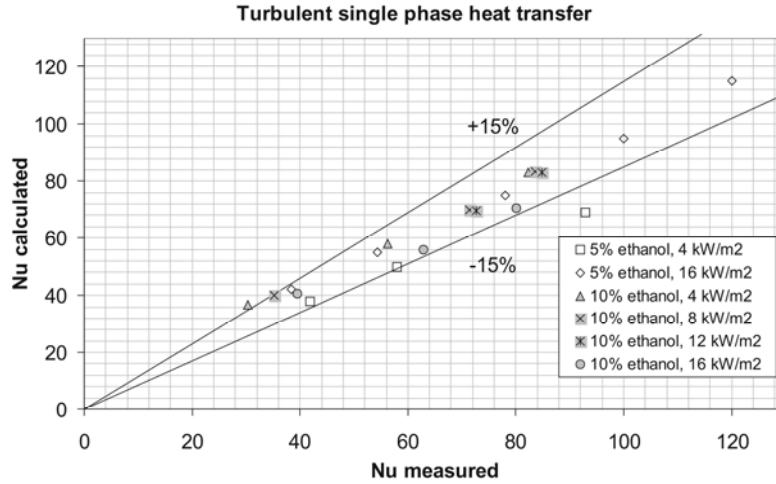
Figure 9.7 Comparison between measured and calculated turbulent heat transfer according to Dittus-Boelter correlation for single phase flow

The relative discrepancy between calculated and measured single phase heat transfer is in range ± 15 % for 90 % of the experimental results. In the analysis that follows, the ice slurry mean heat transfer coefficient will be compared to the values calculated by Dittus-Boelter correlation.

9.3.4 Ice slurry heat transfer

The mean heat transfer coefficient for the tube is plotted in Figure 9.8 versus inlet ice slurry concentration for constant velocity and heat flux. Generally the higher the ice concentration and the velocity the higher is the heat transfer coefficient. Again we see that the imposed heat flux has no or just minor influence on the heat transfer coefficient, e.g. for the velocity of 0.5 m/s and heat flux of 4, 8 and 16 kW/m². Furthermore, after a certain ice concentration threshold for each velocity one can notice a drastic increase in heat transfer. This concentration at which there is a sudden increase depends mainly on the flow velocity. It is specially emphasized for the lowest ice slurry velocity, namely 0.5 m/s. Generally, up to ice concentrations between 10-15 %, the mean heat transfer coefficient shows only slight or no increase in comparison to the single phase. From that point, the heat transfer coefficient increases steadily, with the maximum value reached for the highest ice concentration. In compari-

son to the single phase flow, for some cases the measured ice slurry heat transfer coefficient shows increase with a factor 2 at the highest ice mass fractions.
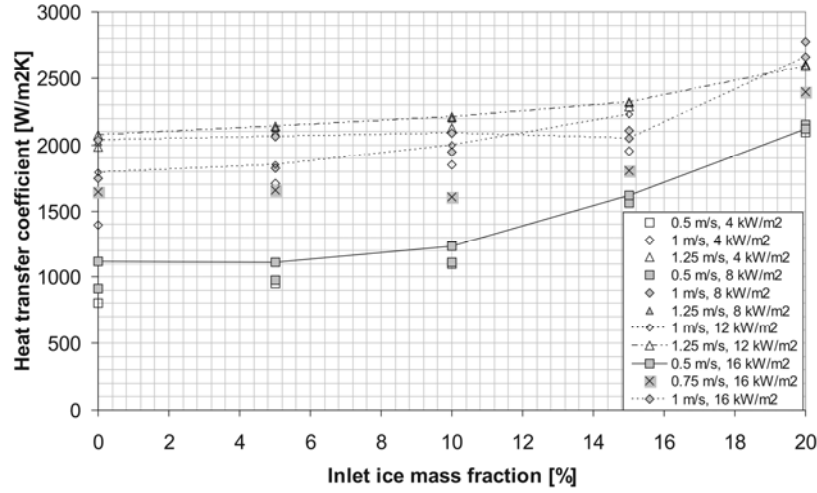
Figure 9.8 Mean heat transfer coefficient vs. inlet ice slurry concentration for constant velocity and heat flux

It is believed that this high relative increase in heat transfer coefficient is a result of the flow pattern change, from homogeneous to heterogeneous flow. With rising content of ice crystals buoyancy and friction forces acting on ice crystals make stratification process more intense (IIR, 2005a).

Figure 9.9 to Figure 9.12 show the ice slurry heat transfer coefficients as a function of inlet ice concentration and tube circumferential position (top, side and bottom of the tube) for constant velocity and heat flux. In addition, the ice slurry (approximate) Reynolds number, Re_{is}, for the inlet conditions is plotted. The figures show that heat transfer coefficient increases with higher ice concentrations and velocities while higher imposed heat flux gives no or just slight increase.

As seen in Figure 9.9 and Figure 9.10 for ice mass fraction from 0 % to ≈ 8 % the heat transfer coefficient is slightly increasing with just small differences between the top, side and bottom of the tube. The ice concentration is too low to give a substantial influence on heat transfer. Above ≈ 8 % ice mass fraction flow separation occurs. The heat transfer coefficient on top of the tube shows the highest value while at tube bottom very low heat transfer is observed (minimum for ice fraction of 8-10 %). It is reasonable to suspect that this decrease in a heat transfer is at least partially a result of conduction in the tube wall, i.e. that the heat flux

123

is not completely homogeneous around the tube perimeter. As more ice crystals are added heat transfer coefficient at the bottom starts to increase again and with 20 % ice it reaches almost the same value as for other locations.
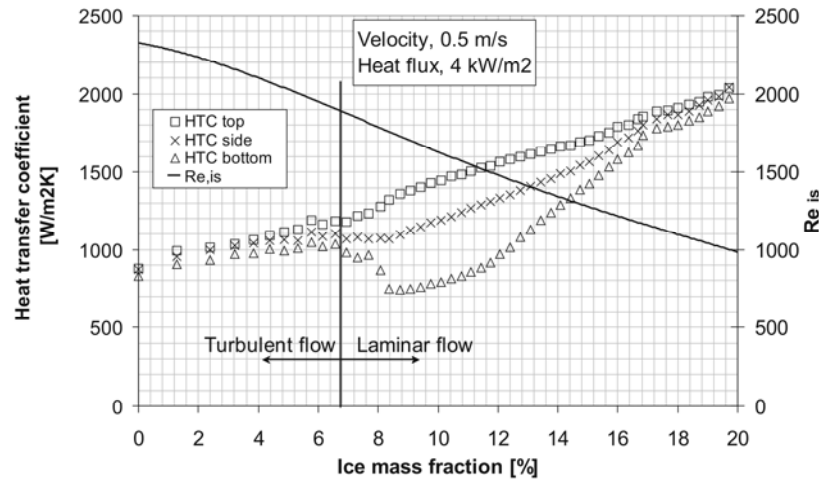
Figure 9.9 Ice slurry heat transfer coefficient versus initial ice concentration for 0.5 m/s and 4 kW/m²

A reason for flow separation to occur is the change in flow pattern. Up to ice fraction of 8 % ice particles have little influence on the flow resulting in a small variation of the ice concentration profile across tube section. Adding more ice particles causes increase in ice slurry viscosity (and consequently decrease in Reynolds number) making flow to shift from turbulent to laminar flow pattern. As long as the flow is turbulent there is enough mixing due to the turbulence to keep the flow homogeneous, while when the flow turns laminar the stratification process will begin due to the lack of mixing. Transition for cases shown in Figure 9.9 and Figure 9.10 is induced for Re=1800-2000.

For the case with a velocity of 0.75 m/s and the heat flux 16 kW/m² turbulent conditions are present up to an ice mass fraction of 13 %. Up to that concentration, heat transfer coefficients were constant at a value of around 1700 W/m²K. At higher ice concentrations, the flow is heterogeneous, with distorted ice concentration profile where most of the ice crystals are at the tube top and less or none are at the tube bottom. This assumption is supported by the observed increase in the heat transfer coefficient at the tube top, as ice particles driven by buoyancy force tend to break the thermal boundary layer and get into direct contact with the tube wall. A different situation takes place at the bottom part of the

124

tube where the heat transfer coefficient is significantly lower as there is no latent heat to stabilize the temperature.
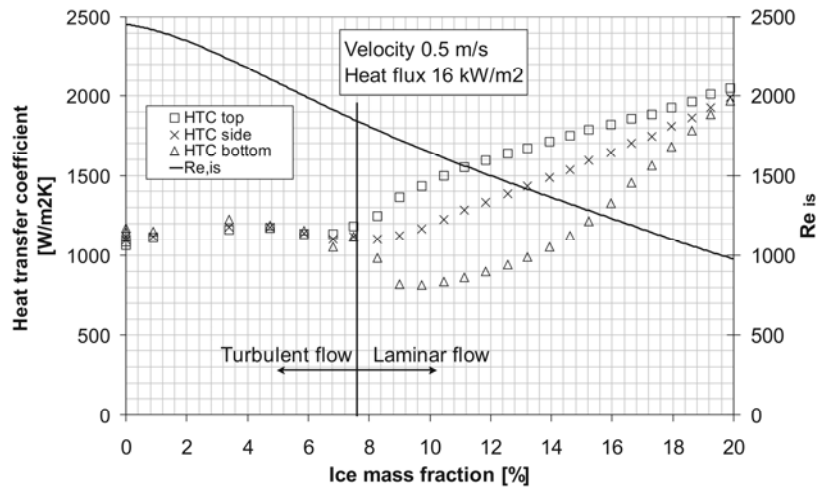
Figure 9.10 Ice slurry heat transfer coefficient versus initial ice concentration for 0.5 m/s and 16 kW/m²
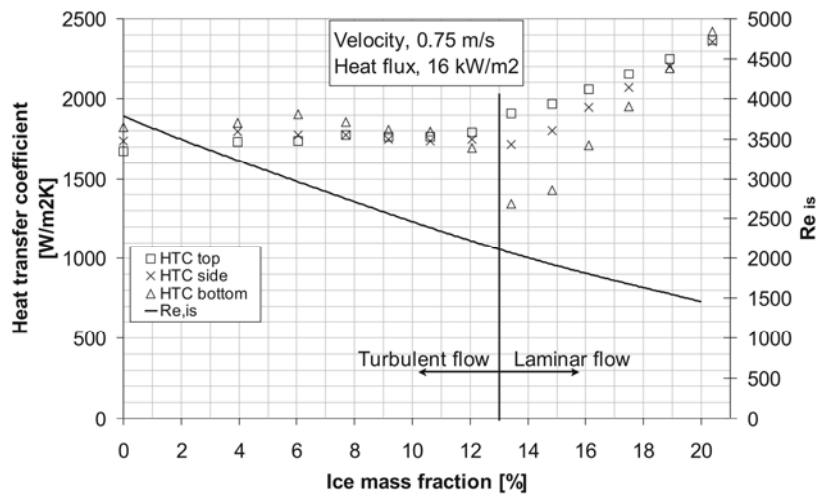
Figure 9.11 Ice slurry heat transfer coefficient versus initial ice mass fraction for 0.75 m/s and 16 kW/m²

As the average ice concentration is increasing the ice front is moving toward the bottom of the tube, which in turn increases heat transfer at the side and bottom of the tube faster than at the tube top. Eventually for an

125

ice concentration of ≥ 20% differences in heat transfer around the periphery of the tube become small again.

If the velocity of ice slurry is high enough, i.e. Reynolds number is higher than the critical (1700-2300) homogeneous flow should be observed without a distinct flow separation threshold. In Figure 9.12, the heat transfer coefficient is plotted against ice concentration for the different tube circumferential locations for the velocity 1.25 m/s and the heat flux of 8 kW/m². As expected, higher velocity generally yields higher heat transfer coefficients. As can be seen there is no notable difference between heat transfer coefficients from one location to another as the flow is turbulent for all ice fractions and more homogeneous with more equal ice concentration distribution across tube cross section than in the previous figures.
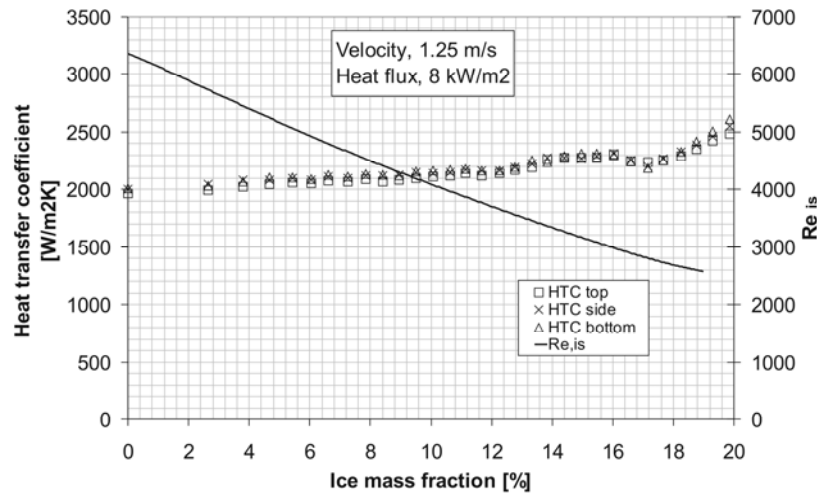
Figure 9.12 Ice slurry heat transfer coefficient versus initial ice mass fraction for 1.25 m/s and 8 kW/m²

For higher velocities the relative heat transfer enhancement (ice slurry to single phase heat transfer for the same velocity and heat flux conditions) is not as large as for cases with lower velocities.

9.3.5 Laminar ice slurry flow

As in the case with single phase flow, the thermal and hydrodynamic entrance length is much larger than the length of the test section for laminar ice slurry flow. Consequently neither the temperature nor the velocity profile could be considered as fully developed in this case. Again, due to test section design, thermal and hydraulic boundary layers are not developing simultaneously.

126

As seen in Figure 9.3, the ice slurry heat transfer coefficient in the laminar region is significantly higher than for single phase flow. In particular, for ice concentration of 20 % the heat transfer coefficient is enhanced at least by a factor of two.

The correlation proposed by Sieder and Tate (Kakac and Yener, 1995), for laminar forced convection in smooth straight circular ducts, cannot be used for heat transfer prediction of ice slurry laminar flow. It strongly underestimates the measured values. None of the experimental values is predicted by this correlation.

Experimental results for laminar ice slurry heat transfer in terms of Nusselt versus inverse Graetz number for constant ice concentration, heat flux and a velocity of 0.5 m/s is shown in Figure 9.13. Beside experimentally obtained results, correlations for single phase flow according to Shah and London (1978) for thermal entry region (eq. 9.12 and 9.13) and by Hausen (Kakac and Yener, 1995) for simultaneously developing region (thermal and hydraulic, eq. 9.11) are plotted in Figure 9.13 as well.
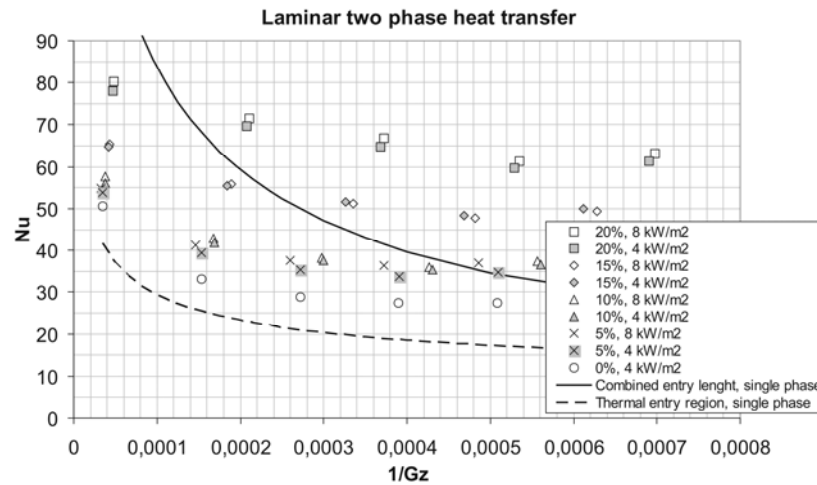
Figure 9.13 Experimental results of laminar ice slurry heat transfer in terms of Nusselt versus inverse Graetz number

As may be observed, the higher the ice fraction the higher the Nusselt number. Heat transfer is more intense at the test section entrance than at the exit, i.e. the value of the Nusselt number strongly decreases along the test tube length. From the entrance to the third measurement location of the test tube, heat transfer is decreasing rapidly followed by an approximately constant value. However, the values stabilize much earlier than

expected, around $Gz^{-1}=0.0005$ which is one hundred times less than for single phase laminar flow.

Based on the experimental results the following correlation for calculating local Nusselt numbers has been derived:

$$Nu(z) = 87.3 \cdot Gz^{0.1} \cdot c_{i,in}{}^{0.67}$$
9.18
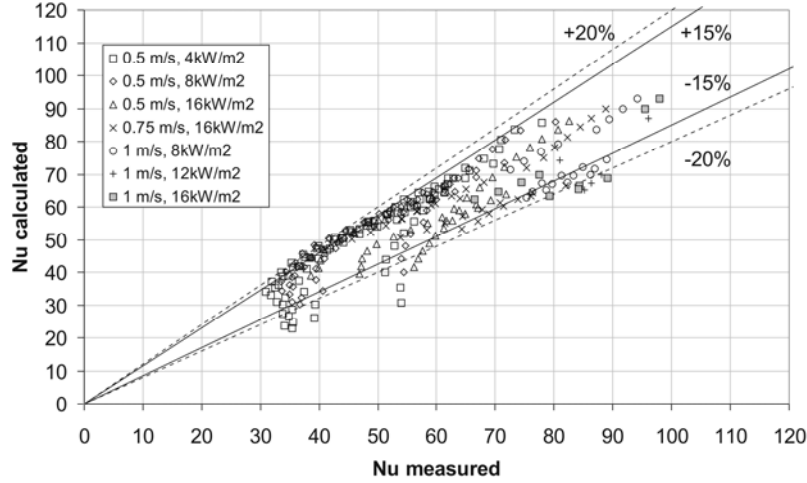
Figure 9.14 Comparison between measured and calculated Nusselt number according to the correlation proposed by eq. 9.18.

With this correlation 75 % of the experimental data points are predicted with relative error less than ± 15 % as seen in Figure 9.14. If the error margin is increased to ± 20 %, more than 91 % of the experimental data points will be predicted by the proposed correlation.

9.3.6 Turbulent ice slurry flow

Using the simple Dittus-Boelter equation based on thermophysical properties of the carrier fluid, approximately 50 % of the experimental data points are predicted with relative error less than $\pm$ 15 % as can be seen Figure 9.15. This correlation serves well for prediction of ice slurry heat transfer coefficient for ice concentration up to approximately 10 % and $Re_{cf} > 2300$ regardless of imposed heat flux. Severe discrepancies occur at higher ice concentrations and this relation is not appropriate anymore. Measured heat transfer coefficients are up to 100 % higher than calculated with this correlation. If Dittus-Boelter equation based on the thermophysical properties of ice slurry is used for prediction of the Nusselt number, the situation is not changed for better. The error is still large.
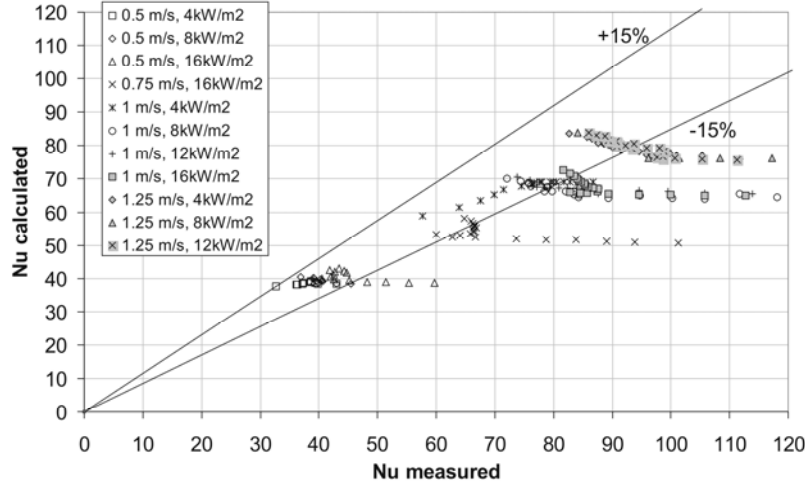
Figure 9.15 Comparison between measured and calculated Nusselt number according to Dittus-Boelter correlation

Christensen and Kauffeld (1997) suggested an empirical correlation based on data for horizontal circular tubes and ice slurry produced from an ethanol solution. The average Nusselt number for an ice concentration above 5 % is described by the relation:

$$\frac{Nu_{is}}{Nu_{cf}} = 1 + 0.103 \cdot c_i - 2.003 \cdot Re_{cf}^{-0.192 \cdot \frac{30 - c_i}{30}} \cdot c_i^{\frac{0.339 \cdot Re_{cf}}{10^4}} \qquad 9.19$$

and for an ice concentration below 5 %:

$$\frac{Nu_{is}}{Nu_{cf}} = 1 \qquad\qquad 9.20$$

Using the correlation proposed by Christensen and Kauffeld (1997) 80 % of the experimental data points were predicted with relative error less than 15 % for the entire range of operating conditions while 95 % of the experimental data points were predicted with relative error less than 25 %.

It should be noted that the experimental results, conclusions and the correlations in this paper are fluid specific, i.e. they are not to be applied for other mixtures e.g. water-salts mixtures with higher density difference between ice and remaining liquid than is the case with alcohol solutions. In horizontal tubes this would affect the behaviour of ice slurry flow, i.e.

flow pattern, critical Reynolds numbers between the laminar and turbulent regimes and finally the heat transfer.

Christensen-Kauffeld
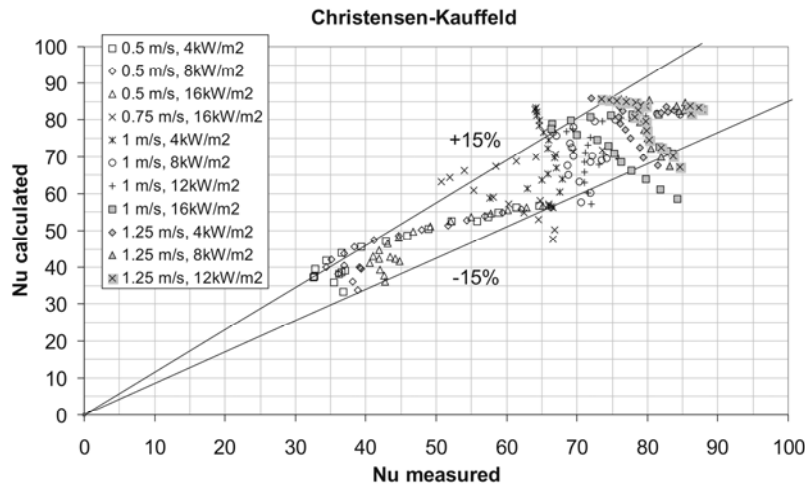
Figure 9.16 Comparison between measured and calculated Nusselt number according to Christensen and Kauffeld correlation

9.4 Conclusion

In order to investigate heat transfer of ice slurry in horizontal tubes and to contribute to clarification of contradicting results published to this date, an experimental investigation of heat transfer behaviour of ice slurry based on ethanol-water mixture in straight horizontal tubes for cooling applications was conducted.

Generally, with higher ice mass fraction and velocity the heat transfer is enhanced. The imposed heat flux has no or just minor influence on the heat transfer coefficient.

Up to ice mass fraction between 10-15 % the mean heat transfer coefficient shows only slight (laminar regime) or no increase (turbulent regime) in comparison to single phase flow. Beyond that ice mass fraction the heat transfer coefficient is increased significantly.

It is believed that this heat transfer enhancement in laminar flow is caused by a heterogeneous flow pattern, where most of the ice crystals float to the top of the tube where they disturb the thermal boundary layer and get into direct contact with the tube wall.

It seems that the ice mass fraction have a greater impact on the heat transfer coefficient than the velocity. The average heat transfer coefficient increases with increased ice fraction, but at higher flow rates increased ice fraction has a reduced effect. The largest relative heat transfer enhancement is found for low flow velocities, namely for laminar flow where the heat transfer is increased by a factor 2 in comparison to single phase flow.

The classical correlation proposed by Sieder and Tate for laminar forced convection in smooth straight circular ducts cannot be used for heat transfer prediction of ice slurry flow. It heavily underestimates measured values.

For turbulent flow the simple Dittus-Boelter equation based on thermophysical properties of the carrier fluid serves well for prediction of mean ice slurry heat transfer coefficient for ice mass fractions up to approximately 10 % and $Re_{cf} > 2300$ regardless of imposed heat flux.

For higher ice mass fractions the correlation proposed by Christensen and Kauffeld gives a good prediction of the experimental mean ice slurry heat transfer coefficients.

10 Performance Comparison of a Static Ice Bank and Dynamic Ice Slurry Cool Thermal Energy Storage Systems

In this study theoretical evaluation of performance of a three ice based cool thermal energy storage systems is conducted, namely static, indirect, external melt ice-on-coil and dynamic ice slurry type storage with a water and ice slurry distribution system. In order to investigate and assess possible economic and energy saving potential of an ice slurry storage system over conventional static type a computer simulation models were used. The systems were compared for high temperature application, for the purpose of milk cooling in the dairy industry. The product temperature that has to be achieved is +3 °C which requires a secondary coolant temperature to be less than +1 °C. Calculations have been performed on basis of specific user supplied load data for a design day, acquired as an actual case for dairy plant "PIK" in the city of Rijeka, Croatia, and local electricity billing rate structure.

The comparison shows that the dynamic CTES system is favourable as to energy consumption in all studied cases.

10.1 Introduction

Several ice making types of cool thermal energy storage (CTES) systems exists on the open market. Most of the CTES systems in food industry are of conventional, static, ice-on-coil type. Only a small percentage of ice based CTES systems in the world are built on ice slurry technology.

A lot of research has in the past been done in the field of static and dynamic CTES technology. Several attempts were made to build and verify dynamic mathematical models of ice bank systems. The types of static CTES systems which are most often referred to in open literature are those classified as direct, external ice-on-coil (Finer et al., 1993; Lopez

133

and Lacarra, 1999; Lee and Jones, 1996) or internal ice-on-coil ice bank system (Chaichana et al., 2001). Finer et al. (1993) and Lopez and Lacarra (1999) developed simple mathematical models of a direct, ice-on-coil ice bank system. Likewise, Lee and Jones (1996) developed analytical models for an indirect, ice-on-coil thermal energy storage system for both charging and discharging modes. As such, the models were simplified to a large extent. Recently Halasz et al. 2009 developed a more complex computer model of a static, indirect, cool thermal storage system with external ice-on-coil building/melting in order to allow the definition of numerous design parameters and operating conditions. The model was experimentally verified by Grozdek et al. (2009).

During the last ten years a great effort has been invested in the field of ice slurry technology. Various phenomena and behaviour of the particular components with ice slurries are investigated (IIR, 2005a; Grozdek et al., 2009). The key problem which is prohibiting wider spread of the ice slurry technology is the high cost of ice slurry production. There are many methods of ice slurry production, yet no single type of ice slurry generator is suitable for all applications. Scraped surface, fluidized bed crystallizer and supercooling are methods for ice slurry production that are commercially applied at present while many others systems such as, vacuum ice, direct contact with immiscible fluid, hydro-scraped and recuperative methods are still under development. Limitations of both the fluidized bed crystallizers and scraped surface ice generators is the minimum concentration of the freezing point depressant that must be used on the ice slurry side. Existing systems operate with minimum concentration of corresponding to the freezing point temperature of -2 °C. Comparison between scraped surface and fluidized bed crystallizer was conducted by Pronk (2006). He came to the conclusion that fluidized bed crystallizers in comparison to the scraped surface systems is an attractive method of ice slurry production concerning investment costs and energy consumption.

The aim of this study is to evaluate the performance of a two ice based cool thermal energy storage systems in order to assess possible economic and energy saving potential of dynamic over conventional static CTES type. Moreover this investigation may contribute as a guideline for future research activities.

Evaluation of the CTES system performance was conducted by comparison of three potential cases by using computer simulation models, i.e. the static CTES system with chilled water as a transport fluid and the dynamic heterogeneous CTES system with chilled water and ice slurry distribution. Calculations have been performed on the basis of a given cooling load for a day as an actual case for dairy plant "PIK" in the city

134

of Rijeka, Croatia, with a given local electricity billing rate. Simulation program for static CTES system is verified with experimental results while the heterogeneous ice slurry storage model is not.

10.2 Simulation model

For the purpose of cheese production in the dairy factory "PIK" in the city of Rijeka, Croatia large quantities of milk are processed on a daily basis. Milk has to be cooled down from +8 °C to the final temperature of +3 °C as quickly as possible. Basically this would require a secondary working fluid (brine) temperature less than +1 °C. The specific user supplied load data for a design day is shown in Figure 10.1. As it may be seen, the consumer heat rate imposed on the cooling system is highly dynamic with the maximum cooling load (800 kW) more than two times higher than the average load (275 kW). The cooling load demand is separated in three stages, whereas the sequence of imposed heat rate is dependant on the fresh milk arrival and pasteurization process.
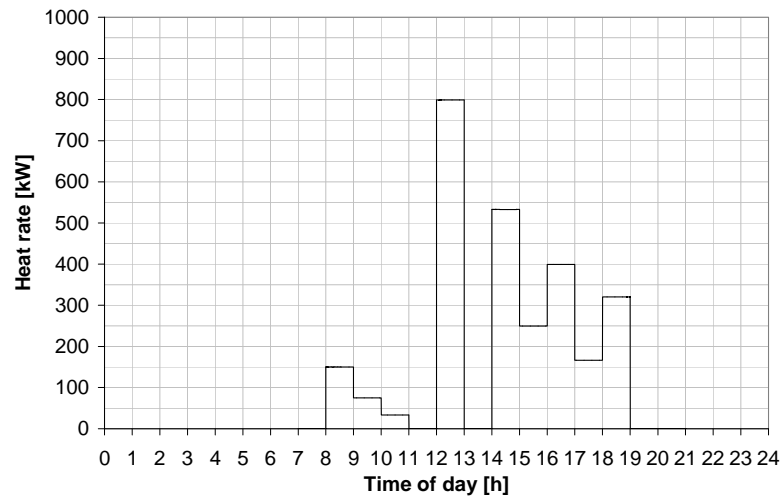
Figure 10.1 User load profile

Three potential cases, where two types of ice storage systems with two types of cooling energy distribution systems are compared and discussed. In a first case static, indirect, external melt ice-on-coil storage system with chilled water as a transport fluid is considered as it is shown in Figure 10.2. In the second case heterogeneous ice slurry storage system with chilled water (Figure 10.3) is examined while as a third case heterogeneous ice slurry storage system with ice slurry distribution is investigated (Figure 10.4). In the two last cases ice is produced by the super-cooling type of ice generator.

For all three cases plain water is used as an energy storage material, with phase change temperature of 0 °C. All three systems can be found in the open market whereas the second and the third cooling systems are less usual.
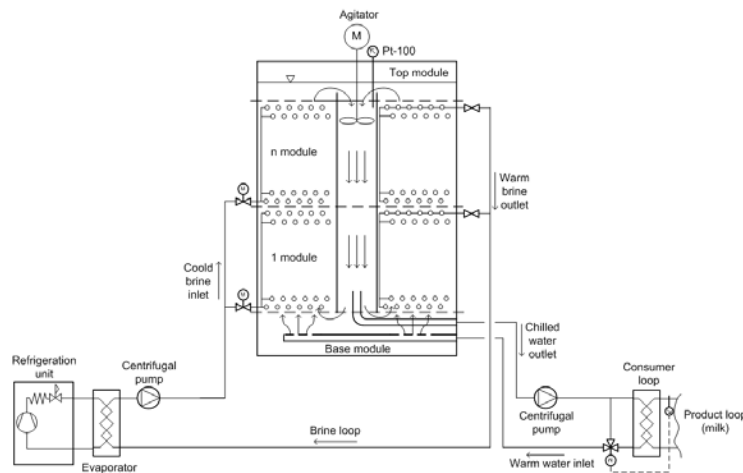
Figure 10.2 External melt ice-on-coil storage system
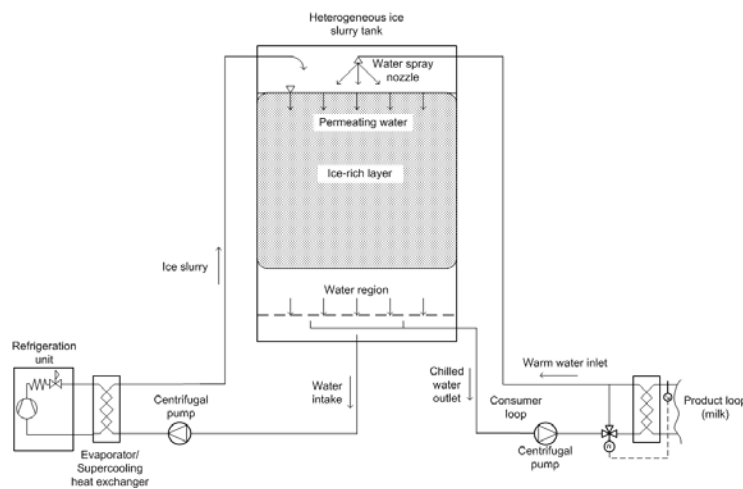
Figure 10.3 Heterogeneous ice slurry storage system with chilled water as a transport fluid
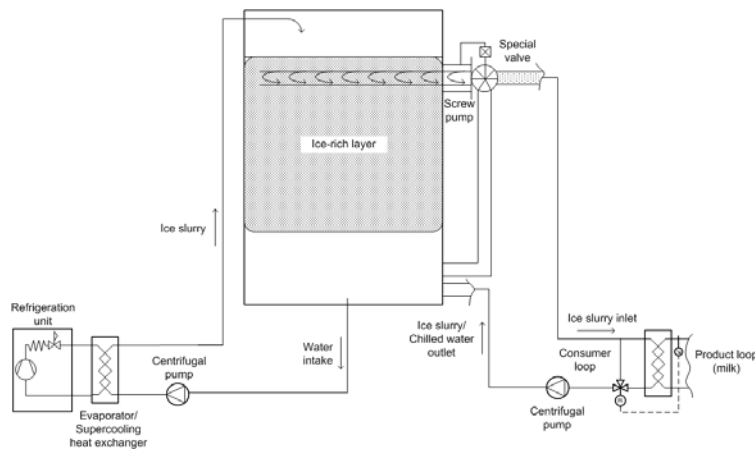
Figure 10.4 Heterogeneous ice slurry storage system with ice slurry as a transport fluid

The melting and charging process for all cases were considered as a separate processes, i.e. full storage system was modelled (Dorgan and Elleson, 1994) where charging of the ice storage was carried during the night time (from 9 p.m. to 7 a.m.) which was limited by the period of cheap electricity. The cool energy stored in the silo is used during day time.

Electricity consumption during off-peak periods in Republic of Croatia is preferred by the local billing rate structure. During on-peak periods (from 7 a.m. to 9 p.m.) the price of electrical energy is 0.085 Eur/kWh while during off-peak period the price is 0.042 Eur/kWh.

10.2.1   Cool thermal energy storage

10.2.1.1   Static CTES, ice bank
In a static, indirect cool thermal storage with external ice-on-coil building/melting, ice is built around the tubes by the brine which is cooled by the refrigeration unit circulating through the tubes. Ice bank system consists of the refrigeration unit cycle, storage unit, i.e. ice silo and consumer cycle, Figure 10.2.

The storage unit is a vertical cylindrical silo built as a stack of up to ten equal modules. The outer part of the silo (of annular cross-section) is used for the ice build-up or melting during upwards flow of water, the central part is used for the downward recirculation of water by means of the propeller (agitator).

Within each module, in an outer annular part, pipes for the flow of brine are spirally wound in a horizontal plane. Each pipe has its own plane.

137

The two vertically adjacent spirals form a staggered arrangement for the upwards flow of water. Submerged pipe coils containing a flow of secondary working fluid are used to build ice on their outer surface. Pipes are made of polypropylene.

On the secondary working fluid side, modules are connected in parallel, so that a total flow of cold brine coming from the refrigerating unit is distributed amongst modules and later collected to be returned to the refrigerating unit. Mixture of water solutions of alcohols or salts are usually used as secondary working fluid.

In the consumers loop, chilled water is circulated from the ice silo to a heat exchanger in product line to provide milk cooling. Heated return water from the consumer is returned to the base module of the silo to be mixed with chilled silo recirculation water.

The detailed description of the simulation model of static, indirect, external melt ice-on-coil storage system can be found in Halasz et al. (2009).

10.2.1.2   Dynamic CTES, water spray method

In order to be able to compare the static and dynamic type storage systems mathematical model of the heterogeneous ice slurry storage system was built. The model considers the melting and charging process. The melting process is based on dynamic model of Tanino and Kozawa (2001) with additional simplifications. The melting process is based on a dynamic model shown in Figure 10.5.

Figure 10.5 Melting model of heterogeneous ice slurry storage

The melting process in a rectangular tank was treated as a one-dimensional problem with uniform temperature distribution in the radial direction. The model consists of water and ice region and only water region placed below ice bed. The warm water is sprayed through the nozzle over the ice bed. Uniform warm water distribution by the nozzle over the tank cross sectional area is assumed. Penetrating through the ice layer the water is cooled while the ice is melted. The water generated by the melting permeates through the ice bed and is mixed with the water in the water region. As a result the height of the ice bed decreases and the water region increases. Other assumptions adopted by the model are as follows:

- o all ice particles are spherical,

- o the number of ice particles during melting doesn't change,

- o ice particles are positioned in the inline arrangement,

- o the water is mixed in only water region,

- o there is no heat transfer to/from environment.

The calculation procedure starts with definition of initial conditions, such as silo size, the inlet water temperature, the particle diameter, mass of the ice in the ice layer, temperature of ice and water in the tank. The calculation procedure is continued by solving the governing equations derived from energy and mass balance in the ice layer and only water region. As a result the water temperature at the tank outlet is obtained.

Energy and mass balance of permeating water in the ice rich layer:

$$M_w c_{pw} \frac{d\vartheta_w}{dt} = \dot{m}_{w,in} c_{pw} \left(\vartheta_{w,in} - \vartheta_w \right) - \dot{m}_{w,melting} c_{pw} \vartheta_w - \Phi_{w\_i} \quad 10.1$$

$$\frac{dM_w}{dt} = \dot{m}_{w,in} + \dot{m}_{w,melting} - \dot{m}_{w,out} \quad\quad 10.2.$$

Ice mass balance: $\dfrac{dM_i}{dt} = -\dot{m}_{w,melting}$ $\quad\quad\quad\quad$ 10.3.

Energy balance of water in the only water region:

$$M_w c_{pw} \frac{\partial \vartheta_{w,out}}{\partial t} = \left(\dot{m}_{w,in} - \frac{\partial H}{\partial t} \cdot A_{tank} \cdot \rho_w \right) c_{pw} \vartheta_w - \dot{m}_{w,out} c_{pw} \vartheta_{out} \quad 10.4.$$

139

Mass of ice (for spherical ice particles): $M_i = \dfrac{4}{3}\pi r_i^3 n \rho_i$ $\qquad$ 10.5.

Mass of ice melting: $\dot{m}_{w,melting} = \dfrac{\alpha_i A_i \vartheta_w}{\Delta h_i}$ $\qquad$ 10.6.

Heat transfer from water to ice surface: $\Phi_{w\_i} = \alpha_i A_i \vartheta_w$ $\qquad$ 10.7.

Heat transfer area: $A_i = 4\pi r^2 n$ $\qquad$ 10.8.

Heat transfer coefficient on water ice interface is calculated according to correlation by Kang et al. (2001) for Nusselt number:

$$Nu = 0.538 \cdot Re^{0.953}$$

10.2.1.3 Dynamic CTES, ice slurry
In this case (Figure 10.4) no special model is used to calculate the temperature of ice slurry at the outlet of the tank. Existence of thermodynamic equilibrium between water and ice crystals in the tank is assumed at all time, i.e. the superheating phenomenon which might occur in reality when ice slurry is imposed to the large heat fluxes and/or high percentage of ice is melted in heat exchangers, is neglected. Even if a superheating of the fluid occurs in the heat exchanger there would be enough time for the ice slurry to reach thermodynamic equilibrium before reaching the storage tank due to the length of the pipeline. Therefore it is assumed that ice slurry of the 0 °C is extracted from the tank.

10.2.2 Ice generator cycle
Two different cases are discussed, building of ice on coils by circulation of brine solution in case of a static ice bank system and production of ice slurry by supercooling of plain water in case of dynamic CTES. In both cases the ice generator cycle consists of pipeline, circulation pump, evaporator and a refrigeration unit.

10.2.2.1 Static CTES system, ice bank system
For a static, indirect CTES system with an external ice-on-coil, ice is built around the tubes by the brine solution which is circulating through the tubes which is cooled by an ordinary refrigeration unit. Brine with a commercial name TEMPER20 with an initial freezing temperature of -20 °C is used as a secondary working fluid.

In case of ice slurry storage system supercooling-type ice generator is considered. The main difference in relation to static ice bank system is that the ice is produced directly by cooling of water below the temperature of the phase change. Namely, the water taken from the bottom of the storage is cooled in the evaporator to be brought into the supercooled state. Ice particles are produced after the evaporator by physically disturbing the flow. According to the research activities carried out up to now, a supercooling of 2 K can be achieved with commercially available systems. Nevertheless the operation of such systems is very sensitive and in order to have continuous production of ice slurry it is necessary to prevent breakdown of supercooling and instantaneous freezing of water inside the evaporator. According to the research of Bedecarrats et al. (2007) to reach the supercooling of 2 K, the water flow inside the evaporator should be laminar and the logarithmic mean temperature difference between water and refrigerant should be kept as small as possible (< 2.5 °C). Moreover, a precise control of refrigeration temperature is important. In order to avoid the sudden breakdown of supercooling inside the heat exchanger and at the same time to maximize the production of ice in given time Bedecarrats et al. (2007) suggested to have supercooling of 1.6 K (corresponds to ice mass fraction of 2 %) with Reynolds number of 3400 and refrigerant temperature of -3.5 °C (these results are valid for tube with inner diameter of 11 mm). The adopted temperature profile in the evaporator/supercooling heat exchanger is shown in Figure 10.6.
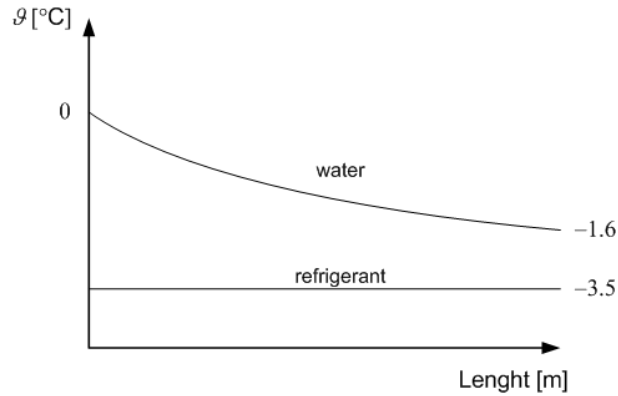
Figure 10.6 Temperature profile in supercooling heat exchanger

10.2.2.3   Refrigeration unit

An ammonia refrigeration unit with a screw compressor is considered for both types of CTES systems. Control of the refrigeration unit capacity and volume ratio is allowed, i.e. compressor performance under full

and part load is modelled according to the manufacturer's data. This allows precise control of the evaporation temperature. The condensation temperature is assumed to be constant at 35 °C.

10.2.2.4   Evaporator
For both types of CTES systems, a shell and tube type of heat exchanger with horizontal circular tubes is considered. In order to simplify the analysis the heat transfer on the ammonia side was considered constant unaffected by the design of the heat exchanger with value of 2000 W/m²K and heat conduction through the pipe wall was considered negligible. Therefore only heat transfer coefficient on brine and water side was modelled.

10.2.2.5   Pipeline
The total pipe length (incoming and outgoing) between cool storages and an refrigeration unit is assumed to be 100 m. The pipeline is sized according to the recommended velocity of approximately 1 m/s.

10.2.2.6   Pump
In both cases the efficiency of the pump is assumed to be 50 %.

10.2.3   Consumer cycle
In the consumer cycle two potential cases are discussed as already mentioned. In a first case chilled water is distributed to the consumer while in the second case ice slurry is used for the transportation of cold.

10.2.3.1   Chilled water as a transport fluid
Chilled water pump is running with continuous water mass flow rate of 38 kg/s which is calculated for the maximum cooling load and the water temperature rise of 5 °C. Regulation of the milk temperature at the heat exchanger outlet is achieved by a three-way regulating valve and a temperature sensor installed in the product circuit. Depending on water temperature at the outlet of the CTES and the consumer load, the cold water flow through the heat exchanger is regulated. The profile of the product temperature and chilled water is shown in Figure 10.7.
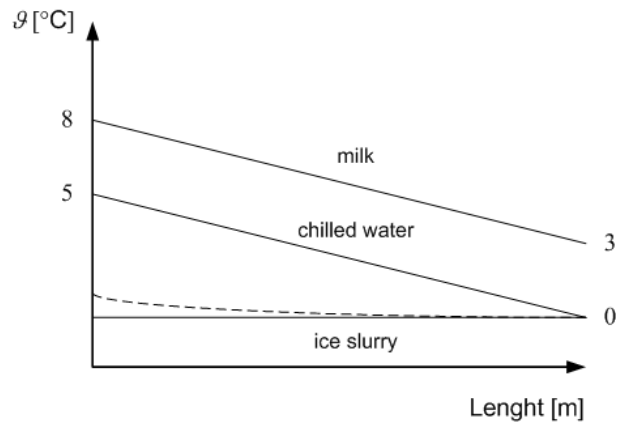
Figure 10.7 Temperature profile in consumer heat exchanger for two cases, with chilled water and ice slurry as transport fluids

10.2.3.2   Ice slurry as a transport fluid

In order to exploit benefits offered by use of ice slurries, instead of chilled water the ice slurry is suggested as a transport fluid to the consumer. The problems related to the heterogeneous ice slurry storage with high ice mass concentrations are connected with ice extraction, i.e. it is impossible to extract the ice particles from the tank without use of auxiliary harvesters and fluidizers. In order to overcome the problem, Egolf et al. (2001) proposed a heterogeneous storage system with screw pump by which the ice slurry with a high ice fraction is pumped from the top of the tank and mixed with liquid from the bottom. By using this method a desired ice fraction can be achieved.

Cooling energy that can be transferred with ice slurries and required pumping power is dependant on the ice mass fraction of the ice slurry. Grozdek et al. (2009) showed that ice slurry with ice mass fraction of 20 % offers maximum values of cooling energy transfer to pumping power ratio. Therefore, in the case when ice slurry is used as a secondary working fluid, an ice mass fraction of 20 % is assumed.

As in the case with plain water flow the ice slurry flow rate is considered constant. The maximum flow rate of ice slurry is calculated as 12 kg/s according to the highest cooling demand by consumer assuming "full melt off" of ice. The regulation of the milk temperature at the heat exchanger outlet is achieved in the same manner as for chilled water.

10.2.3.3   Pipeline

The total pipe length (incoming and outgoing) between cool storage and a consumer heat exchanger is 100 m. The size of the pipeline was chosen

due to a reasonable pressure drop and to have safe operation of ice slurry system.

For cold water distribution systems Recknagel et al. (2006) recommend water velocity to be around 1 m/s. Velocity at this level is assumed to be a good trade-off between pipeline size and induced operating costs.

For ice slurry flow, it is recommended to choose the velocity low enough to be in the region of laminar regime but still high enough to prevent flow separation and system blockage. According to Guilpart et al. (1999) minimum recommended velocity can be calculated from

$$w_{min} = 2.8 \cdot \sqrt{g \cdot d \cdot \left(1 - \frac{\rho_i}{\rho_{cf}}\right)} \qquad 10.9$$

Therefore the velocity of ice slurry in pipes was determined with respect to minimum recommended velocity. The pipes were assumed to be well insulated and no heat transfer with the surrounding was accounted for.

10.2.3.4   Pump
The efficiency of the pump is assumed to be 50 % for chilled water flow while for ice slurry flow it is assumed to be 30 % (Norgaard et al., 2001).

10.2.3.5   Consumer heat exchanger
In order to determine the required size of the heat exchanger for milk cooling in cases when water and ice slurry were used as a secondary coolant, the heat transfer between the secondary coolant and the milk was modelled. In both cases the shell and tube type of heat exchanger with horizontal circular tubes was considered. In order to simplify the analysis, the heat transfer on product side was considered constant at 2000 W/m²K, unaffected by the design of the heat exchanger. Heat conduction through the pipe wall was considered negligible.

The size, i.e. the area of the heat exchanger is directly dependant on the heat transfer coefficient between the tube and the secondary coolant, which is generally dependant on the flow regime and the thermophysical properties of the fluid.

In case of water flow the heat transfer coefficient is calculated according to the following correlations:

$$\alpha = \frac{\lambda}{d} \cdot 1.86 \cdot \left(Re \cdot Pr \cdot \frac{d}{L} \right)^{1/3} \quad \text{for } Re < 2300$$

and

$$\alpha = \frac{\lambda}{d} \cdot \frac{(f/8) \cdot (Re - 1000) \cdot Pr}{1 + 12.7 \cdot (f/8)^{0.5} \cdot (Pr^{2/3} - 1)} \quad \text{for } Re > 2300 \qquad 10.10$$

where f is determined by the Petukhov (Incropera et al., 2006) correlation

$$f = (0.79 \cdot \ln Re - 1.64)^{-2} \quad \text{for } Re > 3000 \qquad 10.11.$$

Friction factor for circular tubes in laminar regime can be calculated from

$$f = \frac{64}{Re} \qquad 10.12.$$

The pressure drop in the heat exchanger is calculated from

$$\Delta p = f \cdot \rho \cdot \frac{L}{d} \cdot \frac{w^2}{2} \qquad 10.13.$$

In case of ice slurry flow, the following correlations are used for determination of the friction factor (IIR, 2005a):

$$f = \frac{64}{Re_{is}} \cdot \left[1 + \frac{He}{6 \cdot Re_{is}} - \frac{He^4}{3 \cdot f^3 \cdot Re_{is}^7} \right] \quad \text{for } Re_{is} < 2300 \qquad 10.14$$

where the Hedstrom number is defined as:

$$He = \frac{d^2 \cdot \tau_0 \cdot \rho_{is}}{\eta_{is}^2} \qquad 10.15$$

and

$$\frac{1}{\sqrt{f}} = \frac{2}{n^{0.75}} \cdot \log_{10}\left(Re_{is} \cdot \left(\frac{f}{4}\right)^{\frac{2-n}{2}}\right) - \frac{0.2}{n^{1.2}} \text{ for } Re_{is} > 2300 \qquad 10.16$$

where n is a fluid behaviour index and is 1 for a Bingham fluid.

Correlations for calculation of heat transfer coefficients of water ice slurry in horizontal circular tubes were not found in an open literature. Instead they are estimated by use of correlations for 10.3 % ethanol water mixture described by following relations. The average Nusselt number for an ice concentration above 5 % is described by the relation (Kauffeld et al., 1999):

$$\left(\frac{Nu_{is}}{Nu_{cf}}\right)_{ethanol-water} = 1 + 0.103 \cdot c_i - 2.003 \cdot Re_{cf}^{-0.192 \cdot \frac{30-c_i}{30}} \cdot c_i^{\frac{0.339 \cdot Re_{cf}}{10^4}} \qquad 10.17$$

and for an ice concentration below 5 %:

$$\left(\frac{Nu_{is}}{Nu_{cf}}\right)_{ethanol-water} = 1 \qquad\qquad 10.18.$$

These correlations have been confirmed by an experimental work on an ice slurry system described in Grozdek et al. (2009). Since in this case water without freezing depressant is used, the heat transfer coefficient on ice slurry side is calculated as:

$$\left(\frac{Nu_{is}}{Nu_{cf}}\right)_{water} = \left(\frac{Nu_{is}}{Nu_{cf}}\right)_{ethanol-water} \qquad\qquad 10.19.$$

10.3 Results and discussion

10.3.1 Static CTES system, ice bank system

The performance of the static, ice bank storage system is evaluated by use of simulation software developed by Halasz et al, 2009. On the basis of a specific user supplied data for a design day, acquired as an actual case (Figure 10.1), the task was to offer an ice bank system which would meet requirements set by a user, i.e. to provide an outlet water temperature to the consumer below 1 °C. As an input parameter the existing module design and its related geometry acquired from the producer was used.

When designing the ice bank systems one has to decide on the number of modules stacked in the silo. According to the manufacturers data the total nominal capacity of one module with average ice thickness of 35 mm is approximately 580 kWh, for 30 mm it is 455 kWh, for 25 mm it is 345 kWh and for 20 mm it is 248 kWh. With a total consumer load of 2750 kWh during a 24 hour period (see Figure 10.1), one silo with five modules and ice thickness of 35 mm should be sufficient or with six modules with ice thickness of 30 mm or with eight modules with ice thickness of 25 mm. The higher the number of stacked modules the lower the ice thickness is required. Consequently, the higher brine temperature at silo inlet is required with higher COP of the refrigeration unit. On the other hand, the higher the number of modules the higher initial cost of the system.

Another decision that has to be made is the choice of the operating parameters, i.e. refrigeration capacity and the brine mass flow rate. The higher the refrigeration capacity the less time is needed to reach the desired ice accumulation but the consequence is higher size and price of the refrigeration equipment. Since the total amount of energy that has to be stored during the night time is 2750 kWh and the charging period is limited to 10 hours the minimum required mean chillers capacity is approximately 275 kW.

The choice of the ice thickness and the choice of the brine mass flow rate has a significant effect on the refrigeration unit COP. Generally, the lower the brine mass flow rate the lower the overall heat transfer coefficient between the water in the silo and the brine. Consequently to achieve desired cooling demand the temperature difference between water and the brine should be higher. Moreover, brine temperature difference between inlet and outlet of the silo should be higher as well. As an effect the nonuniform ice thickness distribution along the tubes occurs which can lead to poor discharge characteristics in a melting mode and difficulties in silo operation. On other hand, the higher the brine mass flow rate the higher the required circulation pump power resulting with higher operating costs of the system.

The product of overall heat transfer coefficient and ice interface area $(kA)_{charging}$ for three different brine velocities (in tube) and 5 module silo is shown in Figure 10.8 for the case of the ice bank system. The figure also shows brine inlet temperatures to the ice silo and brine temperature rise from the tube inlet to the tube outlet, $\Delta \vartheta_b$. As it may be noticed the lowest $(kA)_{charging}$ product is found for velocity of 0.5 m/s. In order to compensate low overall heat transfer coefficient and still to reach the desired ice quantity during the charging period, the brine inlet temperature to the silo has to be low. The reason for such poor heat transfer is that

the brine flow with the velocity of 0.5 m/s is in laminar regime. For the other two velocities 1 and 1.5 m/s, the flow is turbulent and the limiting heat transfer occurs on the water side. Therefore the deviation in $(kA)_{charging}$ and inlet brine temperature between these two cases are small. Further increase in the brine velocity would not give much higher increase in $(kA)_{charging}$ but the pressure drop would significantly increase.
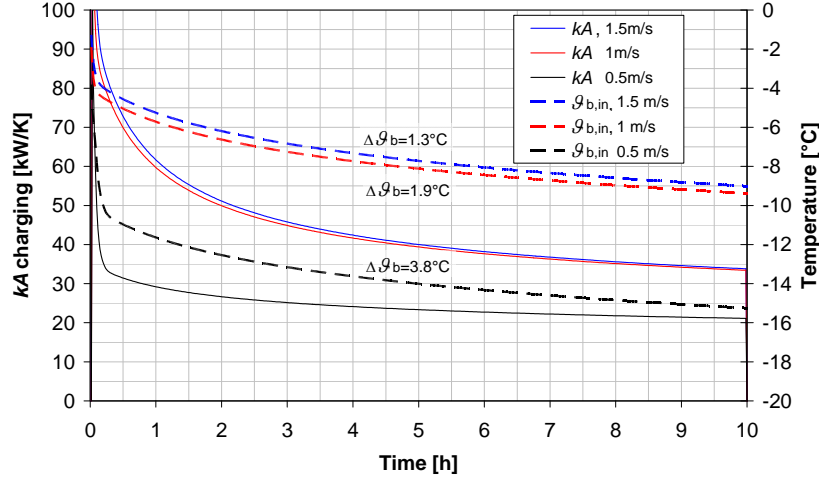
Figure 10.8 $(kA)_{charging}$ and brine inlet temperature versus charging time for 5 module silo

Moreover, the highest deviation of ice thickness between inlet and outlet of the tubes in the ice silo is found for the lowest velocity (7 mm), while for the other two velocities this difference is much lower (3-4 mm). The total brine mass flow rate for the case with a velocity of 0.5 m/s is 22.7 kg/s, for 1 m/s it is 45.5 kg/s while for 1.5 m/s it is 68 kg/s. The brine loop pressure drop for case with velocity of 0.5 m/s is 0.07 bar, for 1 m/s it is 0.47 bar and for 1.5 m/s it is 0.95 bar.

Since the power of the refrigeration unit is usually more than ten times higher than the power of the circulation pump it is more reasonable to design the system which will offer refrigeration unit COP as high as possible (Figure 10.9). It can be concluded that the brine mass flow rate should be chosen high enough to ensure higher heat transfer coefficient than on the water side with bearing in mind increasing circulation pump consumption. For the following analysis brine mass flow rate is chosen to provide velocity in the tube of 1 m/s.

148
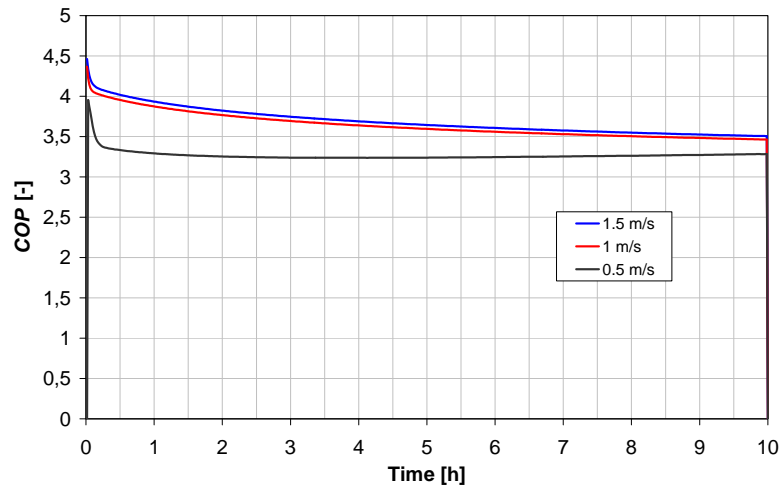
Figure 10.9 COP vs. charging time and brine velocity for 5 module silo

In Figure 10.10 product of overall heat transfer coefficient and ice inter-
face area for ice silo with 5, 6, 7 and 10 modules is shown. Besides, brine
inlet temperatures to the ice silo are shown as well. Calculations are made
for brine velocity inside tubes of 1 m/s.
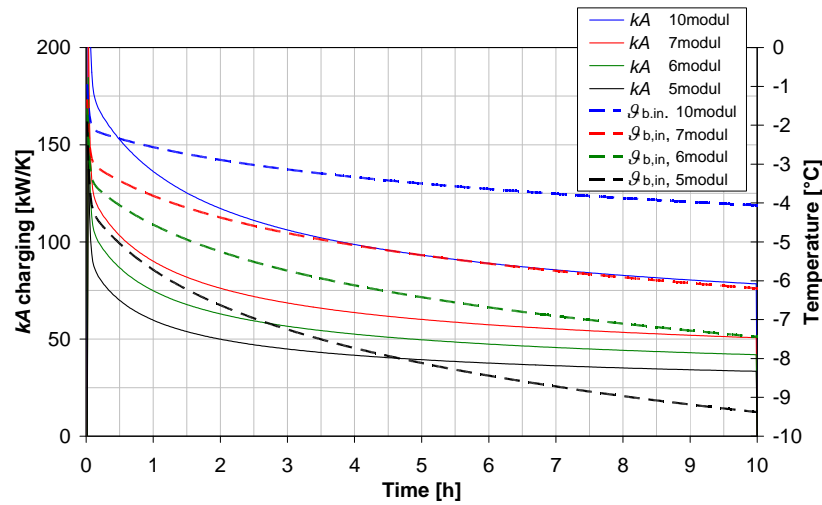
Figure 10.10 $(kA)_{charging}$ and brine inlet temperature versus charging time
for 5, 6, 7 and 10 modules in silo

The desired ice quantity (around 2750 kWh) at the end of the charging
period is reached in all cases. As shown, the higher the number of mod-
ules the higher the $(kA)_{charging}$ product and higher the inlet brine tem-
perature. By increasing the number of modules the area of the heat

transfer rises while the final ice thickness around the tubes is lower. For a silo with 5 modules, average ice thickness at the end of the charging is around 33 mm, for 6 modules is 29 mm, for 7 modules is 26 mm and for 10 modules is 21 mm. Since the resistance to the heat transfer through the ice layer decreases with decreasing ice thickness the required temperature difference between the ice and the brine decreases as well while the refrigeration unit COP rises. In Figure 10.11 it may be noticed that the refrigeration unit COP is raising with added modules but this trend is progressively decreasing. The highest relative increase in COP can be observed for transition from 5 to 6 module silo.
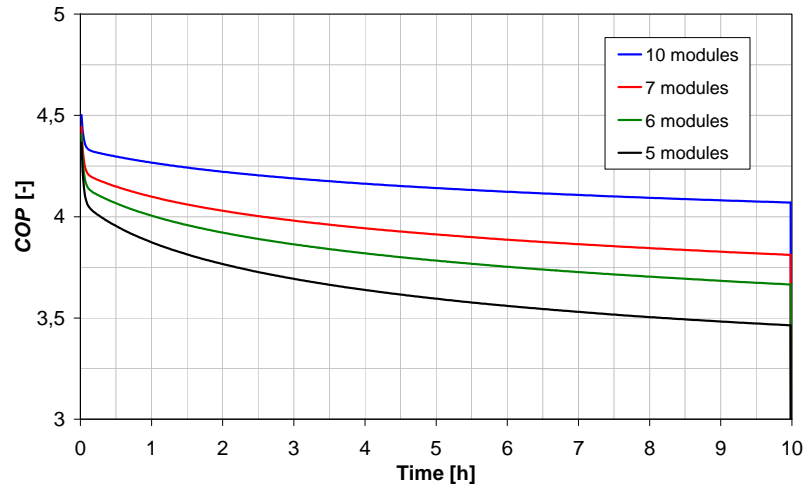
Figure 10.11 COP versus charging time for 5, 6, 7 and 10 modules in silo

Moreover, by increasing the number of modules (and with the condition on brine velocity of 1 m/s) the total brine mass flow rate in circulation increases. The total brine mass flow rate for a case with 5 module silo is 45.5 kg/s, for 6 modules it is 54.5 kg/s, for 7 modules it is 63.5 kg/s, while for 10 modules it is 91 kg/s. By increase of the brine mass flow rate the brine pump power and the pipeline size increases. Since the brine velocity inside the silo was unchanged the silo pressure drop is equal for all cases. In addition, the more modules in silo the higher the initial costs of the system. Therefore for analysis that follows ice silo with 5 modules is considered.

In Figure 10.12 to Figure 10.15 performance and behaviour of the 5 module ice silo versus computational time are presented. Calculation has started at 21 h with no ice on the tubes and with initial temperature of the water, tubes and brine in the silo of 0 °C. In Figure 10.12 storage charging and discharging rates, consumer load and storage inventory is

150

shown. For the first ten hours ice is built on the tubes with rather constant charging rate. At the end of the charging cycle approximately 2750 kWh of energy is stored in form of ice. The discharging cycle starts at 8 a.m. (11th hour of calculation) and lasts up to 7 p.m. In a first discharging period a heat rate of approximately 150 kW is introduced to the ice bank. Since at that moment the ice silo is full, outlet water temperature rises just slightly above 0 °C (Figure 10.13). Therefore the storage discharging rate and the consumer load are almost equal. At 12 h (15th hour of calculation) the ice bank is imposed to the peak cooling load. Due to still high ice content the outlet water temperature rises only to 0.2 °C. In the next four hours (up to 21 h) the outlet water temperature doesn't change much. The highest water temperature rise is observed for the time period between 21 hour and 22 hour. Since at that time only 7 % of ice is still present in the silo due to insufficient ice-water interface area and heat transfer coefficient the water temperature rises to 1 °C.

Figure 10.12 Storage charging and discharging rates, consumer load and storage inventory versus computational time

The higher the heat transfer coefficient between water and ice and the higher the water-ice interface area the higher ice bank capability to ensure the cooling load demands without high outlet water temperature rise.

The water to ice heat transfer coefficient is basically dependant on water velocity around the ice tubes. The water velocity is dependant on agitator capacity and water flow cross sectional area which is a function of spanwise clearance between ice layers. When the ice bank is full the ice interfacial area is high and the water velocity is high as well due to the low

cross sectional area between ice layers. Therefore with high αA product storage, the discharging rate is high with consequently low outlet water temperature.

As ice is melted the ice thickness decreases causing the ice interfacial area to decrease. The water to ice heat transfer coefficient decreases as well due to the increased cross sectional area between ice layers. Therefore storage discharging rate capability decreases and consequently the outlet water temperature rises.
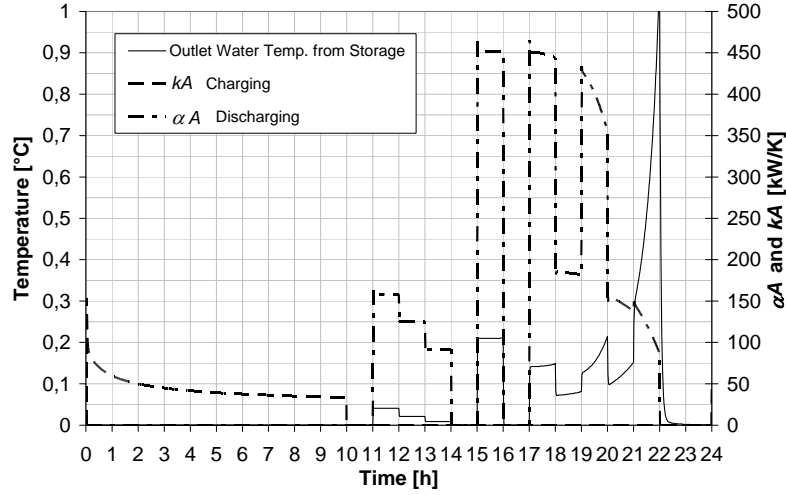
Figure 10.13 Water outlet temperature, kA charging and αA discharging product versus computational time

Silo discharging efficiency can be defined as an ability of an ice bank to reduce the incoming water temperature to the temperature of phase change, 0 °C, which would be the case for an infinitely large ice to water surface area. It is calculated as:

$$\eta_{dis} = \frac{\vartheta_{w,in} - \vartheta_{w,out}}{\vartheta_{w,in}}$$

10.20

The discharging efficiency and the refrigeration unit COP for a five module silo is shown in Figure 10.14. As expected, the discharging efficiency decreases with increasing consumer load and decreasing ice quantity remaining in silo.

152
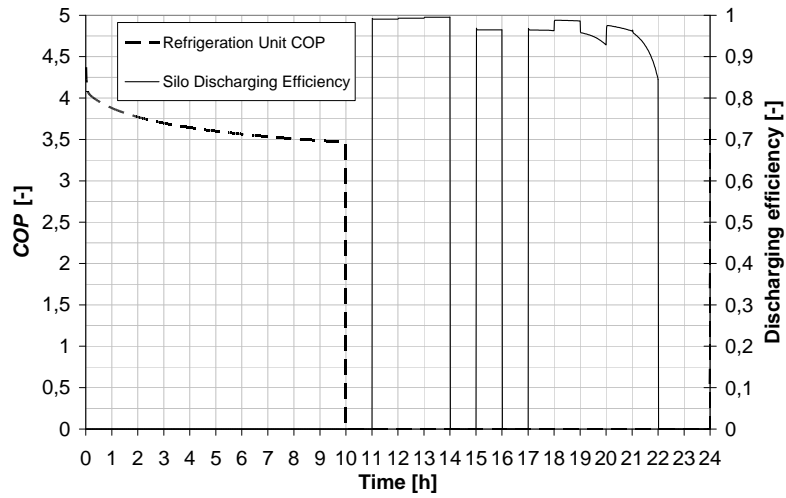
Figure 10.14 Refrigeration unit COP and silo discharging efficiency versus computational time

In Figure 10.15 the evaporation temperature and the brine outlet temperature from evaporator is shown. Evaporator temperature was calculated with condition kA_{evap}=100 kW/K. The refrigeration unit COP is calculated on the basis of evaporation and condensation temperature, charging rate and a manufacturer's data for ammonia type screw compressor (Figure 10.14).
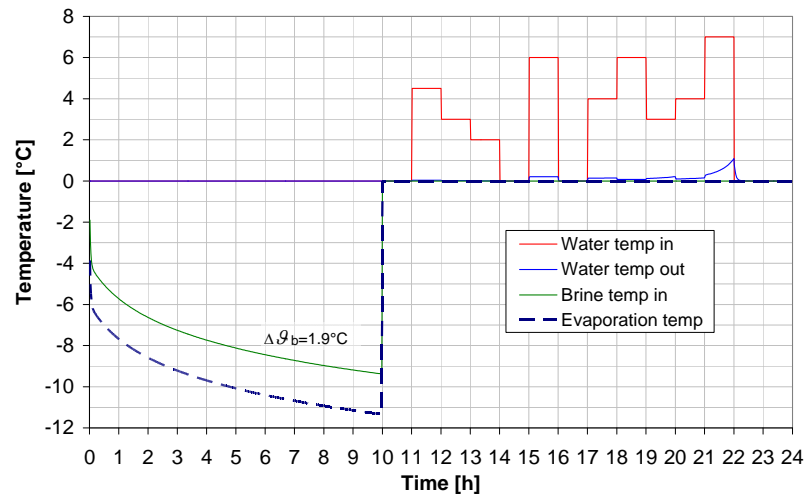
Figure 10.15 Evaporation temperature, water temperature in and out of the silo and brine temperature at silo inlet

Energy consumption of the refrigeration unit in a charging mode is calculated as 772.4 kWh. To calculate the energy consumption of the brine circulation pump the pressure drop in brine pipeline and evaporator are calculated as well.

10.3.2   Dynamic CTES, water spray system

In Figure 10.16 to Figure 10.18 performance of the ice slurry system is shown. Figure 10.16 shows storage charging and discharging heat rates and the storage inventory versus computational time.
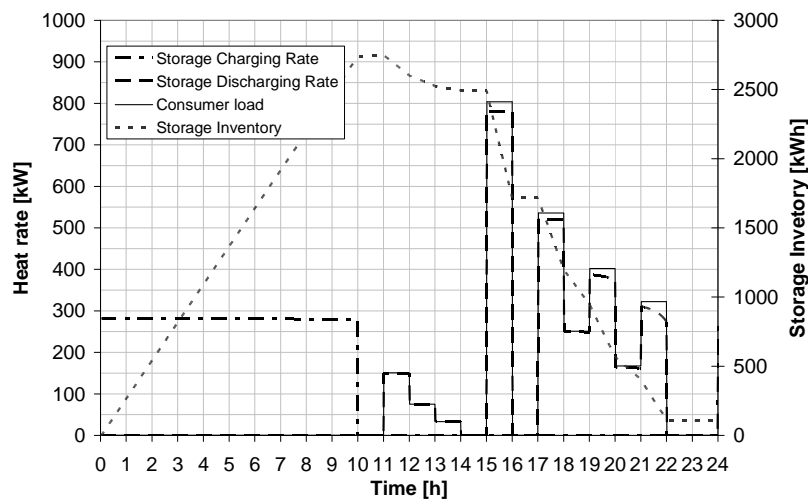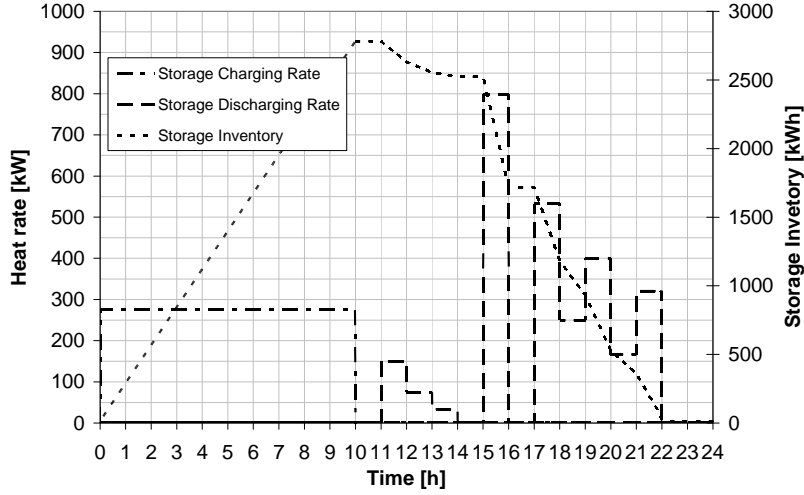
Figure 10.16 Storage charging and discharging rates, consumer load and storage inventory versus computational time

Calculation has started at 21 h with no ice in the tank and with initial temperature of the water of 0 °C. It is assumed that during charging cycle ice particles of spherical form with diameter of 0.4 mm are produced. During the charging period the cooling heat rate is kept constant as it was the case in example of static ice bank system. As it may be observed from the Figure 10.17 unlike static, ice-on-coil CTES systems, the product of heat transfer coefficient and heat transfer area of charging is constant during the period of ice production. This was to be expected since the ice slurry is produced directly by cooling of water from 0 °C to -1.6 °C without ice building on cold evaporator surface. In this case $(\alpha A)_{charging}$ product is related to the heat transfer among water and evaporator surface, i.e. primary refrigerant, while in case of ice bank system $(kA)_{charging}$ was related to the heat transfer among the water and the brine. Therefore the $(\alpha A)_{charging}$ and $(kA)_{charging}$ products should not be compared directly. The kA values in case of ice bank provides information on performance of a heat exchanger (spirally wound tubes as an ex-

154

tra component of the ice silo), but αA in case of the ice slurry system gives information on the performance of the evaporator. The performance of both systems during charging should be evaluated at the level of the refrigeration unit by comparison of their COP. As seen in Figure 10.18 the COP of the ice slurry system is at a constant level of 4.4, while in the case of the ice bank system it is decreasing with time as more ice is deposited on the tubes and has an average value of 3.6. In both cases the characteristics of the same refrigeration unit is used for the COP evaluation.
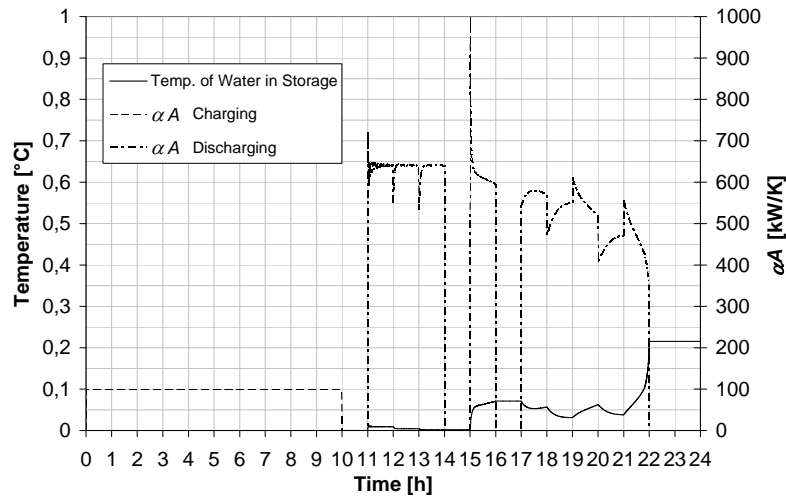
Figure 10.17 Water outlet temperature, αA charging and discharging product versus computational time

During the discharging cycle same heat load is imposed to the ice slurry tank as in case of the ice bank system. During almost the entire cycle the outlet water temperature from the ice tank was slightly higher than 0 °C (Figure 10.17). Only at the end of the cycle a water temperature rise to 0.2 °C is recorded. The reason for such stable outlet temperature is high water-ice interface area, due to the size of ice particles. As shown in Figure 10.17 in the first and second discharging period the $(\alpha A)_{discharging}$ product is at the level of 650 kW/K, while in the last period it progressively decreases as ice is being melted. In comparison to the static system, the ice slurry system shows at least 30 % higher $(\alpha A)_{discharging}$ product. The discharging efficiency curve shows higher values as well.
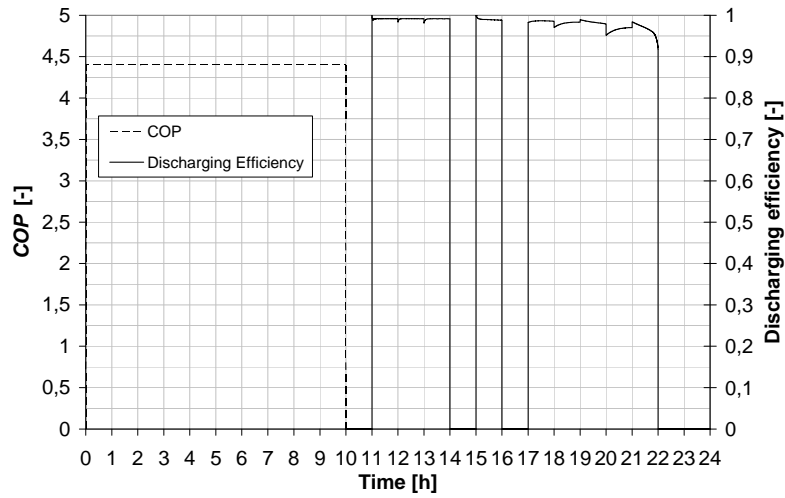
Figure 10.18 Refrigeration unit COP and silo discharging efficiency versus computational time

Energy consumption of the refrigeration unit in a charging mode is calculated as 625.4 kWh.

10.3.3   Pipeline

The sizing of the generator and consumer loop pipelines are carried out according to the maximum cooling demand that occurs during the discharging period (800 kW) and maximum refrigeration load during the charging period (275 kW). The design and operating characteristics of pipelines in consumer and generator loop are shown in Table 10.1.

Table 10.1 Pipeline design and operating characteristics

Loop	Fluid	Mass flow rate [kg/s]	d [m]	w [m/s]	L [m]	$\Delta p/L$ [Pa/m]	Δp [Pa]
Consumer	Ice slurry	12	0.125	1	100	90	9000
	Water	38	0.2	1.2	100	60.42	6420
Generator	Supercooled water	41	0.2	1.3	100	69	6900
	Brine	45.6	0.2	1.25	100	92	9200

10.3.3.1 Chilled water as a transport fluid, consumer loop

The temperature profiles in the consumer loop heat exchanger is shown in Figure 10.7. With a water temperature change in the heat exchanger of 5 °C, the required chilled water mass flow rate is 38 kg/s. For a velocity of 1 m/s the needed diameter of pipeline is 200 mm with specific pressure drop 60.4 Pa/m.

10.3.3.2 Ice slurry as a transport fluid, consumer loop

In Figure 10.19 and Figure 10.20 the transport capability (heat rate transferred by fluid) versus velocity and specific pressure drop respectively of ice slurry for ice mass fraction of 20 % are shown. The line of minimum velocity (w min) below which the ice slurry flow is unstable and may lead to system blockage is plotted as well. By using pipeline DN125 with velocity of 1 m/s (Figure 10.19) the corresponding pressure drop is 90 Pa/m (Figure 10.20) which is twice compared to flow of water. Moreover, required ice slurry mass flow rate considering „full melt off" of ice at highest cooling demand is 12 kg/s (Table 10.1).
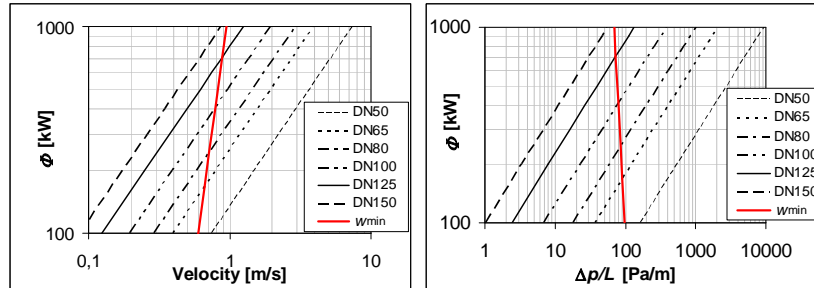
Figure 10.19 and Figure 10.20 Transport capability and specific pressure drop of ice slurry for ice mass fraction of 20 %

Pipeline in the generator loop for supercooled water and secondary working fluid is treated in the similar way. Since the ice mass fraction of ice slurry flow after the supercooler is only 2 %, the pressure drop is calculated as if it is a flow of water. The pipeline diameter for ice slurry flow is almost half the size of when water is used for transport of cold. However pressure drop of the water flow is 30 % lower than for ice slurry flow. In the generator loop the pipelines are of the same size (200 mm) but water flow has approximately 30 % lower pressure drop than the brine flow.

10.3.4   Heat exchangers

10.3.4.1   Consumer loop

Sizing of the consumer loop heat exchangers is carried out for the highest cooling demand of 800 kW (at 12 p.m.) and the outlet water temperature from the ice bank feed to the heat exchanger of 0.2 °C. In case of the dynamic CTES system with water spray method the temperature of the water was less than 0.1 °C. When the ice slurry is used as a secondary fluid it is assumed that the temperature of ice slurry during melting time remains constant at 0 °C. In reality due to limited ice particles surface area and heat transfer coefficient between carrier fluid and ice crystals superheating of ice slurry occurs. As a consequence temperature of ice slurry is higher than 0 °C, as the water is not in thermodynamic equilibrium with ice crystals. Thermodynamic equilibrium is reached further downstream of the heat exchanger, in the pipeline, where ice crystals melt and water temperature decreases reaching the initial freezing temperature. Since the degree of superheating is difficult to asses, its influence is not considered in the process of heat exchanger sizing. For both cases whether the water or ice slurry is used as a transport fluid the heat transfer coefficient on the milk side was considered constant at 2000 W/m²K. In Figure 10.21 heat transfer coefficient (α) and overall heat transfer coefficients (k) and also the specific pressure drop of water and ice slurry flow are shown for tube diameter of 21 mm.
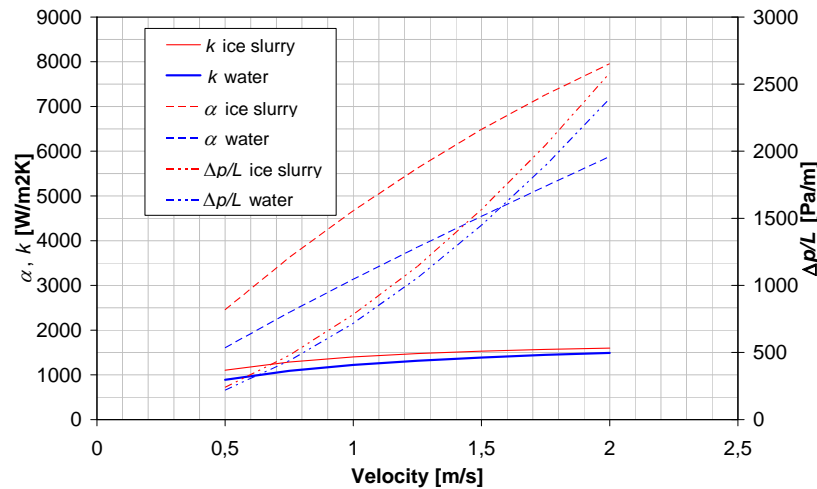
Figure 10.21 Heat transfer coefficient, overall heat transfer coefficient and specific pressure drop of water and ice slurry versus flow velocity for tube diameter of 21 mm

Since the pressure drop of ice slurry flow during melting is exponentially decreasing (Egolf et al., 2001) the logarithmic mean pressure difference method is used to calculate average pressure drop of ice slurry flow in the heat exchangers. The same method is used to calculate the average heat transfer coefficient of ice slurry flow during melting.

From Figure 10.21 it is evident that with increasing velocity the overall heat transfer coefficient is increasing as well. The highest increase is observed in velocity range from 0.5 to 1 m/s since the heat transfer coefficients of water and ice slurry are similar to the heat transfer coefficient on the milk side (2000 W/m²K). With increasing velocity above 1 m/s, due to unchanged heat transfer coefficient on the milk side only a slight increase of overall heat transfer coefficient is observed. Consequently, the area needed of the heat exchanger is decreasing with the same trend (Figure 10.22).
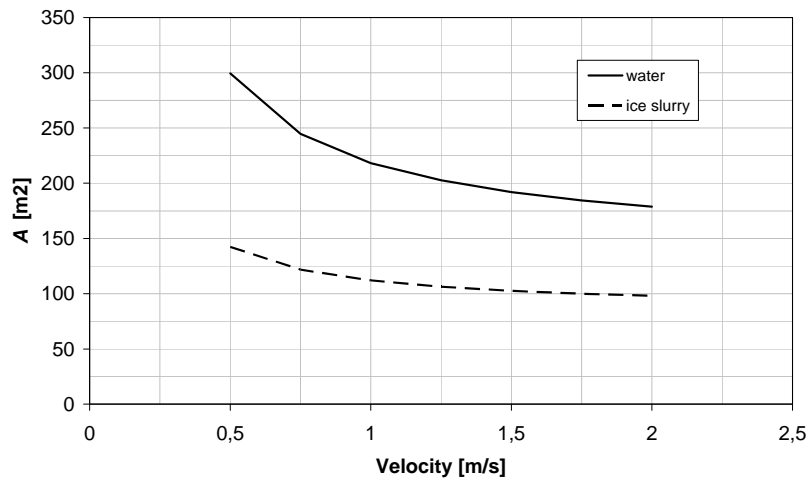
Figure 10.22 Heat exchanger area for water and ice slurry flow for tube diameter of 21 mm

On the other hand with increasing velocity the specific pressure drop in the single tube of the heat exchanger is increasing as well. To avoid the increase length of the tube and to keep lower pressure drop, more parallel tube is suggested with a given heat exchanger area. Specific pressure drop of water and ice slurry flow versus flow velocity for different tube diameters is shown in Figure 10.23.
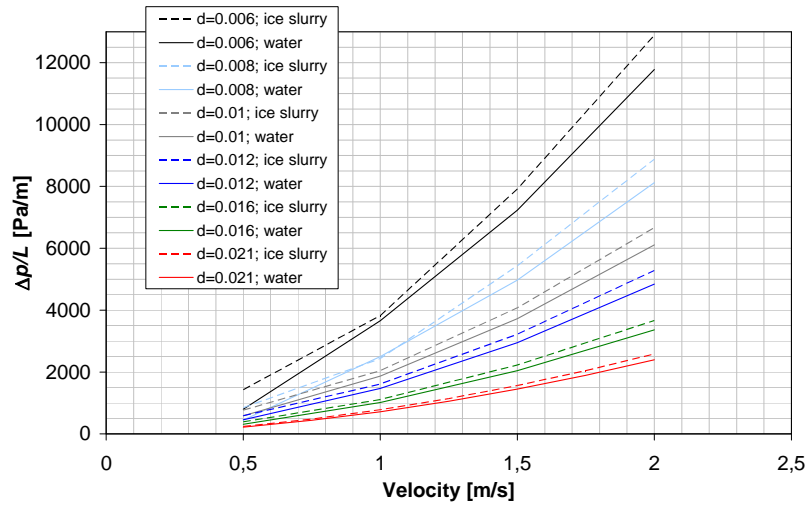
Figure 10.23 Specific pressure drop of water and ice slurry flow versus flow velocity for different tube diameters

In Table 10.2 summary of heat exchangers design and operating characteristics is shown.

Table 10.2 Heat exchangers design and operating characteristics

Loop	Fluid	$\dot{m}$ [kg/s]	d [m]	w [m/s]	k [W/m²K]	$\Delta\vartheta_m$ [°C]	A [m]	N [-]	L [m]	$\Delta p/L$ [Pa/m]	Δp [Pa]
Consumer	Ice slurry	12	0.01	1	1420	5.1	111	156	22	2040	44880
	Water	38	0.01	1	1230	3	217	492	14	1865	26110
Generator	Supercooled water	41	0.012	0.5	1073	2.6	98	738	3.5	457	1600
	Brine	45.6	0.012	1	700	2.75	143	396	9.6	2168	20813

As it may be observed from Table 10.2 in the consumer loop the ice slurry heat exchanger is half the area of the water type heat exchanger. Vice versa the pressure drop of ice slurry heat exchanger is almost twice that of the water type.

10.3.4.2   Generator loop

Dimensioning of the heat exchangers in the generator loop is treated in the similar way as in case of consumer loop. With 275 kW of required cooling capacity for ice production and water supercooled to -1.6 °C the required supercooled water mass flow rate is 41 kg/s. It is calculated that the area of the ice slurry heat exchanger in the generator loop is 30 % lower than of the brine type, but in order to satisfy the condition of

160

Re=3400 (0.5 m/s as a maximum water velocity for 12 mm tube) the number of parallel tubes is much higher with consequently lower pressure drop.

10.3.5   Pumping power

In Table 10.3 the required pumping power and consumed energy in the consumer and generator loop is shown.

Table 10.3 Pumping power and consumed energy for a design day

Loop	Fluid	$\dot{V}$ [m³/s]	Δp [Pa]	P [W]	E_P [kWh]
Consumer	Ice slurry	0.0122	53880	2191	19.72
Consumer	Water	0.038	32530	2472	22.25
Generator	Supercooled water	0.041	8500	697	6.97
Generator	Brine	0.0397	77013	6115	61.15

It can be seen that in the consumer loop the difference in pumping power and consumed energy between ice slurry and water system is low. Even though the pressure drop in the ice slurry circuit is almost double the pressure drop of the water system, due to the much lower volume rate of ice slurry in comparison to the water volume rate, the final pumping power is almost similar. In the generator loop the required pumping power and consumed energy of the brine circuit is almost ten times higher than in the case of supercooled water.

Finally in Table 10.4 the results for different systems solution consumption for a design day are shown. It can be seen that dynamic CTES system consumes approximately 25 % less energy than the static CTES ice bank system. Difference in consumed energy between ice slurry transportation and water system is negligible.

Table 10.4 System consumption

System type		Refrigeration unit consumption [kWh]	Pump consumption [kWh]	Total system consumption [kWh]
Static ice bank system		772.4	83.4	855.8
Dynamic ice slurry system	Ice slurry	625.4	26.7	652.1
	Water	625.4	19.72	647.6

10.4 Conclusion

In the present study results from simulation on performance of a two ice based cool thermal energy storage systems are presented. In particular three cases with two system solutions are examined, static CTES system with chilled water as a transport fluid, dynamic heterogeneous CTES system with chilled water and ice slurry distribution. In the last two cases the ice is produced by a supercooling type of ice generator. In order to investigate and assess possible economic and energy saving potential of an ice slurry storage system over conventional static type a computer simulation models were used.

It is shown that dynamic heterogeneous ice slurry storage system shows better characteristics in both charging and discharging mode in comparison to the static external melt ice-on-coil system. Since the ice slurry is produced directly without ice building on evaporator surface the refrigeration unit COP remains at the same level of 4.4 during charging. On the other hand for the static CTES system the refrigeration unit COP will decrease with building of ice to the average of 3.6. During the entire discharging cycle the dynamic CTES with water spray system show more stable and lower outlet water temperatures than the static CTES system. In case of the dynamic CTES with ice slurry system the temperature of ice slurry in the tank remains at all times at the phase change temperature of 0 °C.

In generator and consumer loops, the dynamic CTES system show advantages to the static CTES system as well. The size of the supercooler heat exchanger is smaller than the heat exchanger for cooling of brine. Moreover, the pressure drop and the pump energy consumption for ice slurry production is much lower than for the brine cooling. In the consumer loop the benefit of using ice slurry as a secondary working fluid is shown through the reduced size of heat exchanger and the pipeline. Required area of the water type heat exchanger is almost twice the area of the ice slurry heat exchanger. Same results can be found for the pipelines.

Finally total energy consumption of dynamic CTES system for a design day is approximately 25 % lower than for the static CTES system. According to the conducted analysis dynamic CTES system with ice slurry distribution show highest economic and energy saving potential.

However, it should be noted that results presented here for CTES system with ice slurry are purely theoretical and should be verified by an experiment. There are many problems of technical nature with operation of ice slurry components and systems in whole which needs yet to be overcome.

162

11 Conclusions and Suggestions for future work

11.1 Conclusions

The experimental investigation of ice slurry pressure drop and heat transfer in horizontal straight tubes for cooling applications have been investigated. In particular mixture of 10.3 % of ethanol water mixture with initial freezing point is considered. Moreover, theoretical evaluation of the performance comparison of a static ice bank and dynamic ice slurry CTES systems has been conducted. The following conclusions can be drawn with relevance to the experimental work and theoretical analysis.

Due to change in size and shape of ice crystals with time the flow behaviour of the ice slurry is time dependant. The pressure drop of ice slurry is generally higher in comparison to the single phase flow in laminar and in turbulent flow regime. However for ice concentrations of 15 % and higher, transition moment from laminar to turbulent flow regime is delayed than in case of single phase fluid. This results in same or even lower ice slurry pressure drop than for single phase flow.

If ice slurry is used for transport of energy it is recommended to keep the concentration of ice particles at level of 20 % while the velocity should be generally at the upper boundary of laminar flow regime. At this concentration ratio of transport capacity to pumping power is found to be at its maximum while the velocity was high enough for proper operation of the system without blockages.

To predict an ice slurry pressure drop in horizontal tubes in laminar regime one can exploit Buckingham-Reiner method which gives good result as long as the buoyancy term is low, i.e. density difference between ice and liquid solution is small or ratio of ice slurry velocity to tube diameter is large.

In order to account for stratification effect, the empirical correlation for ice slurry friction factor in laminar flow regime is derived. It is based on the present experimental data for 10.3 % of ethanol-water mixture. It predicts 82 % of experimental data within accuracy of ±15 %.

In turbulent regime methods of Dodge-Metzner and Tomita show good and relatively accurate prediction capability. In comparison to Tomita method, Dodge and Metzner correlation is less demanding to use.

Beside geometrical characteristics of the straight tubes and thermophysical properties of the carrier fluid the heat transfer of ice slurry is generally a function of ice mass fraction and velocity. The imposed heat flux has no or just minor influence on the heat transfer coefficient.

Up to ice mass fraction between 10-15 % the mean heat transfer coefficient shows only slight (laminar regime) or no increase (turbulent regime) in comparison to single phase flow. Beyond that ice mass fraction the heat transfer coefficient is increased significantly especially in laminar flow regime (by factor 2) since most of the ice crystals float to the top of the tube where they disturb the thermal boundary layer. Moreover, it seems that the ice mass fraction have a greater impact on the heat transfer coefficient than the velocity.

Based on the experimental results, correlation for calculation of local Nusselt number, for laminar ice slurry flow regime and 10.3 % of ethanol-water mixture has been derived. It predicts 75 % of experimental data within accuracy of ±15 %.

For prediction of ice slurry heat transfer in horizontal straight tubes in turbulent regime for ice mass fractions up to 10 % and for Reynolds number greater than 2300 the simple Dittus-Boelter correlation based on thermophysical properties of the carrier fluid can be used with acceptable accuracy. For higher ice mass fractions specially derived correlations should be used such as correlation from Christensen and Kauffeld in case of 10 % ethanol water mixture.

According to the theoretical evaluation it can be concluded that dynamic, ice slurry based CTES systems posses higher economic and energy saving potential than static CTES systems. Regarding production and storage of cold, they show higher and inalterable heat transfer coefficient during charging, higher refrigeration unit COP, higher discharging rates and thereby more stable and lower outlet water temperatures and simpler storage design. Regarding consumption of cold, the benefit of using ice slurry as a transport media is shown through reduced size of heat exchangers and pipelines. In the best case scenario the total energy con-

sumption of dynamic CTES system was found to be approximately 25 % lower than for the static CTES system.

However there are many problems of technical nature with operation of ice slurry components and systems in whole which needs yet to be overcome. Moreover, the cost of ice slurry production components (generators) at present is relatively high in comparison to the static ice building method.

11.2 Suggestions for future work

The experimental investigation of ice slurry pressure drop and heat transfer should be broaden to other secondary fluid pairs and temperature levels potentially interesting for application in industry and building sector. Generally, there is lack of pressure drop and heat transfer information regarding pure water ice slurry in the literature. Knowledge of such correlations is crucial for efficient ice slurry system design near zero temperatures.

Ice slurry production near zero temperature seems to be a major concern in the application of this system solution. Commercially available ice slurry generators (scraped surface, fluidized bed) currently present at the market are not adapted for ice slurry production at temperature levels near zero. There are only few types of ice slurry generators which can operate without freezing point depressants. Still this technology is far from being flawless and universally accepted. A satisfactory solution of this problem would make it possible to compete with static CTES systems.

In order to exploit advantages of heterogeneous storages over homogeneous and to avoid problems related with ice extraction specially designed ice slurry mixing device is needed.

12 Appendix A: Measuring instruments

In this section measuring sensors and instrumentation used in the experiments performed on a static CTES system (ice bank) is discussed. The measuring system consisted of sensors to measure temperature, pressure and flow rates, electronic data acquisition/switch unit and a personal computer. All of the sensors were gathered at a junction box that allowed connection of ten thermocouples, one resistance thermometer, one differential pressure transducer and two flow meters (one vortex type and ultrasonic clamp on type). The analog signals (voltage and current outputs) from the measuring sensors were read by a data logger Agilent 34970A which was connected to a personal computer. The Agilent BenchLink Data Logger 3 software was configured to automate the measuring procedure. The acquisition unit handled 16 channels where 15 were addressed to actual measurement and the last channel corresponded to the thermocouple reference junction. All the data were scanned and recorded in intervals of 5 seconds.

In order to minimize systematic errors all measuring sensors and instrumentations were calibrated and tested against known values prior to experiments.

12.1 Temperature measurements

Temperature measurements at the test facility were conducted by using ten K type thermocouples and one Pt100 temperature sensor. K type thermocouples have a positive chromel wire and a negative alumel wire. A tolerance for a first class K type thermocouple wire is ±1.5 °C between -40 °C and 375 °C. Due to large distance between measurement locations and acquisition unit connection between thermocouples and junction box was accomplished by an extension wire. Resistance thermometers exploit the predictable change in electrical resistance of material with changing temperature. Due to high accuracy and repeatability resistance thermometers are primary choice for measurements below 600 °C. The most common resistance thermometer used in industry is Pt100 sensor. It is made of platinum and has nominal resistance of 100 ohms at 0 °C.

12.1.1   Temperature calibration

12.1.1.1   Thermocouple calibration

Even though all of the thermocouples were of the same type and were cut from the same lot control calibration was carried out in order to determine temperature deviation between them. Calibration itself was conducted in a glycol thermostatic bath at temperature levels of -15 °C, -7 °C, 0 °C and 23 °C in the national laboratory accredited for measurements of temperature, pressure, flow and humidity at the Faculty of Mechanical Engineering and Naval Architecture (FMENA). The ten thermocouples were compared against standard temperature sensor Pt25.5, Hart, with accuracy of ±0.01 °C. In order to preserve consistency the same measuring system and instrumentation arrangement was used during the laboratory testing's and on-site measurements as well.

Since all of the thermocouple joints were of the same size, equal response rate is assumed. In Table 12.1 results of temperature calibration are shown.

Table 12.1 Thermocouple calibration

Thermocouple No.	Temperature				
Standard temperature sensor Pt25.5	-15,15	-7,49	-0,03	5,17	23,68
TC1	-15,1	-7,5	-0,1	5,1	23,6
TC2	-15,1	-7,5	0,0	5,0	23,6
TC3	-15,1	-7,5	0,0	5,0	23,6
TC4	-15,0	-7,4	0,0	5,1	23,7
TC5	-15,0	-7,5	0,0	5,1	23,6
TC6	-15,1	-7,5	-0,1	5,0	23,6
TC7	-15,0	-7,4	0,0	5,2	23,7
TC8	-15,0	-7,4	-0,1	5,1	23,6
TC9	-15,2	-7,7	-0,2	4,9	23,5
TC10	-15,3	-7,8	-0,2	4,8	23,4

The average temperature deviation of each thermocouple in relation to the standard temperature sensor was calculated and entered in the acquisition system as a correction value of the temperature reading.

Uncertainty of the calibrated thermocouple is determined from the following components: uncertainty of the temperature standard, uncertainty of the bridge, uncertainty of gradients and stability of the calibration bath and the resolution of the device under test (DUT):

$$u_{calib\ rig} = \pm\sqrt{u^2_{sensor} + u^2_{bridge} + u^2_{gradient} + u^2_{stability} + u^2_{resolution}}$$

where:

u_{sensor} - measuring uncertainty of the standard temperature sensor, ±0.01 °C

u_{bridge} - measuring uncertainty of the bridge, ±0.004 °C

$u_{gradient}$ - measuring uncertainty due to temperature gradient between measurement locations within the bath, ±0.05 °C

$u_{stability}$ - measuring uncertainty of the bath stability, ±0.05 °C

$u_{resolution}$ - measuring uncertainty of the resolution, $\pm 0.1/\sqrt{3}$ °C.

Therefore the uncertainty of the measuring rig is ±0.1 °C.

12.1.1.2 Resistance thermometer calibration
Calibration of the Pt100 resistance thermometer was conducted in a glycol thermostatic bath between 0 °C and 5 °C at temperature levels of 0 °C, 0.4 °C, 0.6 °C, 1 °C, 3 °C and 5 °C. Again Pt100 temperature sensor was compared against standard temperature sensor SPRT, with accuracy of ±0.005 ° C. Table 12.2 shows results of Pt100 temperature calibration.

Table 12.2 Resistance thermometer (Pt100) calibration

Temperature sensor	Temperature					
Standard temperature sensor SPRT	-0,027	0,387	0,638	1,041	3,034	5,035
Pt100	0,33	0,75	1,00	1,39	3,39	5,39

The uncertainty of the measuring rig is ±0.015 °C.

12.2 Pressure measurements

Omega PX 750 series high performance output differential pressure transducer was used for pressure measurements. Performance data given by the producer are shown in Table 12.3.

Table 12.3 Differential transducer performance data

Type	Range [mbar]	Current [mA]	Accuracy MV* [%]
Omega PX 750	0 - 350	4 - 20	±0.25

* MV – measured value

1 2 . 2 . 1   P r e s s u r e   c a l i b r a t i o n

Differential pressure transducer was calibrated before experiments against the pressure calibrator DRUCK 615 with the uncertainty of 0.025 % within the range of 0-1 bar. The pressure calibrator DRUCK 615 was calibrated in the Laboratory for process measurement (LPM) at the Faculty of Mechanical Engineering and Naval Architecture. LPM is accredited DKD (Deutscher Kalibrierdienst - German Calibration Service) laboratory accredited by PTB (Physikalish-Techniche Bundesanstalt - Physical-Technical Federal Bureau) of Republic of Germany according to the EN ISO/IEC 17025 for temperature and pressure calibrations under the DAR (Deutscher Akkreditieruns Rat - German Accreditation Council) registration number DKD-K-35601. Overall uncertainty of the calibration of the Omega PX 750 which includes uncertainty of the pressure generation, electrical measurements of the Omega 4-20 mA output and hysteresis is 0.1 % of the reading.

When calibrating the differential pressure transducers, the negative pressure port of the differential pressure transducer was opened to the atmosphere and the positive port was connected to the calibration rig. Calibration line is shown in Figure 12.1.
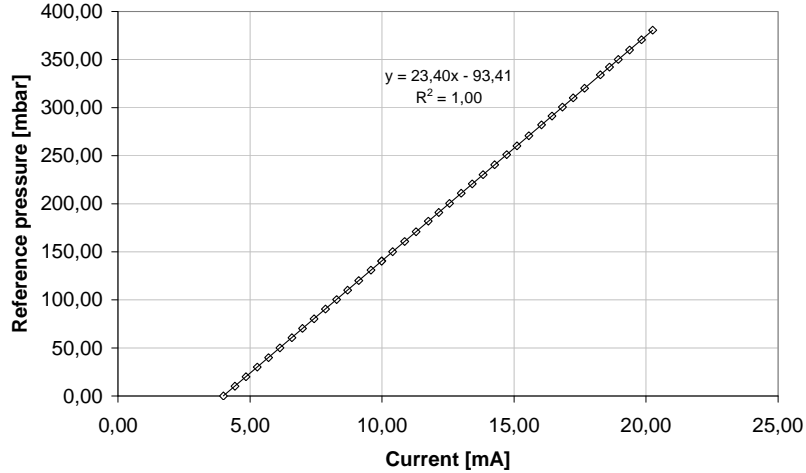
Figure 12.1 Calibration line for the pressure transducer PX 750

12.3 Flow measurements

Secondary refrigerant (mixture of ethylene glycol and water) flow measurements were conducted by Yokogawa digitalYEWFLO vortex type flowmeter (Yokogawa DY 80). According to the manufacturer, flow meter is suitable for measuring flow of liquids, gas and steam. Multiphase and sticky fluids should be avoided. A prerequisite is a minimum Reynolds number of 5000. A special care was taken to ensure proper installation of the flow meter to the test facility. To work properly fully developed flow is required. Therefore it was installed at a safe distance from bends, valves and centrifugal pumps. The flow meter was factory-calibrated for a flow between 0 and maximum flow rate of 100 m^3/h. The analog output signal range of the unit is 4 to 20 mA. The declared accuracy of the flow meter is $\pm$ 0.75 % of the measured value between 0.3 m/s and 10 m/s.

Measurements of the chilled water flow rate were carried out by Sitrans FUE clamp-on ultrasonic type flow meter. The measuring range of the flow meter is from 0 to 12 m/s. For best accuracy operation inside the Reynolds transition region, between 1000 < Re < 5000 should be avoided. The declared accuracy of the flow meter is between $\pm$ 1 and 2 % of the measured value for given pipe diameter and flow velocity. The accuracy of the flow meter was checked for a flow between 0 and 50 m^3/h via volume tank method in the Power Engineering Laboratory at the FMENA. The analog output signal range of the transmitter was 0 - 10 V for a flow between 0 and the adjusted maximum flow rate of 50 m^3/h. In Table 12.4 and Figure 12.2 results of the ultrasonic flow meter calibration is shown. The highest deviation from the declared accuracy can be noticed for the lowest flow rate. For the rest of the control points the accuracy is in rage of $\pm$ 1 %.

Table 12.4 Ultrasonic flow meter calibration

Measurement No.	Referent flow [m^3/h]	Measured flow [m^3/h]
1	3.13	3.42
2	9.42	9.32
3	19.12	19.01
4	23.28	23.12
5	33.75	34.02
6	42.02	42.06
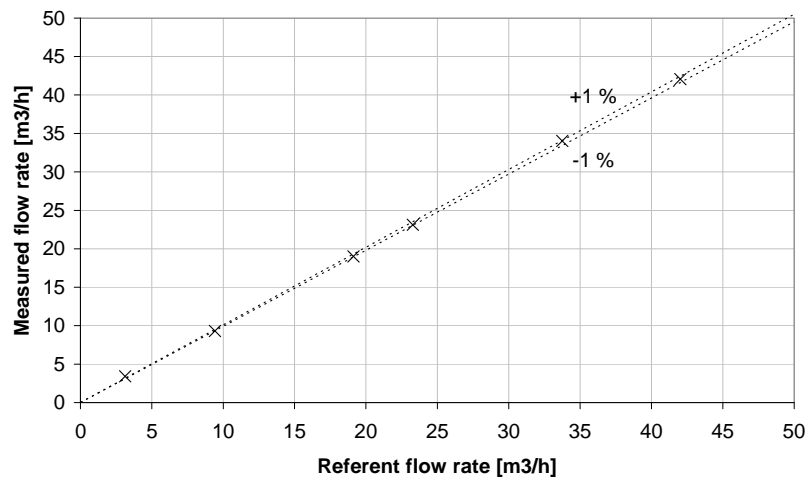
Figure 12.2 Accuracy of the ultrasonic flow meter

13 Appendix B: Uncertainty analysis

Measurement uncertainty is a numerical expression of quality of the measurement result. Any result of measurement is more or less uncertain. There is no doubt that actual value of the physical quantity exists, but it cannot be found out by measurement. In the best case one can estimate the uncertainty of the measurement and determine the range of values for which can be said: there is a high probability that the actual value of the measured quantity is in this range.

The source of errors that occur when performing measurements can be categorized as rough errors, systematic and random errors. Rough errors arise due to insufficient attention and care of the person conducting measurements, negligence, lack of knowledge and selection of an inappropriate measurement procedure. By repetition of the measurements influence of rough errors is reducing.

Systematic errors arise due to imperfection of the measuring procedure and instruments, due to influence of external disturbances on a measured value and the personal influence of the operator. Most of the systematic errors have permanent value and displace measurements in a single direction. This, they can be quantified and taken into account during analysis of the measurement results. Systematic errors of the measuring instruments can be eliminated or minimized by calibration of the measurement equipment.

Random errors are harder to eliminate. They arise due to changes when performing experiments in measurement equipment, object and physical quantity that is being measured, ambient and the measurer. Random errors can be recognized by repetition of the measurements carried out under same conditions. Consequence of the random errors is uncertainty of the measurement result.

Uncertainty of the measurement is expressed by standard deviation. Uncertainty of "type A" (U_A) is determined on basis of frequency distribution of the individual readings gathered by repetition of the measurements. Uncertainty of "type B" (U_B) is usually estimated on basis of as-

sumed frequency distribution of the readings. According to the BIPM/ISO standard, combined uncertainty U is geometrical sum of the individual components,

$$U = \sqrt{U^2{}_A + U^2{}_B}$$
13.1.

It is recommended to express the quality of the measurement result by the combined uncertainty. The expression 1 provides a combined uncertainty at a confidence level corresponding to 1σ (68 %). However, this confidence level is usually not satisfactory and 95 % confidence level is considered. Therefore factor k is introduced. The overall uncertainty is calculated as,

$$U = k \cdot \sqrt{U^2{}_A + U^2{}_B}$$
13.2

where, k is a is normally assigned a value in the range between 2 and 3 which corresponds to the confidence level of 2σ (95 %) and 3σ (99 %) (Nichols and White, 1994).

13.1 Measurement uncertainty "type A"

Random errors are normally stated as "type A" uncertainties. Type A uncertainty is determined by a statistical analysis, repetition of measurements and by calculation of the standard deviation of measured results.

The best estimation of expected value $\bar{x}$ is obtained as a result of N independent measurements under same conditions. Actually it is a mean value and is calculated by

$$\bar{x} = \frac{1}{N} \cdot \sum_{i=1}^{N} x_i$$
13.3.

The statistical dispersion of the variable x around the arithmetic average is determined by standard deviation. Standard deviation measures how spread out the values in a data set are. More precisely, it is a measure of the average difference between the values of the data in the set. If data points are all similar, then the standard deviation will be low (close to zero). The standard deviation computed from a sample of the observations is given by,

$$\sigma_x = \sqrt{\frac{1}{N-1} \cdot \sum_{i=1}^{N} (x_i - \bar{x})^2}$$
13.4.

174

The standard deviation of the mean value, i.e. the uncertainty of the mean value (standard error of the mean) is defined as a ratio of a standard deviation and the root of observation number.

$$\sigma_{\bar{x}} = \frac{\sigma_x}{\sqrt{N}} = \sqrt{\frac{1}{N \cdot (N-1)} \cdot \sum_{i=1}^{N}(x_i - \bar{x})^2}$$
13.5.

If the measurements of the variable x were repeated there is a 68 % probability that each new value would lie within $\bar{x} \pm \sigma_{\bar{x}}$.

Measurement uncertainty of type A is expressed by the standard deviation of the mean value,

$$U_A = \sigma_{\bar{x}}$$
13.6.

Most frequently distribution of the measured results follows normal probability density function.
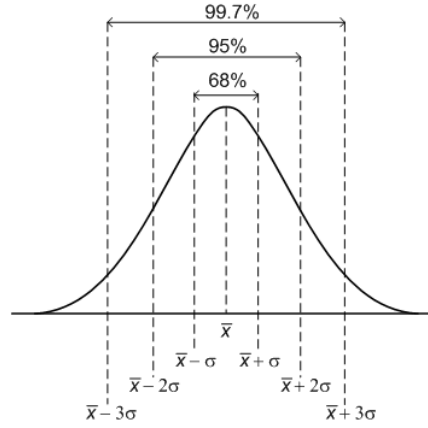
Figure 13.1 Plot of the normal distribution with mean value $\bar{x}$ and standard deviation σ_x

13.2 Measurement uncertainty "type B"

Systematic errors are normally stated as "type B" uncertainties.

Since the measurement error is only seldom determined by the statistical approach, different sources of information which describe measuring uncertainty are used. Due to limited resources, measured value is often a result of only one measurement. In this case measurement uncertainty is

estimated on basis of information which are on disposal, such as previous results of measurement, information acquired from instructions on measuring instrumentation and sensors, calibration certificates etc.

Measurement uncertainty $U(x)$ needs to be significantly smaller then the maximum error a of a measuring instrument $U \ll a$. For example, assume that the producer stated maximum error of the measuring instrument as $-a$ and $+a$. Unless there is no detailed information on distribution of the measuring values within reliable limits, equal probability of a measured value occurrence within the interval $\pm a$ can be assumed. Such distribution is referred to as rectangle distribution.
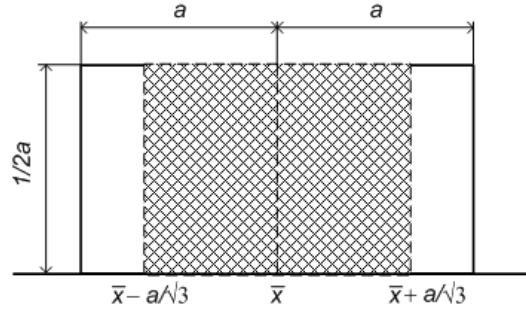
Figure 13.2 Plot of the rectangle distribution with mean value $\bar{x}$ and standard deviation σ_x

Measurement uncertainty of the measured value is equal to the standard deviation of the measured quantity σ_x and for rectangle distribution is

$$U_\mathrm{B} = \sigma_x = \frac{a}{\sqrt{3}}$$
13.7.

13.3 Combined measurement uncertainty

In most cases it is not possible to measure the desired physical quantity directly, but it can be determined indirectly by means of some physical relationship. Generally, indirectly measured physical quantity y is a function of number of independent variables (x_1, …. x_n) which are measured directly:

$$y = f\left(x_1, x_2, ..., x_n\right)$$
13.8.

Each of the variables x_i has its own measurement uncertainty. Absolute uncertainty of the measurement result $U(y)$ is estimated by relation which is based on approximation with the first term of the Taylor series:

$$U(y) = \sqrt{\sum_{i=1}^{n} \left[\frac{\partial y}{\partial x_i} \right]^2 \cdot U^2(x_i)}$$ 13.9.

Partial derivations of the physical quantity by input variables are also called sensitivity coefficients. They indicate how much is measurement result changing with change of the certain input variable x_i.

13.4 Uncertainty of the measurements

13.4.1 Uncertainty of the ice mass measurements

Ice level inside silo was determined by monitoring the change of a water level in a compensation tank. Water level was measured by differential pressure transducer. Ice mass change inside silo during charging or melting process is calculated as

$$\Delta M_i = \Delta V_w \cdot \frac{\rho_w \cdot \rho_i}{\rho_w - \rho_i} = A_{tank} \cdot \Delta h_w \cdot \frac{\rho_w \cdot \rho_i}{\rho_w - \rho_i} \quad .$$

With $\Delta p = \rho_w \cdot g \cdot \Delta h_w$ and $A_{tank} = d_{tank}^2 \cdot \pi / 4$ ice mass change is

$$\Delta M_i = \frac{d_{tank}^2 \cdot \pi \cdot \rho_i \cdot \Delta p}{4 \cdot g \cdot (\rho_w - \rho_i)} .$$

The corresponding partial derivatives are

$$\frac{\partial \Delta M_i}{\partial \Delta p} = \frac{d_{tank}^2 \cdot \pi \cdot \rho_i}{4 \cdot g \cdot (\rho_w - \rho_i)} \text{ and } \frac{\partial \Delta M_i}{\partial d_{tank}} = \frac{d_{tank} \cdot \rho_i \cdot \Delta p}{2 \cdot g \cdot (\rho_w - \rho_i)} .$$

Density of water and ice is dependant on temperature. Since the temperature of water and ice is changing only slightly during measurement procedure influence of water and ice density on uncertainty of the ice mass determination is neglected.

The uncertainty of ice mass may be written

$$U(\Delta M_i) = \pm \sqrt{\left[\frac{\partial \Delta M_i}{\partial \Delta p} \cdot U(\Delta p)\right]^2 + \left[\frac{\partial \Delta M_i}{\partial d_{tank}} \cdot U(d_{tank})\right]^2}.$$

The uncertainty of the pressure measurements is calculated according to the measured pressure and assumed rectangular distribution

$$\Delta p = p_1 - p_2$$
$$U(p) = \frac{0.1\% \cdot p}{100}$$
$$U(\Delta p) = \pm \sqrt{U^2(p_1) + U^2(p_2)}$$

The uncertainty in determination of the compensation tank diameter is assumed as a 2 % of the given value

$$U(d_{tank}) = 2\% \cdot d_{tank} / 100.$$

The uncertainty of the calculated mass of ice was found to be approximately 2.9 % of the calculated ice mass at a 95 % confidence level.

13.4.2   Uncertainty of the charging rate
Charging rate of the ice bank is calculated as

$$\Phi_{ch} = \dot{V}_b \cdot \rho_b \cdot c_{pb} \cdot (\vartheta_{b,out} - \vartheta_{b,in}).$$

Neglecting the uncertainty in the density and specific capacity of the secondary working fluid (brine), an expression for the uncertainty in the measured charging rate can be written as,

$$U(\Phi_{ch}) = \pm \sqrt{\left[\frac{\partial \Phi_{ch}}{\partial \dot{V}_b} \cdot U(\dot{V}_b)\right]^2 + \left[\frac{\partial \Phi_{ch}}{\partial \Delta \vartheta_b} \cdot U(\Delta \vartheta_b)\right]^2}.$$

The corresponding partial derivatives are

$$\frac{\partial \Phi_{ch}}{\partial \dot{V}_b} = \rho_b \cdot c_{pb} \cdot (\vartheta_{b,out} - \vartheta_{b,in}) \text{ and } \frac{\partial \Phi_{ch}}{\partial \Delta \vartheta_b} = \dot{V}_b \cdot \rho_b \cdot c_{pb}.$$

The uncertainty of the measured brine volume flow rate is calculated according to the measured flow rate and assumed rectangular distribution

$$U\left(\dot{V}_b\right)=\frac{a\left(\dot{V}_b\right)}{\sqrt{3}}=\frac{\dfrac{0.75\%\cdot\dot{V}_b}{100}}{\sqrt{3}} \ .$$

The uncertainty of the measured temperature difference is calculated as

$$\Delta\vartheta_b=\vartheta_{b,out}-\vartheta_{b,in}; \quad U\left(\vartheta_b\right)=\pm0.1°C$$

$$U\left(\Delta\vartheta_b\right)=\pm\sqrt{U^2\left(\vartheta_{b,out}\right)+U^2\left(\vartheta_{b,in}\right)}=\pm0.14°C$$

The uncertainty of the calculated charging rate was found to be approximately 14 % at a 95 % of confidence level.

13.4.3 Uncertainty of the discharging rate
Discharging rate of the ice bank is calculated as

$$\Phi_{dis}=\dot{V}_w\cdot\rho_w\cdot c_{pw}\cdot\left(\vartheta_{w,in}-\vartheta_{w,out}\right).$$

Neglecting the uncertainty in the density and specific capacity of the water, an expression for the uncertainty in the measured discharging rate can be written as,

$$U\left(\Phi_{dis}\right)=\pm\sqrt{\left[\frac{\partial\Phi_{dis}}{\partial\dot{V}_w}\cdot U\left(\dot{V}_w\right)\right]^2+\left[\frac{\partial\Phi_{dis}}{\partial\Delta\vartheta_w}\cdot U\left(\Delta\vartheta_w\right)\right]^2} \ .$$

The corresponding partial derivatives are

$$\frac{\partial\Phi_{dis}}{\partial\dot{V}_w}=\rho_w\cdot c_{pw}\cdot\left(\vartheta_{w,in}-\vartheta_{w,out}\right) \text{ and } \frac{\partial\Phi_{dis}}{\partial\Delta\vartheta_w}=\dot{V}_w\cdot\rho_w\cdot c_{pw} \ .$$

The uncertainty of the measured brine volume flow rate is calculated according to the measured flow rate and assumed rectangular distribution

$$U\left(\dot{V}_w\right)=\frac{a\left(\dot{V}_w\right)}{\sqrt{3}}=\frac{\dfrac{1\%\cdot\dot{V}_w}{100}}{\sqrt{3}} \ .$$

The uncertainty of the measured temperature difference is calculated as

$$\Delta\vartheta_{\mathrm{w}} = \vartheta_{\mathrm{w,in}} - \vartheta_{\mathrm{w,out}}; \quad U(\vartheta_{\mathrm{w,in}}) = \pm 0.1°C; \quad U(\vartheta_{\mathrm{w,out}}) = \pm 0.015°C$$

$$U(\Delta\vartheta_{\mathrm{w}}) = \pm\sqrt{U^2(\vartheta_{\mathrm{w,in}}) + U^2(\vartheta_{\mathrm{w,out}})} = \pm 0.101°C$$

The uncertainty of the calculated discharging rate was found to be approximately from 1.9 to 5.9 % at a 95 % confidence level.

13.4.4 Uncertainty of the product of overall heat transfer coefficient and heat transfer area

Product of overall heat transfer coefficient and heat transfer area during process of charging is calculated as

$$kA_{\mathrm{ch}} = \frac{\Phi_{\mathrm{ch}}}{\Delta\vartheta_{\mathrm{LMTD}}} \quad \text{where} \quad \Delta\vartheta_{\mathrm{LMTD}} = \frac{\vartheta_{\mathrm{b,out}} - \vartheta_{\mathrm{b,in}}}{\ln\dfrac{\vartheta_{\mathrm{b,in}}}{\vartheta_{\mathrm{b,out}}}}.$$

Hence, the uncertainty is

$$U(kA_{\mathrm{ch}}) = \pm\sqrt{\left[\frac{\partial kA_{\mathrm{ch}}}{\partial\Phi_{\mathrm{ch}}}\cdot U(\Phi_{\mathrm{ch}})\right]^2 + \left[\frac{\partial kA_{\mathrm{ch}}}{\partial\Delta\vartheta_{\mathrm{LMTD}}}\cdot U(\Delta\vartheta_{\mathrm{LMTD}})\right]^2}.$$

The corresponding partial derivatives are

$$\frac{\partial kA_{\mathrm{ch}}}{\partial\Phi_{\mathrm{ch}}} = \frac{1}{\Delta\vartheta_{\mathrm{LMTD}}} \quad \text{and} \quad \frac{\partial kA_{\mathrm{ch}}}{\partial\Delta\vartheta_{\mathrm{LMTD}}} = -\frac{\Phi_{\mathrm{ch}}}{\Delta\vartheta_{\mathrm{LMTD}}^2}.$$

The uncertainty of the charging rate is already estimated. The uncertainty of the logarithmic mean temperature difference between brine and water is calculated as

$$U(\Delta\vartheta_{\mathrm{LMTD}}) = \pm\sqrt{\left[\frac{\partial\Delta\vartheta_{\mathrm{LMTD}}}{\partial X_1}\cdot U(X_1)\right]^2 + \left[\frac{\partial\Delta\vartheta_{\mathrm{LMTD}}}{\partial X_2}\cdot U(X_2)\right]^2}$$

where $X_1 = \vartheta_{\mathrm{b,out}} - \vartheta_{\mathrm{b,in}}$ and $X_2 = \ln\dfrac{\vartheta_{\mathrm{b,in}}}{\vartheta_{\mathrm{b,out}}}$.

Partial derivatives are

180

$$\frac{\partial \Delta \vartheta_{\text{LMTD}}}{\partial X_1} = \frac{1}{\ln \dfrac{\vartheta_{\text{b,in}}}{\vartheta_{\text{b,out}}}} \quad \text{and} \quad \frac{\partial \Delta \vartheta_{\text{LMTD}}}{\partial X_2} = \vartheta_{\text{b,out}} - \vartheta_{\text{b,in}} \, .$$

The uncertainties of X_1 and X_2 are

$$U(X_1) = \pm\sqrt{U^2(\vartheta_{\text{b,in}}) + U^2(\vartheta_{\text{b,out}})} = \pm 0.14°\text{C} \text{ and}$$

$$U(X_2) = \pm\sqrt{\left[\frac{\partial X_2}{\partial \vartheta_{\text{b,in}}} \cdot U(\vartheta_{\text{b,in}})\right]^2 + \left[\frac{\partial X_2}{\partial \vartheta_{\text{b,out}}} \cdot U(\vartheta_{\text{b,out}})\right]^2} \, .$$

With $\dfrac{\partial X_2}{\partial \vartheta_{\text{b,in}}} = \dfrac{1}{\vartheta_{\text{b,in}}}$ and $\dfrac{\partial X_2}{\partial \vartheta_{\text{b,out}}} = -\dfrac{1}{\vartheta_{\text{b,out}}}$ the uncertainty of the variable X_2 is estimated as $U(X_2) = \pm 0.1°\text{C}$.

The uncertainty of the LMTD between secondary fluid and water is found to be approximately $U(\Delta \vartheta_{\text{LMTD}}) = \pm 0.23°\text{C}$.

Finally, the uncertainty of the product of overall heat transfer coefficient and heat transfer area was found to be approximately 28.9 % at 95 % confidence level.

13.4.5 Uncertainty of the product of heat transfer coefficient and heat transfer area at water-ice interface

Product of water to ice heat transfer coefficient and heat transfer area during process of charging is calculated as

$$\alpha A_i = \frac{\Phi_{\text{w-i}}}{\vartheta_{\text{w}} - \vartheta_{\text{i}}} \, .$$

Heat rate from water to ice is calculated from $\Phi_{\text{w-i}} = \Phi_{\text{in}} - \Phi_{\text{w},\vartheta} - \Phi_{\text{w,M}}$

$$\Phi_{\text{w-i}} = \dot{V}_{\text{w}} \rho_{\text{w}} c_{\text{pw}} (\vartheta_{\text{w,in}} - \vartheta_{\text{w,out}}) - M_{\text{w}} c_{\text{pw}} \frac{d\vartheta_{\text{w}}}{dt} - c_{\text{pw}} (\vartheta_{\text{w}} - \vartheta_{\text{i}}) \frac{dM_{\text{w}}}{dt} \, . \text{ If}$$

the sensible heat rate due to change in mass of water in the tank, $\Phi_{\text{w,M}}$ is neglected the water to ice heat rate is

$$\Phi_{w\text{-}i} = \dot{V}_w \rho_w c_{pw} \left(\vartheta_{w,in} - \vartheta_{w,out}\right) - M_w c_{pw} \frac{\Delta\vartheta_w}{\Delta t} .$$

If the uncertainty of thermophysical properties of water and time measurements are neglected and $\vartheta_i = 0°C$ the uncertainty of αA_i is

$$U(\alpha A_i) = \pm \sqrt{\begin{array}{l}\left[\dfrac{\partial \alpha A_i}{\partial \dot{V}_w} \cdot U(\dot{V}_w)\right]^2 + \left[\dfrac{\partial \alpha A_i}{\partial \vartheta_{w,in}} \cdot U(\vartheta_{w,in})\right]^2 + \left[\dfrac{\partial \alpha A_i}{\partial \vartheta_{w,out}} \cdot U(\vartheta_{w,out})\right]^2 + \\ + \left[\dfrac{\partial \alpha A_i}{\partial M_w} \cdot U(M_w)\right]^2 + \left[\dfrac{\partial \alpha A_i}{\partial \Delta\vartheta_w} \cdot U(\Delta\vartheta_w)\right]^2 + \left[\dfrac{\partial \alpha A_i}{\partial \vartheta_w} \cdot U(\vartheta_w)\right]^2\end{array}}$$

The corresponding partial derivatives are

$$\frac{\partial \alpha A_i}{\partial \dot{V}_w} = \frac{\rho_w c_{pw}\left(\vartheta_{w,in} - \vartheta_{w,out}\right)}{\vartheta_w} ; \quad \frac{\partial \alpha A_i}{\partial \vartheta_{w,in}} = \frac{\dot{V}_w \rho_w c_{pw}}{\vartheta_w}$$

$$\frac{\partial \alpha A_i}{\partial \vartheta_{w,out}} = \frac{-\dot{V}_w \rho_w c_{pw}}{\vartheta_w} ; \quad \frac{\partial \alpha A_i}{\partial M_w} = \frac{c_{pw}\Delta\vartheta_w}{\vartheta_w \Delta t} ; \quad \frac{\partial \alpha A_i}{\partial \Delta\vartheta_w} = \frac{M_w c_{pw}}{\vartheta_w \Delta t}$$

$$\frac{\partial \alpha A_i}{\partial \vartheta_w} = -\frac{\dot{V}_w \rho_w c_{pw}\left(\vartheta_{w,in} - \vartheta_{w,out}\right) - M_w c_{pw} \dfrac{\Delta\vartheta_w}{\Delta t}}{\vartheta^2_w} .$$

The corresponding uncertainties are

$$U(\dot{V}_w) = \frac{a(\dot{V}_w)}{\sqrt{3}} = \frac{\dfrac{1\% \cdot \dot{V}_w}{100}}{\sqrt{3}} ; \quad U(\vartheta_{w,in}) = \pm 0.1°C ;$$

$$U(\vartheta_{w,out}) = \pm 0.1°C ; \quad U(\Delta\vartheta_w) = \pm 0.101°C .$$

The uncertainty of the mass of water is calculated as

$$U(M_w) = \pm \sqrt{\left[\frac{\partial M_w}{\partial V_{w0}} \cdot U(V_{w0})\right]^2 + \left[\frac{\partial M_w}{\partial M_i} \cdot U(M_i)\right]^2} .$$

Mass of water is calculated according to

$$M_w = \left(V_{w0} - \frac{M_i}{\rho_i} \right) \cdot \rho_w \quad \text{where } V_{w0} \text{ is volume of water inside silo}$$

without ice.

It is estimated that the initial water volume can be determined with uncertainty of 7 %. The uncertainty of the ice mass measurements is already estimated as 1.9 % of the given value. Therefore, the uncertainty of the mass of water is $\pm$ 7.1 %.

Finally, the uncertainty of the product of αA_i was found to be approximately from 6 to 14.5 % of the calculated value.

184

14 Nomenclature

14.1 Chapters 3, 4 and 5

14.1.1 Latin letters

A surface area [m²]
a, b coefficients in the friction factor correlation, eq. 3.19
c_f friction factor [-]
c_p specific heat capacity [Jkg⁻¹K⁻¹]
d diameter [m]
h specific enthalpy [Jkg⁻¹]
I investment cost [EUR]
k overall heat transfer coefficient [Wm⁻² K⁻¹], as defined in eq. 3.3, 3.9 and Figure 4.5
L length [m]
M mass [kg]
m mass [kg]
$\dot{m}$ mass flow rate [kgs⁻¹]
n compressor speed [s⁻¹]
Nu Nusselt number
OCT type of oil cooling
P power [W]
$Pr_{\infty,0}$ Prandtl number for water at temperature 0 °C
r radius [m]
Re Reynolds number [-]
RT refrigerant
t time [s]

14.1.2 Greek Symbols

α heat transfer coefficient [Wm⁻²K⁻¹], eq. 3.3, eq. 4.4, Figure 4.12 and Figure 4.14
δ thickness [m]
Δ difference
η dynamic viscosity [Pas]
ϑ temperature [°C]
λ thermal conductivity [Wm⁻¹K⁻¹]

ρ density [kgm^{-3}]

Φ heat rate [W]

14.1.3   Subscripts

b   brine
c   cooling, condensation
comp   compressor
conn   electrical connection
e   evaporation
el   electrical
he   heat exchanger
i   ice
in   inlet
M   mass
ol   oil load
out   outlet
pthx   plate type heat exchanger
RT   refrigerant
s   spiral
s&thx   shell and tube heat exchanger
sl   solid-liquid
t   tube
temp   temperature
tot   total (liquid and solid)
w   water
ww   warm water
1   tube inner surface
2   tube outer surface

14.1.4   Superscripts

cv   control volume

14.2 Chapters 7, 8, 9, 10 and 13

14.2.1   Latin letters

A   additive
a coefficient [-], eq. 8.17, 8.18
b constants [-], eq. 8.25
c concentration [-]
$C_{1..4}$ constants [-], eq. 8.14
c_A initial additive concentration [-]
c_p specific heat capacity [Jkg^{-1}K^{-1}]

186

COP	coefficient of performance [-]
d	pipe inner diameter [m]
d_p	ice particle diameter [m]
E_p	energy consumed by pump [kWh]
f	Darcy friction factor
F	functional relationship
g	gravity constant [ms^{-2}]
Gz	Graetz number [-]
h	enthalpy [Jkg^{-1}]
H	height [m]
He	Hedström number [-]
k	overall heat transfer coefficient [Wm^{-2}K^{-1}]
L	tube length [m]
$\dot{m}$	mass flow rate [kgs^{-1}]
m	coefficient [-], eq. 8.16, 8.19
M	mass [kg]
n	number of ice particles [-], eq. 10.5, 10.8
n	fluid behaviour index [-], eq. 8.20, 10.16
N	number of parallel tubes [-]
p	pressure [Pa]
Δp	pressure drop [Pa]
P	pumping power ratio [Wm^{-1}], Chapter 8
P	pumping power [W], Table 10.3
Pr	Prandtl number [-]
$\dot{q}$	heat flux [Wm^{-2}]
Q	Transport capacity [W]
r	radius [m]
Re	Reynolds number [-]
t	time [s]
U, u	uncertainty [%]
V	volume [m³]
$\dot{V}$	volume flow rate [m³s^{-1}]
w	velocity [ms^{-1}]
z	axial tube distance [m]

14.2.2 Greek Symbols

α	heat transfer coefficient [Wm^{-2}K^{-1}]
$\Delta \vartheta_m$	logarithmic mean temperature difference [°C]
$\Delta \rho = \rho_i - \rho_{cf}$	density difference [kgm^{-3}]
ε	roughness [-], eq. 8.3 to 8.6, shear stress factor [-], eq. 8.24
η	dynamic viscosity [Pas]
η_{dis}	discharging efficiency [-], eq. 10.20
ϑ	temperature [°C]

λ	thermal conductivity [Wm^{-1}K^{-1}]
ρ	density [kgm^{-3}]
τ_0	yield stress [Pa]
Φ	heat rate [W]

14.2.3   Subscripts

b	bulk
b	brine, Chapter 13
c	critical
cf	carrier fluid
ch	charging
cs	cross section
dis	discharging
evap	evaporator
f	liquid
h	hydraulic
i	ice
in	inlet
ip	ice particle
is	ice slurry
l	laminar
LMTD	logarithmic mean temperature difference
m	mean
min	minimum
M	mixture
n	fluid behaviour index
out	outlet
R	reference
t	turbulent
th	thermal
vol	volume
w	water
wall	tube wall
0	initial
x	axial distance

15 References

AEA (2003). AEA Technology. Emissions and Projections of HFCs, PECs and SF6 for the UK and Constituent Countries. Report prepared for the Global Atmosphere Division of the UK Department for Environment, Food, and Rural Affairs.

Andrepont, J.S. (2005). Development in Thermal Energy Storage: Large Applications, Low Temps, High Efficiency and Capital Savings. Proceedings of Association of Energy Engineers (AEE) World Energy Engineering Congress.

ARI Guideline T (2002). Guideline for Specifying the Thermal Performance of Cool Storage Equipment. Air-Conditioning and Refrigeration Institute, Arlington,Virginia, USA, 2002.

ASHRAE (2007). Thermal storage. ASHRAE Handbook – HVAC Applications (SI). Atlanta, USA: American Society of Heating, Refrigerating, and Air-Conditioning Engineering, Inc.

Ayel, V., Lottin, O., Peerhossaini, H. (2003). Rheology, flow behaviour and heat transfer of ice slurries: a review of the state of the art. International Journal of Refrigeration 26 (2003), pp. 95–107.

Bahnfleth, W.P., Joyce, W.S. (1994). Energy Use in a District Cooling System with Stratified Chilled-Water Storage. ASHRAE Transactions 100(1): 1767-1778.

Bedecarrats, J.P., Strub, F., David, T., Castaing-Lasvignottes, J. (2007). Experimental studies of supercooled ice slurry production. 23th International Congres of Refrigeration, Beijing, China.

Bellas, I., Tassou, S.A. (2005). Present and future applications of ice slurries. International Journal of Refrigeration 28 (2005), pp. 115–121.

Billiard, F. (2005). Refrigeration Equipment, Energy Efficiency and Refrigerants. IIR Bulletin 2005. International Institute of Refrigeration.

CENERG (2005). High Efficiency and Low Environmental Impact Air-conditioning Systems, Air-conditioning key figures, Centre for Energy

and   Processes   Available   at
www.cenerg.ensmp.fr/English/themes/syst/html/cles.htm

Chaichana, C., Charters, W. W. S., Aye, L. (2001). An Ice Thermal Storage System, Appl. Therm. Eng., Vol. 21, 1769-1778.

Christensen, K.G., Kauffeld, M. (1997). Heat Transfer Measurement with Ice Slurry, IIR/IIF International Conference heat transfer issues in natural refrigerants, Maryland, USA, pp. 127-141.

Cristopia (2008). Cristopia Energy Systems, http://www.cristopia.com/

Croatian Parliament (2002). Strategija energetskog razvitka Republike Hrvatske. Croatian Parliament decision dated from 19.03.2002.

Doetsch, C. (2001). Pressure drop and flow pattern of ice slurries. Proceedings of the Third IIR Workshop on Ice Slurries, Lucerne.

Dorgan, C.E., Elleson, J.S. (1994). Design Guide for Cool Thermal Storage. Atlanta, USA: American Society of Heating, Refrigeration, and Air-Conditioning Engineering, Inc.

EcoHeatCool (2006). The European Coold Market, Final Report. Euro-Heat and Power.

Egolf, P.W., Vuarnoz, D. Sari, O. (2001), A model to calculate dynamical and steady-state behaviour of ice particles in ice slurry storage tanks, In: Proceedings of the 4th IIR Workshop on Ice Slurries, 12-13 November 2001, Osaka (Japan), Paris: International Institute of Refrigeration, pp.25-39.

Egolf, P.W., Sari, O., Meili, F., Vuarnoz, D. (2001). Pressure drop and heat transfer in a cylindrical heat exchanger with ice slurry flow. In: Proceedings of the 3th IIR Workshop on Ice Slurries, 16-18 May 2001, Lucerne, Swizerland.

Egolf, P.W., Kitanovski, A., Caesar, D.A., Stamatiou, E., Kawaji, M., Bedecarrats, J.P., Strub, F. (2005). Thermodynamics and heat transfer of ice slurries. Int J Refrig 28, pp. 51-59.

Emblik, E. (1951). Eisbildung und Wärmeübergang im Süßwasserkühler, *Kältetechnik* (1), 10-14, *Kältetechnik* (2), 29-34.

Finer, S. I., Cleland, A.C., Lovatt, S. J. (1993). Simple mathematical model for predicting the transient behaviour of an ice-bank system. Int J Refrig., Vol. 16, No. 5, 312-320.

Fiorino, D.P. (1994). Energy Conservation with Thermally Stratified Chilled Water Storage. ASHRAE Transactions 100(1): 1754-1766.

Frei, B., Egolf, P.W. (2000). Viscometry applied to the Bingham Substance Ice Slurry, Proceedings of the Second IIR Workshop on Ice Slurries, 2000, Paris.

Gigiel, A., Badran, R. (1988). Chilling and storage of pig carcasses using high humidity air as produced by an ice bank cooler. International Journal of Refrigeration, Volume 11, Issue 2, Pages 100-104.

Gladis, S. P. (1997). Ice slurry thermal energy storage for cheese process cooling. ASHRAE Transactions, Volume 103, Part 2, pp. 725-729.

Grozdek M., Halasz, B., Ćurko, T., Soldo, V. (2009). Experimental Investigation of an Ice-Bank System Performance. 3rd IIR Conference on Thermophysical Properties and Transport Processes of Refrigeration, Boulder, CO, USA.

Grozdek M., Khodabandeh, R., Lundqvist, P. (2009). Experimental investigation of ice slurry flow pressure drop in horizontal tubes. Experimental Thermal and Fluid Science, Volume 33, Issue 2, January 2009, Pages 357-370.

Grozdek M., Khodabandeh, R., Lundqvist, P., Palm, B., Melinder, Å. (2009). Experimental investigation of ice slurry heat transfer in horizontal tube. International Journal of Refrigeration, Volume 32, Issue 6, September 2009, Pages 1310-1322.

Gschwander, S., Schossig, P., Henning H. M. (2005). Development of Phase Change Slurries Based on Micro-encapsulated Paraffin. Proceedings of the Second conference on phase change material & slurry. Swizerland.

Guilpart, J., Fournasion, L., Lakhdar, M.A., Flick, D., Lallemand, A. (1999). Experimental study and calculation method of transport characteristics of ice slurries, Proceedings of the First IIR Workshop on Ice Slurries, 1999, France.

Guilpart, J., Stamatiou, E., Delahaze, A., Fournasion, L. (2006). Comparison of the performance of different ice slurry types depending on the application temperature. International Journal of Refrigeration 29, Pages 781-788.

Habeebullah, B.A. (2007). An experimental study on ice formation around horizontal long tubes. Int J Refrig., Vol. 30, 789-797.

191

Halasz, B., Grozdek, M., Soldo, V. (2009). Development of Computer Program for Simulation of Ice-Bank System Operation, Part I: Mathematical Modelling. International Journal of Refrigeration, Volume 32, Issue 6, September 2009, Pages 1323-1335.

Hansen, T.M., Kauffeld, M. (2000). Viscosity of ice slurry, Proceedings of the Second IIR Workshop on Ice Slurries, 2000, Paris.

Hansen, T.M., Radosevic, M., Kauffeld, M. (2002). Behavior of Ice Slurry in Thermal Storage Systems, ASHRAE Research Project 1166, 2002.

Hägg, C. (2005). Ice Slurry as Secondary Fluid in Refrigeration Systems. MSc Thesis. Royal Institute of Technology (KTH). Stockholm 2005.

He, B., Martin, V., Setterwall, F. (2004). Phase transition temperature ranges and storage density of paraffin wax phase change materials. Energy 29, 1785–1804.

Henze, G.P, Biffar, B., Kohn, D., Becker, M.P. (2008). Optimal design and operation of a thermal storage system for a chilled water plant serving pharmaceutical buildings. Energy and Buildings (40), pages 1004-1019.

HEP (2008). Hrvatska Elektroprivreda d.d. National Electric Energy Supplier. Croatian Power System, daily power load curve, available at http://www.hep.hr/ops/hees/dijagram.aspx; Tariff models and prices at http://www.hep.hr/ods/en/customers/Tariff.aspx.

IIR (2002). Industry as a partner for sustainable development, International Institute of Refrigeration, UNEP.

IIR (2004). Ice Slurry: a Promissing Technology. Technical Note on Refrigerating Technologies. International Institute of Refrigeration.

IIR (2005a). Handbook on Ice Slurries, Fundamentals and Engineering. International Institute of Refrigeration, Paris, France.

IIR (2005b). French supermarkets turn to ice slurries, IIR Newsletter, no. 21, Paris: International Institute of Refrigeration.

Incropera, F.P., DeWitt, D.P., Bergman, T.L., Lavine, A. (2006). Fundamentals of Heat and Mass Transfer. Weily and Sons. 6th Edition. 2006.

Inženjerski priručnik IP1 (Handbook for Engineers IP1, in Croatian), Školska knjiga, Zagreb, 1996.

Ise, H., Tanino, M., Kozawa, Y. (2001). Ice storage system in Kyoto station building. Information Booklet for the Technical Tour of the Fourth Workshop of IIR Ice Slurry Working Party, Nov 13, 2001 p. 11–6.

Jensen, E.N., Christensen, K.G., Hansen, T.M., Schneider, P., Kauffeld, M. (2000). Pressure Drop and Heat Transfer with Ice Slurry, IIF-IIR Commision B1, B2, E2 for Purdue University, USA.

Kakac, S., Yener, Y. (1995). Convective heat transfer. 2nd Edition. CRC Press, 1995.

Kang, C., Yano, S., Okada, M. (2001). Non-uniform melting in packed beds of fine ice slurry. International Journal of Refrigeration, Volume 24, Pages 338-347.

Kauffeld, M., Christiansen, K.G., Lund, S., Hansen, T.M. (1999). Experience with ice slurry, Proceedings of the First IIR Workshop on Ice Slurries, 1999, France.

Kitanovski, A., Poredos, A. (2002). Concentration distribution and viscosity of ice-slurry in heterogeneous flow, International Journal of Refrigeration 25 (2002), pp. 827–835.

Knodel B.D., France, D.M., Choi, U.S., Wambsganss (2000). Heat transfer and pressure drop in ice-water slurries, Applied Thermal Engineering 20 (2000), pp. 671±685.

Kuriyama, T., Sawahata, Y. (2001) Slurry ice transportation and cold distribution system. Information Booklet for the Technical Tour of the Fourth Workshop of IIR Ice Slurry Working Party, Nov 13, 2001 p. 1–6.

Lee, A.H.W., Jones, J.W. (1996a). Modelling of an ice-on-coil thermal energy storage system. Energy Convers. Mgmt, Vol. 37, 1493-1507.

Lee, A.H.W., Jones, J.W. (1996b). Laboratory performance of an ice-on-coil Thermal-Energy storage system for residential and light commercial applications. Energy, Vol. 21, 115-130.

Liu, Y.H., Zhang Z., Zhao J., Chen P., (1997). Experiment study on friction loss characteristic of pipes with ice slurry. Science et technique du froid. Air conditioning in rise buildings 97 vol. 3, Shangai, pp 9-12.

Lopez, A., Lacarra, G. (1999). Mathematical Modelling of Thermal Storage Systems for Food Industry. Int J Refrig., Vol. 22, 650-658.

Lucas, L. (1998). IIR news, International Journal of Refrigeration, Vol. 21, No., 2, pp. 87-88.

Melinder, Å. (1997). Thermophysical Properties of Liquid Secondary Refrigerants, Tables and diagrames for the Refrigeration Industry. IIR Handbook, Paris, 1997.

Melinder, Å. (2003). Comparing Thermophysical Properties of Liquid Only and Ice Slurry Secondary Fluids. Proceedings of the International Conference on Fluid and Thermal Energy Conversion 2003, Bali, Indonesia.

MINGORP (2007). Energy in Croatia, Annual Energy Report. Republic of Croatia, Ministry of Economy, Labour and Entrepreneurship.

MZOPU (2005). Uredba o tvarima koje oštećuju ozonski sloj, Narodne Novine 120/05, Ministarstvo zaštite okoliša, prostornog uređenja i graditeljstva 12.10.2005.

Nichols, J.V., White, D. R. (1994). Traceable Temperatures - An Introduction to Temperature Measurement and Calibration. John Wiley & Sons, Chichester, England.

Nikolić, V., Grozdek, M., Halasz, B., Ćurko, T. (2009). Analiza isplativosti banke leda u rashladnim postrojenjima (Economic analysis of ice storage application in cooling systems within the industry). Strojarstvo, Journal for Theory and Application in Mechanical Engineering. Accepted for publication.

Norgaard, E., Sorensen, T.A., Hansen, T.M., Kauffeld, M. (2001). Performance of components of ice slurry systems: pumps, plate heat exchanger, fittings. In: Proceedings of the 3th IIR Workshop on Ice Slurries, 16-18 May 2001, Lucerne, Switzerland.

Pronk, P., Ferreira, C.A.I., Witkamp, G.J. (2004). Melting of ice slurry in a tube-in-tube heat transfer coil, Natural working fluids 2004: 6th IIR-Gustav Lorentzen conference, Paris: IIFIIR.

Pronk, P. (2006). Fluidized Bed Heat Exchangers to Prevent Fouling in Ice Slurry Systems and Industrial Crystallizers. PhD thesis, Technische Universiteit Delft, Nederland.

Ralph, K.E.L., Breisch, L. (1997). Dynamic ice harvesting thermal energy storage and powdered eggs. ASHRAE Transactions, Volume 103, Part 2, pp.730–733.

Recknagel, Sprenger, Schramek (2004). Taschenbuch fur Heizung + Klimatechnik. 72 Ausgabe, R. Oldenbourg Industrieverlag GmbH, Muenchen, 2004.

REFPROP v6.0 (1998). Thermodynamic and transport properties of refrigerants and refrigerant mixtures – REFPROP, version 6.0. National Institute of Standards and Technology (NIST), Boulder, CO, USA, 1998.

Saito, A. (2002). Recent advances in research on cold thermal energy storage. International Journal of Refrigeration, Volume 25, 2002, Pages 177-189

Sari, O., Vuarnoz, D., Meili, F., Egolf, P.W. (2000). Visualization of ice slurries and ice slurry flows. Proceedings of the Second IIR Workshop on Ice Slurries, 2000, Paris.

Sari, O., Meili, F., Vuarnoz, D., Egolf, P.W., (2000). Thermodynamics of Moving and Melting Ice Slurries, Proceedings of the 2nd IIR Workshop on Ice Slurries, 2000, Paris, pp. 140-153.

Shah, R. K., London, A. L. (1978). Laminar flow forced convection in ducts. Academic Press, 1978.

Skogsberg, K., Nordell, B. (2001). The Sundsvall hospital snow storage. Cold Regions Science and Technology, Volume 32, Pages 63-70.

Snoek, C., Bellamy J., 1997. Heat transfer measurements of ice slurry in tube flow. Exp. heat transfer. fluid mech thermo, pp. 1993-1997.

Steffe, J. F. (1996). Rheological methods in food process engineering. Freman Press. USA, 1996.

Stutz, B., Reghem, P. (2001). Friction losses of two-phase flow liquid-solid. Proceedings of the Third IIR Workshop on Ice Slurries, 2001, Lucerne.

Tanino, M., Kozawa, Y. (2001). Ice-water two-phase flow behaviour in ice heat storage systems. International Journal of Refrigeration, Volume 24, Pages 639-651.

UNEP (2003). Report of the Refrigeration, Air Conditioning and Heat Pumps Technical Options Committee, Montreal Protocol on Substances that Deplete the Ozone Layer, United Nations Environmental Programme, 2002 Assessment.

VDI 2078 (1996). Berechnung der Kuehllast klimatisierter Raeume (VDI-Kuellastregeln). Beuth Verlag GmbH, Berlin.

Zanki, A.V. (2006). Energy Use and Environmental Impact from Hotels on the Adriatic Coast in Croatia - Current Status and Future Possibilities for HVAC Systems. Doctoral thesis, Royal Institute of Technology (KTH), Stockholm, Sweden.

Zelasko, B.N, Zalewski W. (2006). Momentum transfer of ice slurry flows in tubes, experimental investigations, International Journal of Refrigeration 29, 2006, pp. 418-428.

Zelasko, B.N (2006). Heat transfer of ice slurry flows in tubes. International Journal of Refrigeration 29, pp. 437-450.